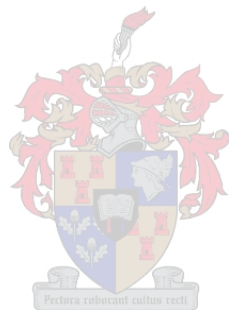


**Investigation of the N-terminal interactions of cardiac  
Myosin-Binding Protein C (cMyBPC) under defined phosphorylation states**

A. Ramburan

Dissertation presented for the Degree of Doctor of Philosophy at Stellenbosch University



Promoter: Prof Johanna C. Moolman-Smook

December 2008

## **DECLARATION**

By submitting this dissertation electronically, I declare that the entirety of the work contained therein is my own, original work, that I am the owner of the copyright thereof (unless to the extent explicitly otherwise stated) and that I have not previously in its entirety or in part submitted it for obtaining any qualification.

Date: December 2008

Copyright © 2008 Stellenbosch University  
All rights reserved

## ABSTRACT

Cardiac myosin-binding protein C (cMyBPC) is a large multi-domain protein (C0 to C10) that is anchored, in the C-zone of the sarcomere, to the light meromyosin portion of myosin and titin *via* its C-terminus domains. The C-terminus domains are further proposed to form a trimeric collar around the thick filament (Moolman-Smook *et al.*, 2002), which is hypothesised to dynamically form and release upon cMyBPC phosphorylation, thereby accommodating or facilitating the changes in the thick filament backbone diameter and affecting crossbridge formation. While the function and some interactors of the C-terminus are known, those of the N-terminus (C0C2) are not as well characterised. The N-terminus is proposed to modulate cardiac contractility *via* phosphorylation of the cMyBPC motif which results in a rearrangement of the myosin crossbridges and the structure of the thick filament (Weisberg and Winegrad, 1996; Levine *et al.*, 2001), impacting on muscle performance (McClellan *et al.*, 2001). The cMyBPC motif is located between domains C1 and C2 and contains three phosphorylation sites (Gautel *et al.*, 1995) that are substrates for PKA and/or a Ca<sup>2+</sup>/calmodulin-regulated kinase upon β-adrenergic stimulation. Since domains C0C2 have a rigid scaffolding structure and sufficient length to extend into the interfilament space (Jeffries *et al.*, 2008), it is possible that this region may modulate cardiac contractility by cycling between binding partners, dependent perhaps on the phosphorylation status of the MyBPC motif. That this region may be of vital importance is further emphasised by reports of mutations linked to hypertrophic cardiomyopathy.

The present study aimed to identify interactors of the C1C2 region of cMyBPC by yeast two-hybrid (Y2H) analyses, under conditions that mimic the various phosphorylation states of the cMyBPC motif, with a view to gaining insight into the function of the N-terminus of cMyBPC. C1C2 bait constructs mimicking the native, monophosphorylated, trisphosphorylated and dephosphorylated conditions of the cMyBPC motif were used to screen cardiac cDNA libraries, in separate Y2H library screens. Putative C1C2 interactors were subjected to *in vitro* co-immunoprecipitation (Co-IP), and three-dimensional *in vivo* co-localisation or live cell bioluminescence resonance energy transfer (BRET) analyses to verify interaction with N-terminus cMyBPC. Additionally, the ability of the cardiac-specific region N-terminus of C1 (C0-pro-ala-rich linker) to autoregulate the interactions of the C1C2 region was tested by Y2H direct protein-protein interaction assays.

The four library screens yielded a total of 27 putative positive interactors of domains C1C2, of which 13 [cardiac troponin I (cTNI); cardiac actin (ACTC); cardiac troponin T (cTNT); cMyBPC C5C10; α-actinin (ACTN2); copper metabolism gene *MURR1* domain 4 (COMM4D); β-enolase (ENO3); phosphodiesterase 4D interacting protein (PDE4DIP); heat shock 27kDa protein family, member 7 (HSPB7); glutamate receptor, ionotropic, NMDA-like 1A (GRINL1A); uveal autoantigen with coiled-coil domains and ankyrin repeats (UACA); spectrin repeat containing, nuclear envelope 1 (SYNE1); and guanine nucleotide-binding protein subunit beta-2-like 1 (GNB2L1)], representing 6 broad groups of interactors which may plausibly relate to the functions of cMyBPC, were investigated in the present study. The Y2H interaction assays showed that only two interactions with C1C2 (COMM4D and ACTN2)

were phosphorylation status dependent, while the remaining interactors bound to either the flanking domains (C1 or C2) or interacted with the cMyBPC motif in a manner not dependent on the phosphorylation status. In a separate Y2H interaction assay, the C0-pro-ala-rich linker was shown to interfere with the interactions of COMMD4, ACTC, cTNI, cTNT, HSPB7 and ENO3 with C1C2 cMyBPC, while no interference was observed for the cMyBPC (C5C10) and PDE4DIP interaction with C1C2 cMyBPC. Protein sequence analyses showed that three interactors (ACTN2, GRINL1A and UACA) had significant homology to myosin S2, a recognised interactor of C1C2, and their interaction with C1C2 may be driven by this homology. Further, these interactors had subcellular localisations incompatible with that of cMyBPC (in the sarcomeric C-zone) and were thus considered physiologically irrelevant interactors. SYNE1 had significant homology to ACTN2 and coupled with an incompatible subcellular localisation was also considered a spurious interactor. *In vitro* Co-IP experiments confirmed the interactions of ACTC, cMyBPC (C5C10), HSPB7 and PDE4DIP with C1C2 cMyBPC, while no interactions were observed for COMMD4 and cTNT with C1C2 cMyBPC. The C0-pro-ala-rich region did not interfere with any of the interactions between C1C2 cMyBPC and the putative interactors. Three-dimensional *in vivo* co-localisation in differentiated H9C2 cardiac myocytes showed that COMMD4, PDE4DIP, HSPB7 and ENO3 exist in the same subcellular space as cMyBPC, while BRET assays suggested that ACTC and cTNI may interact with C1C2 cMyBPC when the cMyBPC motif is unphosphorylated.

The present study has identified and verified numerous novel interactors of C1C2 cMyBPC. These interactors may shed light on the dynamics of PKA-mediated phosphorylation (PDE4DIP), the turnover of cMyBPC in the sarcomere (COMMD4), the preservation of cMyBPC integrity (HSPB7) and the means to generate energy to power the additional work during  $\beta$ -adrenergic stimulation (ENO3). In addition, direct contact with cTNI and ACTC may be the means by which cMyBPC is able to contribute to cardiac contraction and regulation under all conditions. Finally, the role of the C0-pro-ala-rich region with regard to the interactions of C1C2 is not entirely clear and may need to be investigated within the context of muscle cells. This study has identified exciting and novel interactors that will extend our knowledge of cMyBPC and will serve as a platform for future studies on the role and function of cMyBPC, as well as novel potential contributors to cardiac dysfunction.

## OPSOMMING

Kardiale miosien-bindingsproteïen C (cMyBPC) is 'n groot multi-domein (C0 tot C10) proteïen wat ganker is, in die C-sone van die sarkomeer, waar sy C-terminuse domeine aan die ligte meromiosien-deel van miosien en aan titin bind. Dit word gepostuleer dat die C-terminuse domeine 'n trimeriese kraag om die dik filament vorm en die hipotese is dat hierdie kraag dinamies vorm en losmaak met fosforilering van cMyBPC, om sodoende die verandering van die dik filament deursnee te akommodeer of selfs te faciliteer en daardeur kruisbrug-vorming óf te bevorder óf te beperk (Moolman-Smook *et al.*, 2002). Terwyl die funksie van en ten minste sommige van die proteïene wat bind aan die C-terminus van cMyBPC bekend is, is dié van die N-terminus nie so goed gekarakteriseer nie. Die N-terminuse domeine (C0-C2) word gepostuleer om kardiale kontraktiliteit te moduleer deur fosforilering van die MyBPC-motief, wat harrangskikking van die miosien kruisbrue asook van die struktuur van die dik filament veroorsaak (Weisberg and Winegrad, 1996; Levine *et al.*, 2001), wat dan weer 'n impak het op spier werkverrigting (McClellan *et al.*, 2001). Die MyBPC-motief lê tussen die domeine C1 en C2 en bevat drie fosforileringssetels (Gautel *et al.*, 1995) wat substrate is van PKA en/of 'n  $\text{Ca}^{2+}$ /kalmodulien-gereguleerde kinase onder  $\beta$ -adrenerge stimulasie.

Dit word gedink dat die N-terminuse (C0-C2) gebied kardiale kontraktiliteit beïnvloed deur in die tussenfilament ruimte in te strek, waar dit aan verskillende proteienbindings mag deelneem, wat dalk afhang van die fosforilasie-status van die MyBPC-motief. Synde dat hierdie deel 'n rigiede, platform struktuur het en ook lank genoeg is om in die tussen-filament ruimte in te strek, is dit moontlik dat die N-terminaal met ander sarkomeriese proteiene mag bind, wat die voorgestelde rol van regulasie van kardiale kontraktiliteit mag faciliteer. Dat hierdie gebied van groot belang is word onderstreep deur die feit dat mutasies in dié gebied hipertrofiese kardiomiopatie veroorsaak.

Die doel van hierdie studie was die identifikasie van buindingsgenote van die C1C2 gebied van cMyBPC deur gis twee-hibried (G2H) analises, onder toestande wat die verskillende fosforilasietoestande van die cMyBPC-motief weerspieël het, om daardeur 'n insig in die funksie van die N-terminus van cMyBPC te verkry. C1C2 jag-plasmiede, wat die normale, die mono-geflosforileerde, die tris-geflosforileerde en die nie-geflosforileerde toestande van die cMyBPC-motief verteenwoordig het, is gemaak. Hulle is afsonderlik gebruik om 'n hart kDNS-biblioteek in aparte siftings te ondersoek. Moontlike C1C2 bindingsgenote is onderwerp aan *in vitro* ko-immunopresipitasie (Ko-IP) en drie-dimensionele *in vivo* ko-lokalisering of lewendige sel bioluminisensie resonans-energie oordrag (BRET) analises om die interaksie met die N-terminus van cMyBPC te verifieer. Boonop is die vermoë van die hart-spesifieke gebied N-terminaal tot C1, die C0-pro-ala-ryke koppelaar, om die interaksies van die C1C2 gebied te auto-reguleer getoets deur middel van G2H direkte proteien-proteien interaksie-analises.

Die vier biblioteek-siftings het 'n total van 27 moontlike positiewe interakties van domeine C1C2 opgelewer. Daarvan is 13 [troponien I (TNI), kardiale aktien (ACTC), troponien T (TNT), cMyBPC C5-C10, a-aktinien

(ACTN), koper metabolisme geen MURR1 domein 4 (COMMD4), b-enolase (ENO3), fosfodiesterase 4D-interaksie proteen (PDE4DIP), hitte skok 27kDa proteien familie, lid 7 (HSPB7), glutamaat reseptor inostrofies, NDMA-soortige 1A (GRINL1A), uveale outoantigeen met gerolde-spring domein en ankirien herhalings (UACA), spektrien herhalings bevattende nukleale membraan 1 (SYNE) en guanine nukleotied-bindinde protein subeenheid beta-2-soortige 1 (GBN2L1), wat 6 breë kategoriee van bindingsgenote wat geloofwaardige funksionele verbande met cMyBPC verteenwoordig het, in hierdie studie verder ondersoek.

Die G2H interaksie-analises het getoon dat slegs twee interaksies met C1C2, dié van COMMD4 en ACTN2, van die fosforilerings-status van die cMyBPC-domein afhanglik was. Die ander interaktors het gebind aan óf C1 óf C2 óf met die cMyBPC-domein in 'n fosforilerings-status onafhanglike manier. In 'n afsonderlike G2H interaksie-analise, is getoon dat die C0-pro-ala-ryke koppelaar die interaksies tussen C1C2 cMyBPC en COMMD4, ACTC, TNI, TNT, HSPB7 en ENO3 versteur het, terwyl geen steuring in die interaksies van C1C2 cMyBPC met cMyBPC(C5C10) en PDE4DIP opgemerk is. Proteïen-volgorde analises het getoon dat drie moontlike bindingsgenote (ACTN2, GRINL1A, en UACA) beduidende homologie met miosien S2, 'n bekende bindignsgenoot van C1C2, gehad het, wat die rede vir die interaksie met C1C2 kon gewees het. Hierdie drie bindingsgenote se subsellulêre lokalisering is ook nie te vereenselwig met dié van cMyBPC in die C-sone van die sarkomeer nie, en hierdie is dus as valse interaksies beskou. SYNE1, wat beduidende homologie met ACTN2 het en 'n onooreenstemmende subsellulêre lokalisering in vergelyking met cMyBPCn het, is ook as 'n valse interaktor beskou.

*In vitro* Ko-IP eksperimente het die interaksies tussen C1C2 en ACTC, cMyBPC(C5C10), HSPB7 en PDE4DIP bevestig, maar geen interaksie kon met hierdie benadering tussen C1C2 en COMMD4 en TNT aangetoon word nie. Verder het die C0-pro-ala-ryke koppelaar nie die interaksies van C1C2 cMyBPC versteur nie. Drie-dimensionele *in vivo* ko-lokalisering in gedifferensiéerde H9C2 kardiale miosiete het getoon dat COMMD4, PDE4DIP, HSPB7 en ENO3 in dieselfde subsellulêre kompartement as cMyBPC teenwoordig is, terwyl BRET-analises aangedui het dat ACTC en TNI met die cMYBP-domein bind wanneer dit in die nie-gefosforileerde toestand is.

Hierdie studie het verskeie nuwe bindingsgenote van C1C2 cMyBPC geïdentifiseer en geverifieer. Hierdie bindingsgenote kan dalk lig werp op die dinamika van PKA-gemediéerde fosforilering (PDE4DIP), die omset van cMyBPC in die sarkomeer (COMMD4), die behoud van cMyBPC integriteit (HSPB7) en die manier waarop energie gegenereer word vir hoer werkverrigting na  $\beta$ -adrenerge stimulasie (ENO3). Verder kan direkte kontak met ACTC en TNI die manier wees waardeur cMyBPC tot kardiale kontraktiliteit en regulering onder enige omstandighede kan bydra. Die rol van die C0-pro-ala-ryke koppelaar met betrekking tot C1C2 interaksies is nog nie duidelik nie en hoort binne die konteks van spierselle verder ondersoek te word. Die nuwe bindingsgenote van cMyBPC wat deur hierdie studie geïdentifiseer is, brei ons kennis van cMyBPC uit en vorm die basis vir toekomstige studies oor die rol en funksies van cMyBPC asook moontlik nuwe bydraers tot kardiale wanfunksie.

<b>INDEX</b>	<b>PAGE</b>
<b>ACKNOWLEDGEMENTS</b>	viii
<b>LIST OF ABBREVIATIONS</b>	ix
<b>LIST OF FIGURES</b>	xvi
<b>LIST OF TABLES</b>	xxiv
<b>CHAPTER ONE: INTRODUCTION</b>	1
<b>CHAPTER TWO: MATERIALS AND METHODS</b>	69
<b>CHAPTER THREE: RESULTS</b>	104
<b>CHAPTER FOUR: DISCUSSION</b>	150
<b>APPENDIX I</b>	184
<b>APPENDIX II</b>	194
<b>APPENDIX III</b>	196
<b>APPENDIX IV</b>	200
<b>APPENDIX V</b>	201
<b>APPENDIX VI</b>	208
<b>APPENDIX VII</b>	209
<b>THESIS REFERENCES</b>	212

## **ACKNOWLEDGEMENTS**

My heartfelt gratitude to the following individuals who have assisted me through the course of my PhD:

My mentor, Professor JC Moolman-Smook, for your scientific input, guidance and patience throughout the study and write-up of this thesis. Thank you, also, for the financial and moral support. You are a strong woman and brilliant scientist, and I am grateful for having been your student.

Mrs Lundi Korkie, Department of Medical Biochemistry (University of Stellenbosch), for all the technical assistance and advice throughout the library screening and BRET assays. For the many hours you spent in tissue culture with me. Your friendship and support has been invaluable.

Mr Ben Loos, Department of Physiology (University of Stellenbosch), for the technical assistance and his comforting presence at the fluorescence microscope throughout the co-localisation assays.

Dr Muhammed F-R Sayed, Department of Bioinformatics (University of the Western Cape), for your willingness to assist me with the protein sequence analyses.

The Medical Research Council for accepting me into the Research Internship Programme and the financial support.

My many friends and colleagues in the Department of Medical Biochemistry for creating an enjoyable working environment.

Professor Vikash Sewram for giving me a home away from home. Your support and encouragement has made this whole experience so much less daunting. I shall forever be indebted to you.

My loving parents (Ramesh and Saras Ramburan) and brothers (Shandir and Diresh) for letting me pursue my dreams and aspirations no matter where it takes me. For giving me the foundation so I can stand tall by myself. Your unwavering love and support has been invaluable.

Finally, and most importantly, dear God: for showing me that perseverance and faith are endless resources. For watching over me and bringing me to the end of this journey.

## LIST OF ABBREVIATIONS

2-PGA	Two-phospho-D-glycerate
3D	Three-dimensional
5'-UTR	Five prime untranslated region
A	Alanine
aa	Amino acid
A-band	Anisotropic band
ABP	Actin binding protein
ACTA	Actin, skeletal isoform
ACTB	Actin, cytoplasmic isoform
ACTC	Actin, cardiac isoform
ACTG	Actin, smooth muscle isoform
ACTN2	Actinin, alpha 2
<i>ADE2</i>	Phosphoribosylaminoimidazole carboxylase gene
ADP	Adenosine diphosphate
AKAP	A-kinase anchoring protein
ALP	Alpha actinin-associated LIM protein
AMP	Adenosine monophosphate
AMPK	5'-AMP-activated protein kinase
ANOVA	Analysis of variance
AP2B1	Adaptor-related protein complex 2, beta 1 subunit
APAF1	Apoptotic protease activating factor 1
APS	Ammonium persulphate
ASB2	Ankyrin repeat and SOCS box-containing 2
ATCC	American type culture collection
ATP	Adenosine triphosphate
ATP5H	ATP synthase, H <sup>+</sup> transporting, mitochondrial F0 complex
BLAST	Basic local alignment search tool
BLASTN	Basic local alignment search tool (nucleotide)
BLASTP	Basic local alignment search tool (protein)
bp	Base pair
BRET	Bioluminescence resonance energy transfer
CO <sub>2</sub>	Carbon dioxide
C0A <sub>1</sub> A <sub>2</sub> A <sub>3</sub> C2	Phosphorylation-mimic of domain C0 to C2 representing the dephosphorylated state of the cMyBPC motif
C0A <sub>1</sub> P <sub>2</sub> A <sub>3</sub> C2	Phosphorylation-mimic of domain C0 to C2 representing the monophosphorylated state of the cMyBPC motif
C0C2	Construct of domain C0 to C2 representing the native state of the cMyBPC motif
C0P <sub>1</sub> P <sub>2</sub> P <sub>3</sub> C2	Phosphorylation-mimic of domain C0 to C2 representing the trisphosphorylated state of the cMyBPC motif

C1A <sub>1</sub> A <sub>2</sub> A <sub>3</sub> C2	Phosphorylation-mimic of domain C1 to C2 representing the dephosphorylated state of the cMyBPC motif
C1A <sub>1</sub> P <sub>2</sub> A <sub>3</sub> C2	Phosphorylation-mimic of domain C1 to C2 representing the monophosphorylated state of the cMyBPC motif
C1C2	Construct of domain C1 to C2 representing the native state of the cMyBPC motif
C1orf108	Chromosome 1 open reading frame 108
C1P <sub>1</sub> P <sub>2</sub> P <sub>3</sub> C2	Phosphorylation-mimic of domain C1 to C2 representing the trisphosphorylated state of the cMyBPC motif
C2orf29	Chromosome 2 open reading frame 29
Ca <sup>2+</sup>	Calcium
CaCl <sub>2</sub>	Calcium chloride
CamK-II	Calcium/calmodulin-dependent kinase-II
cAMP	Cyclic adenosine monophosphate
CARP	Cardiac ankyrin-repeat protein
CCT7	Chaperonin containing TCP1, subunit 7
cdDNA	Complementary DNA
Cfu	Colony forming units
cGMP	Cyclic guanosine monophosphate
CIAP	<i>Calf intestinal alkaline phosphatase</i>
cMyBPC <sup>-/-</sup>	Homozygous knockout of the cMyBPC gene
cMyBPC <sup>+/+</sup>	Heterozygous knockout of the cMyBPC gene
cMyBPC <sup>A P</sup>	Construct expressing a non-phosphorylatable cMyBPC protein
cMyBPC <sup>t/t</sup>	Construct expressing a truncated cMyBPC protein with domains C8 to C10 deleted
Cn	Calcineurin
CNN1	Calponin 1, smooth muscle isoform
Co-IP	Co-immunoprecipitation
COL1A2	Collagen, type I, alpha 2
COMM <sub>D</sub>	Copper metabolism <i>MURR1</i> domain
CRP	Cysteine-rich protein
cTNC	Troponin C, cardiac isoform
cTNI	Troponin I, cardiac isoform
cTNI-ND	cTNI construct expressing an N-terminus deleted protein
cTNI-PP	cTNI construct expressing a partially phosphorylated protein (serine 23/24)
cTNI-A//P	cTNI construct expressing a completely phosphorylated protein
Cull	Cullin
D	Aspartic acid
dATP	Deoxy-adenosine triphosphate
DBC	DeepBlueC
DCM	Dilated cardiomyopathy
dCTP	Deoxy-cytidine triphosphate
ddH <sub>2</sub> O	Distal deionised water
dGTP	Deoxy-guanosine triphosphate

DMEM	Dulbecco's modified eagle media
DMSO	Dimethyl sulphoxide
DNA	Deoxyribonucleic acid
dNTP	Deoxy-nucleotide triphosphate
DSCR3	Down syndrome critical region 3 protein
DTT	1,4-Dithiothreitol
dTTP	Deoxy-thymidine triphosphate
E1	Ubiquitin-activating enzyme
E2	Ubiquitin-conjugating enzyme
E3	Ubiquitin ligase
<i>E-coli</i>	<i>Escherichia coli</i>
EDTA	Ethylene-diamine-tetra-acetic acid
EIF4A2	Eukaryotic translation initiation factor 4A, isoform 2
ELC	Essential light chain
ENO3	Enolase 3, muscle isoform
ERK2	Extracellular signalling-regulated kinase 2
ETFA	Electron-transfer-flavoprotein, alpha polypeptide
E-Tmod	Tropomodulin, embryonic isoform
F-actin	Filamentous actin
FBXL10	F-box and leucine-rich repeat protein 10
FHL	Four-and-a-half LIM
FLNC	Filamin C, gamma
$F_{\max}$	Maximum $\text{Ca}^{2+}$ -activated force
FNIII	Fibronectin type three domain
Fs	fast skeletal muscle isoform
G	Grams
GABA	Gamma-aminobutyric acid
G-actin	Globular actin
GFP	Green fluorescent protein
GNB2L1	Guanine nucleotide binding protein (G protein), beta polypeptide 2-like 1
GRINL1A	Glutamate receptor, ionotropic, NMDA-like 1A
HCl	Hydrochloric acid
HCM	Hypertrophic cardiomyopathy
<i>HIS3</i>	Imidazoleglycerolphosphate dehydratase gene
HMM	Heavy meromyosin
HOMSTRAD	Homologous structure alignment database
HSP	Heat shock protein
HSPB3	Heat shock 27 kDa protein 3
HSPB7	Heat shock 27 kDa protein family, member 7, cardiovascular isoform
I-band	Isotropic band
Ig	Immunoglobulin
kb	Kilo bases

kDa	Kilo Dalton
KO	Knock-out
KOAc	Potassium acetate
$K_{tr}$	Rate of force development
L	Litre
LB	Luria-Bertani broth
LGMN	Legumain
LiAc	Lithium acetate
LMM	Light meromyosin
LMOD3	Leiomodin 3, foetal isoform
LV	Left ventricular
M	Molar
M6t	Construct expressing a cMyBPC protein from domains C0 to partial deletion of domain C10
M7t	Construct expressing a cMyBPC protein from domains C0 to partial C1 only
mAKAP	Muscle-specific A-kinase anchoring protein
MCS	Multiple cloning site
MDa	Mega Dalton
<i>MELI</i>	Alpha-galactosidase gene
MFC	MURF family conserved
mg	Milligram
MHC	Myosin heavy chain
MHCemb	Myosin heavy chain, embryonic isoform
MHCExoc	Myosin heavy chain, extraocular isoform
MHCneo	Myosin heavy chain, neonatal isoform
ml	Millilitre
MLC	Myosin light chain
MLCK	Myosin light chain kinase
MLP	Muscle LIM protein
mM	Millimolar
MRC	Medical research council
mRNA	Messenger RNA
MURF	Muscle specific RING finger protein
MyBPC	Myosin-binding protein C
<i>MYBPC3</i>	Cardiac myosin-binding protein C gene
MyBPH	Myosin-binding protein H
<i>MYL</i>	Myosin light chain gene
NaCl	Sodium chloride
NaOH	Sodium hydroxide
NcTNC	N-terminus cardiac troponin C
NcTNI	N-terminus cardiac troponin I
NFAT3	Nuclear factor of activated T cells 3

NF-κB	Nuclear factor kappa beta
NH <sub>4</sub>	Ammonium
NMDA	<i>N</i> -methyl- <i>D</i> -aspartate
NMR	Nuclear magnetic resonance
°C	Degrees Celsius
OD	Optical density
ORF	Open reading frame
PAGE	Polyacrylamide gel electrophoresis
PARVA	Parvin, alpha
PBS	Phosphate buffered saline
PCI	Phenol/chloroform/isoamyl alcohol
PCR	Polymerase chain reaction
PDE	Phosphodiesterase
PDE4DIP	Phosphodiesterase 4D interacting protein
PDZ	PSD-95/Disc-large/ZO 1
PEG	Polyethylene glycol
PEP	Two-phosphoenolpyruvate
PEVK	Proline, glutamine, valine and lysine rich domain of titin
PGM5	Phosphoglucomutase 5
Pi	Inorganic phosphate
PIPES	Piperazine-N,N-bis (2-ethanesulfonic acid,) 1.5 Sodium
PKA	Protein kinase A
PKC	Protein kinase C
PKG	Protein kinase G
PLB	Phospholamban
PMSF	Phenylmethylsulphonyl fluoride
PSAP	Prosaposin
QDO	Quadruple dropout
RACK1	Receptor for activated C kinase 1
RET	Non-radiative energy transfer
RFP	Red fluorescent protein
Rho-GEF	Rho-guanine nucleotide exchange factor
RING	Really interesting new gene
RLC	Regulatory light chain
RLCa	Regulatory light chain, atrial isoform
RLCv	Regulatory light chain, ventricular isoform
Rluc	<i>Renilla</i> luciferase
RNA	Ribonucleic acid
Rpm	Revolutions per minute
RSA	Republic of South Africe
S1	Myosin subfragment 1
S2	Myosin subfragment 2

sAnk1	Small ankyrin 1
SB	Sodium borate
SCF	Skp-1-cullin-F-box
SD	Synthetic dropout
SDS	Sodium dodecyl-sulphate
Ser	Serine
SERCA	Sarco endoplasmic reticulum calcium-ATPase
SERPINH1	Serpin peptidase inhibitor, clade H, member 1
SH3	Src homology 3
shSP	Small heat shock protein
Skp1	S-phase kinase-associated protein 1
SLC25A3	Solute carrier family 25 (mitochondrial carrier; phosphate carrier), member 3
SMARCB1	SWI/SNF related, matrix associated, actin dependent regulator of chromatin, subfamily b, member 1
SNF	Sodium neurotransmitter family
SNX3	Sorting nexin 3
SR	Sarcoplasmic reticulum
SRF	Serum response factor
ss	Slow skeletal muscle isoform
SUPV3L1	Suppressor of var1, 3-like
SVIL	Supervillin
SYNE1	Spectrin repeat containing, nuclear envelope 1
Ta	Annealing temperature
TBST	Tris-buffered saline Tween 20
T-cap	Telethonin
TDO	Triple dropout
TE	Tris-EDTA
TEMED	N,N,N',N'-Tetramethylethylenediamine
TG	Transgenic
Thr	Threonine
TK	Titin kinase
TM	Tropomyosin
Tm	Melting temperature
Tmod	Tropomodulin
Tn	Troponin
TNC	Troponin C
TNI	Troponin I
<i>TNNI3</i>	Troponin I type 3, cardiac gene
<i>TNNT2</i>	Troponin T type 2, cardiac gene
TNT	Troponin T
<i>TPM</i>	Tropomyosin gene
Tyr	Tyrosine

UACA	Uveal autoantigen with coiled-coil domains and ankyrin repeats
Ub	Ubiquitin
UBE2V1	Ubiquitin-conjugating enzyme E2 variant 1
UK	United Kingdom
UPS	Ubiquitin-proteasome system
USA	United States of America
UV	Ultraviolet
V	Volts
VLC2	Ventricular light chain 2
$V_{\max}$	Maximal shortening velocity
$V_o$	Unloaded shortening velocity
w/v	Weight per volume
WT	Wild-type
www	World wide web
X- $\alpha$ -Gal	X-alpha-galactosidase
Y2H	Yeast-two hybrid
YFP	Yellow fluorescent protein
YPD <sub>A</sub>	Yeast peptone dextrose adenine
ZASP	Z-disc alternatively spliced PDZ-containing protein
ZNF219	Zinc finger protein 219
ZNF668	Zinc finger protein 668
$\alpha$ -HA	Anti-hemagglutinin
$\alpha$ -MHC	Myosin heavy chain, alpha
$\beta$ -MHC	Myosin heavy chain, beta
$\mu$ l	Microlitre

## LIST OF FIGURES

**Figure 1.1.** Electron micrograph of a single sarcomere showing the major compartments of the sarcomere (I-band, Z-disc, A-band, M-line, C-zone and the H-zone). Actin filaments are the major component of the I-band and extend into the A-band while myosin filaments extend throughout the A-band and overlap in the M-line. Image modified from (Laing and Nowak, 2005).

**Figure 1.2.** The thin filament. The double-stranded filamentous actin (F-actin) forms the principal part of the thin filament. The troponin complex of troponin C, troponin I and troponin T, together with tropomyosin, make the calcium-sensitive switch that activates muscle contraction. A single molecule of nebulin stretches the entire length of the thin filament and determines the length of the thin filament in different muscle fibre types. Image taken from (Laing and Nowak, 2005).

**Figure 1.3.** Model illustrating the interactions of troponin components in the diastolic state and with phosphorylation of Ser23/24 in the unique N-terminus extension of cTnI containing a phosphorylation helix, a proline helix linker and an acidic region. Tropomyosin (TM), cardiac troponin I (cTnI), cardiac troponin T (cTnT), the switch peptide of cTnI (H3; that binds to the hydrophobic patch on cTnC) and the cTnI inhibitory region (Ip) is indicated. In this state both the Ip region and C-terminus domain interact with actin. Image taken from (Solaro *et al.*, 2008).

**Figure 1.4.** (A) Striated muscle sarcomere showing the overlapping arrays of thick and thin filaments. Thick filaments are connected at the M-line and thin filaments at the Z-disc/line. (B) Central portion of the thick filament model showing the helical array (red dashed line) of pairs of myosin heads on the filament surface (each pair represented by a yellow sphere). The green backbone contains myosin tails. (C) The myosin molecule. The tail (S2 and LMM) is a coiled-coil formed from the C-terminus halves of each heavy chain (red and green). Heads (S1) comprise the motor domain (MD) and light chain domain (LCD) which contains the essential light chain (ELC, blue) and regulatory light chain (RLC, yellow). Image taken from (Craig and Woodhead, 2006).

**Figure 1.5.** The cardiac Z-disc/titin cytoskeletal structure and associated proteins. An increasing number of molecules have been identified in the vicinity of the Z-disc/titin cytoskeleton. See section 1.5.1-11 for details. muscle LIM protein (MLP); four-and-a-half LIM domain (FHL); calcineurin (Cn); telethonin (T-cap); muscle-specific RING finger (MURF); Image taken from (Hoshijima, 2006).

**Figure 1.6.** Molecular structure and interactions of titin. Titin is a highly modular protein, comprising mainly immunoglobulin and fibronectin type III domains. These domains are arranged in patterns specific for sarcomeric substructures (the Z-disc, I-band, A-band and M-line) where they serve as regulatory or ligand-

binding sites. Interactions with proteins for each region are described in section 1.6. Image taken from (Lange *et al.*, 2006).

**Figure 1.7.** The transition of Z-bodies (containing  $\alpha$ -actinin) in premyofibrils and nascent myofibrils to Z-discs in mature myofibrils. In this premyofibril model, assembly begins at the edges of muscle cells with premyofibrils composed of mini-sarcomeres that contain sarcomeric proteins in the  $\alpha$ -actinin enriched Z-bodies and thin filaments of actin, troponins and tropomyosin. Non-muscle myosin II filaments are present in the mini-sarcomere of the premyofibrils. Z-bodies in adjacent fibrils begin to align in nascent myofibrils, forming beaded Z-discs that gradually become linear Z-discs in mature myofibrils. Titin molecules and muscle myosin II thick filaments are also present in the nascent myofibrils. The thick filaments in the nascent myofibrils are not aligned, but are overlapped. M-line proteins are recruited to the mature myofibrils, thick filaments become aligned into A-bands, while non-muscle myosin II proteins are absent. Image taken from (Sanger *et al.*, 2006).

**Figure 1.8.** Sarcomere protein turnover and Z-disc/M-line-associated ubiquitin (Ub) ligase complexes. Ubiquitination-dependent protein turnover may critically regulate turnover of cardiac proteins. Selective localisations of E3 ubiquitin ligase complex components have been identified: MURFs at the M-line titin and atrogin-1 at the Z-disc. In addition to their direct interaction with sarcomeric proteins, M-line MURF may regulate the SRF transcriptional factor, and atrogin-1 binds and induces degradation of calcineurin (Cn) at the Z-discs. Collectively, sarcomere-associated ubiquitin ligase components may serve as critical regulators of both protein synthesis and degradation. Image taken from (Hoshijima, 2006).

**Figure 1.9.** Simplified kinetic scheme of the crossbridge cycle. M, myosin; A, actin. Main reaction pathways are indicated by heavy arrows. See section 1.8.1 for details. Diagram taken from (Schaub *et al.*, 1998).

**Figure 1.10.** The three-dimensional ribbon structure of the autoinhibited form of titin kinase. Red, regulatory tail; cyan, catalytic loop; green, activation segment; magenta, P+1 loop. The side chains of residues D127, R129 and Y-170 are highlighted in yellow. The autoinhibited TK shows how Tyr-170 of the P+1 loop inhibits the active site. The  $\alpha$ R2 helix binds to the kinase ATP-binding site and specifically interacts with the residues involved in catalysis while the C-terminus part of the regulatory tail,  $\beta$ R1, forms a  $\beta$ -sheet with  $\beta$ C10 and  $\beta$ C11. TK activation therefore requires release of autoinhibition, in particular the removal of autoinhibitory tail from the active site upon phosphorylation of Tyr170 and  $\text{Ca}^{2+}$ /calmodulin-binding to the N-terminus  $\alpha$ R1 helix (Mayans *et al.*, 1998). Image taken from (Mayans *et al.* 1998).

**Figure 1.11.** (A) Schematic representation of phospholamban. Horizontal lines denote the membrane boundaries and amino acids are shown in circles (taken from Bhupathy *et al.*, 2007). (B) Structural models of pentameric phospholamban; the extended helix/sheet; continuous helix; pinwheel and bellflower pentamers. Image taken from (Traaseth *et al.*, 2007)

**Figure 1.12.** The proposed arrangement of cMyBPC in the thick filament. (A) The trimeric collar model has three cMyBPC molecules forming a collar around the thick filament, with domains C5C7 of one molecule interacting with domains C8C10 of the next (Moolman-Smook *et al.*, 2002). The N-terminus domains (C0C4) extend into the interfilament space where the cMyBPC motif interacts with myosin S2. [Image taken from Moolman-Smook *et al* (2002)] (B) The second model has domains C7C10 running axially along the myosin filament with the N-terminus (pro-ala-rich insert) interacting with actin. [Image taken from Squire *et al* (2003)]

**Figure 1.13.** Schematic representation of cMyBPC domain organisation. The interactions with cMyBPC represented by solid black lines indicate established interactions while those in broken black lines represent interactions that require independent verification. Ig domains are shown in pink circles; FNIII domains in blue squares; linker sequences between domain C0C1 and C4C5 in solid blue lines; cardiac-specific insert in C5 in green rectangle and phosphorylation sites between C1C2 in purple octagons.

**Figure 2.1.** Representation of the C0C2 and C1C2 cMyBPC phosphorylation mimics generated by PCR-mediated site-directed mutagenesis (Section 2.2.3). The serine residues in each of the three phosphorylation sites (P1, P2 and P3) were substituted with either alanine or aspartic acid to represent constitutive dephosphorylation or constitutive phosphorylation, respectively.

**Figure 2.2.** Schematic representation of PCR site-directed mutagenesis PCR. Step A shows the outer forward (C0-F) and reverse (C2-R) primers, two sets of mutagenesis primers (C1A<sub>1</sub>A<sub>2</sub>-F/R and C1A<sub>3</sub>-F/R), and the MyBPC cDNA template that was used in various PCR reactions (Steps B, C, D, E) to generate a full length PCR product representing the dephosphorylated cMyBPC C0C2 mimic, C0A<sub>1</sub>A<sub>2</sub>A<sub>3</sub>C2. A similar protocol was followed to produce the three phosphorylation mimics of the C1C2 fragment, except that the C1-F primer was used in stead of C0-F.

**Figure 2.3.** Schematic representation of the Co-IP protocol. Protein A; ▲ Protein B; ■ Anti-Myc Antibody; ▽ Anti-HA Antibody; △ Protein G agarose ● . Experiments 1 and 2 represent the immunoprecipitation of Proteins A and B using the appropriate antibodies. On a 15% SDS-PAGE gel, the immunoprecipitation is represented by a single band as seen in lanes 1 and 2. Experiment 3 represents a Co-IP reaction showing an interaction between Proteins A and B. This interaction is seen as two bands (lanes 3) on the gel; one band for each protein. Experiment 4 shows a Co-IP reaction where Proteins A and B do not interact with each other. After the 5 TBST washes, unbound proteins are washed away, leaving only proteins bound to the Myc antibody and hence only one band is seen in lane 4. Experiment 5 shows the Protein G agarose control. As this is a negative control, Protein B should not interact with the Protein G agarose in the absence of an antibody, hence there should be no band in lane 5.

**Figure 3.1.** Linear growth curves of yeast strain AH109 transformed with non-recombinant pGBK and pGBK-cMyBPC bait constructs. In order to determine whether the bait constructs had toxic effects on the AH109 strain, the growth rate of the pGBK-bait transformants were compared to the non-recombinant pGBK. The growth rate was determined by calculating the slope of each of the curves. The slopes were comparable indicating that the bait constructs had no toxic effect on the growth of the host yeast strain.

**Figure 3.2.** Autoradiograph of radioactive-labelled proteins from coupled *in vitro* transcription-translation reactions (15% SDS-PAGE gel). A and B show translated bait-mimics of C0C2 and C1C2 representing various phosphorylation states of the cMyBPC motif. C and D show translated prey proteins. Lanes A1, B6, C1 and D1 show the positions of the non-radioactive High-Range Rainbow™ molecular weight marker bands, as transferred from the dried polyacrylamide gel. The red arrow indicates the band of interest. Lane D2 shows the translation of protein not used in the present study.

**Figure 3.3.** Autoradiograph of 20% SDS-PAGE gel showing the Co-IP of C0C2 and C1C2 cMyBPC phosphorylation-mimics with HSPB7 protein. The antibody used for immunoprecipitation is indicated within brackets. Two bands in each Co-IP lane in conjunction with a clear negative control lane suggests that HSPB7 interacted with the bait phosphorylation mimic.

**Figure 3.4.** Autoradiograph of 20% SDS-PAGE gel showing the Co-IP of C0C2 and C1C2 cMyBPC phosphorylation-mimics with PDE4DIP protein. The antibody used for immunoprecipitation is indicated within brackets. Two bands in each Co-IP lane in conjunction with a clear negative control lane suggests that PDE4DIP interacted with the bait phosphorylation mimic.

**Figure 3.5.** Autoradiograph of 17.5% SDS-PAGE gel showing the Co-IP of C0C2 and C1C2 cMyBPC phosphorylation-mimics with ACTC1 protein. The antibody used for immunoprecipitation is indicated within brackets. Two bands in each Co-IP lane in conjunction with a clear negative control lane suggests that ACTC1 interacted with the bait phosphorylation mimic.

**Figure 3.6.** Autoradiograph of 17.5% SDS-PAGE gel showing the Co-IP of C0C2 and C1C2 phosphorylation-mimics with COMMD4 protein. The antibody used for immunoprecipitation is indicated within brackets.

**Figure 3.7.** Densitometer estimate of COMMD4 precipitated in the Co-IP lanes only. The yellow bar in lanes 2-9 shows that the amount of COMMD4 precipitated after the negative control (lane 10) has been subtracted is less than the negative control and therefore COMMD4 does not precipitate with the C0C2 and C1C2 baits, respectively. The estimate amount of each protein is indicated above the bars.

**Figure 3.8.** Autoradiograph of 20% SDS-PAGE gel showing the Co-IP of C0C2 and C1C2 phosphorylation-mimics with cTNT protein. The antibody used for immunoprecipitation is indicated within brackets.

**Figure 3.9.** Densitometer estimate of cTNT precipitated in the Co-IP lanes only. The yellow bar in lanes 2-9 shows that the amount of cTNT precipitated after the negative control (lane 10) has been subtracted is less than the negative control and therefore cTNT does not precipitate with the C0C2 and C1C2 baits, respectively. The estimate amount of each protein is indicated above the bars.

**Figure 3.10.** Autoradiograph of 20% SDS-PAGE gel showing the Co-IP of C0C2 and C1C2 phosphorylation-mimics with ENO3 protein. The antibody used for immunoprecipitation is indicated within brackets.

**Figure 3.11.** Densitometer estimate of ENO3 precipitated in the Co-IP lanes only. The yellow bar in lanes 2-9 shows that the amount of ENO3 precipitated after the negative control (lane 10) has been subtracted is more than the negative control and therefore ENO3 precipitates with the C0C2 baits. Estimate values for the ENO3+C1C2 baits could not be determined as the bands separated too close together. The estimate amount of each protein is indicated above the bars.

**Figure 3.12.** Autoradiograph of 20% SDS-PAGE gel showing the Co-IP of C0C2 and C1C2 phosphorylation-mimics with cTNI protein. The antibody used for immunoprecipitation is indicated within brackets.

**Figure 3.13.** Densitometer estimate of cTNI precipitated in the Co-IP lanes only. The yellow bar in lanes 2-9 shows that the amount of cTNI precipitated after the negative control (lane 10) has been subtracted is more than the negative control and therefore cTNI precipitates with the C0C2 baits (except the C0P<sub>1</sub>P<sub>2</sub>P<sub>3</sub>C2+cTNI interaction). Estimate values for the cTNI+C1C2 baits could not be determined as the bands separated too close together. The estimate amount of each protein is indicated above the bars.

**Figure 3.14.** Autoradiograph of 20% SDS-PAGE gel showing the Co-IP of C0C2 and C1C2 phosphorylation-mimics with cMyBPC (C5C10) protein. The antibody used for immunoprecipitation is indicated within brackets.

**Figure 3.15.** Densitometer estimate of cMyBPC (C5-10) precipitated in the Co-IP lanes only. The yellow bar in lanes 2-9 shows that the amount of cMyBPC (C5-10) precipitated after the negative control (lane 10) has been subtracted is more than the negative control and therefore cMyBPC (C5-10) precipitates with the C0C2 and C1C2 baits, respectively. The estimate amount of each protein is indicated above the bars.

**Figure 3.16.** Live cell fluorescence imaging of COMMD4 and cMyBPC co-localisation in differentiated H9C2 cardiac myocytes. (A) GFP-tagged C1C10 cMyBPC (green). (B) YFP-tagged COMMD4 (red). (C) Co-localisation of COMMD4 and C1C10 cMyBPC generated from Z-stack (yellow). (D) Overlay of images A-C with Hoechst H-33342 labelling of the nuclei (blue). Magnification: 60X oil immersion before 70% reduction.

**Figure 3.17.** Live cell fluorescence imaging of PDE4DIP and cMyBPC co-localisation in differentiated H9C2 cardiac myocytes. (A) GFP-tagged C1C10 cMyBPC (green). (B) YFP-tagged PDE4DIP (red). (C) Co-localisation of PDE4DIP and C1C10 cMyBPC generated from Z-stack (yellow). (D) Overlay of images A-C with Hoechst H-33342 labelling of the nuclei (blue). Magnification: 60X oil immersion before 70% reduction.

**Figure 3.18.** Live cell fluorescence imaging of HSPB7 and cMyBPC co-localisation in differentiated H9C2 cardiac myocytes. (A) GFP-tagged C1C10 cMyBPC (green). (B) RFP-tagged HSPB7 (red). (C) Co-localisation of HSPB7 and C1C10 cMyBPC generated from Z-stack (yellow). (D) Overlay of images A-C with Hoechst H-33342 labelling of the nuclei (blue). Magnification: 60X oil immersion before 70% reduction.

**Figure 3.19.** Live cell fluorescence imaging of ENO3 and cMyBPC co-localisation in differentiated H9C2 cardiac myocytes. (A) GFP-tagged C1C10 cMyBPC (green). (B) RFP-tagged ENO3 (red). (C) Co-localisation of ENO3 and C1C10 cMyBPC generated from Z-stack (yellow). (D) Overlay of images A-C with Hoechst H-33342 labelling of the nuclei (blue). Magnification: 60X oil immersion before 70% reduction.

**Figure 3.20.** Bar graph of BRET values determined from differentiated H9C2 cardiac myocytes co-transfected with cTNI-GFP and C1C10 cMyBPC-Rluc, and respective controls. Values represent means  $\pm$ S.E for five independent transfections. Experiments were performed in duplicate and statistical comparisons were carried out using a one-way analysis of variance (ANOVA) followed by Bonferroni's multiple comparison post-test, comparing all pairs. Graph A shows the respective interactions in unstimulated cells while graph B shows the same interactions in cells stimulated for maximal cMyBPC phosphorylation. There were no statistically significant differences between the C1C10 cMyBPC/cTNI pair and either the C1C10 cMyBPC control or the cTNI control in either stimulated or unstimulated cells, respectively.

**Figure 3.21.** Bar graph of BRET values determined from differentiated H9C2 cardiac myocytes co-transfected with ACTC1-GFP and C1C10 cMyBPC-Rluc, and respective controls. Values represent means  $\pm$ S.E for five independent transfections. Experiments were performed in duplicate and statistical comparisons were carried out using a one-way analysis of variance (ANOVA) followed by Bonferroni's

multiple comparison post-test, comparing all pairs. Graph A shows the respective interactions in unstimulated cells while graph B shows the same interactions in cells stimulated for maximal cMyBPC phosphorylation. There were no statistically significant differences between the C1C10 cMyBPC/ACTC1 pair and either the C1C10 cMyBPC control or the ACTC1 control in either stimulated or unstimulated cells, respectively.

**Figure 3.22.** Bar graph of BRET values determined from differentiated H9C2 cardiac myocytes co-transfected with cTNI-GFP and C2C10 cMyBPC-Rluc, and respective controls. Values represent means  $\pm$ S.E for two independent transfections. Experiments were performed in duplicate and statistical comparisons were carried out using a one-way analysis of variance (ANOVA) followed by Bonferroni's multiple comparison post-test, comparing all pairs. Graph A shows the respective interactions in unstimulated cells while graph B shows the same interactions in cells stimulated for maximal cMyBPC phosphorylation. There were no statistically significant differences between the C2C10 cMyBPC/cTNI pair and either the C2C10 cMyBPC control or the cTNI control in either stimulated or unstimulated cells, respectively.

**Figure 3.23.** Bar graph of BRET values determined from differentiated H9C2 cardiac myocytes co-transfected with ACTC1-GFP and C2C10 cMyBPC-Rluc, and respective controls. Values represent means  $\pm$ S.E for two independent transfections. Experiments were performed in duplicate and statistical comparisons were carried out using a one-way analysis of variance (ANOVA) followed by Bonferroni's multiple comparison post-test, comparing all pairs. Graph A shows the respective interactions in unstimulated cells while graph B shows the same interactions in cells stimulated for maximal cMyBPC phosphorylation. There were no statistically significant differences between the C2C10 cMyBPC/ACTC1 pair and either the C2C10 cMyBPC control or the ACTC1 control in either stimulated or unstimulated cells, respectively.

**Figure 3.24.** Bar graph of BRET values determined from differentiated H9C2 cardiac myocytes co-transfected with C2C10 MCS, C3C10 MCS, C7C10 MCS, and the respective controls. Values represent means  $\pm$ S.E for two independent transfections. Experiments were performed in duplicate and statistical comparisons were carried out using a one-way analysis of variance (ANOVA) followed by Bonferroni's multiple comparison post-test, comparing all pairs. Graph A shows the respective interactions in unstimulated cells while graph B shows the same interactions in cells stimulated for maximal cMyBPC phosphorylation. There were no statistically significant differences between each of the tests and the controls in either stimulated or unstimulated cells, respectively.

**Figure 4.1** CLUSTAL W multiple sequence alignment showing the homology between C1C2 cMyBPC and the inhibitory region of cTNI.

**Figure 4.2.** The hypothesised transition of the thick filament from the tight (A) to loose (B) structure upon  $\beta$ -adrenergic stimulation. In the tight structure, cMyBPC domains C5:C8, C6:C9 and C7:C10 interact. Upon  $\beta$ -

adrenergic stimulation and trisphosphorylation of the cMyBPC motif, the thick filament adopts the loose structure with a wider diameter which is proposed to be facilitated by the widening of the cMyBPC collar. Thus, domains C2 or C3 may now interact with domain C10. Image A taken from Moolman-Smook *et al* (2002) and image B from W.J de Lange (2004).

**Figure 4.3.** SDS-PAGE gel showing Co-IP reactions between cMyBPC clones (C412 and P62) and baits (C1C2 and C1P<sub>1</sub>P<sub>2</sub>P<sub>3</sub>C2). Gels A and B show that cMyBPC clones interact much stronger with C1P<sub>1</sub>P<sub>2</sub>P<sub>3</sub>C2 bait than the C1C2 bait. The antibody used for immunoprecipitation is shown in brackets. Image taken from (Unpublished data; Moolman-Smook *et al.*, 2004)

**Figure 4.4.** Proposed interactions for the N-terminus cMyBPC. See text for details

## LIST OF TABLES

**Table 2.1.** Nucleotide sequences of primers used for the amplification of the C1C2 and C0C2 PCR products, representing the different phosphorylation states of the cMyBPC motif

**Table 2.2.** Primer sequences and annealing temperatures used for the amplification of inserts from Y2H cloning vectors

**Table 2.3.** Primers for the generation of products used in *in vitro* transcription and translation experiments

**Table 2.4.** Primers for the generation of products used for BRET assays

**Table 2.5.** Primers for the generation of products used in *in vivo* co-localisation experiments

**Table 2.6.** Primers for the generation of products used for In-Fusion cloning

**Table 2.7.** Primers for Co-localisation and BRET assay insert screening

**Table 2.8.** Primer pairs and annealing temperatures used for the amplification of C1C2 and C0C2 PCR products, representing the different phosphorylation states of the cMyBPC motif

**Table 2.9.** Transfection experiment layout for BRET assay

**Table 2.10.** Transfection experiment layout for MCS BRET assay

**Table 2.11.** Transfection experiment layout for *in vivo* co-localisation assay

**Table 2.12.** Excitation and emission spectra, and filter requirements of fluorescent proteins used in *in vivo* co-localisation

**Table 3.1.** Effect of bait constructs in pGBK, Y2H bait vector, on AH109 mating efficiency

**Table 3.2.** Activation of nutritional and colourimetric reporter genes by prey-C1C2 interaction. Tabulated are representative scoring of the 460 clones that activated the *HIS3* reporter gene, 162 clones that activated the *ADE2* reporter gene and 103 clones that were able to activate the *MEL1* reporter gene.

**Table 3.3.** Identification of C1C2 putative interactor clones from the Y2H cardiac cDNA library screen. Putative interactors represented by multiple clones are shown first, arranged from highest to lowest activators

of nutritional and colourimetric reporter genes. Putative interactors represented by a single clone are arranged in the same manner.

**Table 3.4.** Interaction of C1C2 preys with heterologous baits in specificity tests. Tabulated are the scores of the clones considered as putative interactors.

**Table 3.5.** Activation of nutritional and colourimetric reporter genes by prey-C1P<sub>1</sub>P<sub>2</sub>P<sub>3</sub>C2 interaction. Tabulated are representative scoring of the 500 clones that activated the *HIS3* reporter gene, 353 clones that activated the *ADE2* reporter gene and 232 clones that were able to activate the *MEL1* reporter gene.

**Table 3.6.** Identification of C1P<sub>1</sub>P<sub>2</sub>P<sub>3</sub>C2 putative interactor clones from the Y2H cardiac cDNA library screen. Putative interactors represented by multiple clones are shown first, arranged from highest to lowest activators of nutritional and colourimetric reporter genes. Putative interactors represented by a single clone are arranged in the same manner.

**Table 3.7.** Interaction of C1P<sub>1</sub>P<sub>2</sub>P<sub>3</sub>C2 preys with heterologous baits in specificity tests. Tabulated are the scores of the clones considered as putative interactors.

**Table 3.8.** Activation of nutritional and colourimetric reporter genes by prey-C1A<sub>1</sub>P<sub>2</sub>A<sub>3</sub>C2 interaction. Tabulated are representative scoring of the 1680 clones that activated the *HIS3* reporter gene, 1035 clones that activated the *ADE2* reporter gene and 138 clones that were able to activate the *MEL1* reporter gene.

**Table 3.9.** Interaction of C1A<sub>1</sub>P<sub>2</sub>A<sub>3</sub>C2 preys with heterologous baits in specificity tests. Tabulated are representative scores of the 138 clones that were screened.

**Table 3.10.** Identification of the fourteen C1A<sub>1</sub>P<sub>2</sub>A<sub>3</sub>C2 putative interactor clones from the Y2H cardiac cDNA library screen. Putative interactors represented by multiple clones are shown first, arranged from highest to lowest activators of nutritional and colourimetric reporter genes. Putative interactors represented by a single clone are arranged in the same manner.

**Table 3.11.** Activation of nutritional and colourimetric reporter genes by prey-C1A<sub>1</sub>A<sub>2</sub>A<sub>3</sub>C2 interaction. Tabulated are representative scoring of the 437 clones that activated the *HIS3* reporter gene, 225 clones that activated the *ADE2* reporter gene and 139 clones that were able to activate the *MEL1* reporter gene.

**Table 3.12.** Interaction of C1A<sub>1</sub>A<sub>2</sub>A<sub>3</sub>C2 preys with heterologous baits in specificity tests. Tabulated are representative scores of the 139 clones that were screened.

**Table 3.13.** Identification of the sixteen C1A<sub>1</sub>A<sub>2</sub>A<sub>3</sub>C2 putative interactor clones from the Y2H cardiac cDNA library screen. Putative interactors represented by multiple clones are shown first, arranged from highest to lowest activators of nutritional and colourimetric reporter genes. Putative interactors represented by a single clone are arranged in the same manner.

**Table 3.14.** Summary of clones screened by Y2H

**Table 3.15.** Y2H direct protein-protein interaction assay investigating bait:prey interactions between the C1C2 phosphorylation mimics and the effect of domain C0, using C0C2 phosphorylation mimics.

**Table 3.16.** Predicted molecular weights and approximate molecular weights of fusion proteins used in the co-immunoprecipitation analysis.

**Table 3.17.** Correlation of data between Y2H direct protein-protein interactions and Co-IP\*.

# CHAPTER ONE: INTRODUCTION

INDEX	PAGE
<b>1. THE SARCOMERE</b>	<b>4</b>
<b>1.1 THIN FILAMENTS AND I-BAND COMPONENTS</b>	<b>5</b>
<b>1.1.1 Actin</b>	<b>5</b>
<b>1.1.2 Tropomyosin</b>	<b>6</b>
<b>1.1.3 The troponins</b>	<b>7</b>
<b>1.1.3.1 Troponin C</b>	<b>7</b>
<b>1.1.3.2 Troponin I</b>	<b>7</b>
<b>1.1.3.3 Troponin T</b>	<b>8</b>
<b>1.1.4 CapZ and Tropomodulin</b>	<b>9</b>
<b>1.2 NEBULIN AND NEBULETTE</b>	<b>9</b>
<b>1.3 THICK FILAMENTS AND A-BAND COMPONENTS</b>	<b>10</b>
<b>1.3.1 Myosin</b>	<b>10</b>
<b>1.3.2 The myosin light chains (MLC)</b>	<b>11</b>
<b>1.3.3 Thick Filament-Associated Proteins</b>	<b>12</b>
<b>1.3.3.1 Myosin-Binding Proteins C and H (MyBPC and MyBPH)</b>	<b>12</b>
<b>1.3.3.2 Adenosine Monophosphate Deaminase (AMP-Deaminase)</b>	<b>12</b>
<b>1.4 THE M-LINE</b>	<b>12</b>
<b>1.4.1 Myomesin and M-protein</b>	<b>12</b>
<b>1.4.2 Creatine Kinase and Enolase</b>	<b>13</b>
<b>1.4.3 Muscle-specific RING finger proteins (MURF)</b>	<b>13</b>
<b>1.4.4 Muscle-Specific Calpain 3/p94</b>	<b>13</b>
<b>1.5 THE Z-DISC</b>	<b>13</b>
<b>1.5.1 <math>\alpha</math>-Actinin 2</b>	<b>14</b>
<b>1.5.2 Zyxin</b>	<b>14</b>
<b>1.5.3 Muscle LIM Protein (MLP)</b>	<b>15</b>
<b>1.5.4 The ALP-Enigma Family</b>	<b>15</b>
<b>1.5.5 FHL protein family</b>	<b>16</b>
<b>1.5.6 The Calsarcin Family</b>	<b>16</b>
<b>1.5.7 Palladin–myotilin–myopalladin family</b>	<b>16</b>
<b>1.5.8 Filamin</b>	<b>16</b>
<b>1.5.9 Telethonin/T-Cap</b>	<b>16</b>
<b>1.5.10 Obscurin</b>	<b>17</b>
<b>1.5.11 Phosphodiesterase 5A</b>	<b>17</b>
<b>1.6 TITIN</b>	<b>17</b>
<b>1.6.1 Z-Disc Titin</b>	<b>18</b>
<b>1.6.2 I-Band Titin</b>	<b>18</b>

1.6.3 A-Band Titin	19
1.6.4 M-Line Titin	19
<b>1.7 SARCOMERIC DEVELOPMENT AND MAINTENANCE</b>	<b>19</b>
1.7.1 Sarcomerogenesis	19
1.7.1.1 Premyofibril model	20
1.7.2 Sarcomeric protein integration and exchange	21
1.7.3 Sarcomeric protein degradation	21
1.7.3.1 The ubiquitin-proteasome system (UPS)	21
<b>1.8 CARDIAC CONTRACTION</b>	<b>23</b>
1.8.1 The crossbridge cycle	24
<b>1.9 MODULATION OF CARDIAC CONTRACTILITY</b>	<b>24</b>
1.9.1 Role of $\text{Ca}^{2+}$ in the regulation of cardiac contractility	25
1.9.2 Regulation by the troponin-tropomyosin complex	26
1.9.3 Adrenergic stimulation and contractile protein phosphorylation	27
1.9.3.1 REGULATORY MYOSIN LIGHT CHAIN (RLC)	28
1.9.3.1.1 Phosphorylation of RLC	28
1.9.3.1.2 Effect of RLC phosphorylation	29
1.9.3.1.2.1 Conformational changes and effect on thick filament	29
1.9.3.1.2.2 ATPase	30
1.9.3.1.2.3 Force and $\text{Ca}^{2+}$ -sensitivity	30
1.9.3.1.2.4 Cardiac function and myofibrillogenesis	31
1.9.3.1.2.5 Stretch activation	32
1.9.3.2 TITIN	32
1.9.3.2.1 Phosphorylation of I-band Titin	32
1.9.3.2.2 Titin kinase	33
1.9.3.2.2.1 Function of TK	34
1.9.3.3 PHOSPHOLAMBAN	35
1.9.3.3.1 Phosphorylation of phospholamban	37
1.9.3.3.2 Regulation of basal myocardial contractility by PLB	37
1.9.3.4 TROPONINS	38
1.9.3.4.1 Cardiac Troponin I (cTNI)	38
1.9.3.4.1.1 Phosphorylation by PKA	39
1.9.3.4.1.2 Effect of PKA phosphorylation	40
1.9.3.4.1.3 Phosphorylation by PKC	41
1.9.3.4.1.4 Effect of PKC phosphorylation	42
1.9.3.4.2 Cardiac Troponin T (cTNT)	42
1.9.3.4.2.1 Phosphorylation by PKC	42

<b>1.9.3.5 CARDIAC MYOSIN-BINDING PROTEIN C</b>	<b>43</b>
<b>1.9.3.5.1 Structure</b>	<b>43</b>
<b>1.9.3.5.2 Isoforms</b>	<b>44</b>
<b>1.9.3.5.3 Other MyBPC'S</b>	<b>44</b>
<b>1.9.3.5.4 Models of Arrangement</b>	<b>44</b>
<b>1.9.3.5.5 N-Terminus Region (Domains C0C2)</b>	<b>46</b>
<b>1.9.3.5.5.1 Domain C0 and C0C1 linker</b>	<b>46</b>
<b>1.9.3.5.5.2 Domain C1-cMyBPC motif-C2</b>	<b>47</b>
<b>1.9.3.5.6 Central Domains (C3C6)</b>	<b>48</b>
<b>1.9.3.5.6.1 Domains C3 and C4</b>	<b>48</b>
<b>1.9.3.5.6.2 Domain C5</b>	<b>48</b>
<b>1.9.3.5.6.3 Domain C6</b>	<b>48</b>
<b>1.9.3.5.7 C-Terminus Domains (C7C10)</b>	<b>48</b>
<b>1.9.3.5.7.1 Domain C7</b>	<b>49</b>
<b>1.9.3.5.7.2 Domain C8</b>	<b>49</b>
<b>1.9.3.5.7.3 Domain C9</b>	<b>49</b>
<b>1.9.3.5.7.4 Domain C10</b>	<b>49</b>
<b>1.9.3.5.8 C-terminus versus N-terminus</b>	<b>49</b>
<b>1.9.3.5.9 Interactions with Myosin</b>	<b>49</b>
<b>1.9.3.5.9.1 Myosin S2 and cMyBPC</b>	<b>50</b>
<b>1.9.3.5.9.2 Phosphorylation of cMyBPC motif</b>	<b>50</b>
<b>1.9.3.5.9.3 Other myosin interactions with cMyBPC</b>	<b>51</b>
<b>1.9.3.5.10 Interaction with Actin</b>	<b>52</b>
<b>1.9.3.5.11 Function of cMyBPC</b>	<b>54</b>
<b>1.9.3.5.11.1 Thick filament stability and cardiac function</b>	<b>54</b>
<b>1.9.3.5.11.2 Structure of the thick filament and effect on crossbridges</b>	<b>59</b>
<b>1.9.3.5.11.3 Actomyosin ATPase Activity</b>	<b>61</b>
<b>1.9.3.5.11.4 Effect on force and kinetics of force Production</b>	<b>61</b>
<b>1.9.3.5.11.5 Effect on <math>\text{Ca}^{2+}</math>-sensitivity</b>	<b>64</b>
<b>1.9.3.5.11.6 cMyBPC as an internal load</b>	<b>66</b>
<b>1.10 CARDIOMYOPATHY</b>	<b>67</b>
<b>1.10.1 Hypertrophic Cardiomyopathy</b>	<b>67</b>
<b>1.10.2 Dilated Cardiomyopathy</b>	<b>67</b>
<b>1.11 IN THE PRESENT STUDY</b>	<b>68</b>

# CHAPTER ONE: INTRODUCTION

Contraction of muscle underlies all movement, and indeed life itself, in higher organisms. Striated muscle, viz. cardiac and skeletal muscle, is characterised by the precise organisation of the contractile proteins into striated myofibrils. The myofibrils are, in turn, made up of a repeated unit known as the sarcomere. The mammalian sarcomere is  $2\mu\text{m}$  in length and can shorten to  $\sim 70\%$  of its original length during contraction (Au, 2004). Over recent years, the sarcomere has been shown to be more complex than previously envisaged, being redefined as a dynamic network of proteins capable not only of generating force, but of signalling with other cellular compartments and interaction with metabolic enzymes, and capable of controlling many facets of striated muscle biology (Boateng and Goldspink, 2008). Understanding the intricate interplay of components of the sarcomere is vital for understanding the process and regulation of contraction in striated muscle in health and disease. The focus of this thesis is on one particular striated muscle protein, cardiac myosin-binding protein C (cMyBPC), which plays an integral role in sarcomeric structure and regulation of contraction. This study has identified a number of novel putative interactors of the N-terminus of cMyBPC, by means of yeast two-hybrid (Y2H) analysis. In order to provide context for interpretation of the results of this study, the following chapter will briefly describe the known and lesser-known components of the sarcomere, striated muscle contraction and its regulation before focussing on a few cardiac phosphoproteins which play a role in the regulation of cardiac contractility.

## 1. THE SARCOMERE

The sarcomere is the functional unit of muscle contraction in both skeletal and cardiac muscle. The sarcomere is divided into four major compartments: the Z-disc/Z-line, I-band, A-band and M-line, with one sarcomere being defined as the region between two Z-discs (Laing and Nowak, 2005) (Figure 1.1). The I-band contains the Z-disc and thin filaments. The A-band comprises the area where thin filaments overlap with myosin-containing thick filaments (C-zone), an area of thick filaments only (H-zone) as well as the M-line. The area of overlap between the A-band and the I-band is known as the D-zone while the P-zone is the area of overlap between the A-band and the M-line. Besides the thick and thin filaments, the sarcomere contains a third filament system, which is made up of single molecules of titin spanning half-sarcomeres from M-line to Z-disc. Another giant protein, nebulin, spans the length of the actin filaments and forms the fourth filament system in skeletal muscle (Clarke *et al.*, 2002). Nebulin was thought to be expressed exclusively in skeletal muscle, but recent data showed the presence of nebulin isoforms in cardiac muscle too (Panaviene *et al.*, 2007). It is important to note that in vertebrate striated muscle, the ultrastructure and molecular composition of the sarcomeres are remarkably similar; however, despite this apparent uniformity, there is a high degree of molecular variability due to the existence of multiple isoforms of each myofibrillar component. This chapter will mainly describe myofibrillar protein isoforms present in cardiac muscle, although some reference will be made to the skeletal isoforms. The latter will be described as a single entity, although it is important to note that, even within skeletal muscle, isoforms differ according to fibre type.

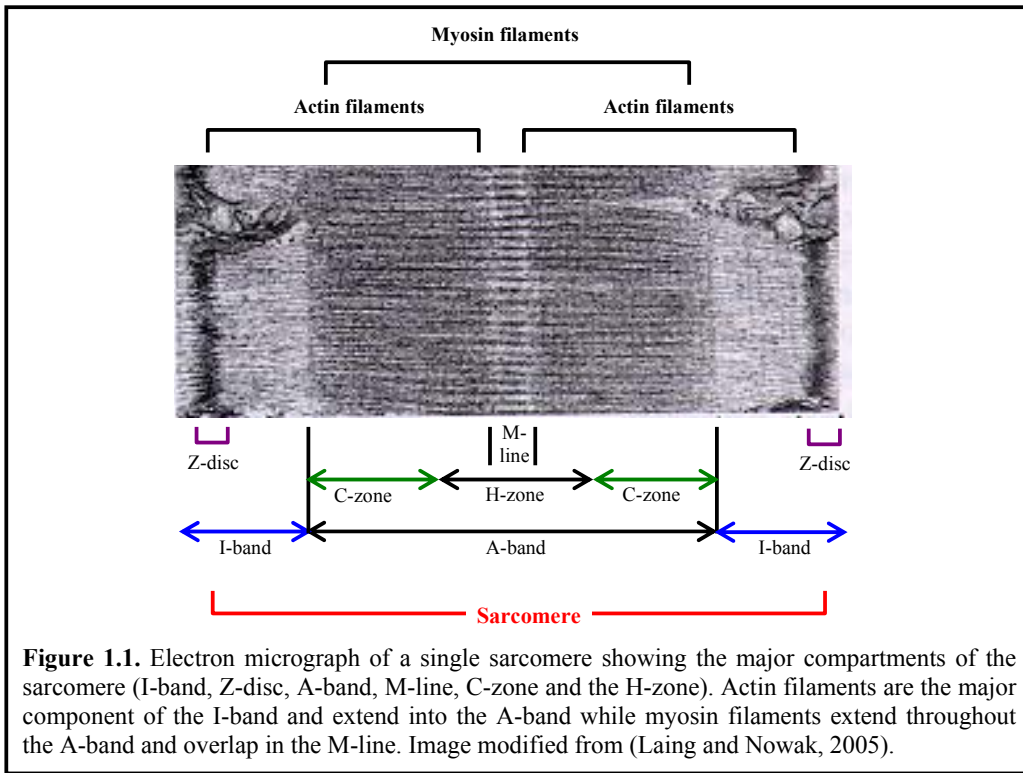


**Figure 1.1.** Electron micrograph of a single sarcomere showing the major compartments of the sarcomere (I-band, Z-disc, A-band, M-line, C-zone and the H-zone). Actin filaments are the major component of the I-band and extend into the A-band while myosin filaments extend throughout the A-band and overlap in the M-line. Image modified from (Laing and Nowak, 2005).

## 1.1 THIN FILAMENTS AND I-BAND COMPONENTS

The thin filament is composed primarily of actin (Section 1.1.1), which is anchored in the Z-disc, spans the I-band, and interdigitates with thick filaments in the A-band. Present along the length of the actin filaments are actin-associated proteins such as the troponins (Section 1.1.3), nebulin/nebulette (Section 1.2) and tropomyosin (Section 1.1.2), while at the pointed and barbed ends of the actin filaments tropomodulin and CapZ (Section 1.1.4) are present, respectively. In addition, this part of the sarcomere contains a segment of titin, (I-band titin; Section 1.6.2) which has elastic modules that function as a molecular spring for the reversible, mechanical stretch response required for efficient contractile activity. Further, the I-band functions to link the region of active force generation (the A-band) with the bordering Z-discs (Clarke *et al.*, 2002).

### 1.1.1 Actin

Actin is a ubiquitous molecule that plays a fundamental role in diverse cellular processes such as muscle contraction, maintenance of the cytoskeleton, cell motility and cytokinesis (dos Remedios *et al.*, 2003). In higher vertebrates, six actin isoforms are recognised:  $\alpha$ -cardiac (ACTC1),  $\alpha$ -skeletal (ACTA1),  $\gamma$ -smooth muscle (ACTG2),  $\alpha$ -smooth muscle (ACTA2),  $\gamma$ -cytoplasmic isoactin (ACTG1) and  $\beta$ -cytoplasmic (ACTB). The expression of these isoforms is developmentally regulated in a temporal and tissue-specific manner. The cytoplasmic actins (ACTG1 and ACTB) are ubiquitously expressed in all cell types and throughout development, while the other actin isoforms are expressed specifically in striated (ACTA1 and ACTC1) and smooth muscle (ACTG2 and ACTA2). Cardiac  $\alpha$ -actin is the main actin isoform in the adult heart although skeletal  $\alpha$ -actin is also present (Bertola *et al.*, 2008).

Actin is expressed as a globular monomer (globular actin or G-actin), which polymerises, in an ATP-dependent reaction, to form fibres (F-actin) with a double helical structure (Figure 1.2). The atomic structure of G-actin shows that actin monomers have four domains: subdomains one and two have been named the “small domain”, while subdomains three and four form the “large domain” (Clarke *et al.*, 2002). A cleft flanking the “large domains” houses the sites for nucleotide-binding and divalent ion-binding. Subdomains one and three form the “barbed ends”, while subdomains two and four form the “pointed ends”. Subdomain one binds to and activates the myosin head upon their association (dos Remedios *et al.*, 2003). The motor activity of the myosin heads then moves the thin filaments past the thick filaments, resulting in muscle contraction, which is described in section 1.8.

### 1.1.2 Tropomyosin

Tropomyosin (TM; ~37 kDa) comprises two  $\alpha$ -helical chains organised as a coiled-coil rod that associates with actin filaments in nearly all eukaryotic cells (Figure 1.2). In striated muscle cells, TM has multiple isoforms ( $\alpha$ -TM,  $\beta$ -TM and the slow twitch fiber  $\alpha$ -TM) which are encoded by different genes (Gunning *et al.*, 2008). TM forms homodimers or heterodimers that associate head-to-tail to create parallel coils that span the length of the actin filaments. All TM dimers extend along seven actin monomers. The interaction of TM along each of the two grooves of the thin filament is highly co-operative and occurs in a head-to-tail manner. The TM-binding site on actin is approximately the same site as that for myosin; hence TM interferes with the actin/myosin interaction (Gunning *et al.*, 2008). The principal role of the TM dimer is to work jointly with the troponin complex (in a 1:1 ratio) (Section 1.1.3) in regulating muscle contraction, which involves a  $\text{Ca}^{2+}$ - and troponin-mediated conformational rearrangement of TM on the thin filament (described in Section 1.9.1). In addition, TM stabilises the thin filament by increasing its stiffness, inhibiting its fragmentation and slowing depolymerisation and polymerisation at the pointed ends where TM interacts with tropomodulin (Weigt *et al.*, 1990) (Section 1.1.4).

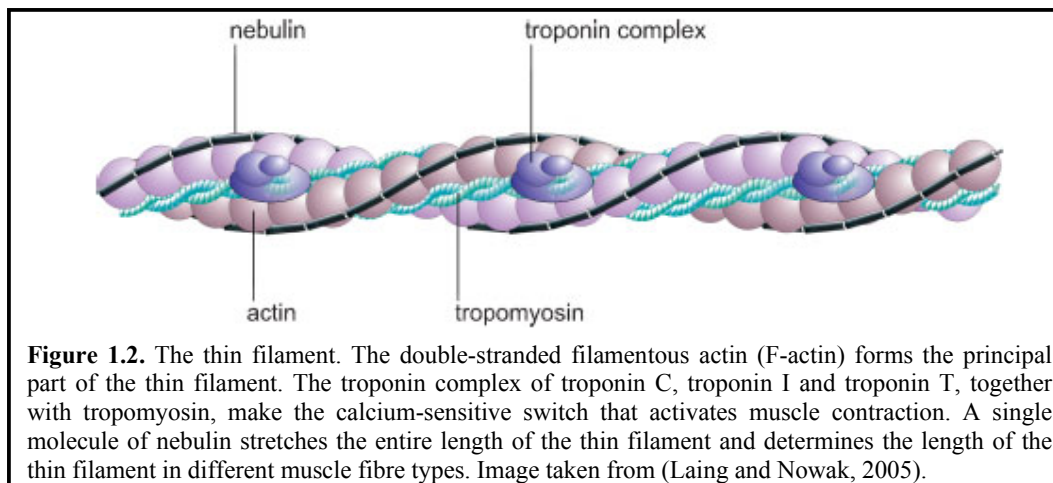


**Figure 1.2.** The thin filament. The double-stranded filamentous actin (F-actin) forms the principal part of the thin filament. The troponin complex of troponin C, troponin I and troponin T, together with tropomyosin, make the calcium-sensitive switch that activates muscle contraction. A single molecule of nebulin stretches the entire length of the thin filament and determines the length of the thin filament in different muscle fibre types. Image taken from (Laing and Nowak, 2005).

### 1.1.3 The troponins

The troponin (Tn) complex is composed of three proteins: the calcium ( $\text{Ca}^{2+}$ )-binding subunit, troponin C (TNC), the inhibitory subunit, troponin I (TNI), and the tropomyosin-binding subunit, troponin T (TNT). This complex interacts with actin (in a 1:7 ratio) and TM to modulate force generation. The Tn subunits are expressed as a number of isoforms whose expression patterns differ during development and among fiber types, and they contribute to the distinct contractile properties of striated muscle (Westfall and Metzger, 2001).

#### 1.1.3.1 Troponin C

There are two isoforms of TNC in striated muscle, encoded by two different genes; one encoding the skeletal isoform (sTNC) and the other the cardiac (cTNC)/slow skeletal (ssTNC) isoform (Tobacman, 1996). TNC (~18 kDa) is a dumbbell shaped protein with two globular heads (N-terminus and C-terminus domains) connected by a long central helix (Figure 1.3). Each globular head has two  $\text{Ca}^{2+}$ -binding sites; sites I/II are located on the N-terminus, while sites III/IV are located on the C-terminus (Clarke *et al.*, 2002). The N-terminus of cTNC/ssTNC has a single functional regulatory  $\text{Ca}^{2+}$ -binding site (site II), which triggers contraction, whereas fast skeletal TNC has two sites (site I and II). The functional consequence of this difference is described in section 1.9.2.

#### 1.1.3.2 Troponin I

There are three closely related TNI genes, selectively expressed in cardiac (cTNI), fast skeletal (fsTNI) or slow skeletal (ssTNI) muscle. Human cTNI is a rod-like and flexible protein that can be divided into six distinct structural segments: the N-terminus cardiac-specific extension (cTNI<sub>1-30</sub>), the IT-arm region (cTNI<sub>34-136</sub>), the inhibitory region (cTNI<sub>128-147</sub>), the switch or triggering region (cTNI<sub>147-163</sub>), and the C-terminus region (cTNI<sub>164-210</sub>) (Li *et al.*, 2004; Solaro *et al.*, 2008) (Figure 1.3).

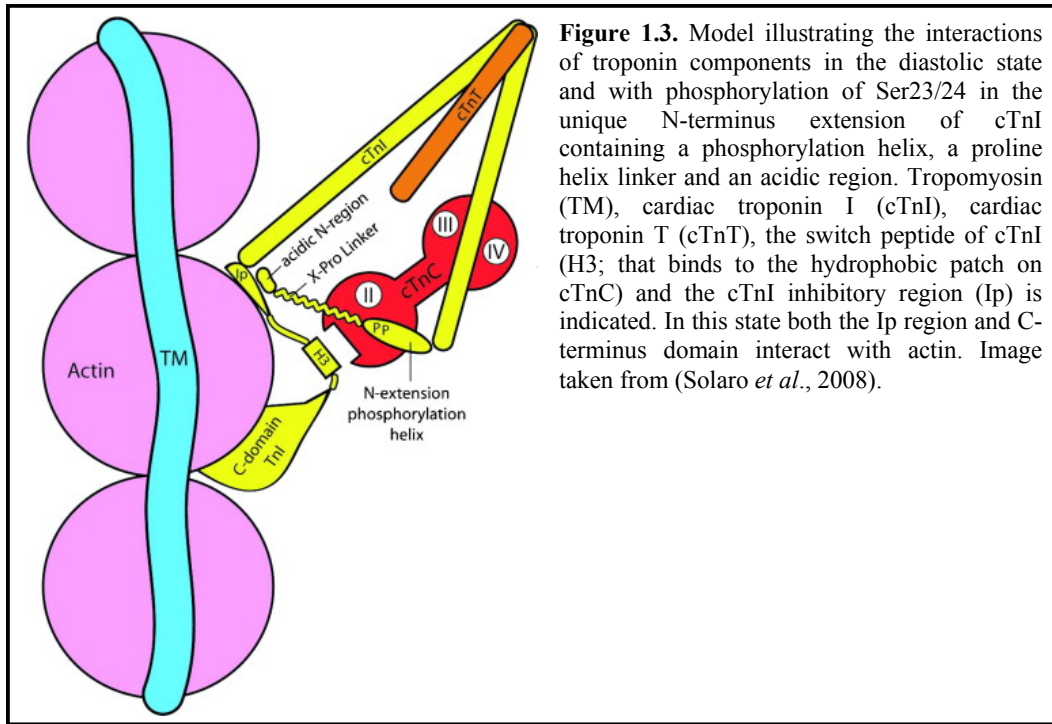
##### *N-terminus cardiac specific region*

This region comprises an acidic N-terminus segment, an extended rigid polyproline helix (residues 11-19), and a C-terminus helix (residues 21-30) containing serial serine (Ser) residues at positions 23 and 24, which are substrates for protein kinase A (PKA) (Howarth *et al.*, 2007). In the unphosphorylated state, N-terminus cTNI (NcTNI) interacts with cTNC's inactive  $\text{Ca}^{2+}$ -binding site I, largely through a series of weak electrostatic and hydrophobic interactions such that the acidic N-terminus region does not strongly contact cTNC (Abbott *et al.*, 2001). The effect of protein kinase phosphorylation on cTNI is described in section 1.9.3.4.1.

##### *IT-arm region*

The IT-arm binds to the C-terminus of cTNC in a  $\text{Ca}^{2+}$ -dependent manner, anchoring cTNC to the thin filament and giving rise to an anti-parallel arrangement of the TNI-TNC complex (Kleerekoper *et al.*, 1995). This region also binds to TNT and the location of these binding sites provides for transfer of a

conformational signal induced by binding of  $\text{Ca}^{2+}$  to TNC, through TNI, to TNT and tropomyosin. Physiological regulation of the interactions of this region with the rest of the thin filament appears to be accomplished by protein kinase C (PKC) phosphorylation at residues Ser43/45 (Filatov *et al.*, 1999).



### Inhibitory region

This region contains a highly basic stretch of amino acids that binds either to actin-TM or  $\text{Ca}^{2+}$ -TNC, thus forming a key part of the molecular switch responsible for turning on the thin filament and is thus referred to as the inhibitory region (Solaro *et al.*, 2008) (Figure 1.3). A PKC-sensitive phosphorylation site at Thr144 is also present (Section 1.9.3.4.1.3).

### Switch region and C-terminus region

The switch region and the C-terminus mobile domain undergo disordered-ordered structural transitions depending on the  $\text{Ca}^{2+}$ -bound state of the regulatory  $\text{Ca}^{2+}$ -binding site in the N-terminus of cTNC (NcTNC) (Solaro *et al.*, 2008). In the resting state (diastole), the inhibitory region and the second actin-binding site in the C-terminus mobile domain interact with actin to prevent strong, force generating reactions with the myosin head (Figure 1.3). Upon  $\text{Ca}^{2+}$ -binding to the NcTNC regulatory site, the switch region of cTNI binds to a newly exposed hydrophobic patch on NcTNC, releasing both the inhibitory region and the second actin-binding site (C-terminus) from actin (Li *et al.*, 1999) allowing actomyosin interaction (Section 1.8).

#### 1.1.3.3 Troponin T

TNT (~37-39 kDa) exists as three different isoforms that are unique in structure; one each for slow skeletal, fast skeletal and cardiac muscle, which are encoded by three different genes (Li *et al.*, 2004). TNI and TNC

bind to TNT at its globular C-terminus, while the binding site for TM and actin is on its extended N-terminus (Chen *et al.*, 1997). In the absence of  $\text{Ca}^{2+}$ , the troponin-TM complex is fixed on actin through TNI. In the presence of  $\text{Ca}^{2+}$ , when the contacts between TNI and actin become weak, TNT plays a crucial role in fixing of the whole troponin complex on the actin filament (Filatov *et al.*, 1999). The addition of TNT to the TNI-TNC complex provides for deeper inhibition of actomyosin ATPase in the absence of  $\text{Ca}^{2+}$  and adds to the activation of actomyosin ATPase activity in the presence of  $\text{Ca}^{2+}$ ; thus TNT also plays an important role in the regulation of actomyosin ATPase activity (Filatov *et al.*, 1999). TNT also has sites for PKC phosphorylation (Section 1.9.3.4.2).

#### 1.1.4 CapZ and Tropomodulin

CapZ and tropomodulin play key roles in the assembly and maintenance of thin filaments. In striated muscle, CapZ is a dimer composed of  $\alpha$  (~36 kDa) and  $\beta$  (~32 kDa) subunits, which are both required for capping at the barbed end of actin where it is involved in the nucleation and stabilisation of actin filaments. CapZ also interacts with  $\alpha$ -actinin to anchor the thin filament to the Z-disc (Frank *et al.*, 2006).

At the pointed end, actin dynamics and filament length are regulated by the tropomodulin (Tmod; ~40 kDa) family of proteins. Tmod1 (or E-Tmod), the predominant isoform in striated muscle, is expressed in embryonic and adult cardiac as well as slow skeletal muscle, while Tmod4 is expressed in fast skeletal muscle (Fritz-Six *et al.*, 2003). Tropomodulin has a relatively low affinity for actin, which is increased in the presence of TM. Therefore, the full capping activity of Tmod is dependent on its association with both actin and TM. The primary actin-binding region resides within the C-terminus while the N-terminus half of Tmod binds TM (Fowler *et al.*, 1993).

### 1.2 NEBULIN AND NEBULETTE

Nebulin (600–900 kDa) and nebulette (~107 kDa) are sarcomeric actin-binding proteins that interact with both the thin filaments and Z-discs of striated muscles. Nebulin was originally identified as one of the giant proteins in skeletal muscle and has been proposed to serve as a thin filament ruler for vertebrate striated muscles (Holmes and Moncman, 2008). The N-terminus of nebulin extends to the pointed ends of the thin filaments while its C-terminus is partially inserted into the Z-discs (McElhinny *et al.* 2001). Nebulin isoforms have also been identified in cardiac muscle where they may function to stabilise cytoskeletal linkages to the Z-disc by interacting with actin, desmin, CapZ and myopalladin (Panaviene *et al.*, 2007). Further, a cardiac-specific petite nebulin, nebulette, has been identified (Holmes and Moncman, 2008). The C-terminus region of nebulette is virtually identical to that of nebulin, while it has a unique N-terminus end. It has been proposed that nebulette's role in cardiac cells may be distinct to that of nebulin as it is considerably smaller than nebulin; there are also some differences between the spectrum of proteins that interact with nebulette (actin, myopalladin, filamin-C, Z-disc alternatively spliced PDZ-containing protein [ZASP], TM and  $\alpha$ -actinin) compared to those that interact with nebulin (Holmes and Moncman, 2008).

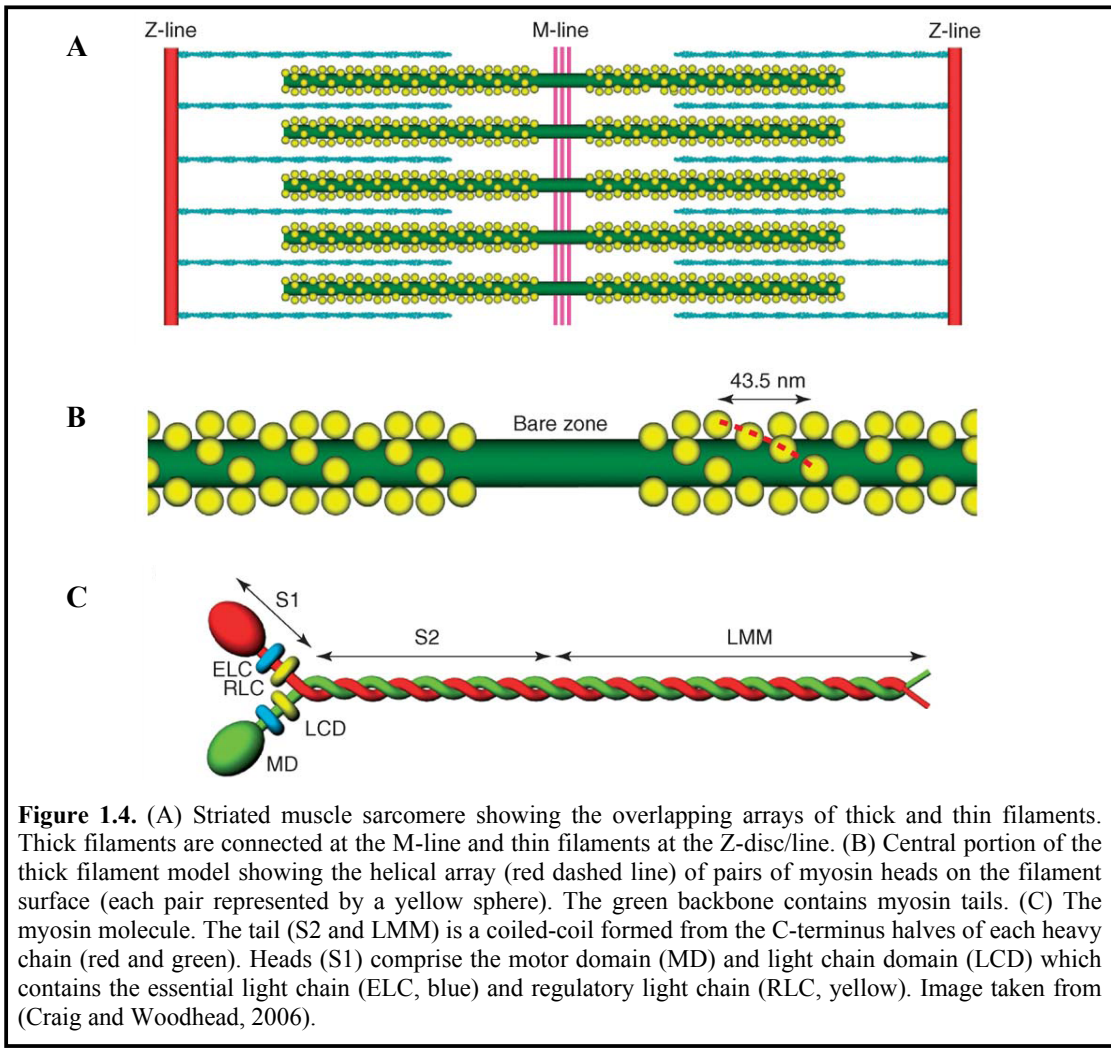
## 1.3 THICK FILAMENTS

The thick filaments (myosin and associated proteins) lie in a region towards the middle of the sarcomere called the A-band. Within this region, the pointed ends of the thin filaments interdigitate with the thick filaments and myosin crossbridges that extend from the thick filaments and cyclically interact with the thin filaments (Figure 1.4A). The crossbridges are located in C- and D-zones while the bare-zone contains the myosin tails (Figure 1.4B) that are anchored and aligned in the M-line (Section 1.4). The C-terminus portion (~2 kDa) of titin, spanning the A-band (Section 1.6.3) and M-line (Section 1.6.4), is widely accepted to act as a molecular blueprint that specifies the sarcomeric architecture of this region (Laing and Nowak, 2005).

### 1.3.1 Myosin

The thick filaments are composed primarily of myosin, which binds and hydrolyses ATP, interacts with actin and ultimately produces movement and force (Section 1.8). At least eight myosin heavy chains (MHC) have been identified in mammals, each encoded by a separate gene: MHCIIa, MHCIIx, and MHCIIb are found in fast skeletal muscle fibers; MHCexoc is expressed in extraocular muscle fibers; and MHCemb (embryonic) and MHCneo (neonatal) are expressed in muscle at different developmental stages. There are two cardiac MHC isoforms,  $\alpha$ -MHC and  $\beta$ -MHC, which are both expressed in a tissue-specific manner in the normal heart:  $\alpha$ -MHC is preferentially expressed in the atrium and  $\beta$ -MHC is almost exclusively expressed in the ventricle of larger mammals.  $\beta$ -MHC is also expressed in slow skeletal muscle (Schiaffino and Reggiani, 1996). Each myosin is basically a hexameric protein comprising two heavy chains (~220 kDa) and four light chains (MLC; ~20 kDa) (Figure 1.4C). Two of the light chains belong to the essential light chain (ELC; Section 1.3.2) family, while the other two, which contain sites suitable for phosphorylation, are referred to as the regulatory light chains (RLC; Section 1.3.2). The MLCs are proposed to fine tune myosin motor activity and augment the versatility of its kinetics (Schiaffino and Reggiani, 1996).

The myosin molecule is divided into two functional regions, the head and the rod (Figure 1.4C). The N-terminus portion of each MHC and two light chains (one of each type) comprise the myosin head domain (the S1 fragment) that makes up the crossbridges. The head domain, which forms the catalytic motor, includes the binding sites for nucleotides and actin (Rayment *et al.*, 1993a). The attachment site for the MLCs is referred to as the lever arm domain and is linked to the motor domain by a small converter region. The elongated rod portion of myosin is made up of the C-terminus regions of the two heavy chains and is referred to as light meromyosin (LMM), which contains coiled-coil domains implicated in myosin polymerisation at their very C-terminus ends. The proximal one third of the tail, which acts as a flexible link connecting the myosin heads to the thick filament core is referred to as subfragment 2 (myosin S2) (Craig and Woodhead, 2006).



### 1.3.2 The myosin light chains (MLC)

In striated muscle, the ELC has isoforms for fast skeletal, slow skeletal, ventricular and atrial muscle which are encoded by different genes (Hernandez *et al.*, 2007). While within the RLC family, isoforms for ventricular (RLC<sub>v</sub>), atrial (RLC<sub>a</sub>) and skeletal muscle are present. Together with calmodulin and troponin C, both types of MLCs belong to the EF-hand Ca<sup>2+</sup>-binding superfamily of proteins (Schiaffino and Reggiani, 1996). In striated muscle, the ELC binds to and stabilises the neck region of MHC closest to the head of the MHC (Figure 1.4C). In addition, it interacts with the C-terminus domain of actin, thus tethering MHC to actin. Relieving or weakening of the MHC/actin tether has been shown to accelerate crossbridge cycling kinetics and enhances tension output, thus increasing contractility (Hernandez *et al.*, 2007). The RLC binds to the neck further than the ELC from the head of MHC and can be phosphorylated by a MLC-specific kinase. The function of RLC, in addition to the consequences of its phosphorylation, in cardiac muscle is described in Section 1.9.3.1.

### **1.3.3 Thick Filament-Associated Proteins**

In addition to myosin, a number of other proteins have been recognised as part of the thick filament and M-line region of the sarcomere. Proteins in this region contain variable copies of fibronectin type III (FNIII) and immunoglobulin (Ig)-like domains and are implicated in thick filament assembly and regulation of muscle contraction (Agarkova *et al.*, 2003).

#### **1.3.3.1 Myosin-Binding Proteins C and H (MyBPC and MyBPH)**

MyBPC (~140 kDa) and MyBPH (~58 kDa) are myosin-binding proteins that are both localised to the C-zone of the thick filament (Oakley *et al.*, 2004). As the cardiac isoform of MyBPC is the subject of investigation in the present study, it, as well as its parologue MyBPH, is described in section 1.9.3.5.

#### **1.3.3.2 Adenosine Monophosphate Deaminase (AMP-Deaminase)**

AMP-deaminase is involved in the regulation of adenosine metabolism, as the sensor of a cell's changing energy requirements. Vigorous muscle contraction activates AMP-deaminase when large portions bind to the myofibril interacting with myosin S2 and A-band titin (Koretz *et al.*, 2003; Clarke *et al.*, 2002).

## **1.4 THE M-LINE**

The M-line region, located in the centre of the A-band (Figure 1.1), forms the anchoring site for the thick filaments and functions to stabilise the sarcomere, similar to the Z-disc. In this region, the myosin filaments are cross-linked by transverse, electron-dense M-bridges (likely composed of myomesin and M-protein [Section 1.4.1]), which function like spacers providing the optimal transverse distances between contractile filaments during contraction (Agarkova and Perriard, 2005). The C-terminus of titin also overlaps here (Section 1.6.4).

### **1.4.1 Myomesin and M-protein**

Myomesin (~185 kDa) is characterised by a unique N-terminus domain followed by 12 repeating FNIII and Ig domains organised as an antiparallel staggered dimer (Obermann *et al.*, 1996). The first N-terminus domain of myomesin interacts with LMM while FNIII domains (My4-6) interact with M-line titin, thus myomesin connects these filament systems. Myomesin also plays an important role in myofibrillogenesis by organising myosin during embryonic development (Obermann *et al.*, 1997).

M-protein (~165 kDa) contains 12 Ig and FNIII domains organised in an order identical to myomesin. The co-operative interaction of two N-terminus M-protein Ig domains is required for its interaction with LMM and is responsible for targeting M-protein to the M-line. M-protein may act together with myomesin and MyBPC to fix the thick filament components to titin in fast skeletal and cardiac muscle (Nave *et al.*, 1989).

#### **1.4.2 Creatine Kinase and Enolase**

Creatine kinase (~43 kDa) is an enzyme localised primarily at cellular sites of energy production and consumption (Au, 2004). It functions to catalyse a reversible phosphotransferase reaction between creatine and ATP that produces creatine phosphate and ADP (adenosine diphosphate). Fast regeneration of ATP from ADP is necessary at times of high energy demand, such as during prolonged muscle contraction (Au, 2004). There are muscle-, brain- and mitochondrial-specific isoforms of creatine kinase, of which the mitochondrial isoform is expressed ubiquitously and sarcomerically (Au, 2004). The brain- and muscle-specific isoforms cannot localise to the M-line but, a small portion (~5-10%) of the muscle-specific isoform is bound to the M-line where it may play a structural role (Clarke *et al.*, 2002). At the M-line, creatine kinase associates with  $\beta$ -enolase, a glycolytic enzyme, which can also localise to the Z-disc and may too be involved with local ATP production (Foucault *et al.*, 1999)

#### **1.4.3 Muscle-specific RING finger proteins (MURF)**

MURF1 and its closely related members, MURF2 and MURF3, are expressed in cardiac and skeletal muscle (Hoshijima, 2006). MURF proteins (~40 kDa) are characterised by an N-terminus RING finger domain, a MFC (MURF family conserved) domain, a B-box domain, leucine-rich coiled-coil domains, and an acidic C-terminus. MURF1 is a myofibrillar protein that interacts with M-line titin, close to the kinase domain (Section 1.9.3.2.2). In this region, MURF1 may play a regulatory role in the maintenance and turnover of myofibrils (Powell, 2006). MURF2 is thought to act as a link between microtubule-associated MURF3 and MURF1, as MURF2 localises to both the M-line region of titin and to microtubules. MURF3 stabilises microtubules in the presence of depolymerising agents. The MURFs have been implicated in various cellular functions, including ubiquitination, signalling and transcription (Gotthardt *et al.*, 2003). Consistently, multiple MURF-interacting proteins have been identified, which include the serum response factor (SRF), glucocorticoid modulatory element-binding protein 1, PKC-adaptor RACK1, cardiac and skeletal TNI, TNT, nebulin, MLC, myotilin, T-cap and a series of enzymes that are related to energy metabolism (Hoshijima, 2006). These proteins do not necessarily interact with the MURFs simultaneously but perhaps consecutively.

#### **1.4.4 Muscle-Specific Calpain 3/p94**

Calpain 3/p94 is a striated muscle-specific, non-lysosomal  $\text{Ca}^{2+}$ -dependent, intracellular cysteine protease, which modulates cellular function by limited and specific proteolysis. Calpain 3 binds near titin's C-terminus and within the titin N2A element in skeletal muscle and N2BA element in cardiac muscle, implicating a role for titin in protein turnover (Granzier and Labiet, 2002).

### **1.5 THE Z-DISC**

Thin filaments, titin, and nebulin filaments are anchored in the Z-disc, making it the primary conduit of force generated by contraction (Clarke *et al.*, 2002). Z-discs are attached to the sarcolemma and to the extracellular matrix at specific sites called costameres. At these sites, Z-disc-associated linker molecules connect the sarcomere with two transmembrane adhesion molecule complexes, the dystroglycan-sarcoglycan complex

and the integrin receptor complex (Epstein and Davis, 2003). The major component of the Z-disc is the muscle-specific  $\alpha$ -actinin 2, which is able to bind many different proteins (Figure 1.5). Thus, the Z-disc is a complex protein network made up of numerous structural as well as signal transduction components; functioning as a biomechanical sensor that can react to variation in tension at the sarcolemma. Further, the Z-disc maintains muscle homeostasis and plays an important role during sarcomerogenesis (Clarke *et al.*, 2002) (Section 1.7.1.4).

### 1.5.1 $\alpha$ -Actinin 2

$\alpha$ -Actinin 2 (~97 kDa) is a member of the spectrin superfamily, of which  $\alpha$ -spectrin,  $\beta$ -spectrin and dystrophin are members. There are four  $\alpha$ -actinin isoforms, encoded by separate genes:  $\alpha$ -Actinin 1 and -4 are non-muscle isoforms involved in actin filament bundling and attach to cellular membranes.  $\alpha$ -Actinin 2 and -3 are both present in striated muscle;  $\alpha$ -actinin 3 expression is restricted largely to fast skeletal muscle fibres where some of its variants may enhance athletes' performance in sprint-type activities (MacArthur and North, 2004). Only  $\alpha$ -actinin 2 is expressed in cardiac muscle (Clarke *et al.*, 2002).

$\alpha$ -actinin 2 is characterised by an actin-binding domain on the N-terminus, a central rod domain composed of four spectrin-repeats, and a C-terminus domain with similarity to calmodulin. The rod domains of  $\alpha$ -actinin monomers are arranged to form antiparallel dimers that cross-link titin and actin filaments from adjacent sarcomeres (Djinovic-Carugo *et al.*, 1999).

Aside from its interaction with actin filaments,  $\alpha$ -actinin has emerged as a major multivalent platform for a number of protein-protein interactions, which can occur simultaneously due to its modular nature. The globular N-terminus domain binds zyxin (Section 1.5.2) and the cysteine-rich protein (CRP) family members (Section 1.5.3), while the central four spectrin repeats bind calsarcins (Section 1.5.6),  $\alpha$ -actinin-associated LIM proteins (ALP) (Section 1.5.4), myotilin (Section 1.5.7) and titin (Section 1.6.1). Other interactions that have been mapped to the C-terminus of  $\alpha$ -actinin include those with cypher/ZASP/oracle (Section 1.5.4) and myopalladin (Section 1.5.8). Together, these protein interactions may provide tensile integrity to the Z-disc and also serve as additional docking sites for other Z-disc-associated proteins (Frank *et al.*, 2006) (Figure 1.5).

### 1.5.2 Zyxin

Zyxin is a cytoskeletal protein that plays an important role in the organisation of actin filaments at focal adhesion sites by making multiple contacts with structural and regulatory proteins such as  $\alpha$ -actinin and cysteine-rich cytoskeletal protein (CRP) (Li and Trueb, 2001). Zyxin can also shuttle between the nucleus and cytoplasm and is therefore a candidate to mediate signals between the two compartments (Crawford *et al.*, 1992).

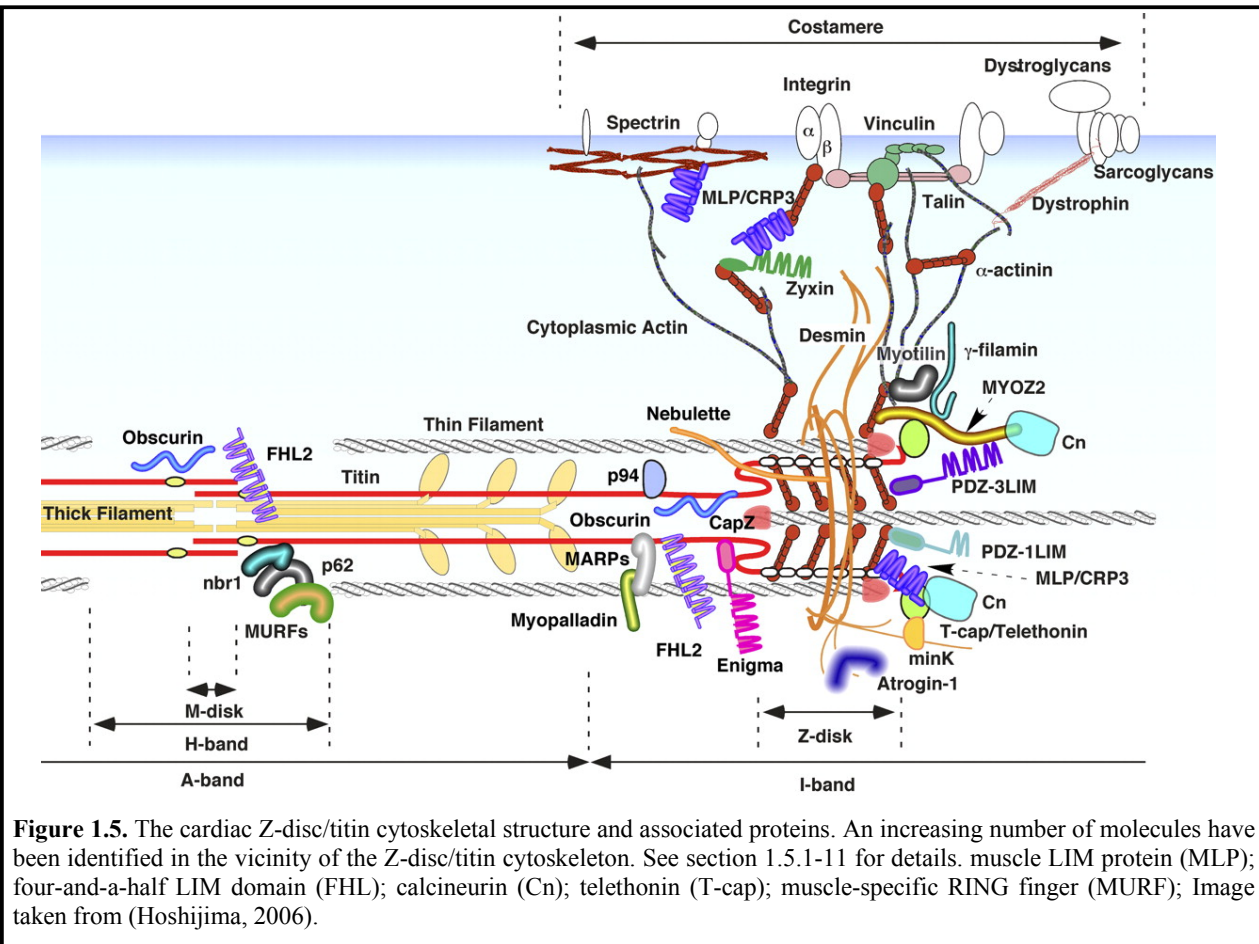


**Figure 1.5.** The cardiac Z-disc/titin cytoskeletal structure and associated proteins. An increasing number of molecules have been identified in the vicinity of the Z-disc/titin cytoskeleton. See section 1.5.1-11 for details. muscle LIM protein (MLP); four-and-a-half LIM domain (FHL); calcineurin (Cn); telethonin (T-cap); muscle-specific RING finger (MURF); Image taken from (Hoshijima, 2006).

### 1.5.3 Muscle LIM Protein (MLP)

MLP (~23 kDa), the striated muscle-specific CRP, localises to the Z-disc and the intercalated disc in both embryonic and adult muscle (Arber *et al.*, 1997). This protein comprises two LIM domains, the first of which interacts with  $\alpha$ -actinin. Additionally, T-cap, zyxin, calcineurin and  $\beta$ -spectrin have been identified as MLP-interactors, supporting its role as a scaffold or linker protein, stabilising the Z-disc (Arber *et al.*, 1997). However, upon hypertrophic stimulation MLP can also translocate from the Z-disc to the nucleus where it interacts with muscle transcriptional regulators (Hoshijima, 2006).

### 1.5.4 The ALP-Enigma Family

The cytoskeletal ALP ( $\alpha$ -actinin-associated LIM protein)-enigma family is characterised by an N-terminus PDZ domain and one/three C-terminus LIM domains. Members of this family, including enigma (~55 kDa), ALP (~36 kDa), and cypher/ZASP/oracle (~77 kDa), are expressed in striated muscle and localise to the Z-disc (Clarke *et al.*, 2002). The N-terminus PDZ domain of these proteins interact with  $\alpha$ -actinin, except enigma, which binds TM. Additionally, enigma and cypher interact with PKC isoforms, while cypher is also linked to the phosphatase calcineurin by associating with members of the calsarcin family (Section 1.5.6) (Frey and Olson 2002). The ALP-enigma proteins may serve to anchor signalling molecules at the Z-disc.

### **1.5.5 FHL protein family**

The Four-and-a-half LIM (FHL) family of proteins constitute a family of 5 members: FHL1, FHL2, FHL3, FHL4 and ACT. FHL1-3 are expressed in striated muscles and localise predominantly to the Z-disc, while FHL4 and ACT are not expressed in striated muscle (Lange *et al.*, 2002). FHL2 also localises to the I-band and M-band of titin where it interacts with the N2B and is2 regions. FHL1-3 interacts with extracellular signalling-regulated kinase 2 (ERK2) and regulates hypertrophic signalling by inhibiting ERK2 nuclear translocation, in addition to participating in the regulation of cell survival (Johannssen *et al.*, 2006).

### **1.5.6 The Calsarcin Family**

The calcareins (calcineurin-associated sarcomeric protein) are a striated muscle-specific family of proteins, localised to the Z-disc. Calsarcin1-3 (~32 kDa) are composed of  $\alpha$ -helical domains on the N- and C-terminus, separated by a glycine-rich central domain (Clarke *et al.*, 2002). The myocardial-specific calsarcin 2 (also known as myozentin) interacts with filamin C,  $\alpha$ -actinin, cypher and telethonin, and may be responsible for anchoring calcineurin to the Z-disc. Calcineurin plays an important part in the initiation of hypertrophic signalling by activating NFAT3 (nuclear-factor-of activated-T-cells), a Z-disc-associated transcription factor, which subsequently translocates to the nucleus. Here, in co-operation with other transcription factors, they activate the pro-hypertrophic gene program (Olson and Williams, 2000).

### **1.5.7 Palladin–myotilin–myopalladin family**

Members of the palladin–myotilin–myopalladin family are important structural elements of the sarcomere Z-disc and are characterised by conserved Ig domains in the C-terminus part of the protein (Bang *et al.*, 2001). Myotilin (57 kDa) and myopalladin (~145 kDa) are mainly expressed in striated muscle, whereas palladin is widely expressed in mesenchymal and epithelial cells. All members of this family interact with  $\alpha$ -actinin; myotilin also binds actin, filamin C and the calcareins while myopalladin interacts with nebulin/nebulette and cardiac ankyrin-repeat protein (CARP; Bang *et al.*, 2001). Members of this family appear to have key roles in the dynamic molecular events mediating myofibril assembly and in the organisation and/or maintenance and integrity of the sarcomeres (Carlsson *et al.*, 2007).

### **1.5.8 Filamin**

The striated muscle-specific  $\gamma$ -filamin (~300 kDa) forms a family with  $\alpha$ - and  $\beta$ -filamin that comprises an N-terminus actin-binding domain followed by 24 Ig-like domains.  $\gamma$ -Filamin (also known as filamin 2 or filamin C) interacts with a number of proteins (such as  $\delta$ - and  $\gamma$ -sarcoglycan,  $\beta$ 1D-integrin, myotilin and the calcarein family) and may function as a crucial link connecting the cell membrane and the sarcomere (Frank *et al.*, 2006).

### **1.5.9 Telethonin/T-Cap**

Telethonin (19 kDa; also known as titin cap or T-cap) interacts with N-terminus titin domains (Z1-Z2) to anchor the giant protein to the Z-disc. It also serves to link titin to other Z-disc-associated proteins such as

the calsarcin family, MURF1, MURF2, potassium channel subunit minK and MLP (Linke, 2008). During development, T-cap transiently localises to the M-line where it is phosphorylated by the titin kinase region (located at the M-line) (Section 1.9.3.2.2) and perhaps plays a role in the assembly of M-line (Weinert *et al.*, 2006).

### 1.5.10 Obscurin

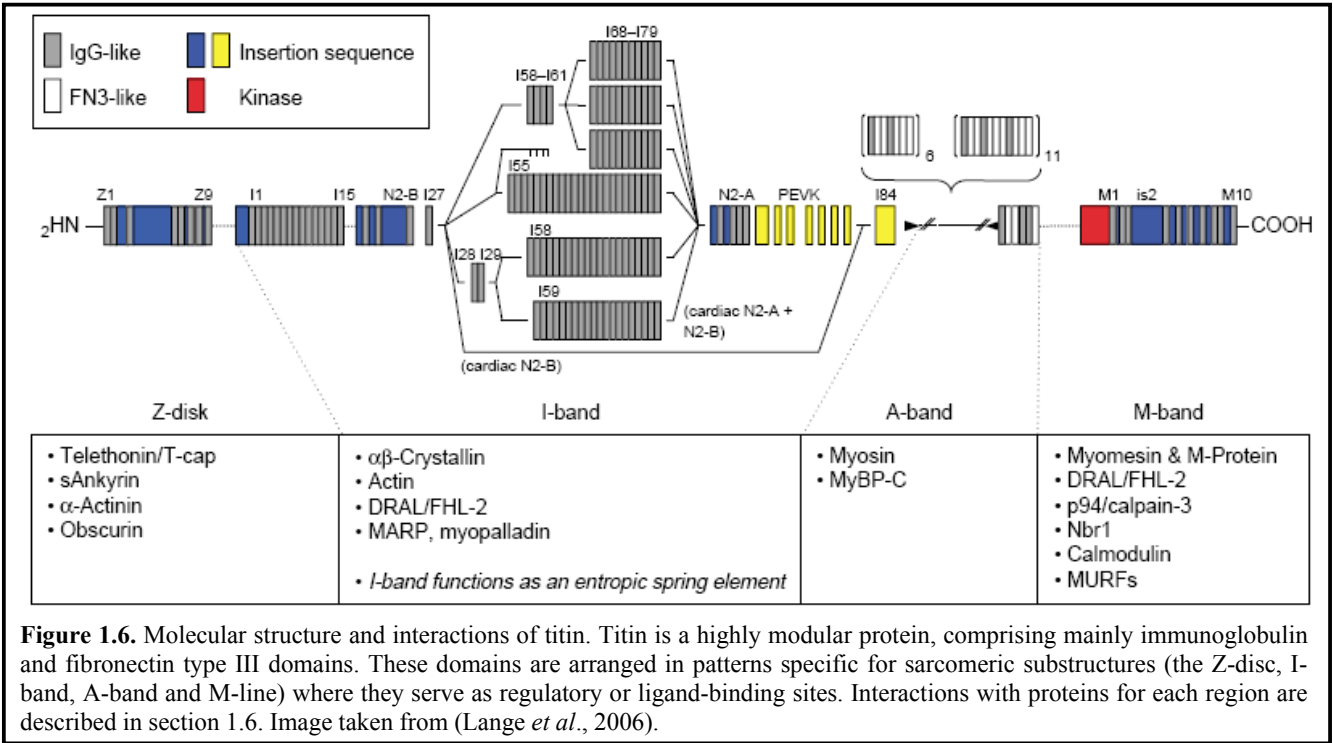
Obscurin (~700–800 kDa) is a complex, large, multi-domain protein that is expressed in striated muscle. The N-terminus contains 49 Ig and two FNIII domains, followed by a complex region consisting of four additional Ig domains flanked by non-modular sequences, an IQ motif and a conserved SH3 domain adjacent to Rho-Guanine Nucleotide Exchange Factor (Rho-GEF) and pleckstrin homology domains (Young *et al.*, 2001). The C-terminus end of the protein contains several consensus phosphorylation motifs for ERKs. Obscurin is present at the M-line, in adult muscle, but at the Z-disc during developmental stages where it participates in sarcomere assembly and integration with other sarcoplasmic elements. Obscurin interacts with titin and the sarcoplasmic reticulum membrane protein small ankyrin 1 (sAnk1) (Borisov *et al.*, 2008).

### 1.5.11 Phosphodiesterase 5A

Phosphodiesterase 5A is a cyclic guanosine monophosphate (cGMP)-specific phosphodiesterase (PDE) that localises to the cytosol of the Z-disc in myocardial tissue. This protein is a member of the PDE superfamily (11 families; >70 isozymes) that locally degrades cGMP and/or cyclic adenosine monophosphate (cAMP) depending on the PDE isoform. PDEs are targeted to distinct subcellular compartments by scaffolding proteins such as myomegalin, muscle-specific A-kinase anchoring protein (mAKAP) and β-arrestins (Osadchii, 2007). Thus PDEs, along with A-kinase anchoring proteins (AKAPs), contribute to the specificity of cAMP/cGMP signalling by targeting the kinases that respond to these second messengers to specific intracellular sites and signalling complexes within the cell by spatially restricting cAMP/cGMP gradients at specific intracellular sites through degradataion (PDEs) (Houslay *et al.*, 2007).

## 1.6 TITIN

The giant, modular protein titin (also known as connectin) makes up the third filament system of striated muscle (Figure 1.6). It is the largest protein identified to date (4.2 MDa) and is the third most abundant muscle protein after actin and myosin (Bang *et al.*, 2001). The 38138 amino acid residues of titin are encoded by a single gene, and several splice variants of this gene have been recognised (Bang *et al.*, 2001). Fibronectin type III and Ig domains (132 and 168 domains, respectively) make up the majority (~90%) of the titin molecule, while the remaining 10% is comprised of 17 non-repetitive sequences that are positioned between the Ig and FNIII repeats. One inter-domain insertion includes a kinase domain and the other 16 have no significant resemblance to each other or to other identified proteins (Clarke *et al.*, 2002). As titin spans half the sarcomere, it associates with components in all compartments of the sarcomere. These interactions and the function of titin within the various compartments are summarised below.



### 1.6.1 Z-Disc Titin

The N-terminus of titin, the first ~80 kDa of the protein, spans the entire Z-disc (Figure 1.6) (Young *et al.*, 1998). This region is cross-linked *via*  $\alpha$ -actinin, not only to actin but to a variety of Z-disc-associated proteins [sAnk1, T-cap (Section 1.5.9), nebulin/nebulette (Section 1.2), filamin C (Section 1.5.8) and obscurin (Section 1.5.10)], creating a complex involved in the stabilisation of the Z-disc and signalling in response to stretch (Linke, 2008).

### 1.6.2 I-Band Titin

Myofibrils produce an independent passive force in addition to the active force produced by the actomyosin ATPase (LeWinter *et al.*, 2007). This passive force preserves the overlap of the thick and thin filaments when inactivated myofibrils are shortened below or stretched beyond their resting length. Upon stretch, the I-band region of titin (Figure 1.6) is responsible for this passive tension development and contains spring-like elements (tandem stretches of Ig domains with unique sequences inserted in between) that contribute to the degree of myofibril stiffness (LeWinter *et al.*, 2007). One insert is the PEVK domain, so named because it is rich in proline, glutamine, valine, and lysine residues (Labeit and Kolmerer, 1995). The structure of the PEVK domain has been characterised as a random coil, but it may actually assume a variety of elastic conformations (Li *et al.*, 2001). In addition, the I-band region contains the N2 region, of which there are two forms (N2A and N2B), which function as additional spring elements. Skeletal titin contains only N2A sequences, whereas cardiac titin contain N2B only or N2BA (N2B and N2A) sequences. During  $\beta$ -adrenergic stimulation, the N2B sequence of cardiac titin can be phosphorylated by PKA (Section 1.9.3.2; Yamasaki *et al.*, 2002), resulting in decreased myocardial passive stiffness (van Heerebeek *et al.*, 2006).

When a sarcomere is stretched from slack length, the spring elements are recruited in a sequential order: At low forces, the Ig domains extend first presumably by straightening inter-domain linkers, while at higher forces and greater stretch, the PEVK and N2A regions unravel additionally (Granzier and Labeit, 2002). In cardiac muscle, the N2B region provides further extensibility at still higher levels of stretch (Trombitas *et al.*, 1999). Thus, the I-band region of titin has elastic properties suggesting that titin may function as a bi-directional molecular spring and may govern some aspects of myofibrillar stiffness. To protect this extensible region from denaturation due to unfolding upon fiber stretching during  $\beta$ -adrenergic stimulation, the N2B region interacts with a heat shock protein and chaperone,  $\alpha$ B-crystallin (Bullard *et al.*, 2004). Further, N2B interacts with various metabolic enzymes *via* the LIM protein, FHL2 (Section 1.5.5) (Lange *et al.*, 2002); in addition, the I-band of titin also interacts with the thin filament, but before contraction or stretch, the thin filaments may be freed from titin (Yamasaki *et al.*, 2001).

### 1.6.3 A-Band Titin

The ~2 MDa A-band region of titin (Figure 1.6) has been proposed to function as a template for the precise assembly and exact length of the thick filaments. This functionally inextensible region is composed of Ig and FNIII domains that are largely arranged in a super-repeat pattern of either seven or eleven domains (Linke, 2008). Specifically, the eleven-domain super-repeat occurring in the C-zone of titin may dictate the number and position of MyBPC and myosin molecules as they correspond to the 11x43nm repeats of the thick filament in the C-zone (Houmeida *et al.*, 1995). Additionally, within these super-repeats the first Ig domain has been shown to have MyBPC-binding sites (Freiburg and Gautel, 1996).

### 1.6.4 M-Line Titin

The M-line region of titin (Figure 1.6) comprises the ~250 kDa C-terminus region of titin housing the catalytically active kinase domain that is thought to play a role in sarcomerogenesis and mechanotransduction (Labeit and Kolmerer, 1995). Within the kinase domain there is a binding site for calmodulin, which is involved in the activation of this domain (Mayans *et al.*, 1998) (Section 1.9.3.2.2). The binding site for MURF1 (Section 1.4.3) is just N-terminus of the kinase domain and several other proteins described in section 1.4 are known to interact with M-line titin. The functions of this part of titin include involvement in thick filament assembly, M-band formation and even maturation of other parts of the sarcomere in cardiac cells (Musa *et al.*, 2006). Further, the kinase domain implicates titin in signalling pathways and protein turnover (Granzier and Labeit, 2004).

## 1.7 SARCOMERIC DEVELOPMENT AND MAINTENANCE

### 1.7.1 Sarcomerogenesis

Sarcomerogenesis is the assembly of sarcomeric and associated proteins in a highly ordered, physically compartmentalised structure with individual components assembled into a complex, three-dimensional latticework. Despite the differences in functional specialisation that different muscles types acquire during development, the basic process of assembly of proteins into myofibrils appears to take place in a step-wise

manner (Sanger *et al.*, 2004). The currently accepted model is the “premyofibril model” (Figure 1.7), which has replaced earlier models on the process of assembly events leading to the mature myofibril (Sanger *et al.*, 2005).

### 1.7.1.1 Premyofibril model

This model was originally proposed for the formation of mature myofibrils in cardiac muscle cells, and experiments on primary embryonic avian myoblasts as well as a transformed mouse skeletal muscle cell line (derived from the limb muscles of *H-2K<sup>b</sup>-tsA58* transgenic mice) provide support for this model (Sanger *et al.*, 2002). Premyofibrils form along the plasma membrane consisting of mini-sarcomeres containing  $\alpha$ -actinin, actin and non-muscle myosin II (Figure 1.7). In this structure, non-muscle myosin II filaments interdigitate with actin filaments that contain muscle isoforms of troponins and tropomyosin, while the barbed ends of the actin filaments are embedded in Z-bodies (containing  $\alpha$ -actinin). In the earliest steps, the premyofibrils associate at the level of their Z-bodies and as the premyofibrils begin to align and grow in width, titin and muscle myosin II appear in the now nascent myofibrils. In the progression from nascent myofibrils to mature myofibrils, the Z-bodies transform from aligned Z-bodies to Z-discs, the muscle myosin II filaments align into A-bands, and non-muscle myosin II is no longer detected. It is unclear how the loss of non-muscle myosin II is accomplished during the transformation of nascent myofibrils into mature myofibrils. It is similarly unclear how the myriad of proteins in the Z-disc are assembled in the transition of Z-bodies in the premyofibrils and nascent myofibrils to the typical Z-discs of mature myofibrils. C-zone and M-line proteins are recruited to the A-bands of the mature myofibrils, and may be responsible for the final alignment of the thick filaments (Sanger *et al.*, 2005).

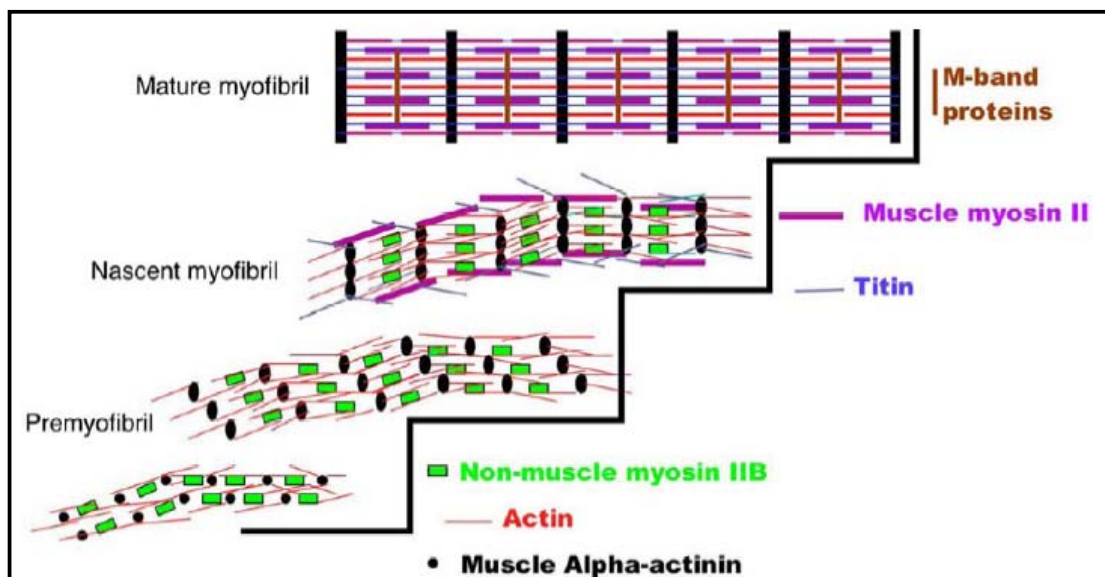


**Figure 1.7.** The transition of Z-bodies (containing  $\alpha$ -actinin) in premyofibrils and nascent myofibrils to Z-discs in mature myofibrils. In this premyofibril model, assembly begins at the edges of muscle cells with premyofibrils composed of mini-sarcomeres that contain sarcomeric proteins in the  $\alpha$ -actinin enriched Z-bodies and thin filaments of actin, troponins and tropomyosin. Non-muscle myosin II filaments are present in the mini-sarcomere of the premyofibrils. Z-bodies in adjacent fibrils begin to align in nascent myofibrils, forming beaded Z-discs that gradually become linear Z-discs in mature myofibrils. Titin molecules and muscle myosin II thick filaments are also present in the nascent myofibrils. The thick filaments in the nascent myofibrils are not aligned, but are overlapped. M-line proteins are recruited to the mature myofibrils, thick filaments become aligned into A-bands, while non-muscle myosin II proteins are absent. Image taken from (Sanger *et al.*, 2006).

### **1.7.2 Sarcomeric protein integration and exchange**

Once the sarcomere is established, integration and exchange of new proteins into the structure occur continuously. The half-life of contractile proteins is quite long compared with soluble cytosolic cellular components; the half-life of myosin in the heart is about ~15 days (Papageorgopoulos *et al.*, 2002). However, the turnover rate of myofibrillar proteins varies; the subunits of troponin have a turnover rate of 3-5 days under steady-state conditions, suggesting that there is an assembly pool of myofibrillar proteins available for exchange (Martin, 1981). Consistent with this hypothesis, two pools of troponin have been identified: the majority of troponin is myofibril-bound and the remaining troponin is found as a soluble, cytoplasmic pool, which probably serves as a precursor pool for the synthesis of the troponin complex (Adamcova and Pelouch, 1999). In transiently transfected skeletal muscle cells, MyBPC intracellular pools were shown to be regulated by muscle-specific members of the ubiquitin-proteasome system; in addition MyBPC had a half-life of 3 hours suggesting that this is a very short lived protein (Bosch-Comas *et al.*, 2006)

Little is known about the fate of newly synthesised sarcomeric proteins and the mechanism of their incorporation into the sarcomere (Boateng and Goldspink, 2008). The involvement of muscle-specific factors in this process was suggested by the finding that the folding of a chimeric myosin green fluorescent protein (GFP)-tagged construct was improved in the presence of muscle cell extract. Immuno-colocalisation of the myosin-GFP folding intermediates showed that they were associated with protein chaperones, viz. heat shock proteins (Srikakulam and Winkelmann, 2004). This data, in addition to data from studies in *Caenorhabditis elegans*, support the role of chaperone complexes in the assembly of the contractile protein apparatus (Barral *et al.*, 2002). Chaperones are known to closely associate with the cytoskeletal network and, in circumstances where cytoskeletal homeostasis is affected (elevated temperatures, exposure to toxins, inflammation, ischaemia and hypoxia), chaperone proteins are believed to bind to and stabilise the unstable conformers. This binding adaptively facilitates the assembly, disassembly or folding/refolding of cytoskeletal proteins and prevents aberrant protein aggregation in an attempt to restore cellular function (Kumarapeli and Wang, 2004).

### **1.7.3 Sarcomeric protein degradation**

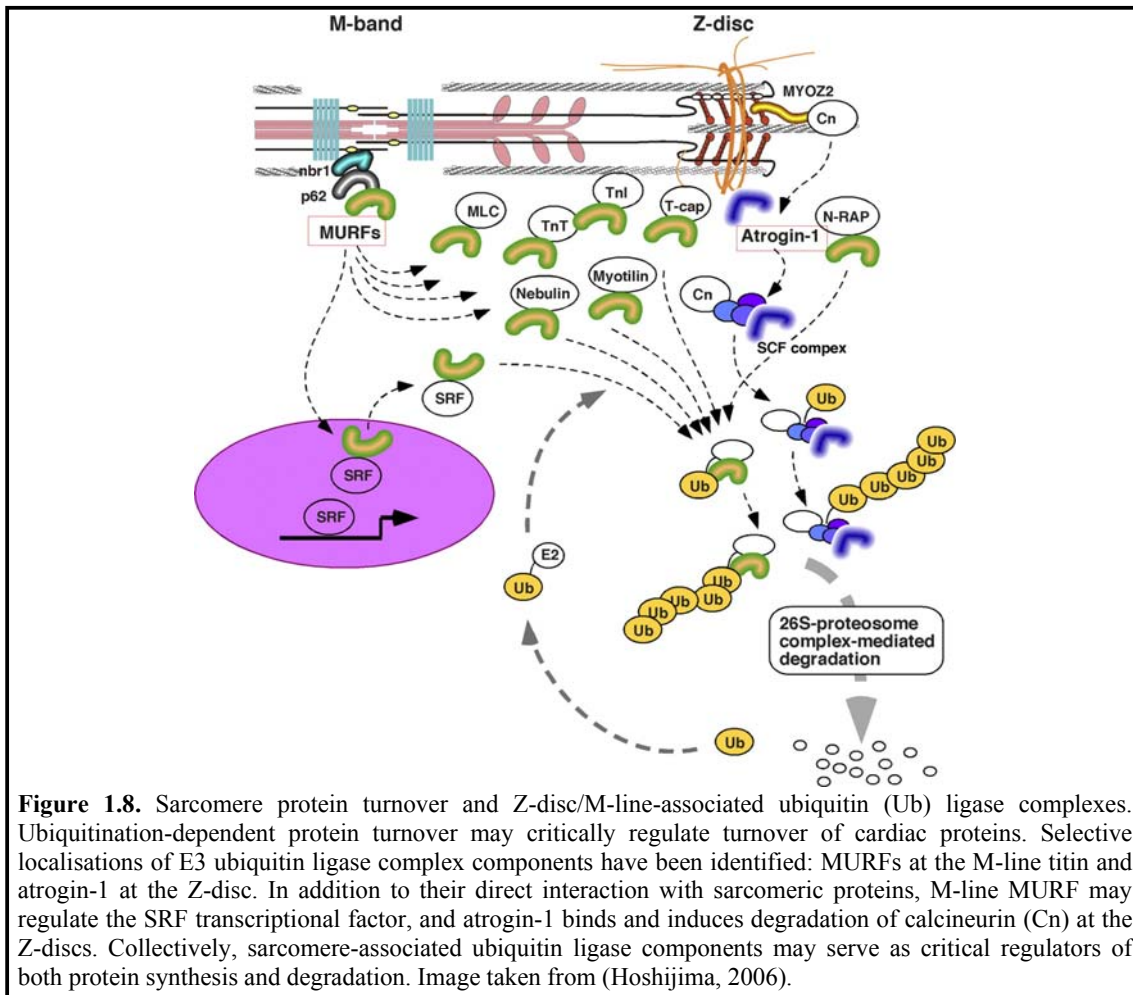
All intracellular protein constituents, including the cytoskeletal protein subunits such as sarcomeric proteins, undergo a continuous process of degradation and re-synthesis (Hoshijima, 2006). The rates of flux of intracellular protein constituents through these two opposing metabolic pathways ultimately determines the changes in protein mass observed during normal growth, hypertrophy, and atrophy of cardiac and skeletal muscles (Samarel, 1991). The degradation process is facilitated by the ubiquitin-proteasome system.

#### **1.7.3.1 The ubiquitin-proteasome system (UPS)**

The UPS eliminates damaged and misfolded proteins and closely regulates cellular processes by rapid proteolysis and modulation of many intracellular proteins (Powell, 2006). The UPS is found primarily in the cytosol in association with the cytoskeleton, endoplasmic reticulum, the plasma membrane and nucleus

(Willis and Patterson, 2006). In this pathway, protein substrates are first marked for degradation by covalent linkage to multiple ubiquitin molecules in three steps. First, the ubiquitin-activating enzyme (E1) forms a covalent bond with ubiquitin in an ATP-dependent process. The ubiquitin-conjugating enzyme (E2) subsequently transfers ubiquitin from the E1 to itself. While some E2s can directly add ubiquitin to a substrate, however, a third step involving an E3 enzyme (ubiquitin ligase) is generally required. The E3 recognises its specific substrate and transfers ubiquitin from the E2 to a substrate lysine (Powell, 2006). There is only one E1 enzyme, while approximately a dozen different types of E2 enzymes and hundreds of E3 ubiquitin ligases have been described (Willis and Patterson, 2006). In general, if the substrate is to be degraded by the 26S proteasome, it must be polyubiquitinated, which occurs *via* successive addition of conjugated ubiquitin by an elongation factor (E4). Once a substrate is polyubiquitinated, it is either recognised directly by the proteasome or bound to some shuttling protein (such as a chaperone), which transports it to the proteasome (Powell, 2006).

While the process of sarcomeric protein turnover is still being elucidated, several factors potentially involved with the UPS have been identified in association with the sarcomere. At the M-line (Figure 1.8), the nbr1 (neighbour of *BRCA1* gene 1) protein and p62, which both have the ubiquitin-associated domain, together with MURF1 and MURF2 (Section 1.4.3), complex with the titin kinase domain. *MURF1* is among a small subset of genes up-regulated in models of skeletal muscle atrophy and MURF1-deficient mice are resistant to skeletal muscle atrophy, consistent with the view that MURF1 regulates muscle protein degradation (Bodine *et al.* 2001). A number of sarcomeric proteins have been identified as interactors of the MURFs, suggesting that they may be involved in the turnover of myofibril proteins. Also, MURFs have been found to interact with cardiac enzymes required for energy production, suggesting a link between cardiac metabolism and muscle turnover. Another protein upregulated in models of skeletal muscle atrophy was Atrogin 1 [muscle atrophy F-box protein (FBX032)] (Bodine *et al.*, 2001). Atrogin 1 forms part of the SCF (Skp-1-cullin-F-box) ubiquitin ligase complex, which localises to the cardiac Z-disc (as an  $\alpha$ -actinin interactor) and regulates the protein level of calcineurin A (Hoshijima, 2006). Although the mechanism(s) by which these muscle-specific E3s act has not been fully elucidated, it is apparent that they are involved in myofibrillar degradation (Powell, 2006).



## 1.8 CARDIAC CONTRACTION

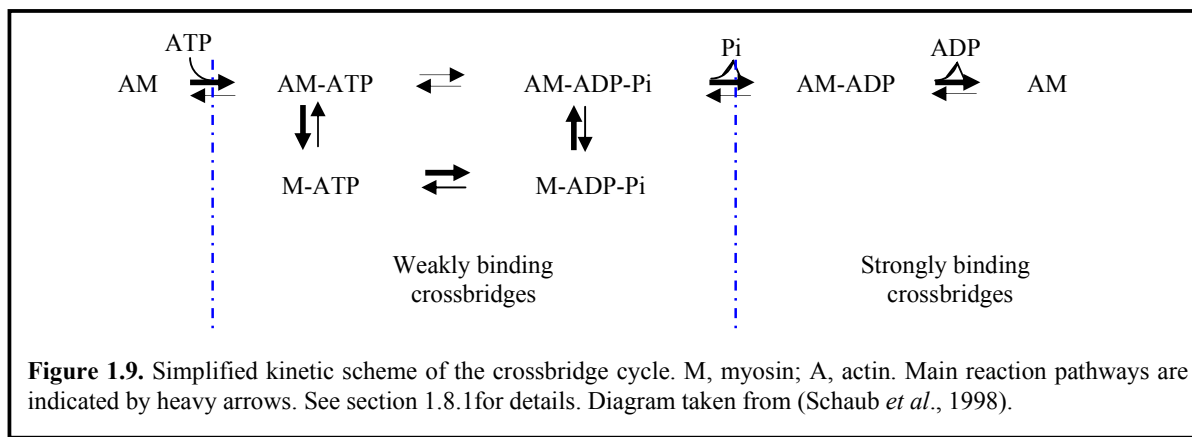
Activation of the cardiac sarcomere is a co-operative multi-step process that involves complex protein-protein interactions. These interactions ultimately result in the activation of the thin filament and the subsequent interaction between actin and myosin that leads to ATP hydrolysis and myofilament force development. The “sliding filament” theory of muscle contraction, originally proposed by Huxley (1957), suggested that force generation results from the sliding movement of the thick filaments relative to the thin filaments, which is mediated by the cyclical attachment and detachment of myosin crossbridges to actin. The “swinging crossbridge” model, a subsequent modification of the sliding filament model, hypothesised that a swinging motion of the myosin head was a significant factor for progression along the thin filament (Huxley, 1969; Lynn and Taylor, 1971). This model also included a role for ATP hydrolysis. A modification of the “swinging crossbridge model” followed after structural and spectroscopic observations showed that the relative movement of actin and myosin arise from the head of myosin acting as a lever (Huxley, 2000). In this “lever-arm” model, the power stroke is produced not by movement of the myosin head (at the point of actin attachment), but by the pivoting movement of the myosin rod at the hinge region. The lever arm rotation was attributed to the transition between two conformations of the myosin head, “open” and “closed”, that affects nucleotide affinity and hydrolysis, and that are determined by actin-binding. It has subsequently

been proposed that altered orientation of both the myosin head and the  $\alpha$ -helical rod may contribute to the overall displacement of actin (Fatkin and Graham, 2002).

### 1.8.1 The crossbridge cycle

The crossbridge cycle is a series of reactions that result in the force-generation required for filament movement, causing the sarcomere to shorten, and, in turn, the muscle to contract. During this cycle, the myosin head undergoes a series of conformational changes (structural and mechanical), during the cleavage of ATP to ADP and inorganic phosphate (Pi). The simplified crossbridge cycle scheme combines the mechanical and kinetic cycles and delineates the main intermediate states in the actin-myosin interaction (Schaub *et al.*, 1998) (Figure 1.9).

The affinity of myosin (M) for actin (A) changes during the crossbridge cycle. The start of the cycle begins with myosin bound to actin in the “rigor” conformation. The binding of ATP to myosin reduces the affinity of myosin for actin, causing the two proteins to separate. Myosin then hydrolyses ATP, and this leads to a “cocked” conformation, priming the conformational change required for the “power stroke”. The weak association of the M-ADP-Pi complex with actin results in the release of Pi that increases the affinity of myosin for actin. These force generating crossbridges bind to actin with positive co-operativity, resulting in an increased resistance to passive stretch. This step is immediately followed by a large conformational change in myosin (the power stroke), and the simultaneous release of ADP re-establishes the initial “rigor” position. *In vivo*, upon binding of a new substrate ATP, the crossbridge dissociates from actin and the cycle is ready to start again (Schaub *et al.*, 1998; Au, 2004).



## 1.9 MODULATION OF CARDIAC CONTRACTILITY

Crossbridge cycling at the molecular level is manifested as cardiac contractility at organ level. The *in vivo* control systems that regulate cardiac contractility are multi-layered and complex. Contractility is largely determined by nervous outflow to the heart and circulating chemical messengers, but mechanisms intrinsic to the myocardium also contribute to these control systems (Metzger and Westfall, 2004).

Physiological regulation of contraction can occur at three different locations in the myocardial contractile apparatus: cytosolic concentration of  $\text{Ca}^{2+}$  ions that activate thin filament proteins (Section 1.9.1), the thin filament proteins themselves (Section 1.9.2), and thick filament proteins (Section 1.9.3.1 and 1.9.3.5). In addition, phosphorylation of specific serine (Ser) and threonine (Thr) residues on sarcomeric thin and thick filament proteins by several different kinases also represents a major physiological mechanism for alteration of myofilament properties (Metzger and Westfall, 2004). The effect of this regulatory mechanism is described in sections 1.9.3.1-5 of this chapter and ties in closely with the current study.

### **1.9.1 Role of $\text{Ca}^{2+}$ in the regulation of cardiac contractility**

$\text{Ca}^{2+}$  is the physiological activator and an important regulator of the contractile machinery in both skeletal and cardiac muscle. The activation of the contractile apparatus is initiated upon the entry of  $\text{Ca}^{2+}$  into the cell via voltage-gated L-type channels in the sarcolemmal membrane during membrane depolarisation. This transient increase in the cytosolic  $\text{Ca}^{2+}$  concentration is not sufficient to directly activate the myofilaments, but instead serves as a trigger to release  $\text{Ca}^{2+}$  from the sarcoplasmic reticulum (SR) via ryanodine receptors (Bers, 2005). The free  $\text{Ca}^{2+}$  binds to TNC and activates the thin filament as described in section 1.9.2. Relaxation is initiated by dissociation of  $\text{Ca}^{2+}$  from TNC, followed by its rapid reuptake into the SR by the SR  $\text{Ca}^{2+}$ -ATPase (SERCA) pump. SERCAs are 110 kDa transmembrane ATP-driven  $\text{Ca}^{2+}$  pumps that comprise of a large cytoplasmic region and a transmembrane domain that constitutes the  $\text{Ca}^{2+}$  channel. SERCA2a is the major isoform expressed in the developing and adult mammalian heart and is regulated by phospholamban (PLB; Section 1.9.3.3), a 52-amino acid phosphoprotein (Ha *et al.*, 2007). The sarcolemmal  $\text{Na}^+/\text{Ca}^{2+}$  exchanger and the mitochondrial  $\text{Ca}^{2+}$  uniporter are also responsible for  $\text{Ca}^{2+}$  uptake, although to a much smaller extent than SERCA (Mattiazzi *et al.*, 2005). The net result of these changes is the cyclic increase and decrease in  $\text{Ca}^{2+}$  and contractility. Changes in the rate and/or force of contraction are needed in stressful circumstances to increase cardiac output and this is achieved by the processes that enhance the  $\text{Ca}^{2+}$ -mediated responses mentioned above. These  $\text{Ca}^{2+}$  handling proteins (such as L-type  $\text{Ca}^{2+}$  channels, ryanodine receptors, SERCA and PLB) are substrates of protein kinase A (Section 1.9.3) and phosphorylation of these proteins increases the intracellular  $\text{Ca}^{2+}$  transient and contraction amplitudes, and accelerate their kinetics (Song *et al.*, 2001).

$\text{Ca}^{2+}$  also influences the activation state of the thin filament, which is an important factor affecting the probability of force generation. A two-state and a three-state model of the thin filament activation has been proposed (Brenner, 1988). In the two-state model system, myosin is prevented from binding to the thin filament in the “off-state”, while it binds co-operatively in the “on-state” (Brenner, 1988). However,  $\text{Ca}^{2+}$  activation may not just exert an “on-off” action on actin-myosin interaction and thus a three-state model has been proposed. In this model the thin filament is either in a “blocked”, “closed”, or “open” conformation (Tobacman and Butters, 2000). The transition from the “closed” to the “open” state is influenced by the level of activating  $\text{Ca}^{2+}$  (Maytum *et al.*, 1999). In the “blocked” (off) state,  $\text{Ca}^{2+}$  is not bound to TNC and crossbridge binding does not occur. In the “closed” (off) state, weak crossbridges form when  $\text{Ca}^{2+}$  binds to

TNC, while in the “open” (on) state,  $\text{Ca}^{2+}$  is bound to TNC and crossbridges are strongly bound. Thus, this three-state model proposes that  $\text{Ca}^{2+}$  may determine whether or not crossbridges bind and the strength of binding. Further, it has been suggested that changes in  $\text{Ca}^{2+}$  activation may modify the number of crossbridges attached and the kinetics of crossbridge attachment and detachment (Wannenburg *et al.*, 2000). Thus, it is clear that the activation of the contractile apparatus by  $\text{Ca}^{2+}$  involves a molecular rearrangement of contractile proteins leading to altered protein-protein interactions in the thin filament. These events ultimately lead to strong crossbridge binding, ATP hydrolysis by myosin, force development, and mechanical work generation (de Tombe, 2003).

### 1.9.2 Regulation by the troponin-tropomyosin complex

The key events in the regulation of cardiac contractility involve reversible  $\text{Ca}^{2+}$ -binding to TNC, structural changes within the trimeric troponin complex associated with the binding, and changes in the interaction between the TNC-TNI interface.  $\text{Ca}^{2+}$ -binding is considered the trigger of activation and the change in the TNC-TNI linkage is the switch between activation and deactivation (Dong *et al.*, 2006).

The initiation of muscle contraction begins with the saturation of the regulatory sites of TNC by  $\text{Ca}^{2+}$ . In skeletal muscle, the binding of  $\text{Ca}^{2+}$  induces conformational changes in skeletal TNC that expose hydrophobic residues, which may play a significant role in the formation of tight contacts between skeletal TNI and TNC (Herzberg *et al.*, 1986) and weakens the interaction between skeletal TNI and actin-TM. In the absence of  $\text{Ca}^{2+}$ , the  $\text{Ca}^{2+}$ -binding sites are in the so-called “closed” configuration. In this state, the hydrophobic residues form contacts with each other and are shielded from  $\text{Ca}^{2+}$ . After saturation of  $\text{Ca}^{2+}$ , the helices move apart, exposing the hydrophobic residues to  $\text{Ca}^{2+}$ , and the  $\text{Ca}^{2+}$ -binding sites change to their so-called “open” conformation (Houdusse *et al.*, 1997). Since cTNC has lost the ability to bind  $\text{Ca}^{2+}$  at site I, the N-terminus domain remains in the so-called “closed” conformation and the presence of both  $\text{Ca}^{2+}$  at site II and cTNI are required to stabilise the “open” conformation of the N-terminus of cTNC (Li *et al.*, 1999; Dong *et al.*, 1999). Despite the differences in  $\text{Ca}^{2+}$  binding capacity between the skeletal and cardiac isoforms of TNC, both regulate muscle contractile activity.

Once the N-terminus of cTNC has taken on the more open conformation, a hydrophobic patch within the domain becomes exposed and makes possible a strong interaction of this patch with the regulatory region of cTNI (McKay *et al.*, 1999). This hydrophobic interaction is facilitated by a large conformational change of a downstream segment of cTNI (the inhibitory region) from a  $\beta$ -turn/coil motif to an extended conformation (Dong *et al.*, 2003). This conformational change may be a consequence of the release of the inhibitory region from actin, triggered by  $\text{Ca}^{2+}$ -activation. An alternate view is that the regulatory region simply slides into the open N-terminus to interact with the exposed hydrophobic pocket, thus stabilising the  $\text{Ca}^{2+}$ -saturated N-terminus. This movement drags on the downstream inhibitory region, which in turn breaks its contact with actin. These changes free the thin filament from its inhibitory state, supporting actin-myosin contact and

force generation. Once some strongly bound crossbridges have formed, the binding of additional crossbridges is greatly enhanced in a co-operative manner (Dong *et al.*, 2006).

Upon decline of cytosolic  $\text{Ca}^{2+}$  concentrations to diastolic levels,  $\text{Ca}^{2+}$  dissociates from TNC and restores the inhibitory action of TNI on actomyosin interaction. While the stimulation of  $\text{Ca}^{2+}$  reuptake into the SR to some extent speeds up relaxation, the efficiency of this mechanism is limited by the rate at which  $\text{Ca}^{2+}$  dissociates from TNC, which is a prerequisite for relaxation to occur at the actomyosin crossbridge level. Hence, mechanisms that decrease the  $\text{Ca}^{2+}$  affinity of TNC will favour rapid relaxation (Kögler, 2006).

### 1.9.3 Adrenergic stimulation and contractile protein phosphorylation

Long term regulation of protein-protein interactions in the sarcomere is achieved by changes in gene expression patterns (Schiaffino and Reggiani, 1996). On the other hand, short-term dynamic adaptations are mediated by protein phosphorylation of specific proteins by the action of dedicated kinases (Gruen *et al.*, 1999a), which often occurs in response to stress. Under the latter conditions (i.e. during a “flight-fight-or-fright” reaction), a variety of neurohumoral factors are generated and released from the sympathetic nervous system and adrenal medulla that stimulates cardiac  $\beta$ - and  $\alpha$ -adrenoreceptors (Pi *et al.*, 2002). Stimulation of  $\beta$ -adrenergic receptors has profound effects on myocardial function and can be broadly summarised as increases in cardiac pressure generation (inotropy), relaxation rate (lusitropy), and cardiac contractile frequency (chronotropy). These changes are beneficial during “flight-fight-or-fright” response because the net result is an overall increase in power output by the myocardium (Metzger and Westfall, 2004).

Upon  $\beta$ -adrenergic stimulation, there is a rapid formation of the intracellular second messenger cAMP (cyclic adenosine monophosphate), which directly activates protein kinase A (PKA). The activated catalytic subunit of PKA is known to have multiple intracellular targets in cardiac muscle, including the sarcolemmal  $\text{Ca}^{2+}$  channel, phospholamban of the sarcoplasmic reticulum, titin, TNI and cMyBPC (Katz and Lorell, 2000). These proteins undergo orchestrated functional changes that together comprise the positive inotropic and lusitropic effects caused by  $\beta$ -adrenoreceptor activation. These effects serve to enhance cardiac output: the positive inotropic effect boosts myocyte contractility by optimising  $\text{Ca}^{2+}$  homeostasis, mainly *via* phosphorylation of  $\text{Ca}^{2+}$ -handling proteins (Section 1.9.1). The positive lusitropic effect accelerates myocyte relaxation, thereby facilitating an increase in cardiac output *via* elevation of heart rate (Kögler, 2006). The intracellular level of cAMP is maintained by phosphodiesterases (PDEs; Section 1.5.11), which hydrolyse cAMP after  $\beta$ -adrenergic activation (Houslay *et al.*, 2007).

The stimulation of cardiac  $\alpha$ -adrenoreceptors, on the other hand, results in mobilisation of lipid second messengers (including fatty acids and diacylglycerols), which activate the lipid-dependent protein kinase C (PKC) family. Adenosine, endothelin 1, opiates and angiotensin II are among the stress-related agonists that stimulate PKC in the heart and phosphorylate a wide range of intracellular proteins, including ion pumps, ion channels, exchangers, and myofilament proteins (Pi *et al.*, 2002). The mechanisms by which PKC pathways

regulate cardiac contractility remains poorly understood, as there are multiple PKC isoforms of uncertain function, multiple sites of action of PKC phosphorylation and multiple pathways of PKC activation. Additionally, the effects of  $\alpha$ -adrenergic agonists thought to stimulate the PKC pathway have both positive and negative inotropic effects, depending on the frequency of stimulation and inotropic state of the preparations (Pi *et al.*, 2002). Studies utilizing RT-PCR identified the presence of  $\alpha$ ,  $\delta$ ,  $\epsilon$ ,  $\eta$ , and  $\zeta$  PKCs in rat cultured cardiomyocytes, including abundant expression of both  $\beta$ I and  $\beta$ IIIPKC in human and rat cardiomyocytes (Churchill *et al.*, 2008).

Not only are the molecular effects of adrenergic stimulation on contractile function not yet fully understood, but other kinases also affect the phosphorylation state of some sarcomeric proteins. As these processes may occur simultaneously, it is difficult to define the individual contribution of each phosphoprotein to these effects. For the purpose of this thesis, the effects of phosphorylation on the myosin regulatory light chain (RLC), titin, phospholamban (PLB), cardiac troponin I (cTNI) and myosin-binding protein C (cMyBPC) will be described further. Although PLB is not a sarcomeric protein and thus does not strictly fall within the scope of this thesis, it is prominent among the proteins (cTNI and cMyBPC) responsible for the enhanced lusitropy (rate of relaxation) and will therefore be described.

### **1.9.3.1 REGULATORY MYOSIN LIGHT CHAIN (RLC)**

In smooth muscle, the function of RLC is to initiate contraction (upon its phosphorylation by smooth muscle myosin light chain kinase) (Szczesna-Cordary, 2003). However, in striated muscle, initiation of contraction is fulfilled by the thin filament (upon a rise in  $\text{Ca}^{2+}$  concentration); thus the function of RLC in striated muscle is not as well understood, although it is thought to play a modulatory role in muscle contraction. The following sections describe some of the functions attributed to RLC phosphorylation in cardiac muscle, specifically.

#### **1.9.3.1.1 Phosphorylation of RLC**

Myosin light chain kinase (MLCK) is a  $\text{Ca}^{2+}$ -calmodulin-dependent kinase that phosphorylates cardiac, skeletal and smooth muscle RLC. Kinase isoform expression is predominantly tissue-specific (Chan *et al.*, 2008), although, skeletal and smooth muscle MLCK expression have also been observed in cardiac muscle (Chan *et al.*, 2008). The N-terminus Ser14 of human RLCv, and Ser21 and Ser22 of human RLCa are phosphorylated by MLCK, consequently human RLCv isoforms are monophosphorylated, while human RLCa may be mono- or diphosphorylated. Ser14 is also phosphorylated by PKC *in vitro* and *in situ* (Morano, 1999). On the other hand,  $\beta$ -adrenergic stimulation does not increase RLC phosphorylation; accordingly PKA is not thought to be able to phosphorylate RLC (England *et al.*, 1984). Protein phosphatases 1 and/or 2A have been implicated in the dephosphorylation of RLC (Venema *et al.*, 1993).

Cardiac muscle exhibits very low rates of RLC phosphorylation and dephosphorylation because of the very low MLCK and phosphatase activities (Sweeney *et al.*, 1993). Despite this, there exists a gradient of RLC

phosphorylation across the ventricular wall in rat heart, such that RLC in the epicardium is hyperphosphorylated while RLC in the endocardium is hypophosphorylated (Davis *et al.*, 2001). This pattern of RLC phosphorylation corresponds to the pattern of a skeletal-like MLCK expression, with large amounts expressed at the epicardium and low amounts at the endocardium. This spatial pattern for RLC phosphorylation has been proposed to explain the force mismatch during ventricular systole that produces the “wringing” motion (epicardial fiber shortening predominating over endocardial fiber shortening), which aids pump function by perhaps determining the amount, timing and rate of force generation across the ventricular wall (Davis *et al.*, 2001).

#### **1.9.3.1.2 Effect of RLC phosphorylation**

##### **1.9.3.1.2.1 Conformational changes and effect on thick filament**

Structurally, the RLC comprises of two globular domains, connected by a flexible region that may bend to move the N- and C-terminus close to each other (Sweeney *et al.*, 1993). The N-terminus is rich in basic residues, displaying a segmental mobility independent of the rest of the molecule and assumes an extended “antenna-like” mobile conformation (Levine *et al.*, 1988). It has been suggested that phosphorylation may induce a conformational change in the N-terminus, resulting in a more compact and/or less flexible structure (Ritz-Gould *et al.*, 1980). Considering RLCs close association with myosin, any conformational change in RLC would likely affect the underlying  $\alpha$ -helical region of the MHC. As such, there have been studies investigating the effect of RLC extraction as well as RLC phosphorylation on the thick filament. When thick filaments (obtained from arthropod striated muscles) were exposed to phosphorylating conditions, there was a conformational change in the order of the myosin heads from helically ordered (characteristic of the relaxed state) to disordered (Levine *et al.*, 1991). Extreme disorder was also reported after removal of RLC from thick filaments. In these experiments, the myosin heads reached much greater radii from the filament backbone than was seen after RLC phosphorylation. These observations suggest that RLC may play an important role in maintaining the relaxed, ordered arrangement of myosin heads (Margossian *et al.*, 1992), at least in arthropod muscle.

The conformation change in the myosin head upon RLC phosphorylation may be explained by the hypothesis proposed by Sweeney *et al* (1994), which suggested that RLC phosphorylation neutralised the positively charged amino acids N-terminus from the phosphorylatable serine residue. It is possible that ionic interactions between these residues and negatively charged regions of myosin (either within the underlying myosin rods or within the light or heavy chains in the neighbouring myosin heads) stabilise and help maintain the ordered organisation of the myosin heads in the RLC-unphosphorylated state (Sweeney *et al.*, 1994). By neutralising the overall positive charge of the RLC N-terminus, phosphorylation may effectively free the myosin heads from their association with other myosin molecules. The free heads would be more mobile and appear disordered. With increased proximity to the thin filament, phosphorylated heads are more likely to be involved in actin-myosin interactions, than the stable, RLC-unphosphorylated variety (Levine *et al.*, 1998).

Thus, in summary, it is proposed that the association of the unphosphorylated RLC with MHC increases the structural order of the myosin filament, moving the crossbridge closer to the myosin filament backbone, which reduces the probability of crossbridge attachment to the actin filament at submaximal  $\text{Ca}^{2+}$  concentrations. This reduces the number of crossbridges in the force-generating states and thus force and stiffness at submaximal  $\text{Ca}^{2+}$ -activation are low. Phosphorylation of RLC relieves this relative inhibition, allowing the crossbridges to swing out from the thick filament backbone towards the actin filament, increasing the probability of attachment and force generation, which is most pronounced at low  $\text{Ca}^{2+}$ -activation levels (Morano, 1999).

#### 1.9.3.1.2.2 ATPase

Functionally, RLC is not essential for enzymatic hydrolysis of ATP by myosin; rather, it may act to modulate the ATPase activity. Removal of RLC causes enhanced ATPase activity, an effect which was abrogated by the re-addition of unphosphorylated RLC (Malhotra *et al.*, 1979). In contrast, re-addition of phosphorylated RLC to a RLC-free myosin preparation does not inhibit actin-activated ATPase to the same extent as non-phosphorylated RLC (Morano, 1999).

#### 1.9.3.1.2.3 Force and $\text{Ca}^{2+}$ -sensitivity

Phosphorylation of RLC by MLCK, in chemically skinned cardiac fibers, resulted in an increase in myofilament  $\text{Ca}^{2+}$ -sensitivity (Szczesna-Cordary *et al.*, 2002; Pi *et al.*, 2003; Olsson *et al.*, 2004) and maximum steady-state force (Szczesna-Cordary *et al.*, 2002). Further, there was acceleration in the rate of force development ( $k_{tr}$ ) in myocardium at low levels of activation (Olsson *et al.*, 2004) and a slowing down of relaxation following RLC phosphorylation (Patel *et al.*, 1998). In these fibers, RLC phosphorylation increased the  $\text{Ca}^{2+}$ -sensitivity of the myofibrillar apparatus, thus decreasing the  $\text{Ca}^{2+}$  concentration required to elicit tension (Persechini *et al.*, 1985). Such effects are limited to submaximal  $\text{Ca}^{2+}$  concentrations suggesting that the net effect of displacement was to speed the co-operative recruitment of crossbridges to force-generating states, which would increase both force and the rate of force development. Likewise, slowed rates of relaxation would be a consequence of increased likelihood of crossbridge re-binding to actin once detached and not due to a slower rate of detachment (Moss and Fitzsimons, 2006).

RLC phosphorylation occurs within a few seconds of repetitive simulation of skeletal muscle contractions at physiological frequencies (Sweeney *et al.*, 1993), whereas minutes are required for dephosphorylation, even in resting muscle with inactive kinase. Sweeney *et al* (1993) postulated that RLC phosphorylation in vertebrate striated muscle acts as a factor enhancing the performance of muscle, a kind of “memory” that the muscle has been recently active. RLC phosphorylation enhances the force if the muscle was recently activated and allows the force to be maintained at a certain level, even if, during prolonged contractions, the  $\text{Ca}^{2+}$  concentration decreases (Stepkowski, 1995). Such a modulatory mechanism is economical because when RLC is phosphorylated, the cascade of events associated with activation requires only a small increase in  $\text{Ca}^{2+}$  thus, less  $\text{Ca}^{2+}$  must be pumped back into the SR, at a decreased energy cost (Sweeney *et al.*, 1993).

#### **1.9.3.1.2.4 Cardiac function and myofibrillogenesis**

The importance of RLC in cardiac function is evident from findings that mutations in *MYL2* underlie some cases of hypertrophic cardiomyopathy (Szczesna-Cordary *et al.*, 2005) (Section 1.10.1). RLC phosphorylation appears to be important in cardiac development, as inhibition of MLCK disrupted thick filament assembly in embryonic myocytes in culture (Li *et al.*, 2004). It is thought that when  $\text{Ca}^{2+}$  increases during development, MLCK is activated; RLC is phosphorylated and contributes critically to thick filament assembly (Li *et al.*, 2004).

Partial replacement of the ventricular RLC with isoforms that are normally expressed in fast skeletal muscle fibers resulted in decreased left ventricular contractility and relaxation, although the unloaded shortening velocity of the isolated ventricular cardiomyocytes was not appreciably different (Gulick *et al.*, 1997). Ventricular dysfunction was also observed in another study where the total disruption of the murine cardiac ventricular RLC gene resulted in sarcomeric disassembly, an embryonic form of dilated cardiomyopathy (DCM; Section 1.10.2) and the early death of homozygous embryos. Drastic changes in the ventricular structure and function were also observed in muscle expressing the atrial isoform of RLC. The authors concluded that the ventricular isoform of RLC has a unique function in the maintenance of cardiac contractility and ventricular chamber morphogenesis during mammalian cardiogenesis (Chen *et al.*, 1998).

Heterozygous RLC knockout mice, on the other hand, showed that, while there was a 50% reduction in RLC ventricular mRNA, normal levels of protein were detected (Minamisawa *et al.*, 1999). Further, heterozygote mice exhibited cardiac function comparable to that of wild-type (WT) controls and demonstrated no significant differences in contractility and response to  $\text{Ca}^{2+}$  in unloaded cardiomyocytes. Thus, heterozygous mice showed neither a molecular nor a physiological cardiac phenotype, suggesting that post-translational compensatory mechanisms may play a major role in maintaining the level of the ventricular RLC in murine hearts (Minamisawa *et al.*, 1999). As most human cases of hypertrophic cardiomyopathy (HCM; Section 1.10.1) are as a result of heterozygous mutations, this study suggests that the mechanism by which the HCM-mutant protein causes disease is perhaps by acting as a “poison peptide”, incorporating into the sarcomere and affecting normal contractile function.

In the zebrafish embryonic heart, where a single isoform of cardiac RLC is expressed at all stages of development, RLC gene ablation resulted in a failure of both cardiac thick filament assembly (even while thin filament assembly was evident) and myofibrillogenesis, leading to embryonic lethality (Rotterbauer *et al.*, 2006). Control experiments showed that this effect was caused by absence of RLC expression and occurred in a cell autonomous manner. These results indicated that RLC was required for thick filament assembly, in this model, but whether this is because of a structural or contractile effect of RLC is presently unknown (Rotterbauer *et al.*, 2006).

The transgenic over-expression of a non-phosphorylatable ventricular RLC (Ser residue replaced with non-phosphorylatable alanine residue) in the atria and ventricles of mice, resulted in a spectrum of cardiovascular alterations that were observed by both gross histology and transmission electron microscopy analyses. Mature animals displayed both atrial hypertrophy and dilation, and echocardiographic analysis revealed that severe tricuspid valve insufficiency, a consequence of chamber enlargement, resulted in a detectable regurgitation jet. These findings confirmed the importance of regulated RLC phosphorylation in maintaining normal cardiac function (Sanbe *et al.*, 1999). Similarly, when the non-phosphorylatable RLC was expressed in the indirect flight muscles of *Drosophila*, the resultant flies showed normal myofibrillogenesis, but had reduced power output and flight ability, resulting from a marked reduction in the stretch activation of the indirect flight muscle (Tohong *et al.*, 1995). Thus, depending on the model, RLC phosphorylation appears to affect myofibrillogenesis differently but appears essential for normal cardiac function.

#### **1.9.3.1.2.5 Stretch activation**

Phosphorylation of RLC also affects the stretch activation response differently across species. Tohong *et al* (1995) showed a marked reduction in the stretch activation of the indirect flight muscle of *Drosophila* when non-phosphorylatable RLC was expressed. These findings contrast with the study by Stelzer *et al* (2006a), who found that RLC phosphorylation significantly accelerated the stretch activation response in murine ventricular myocardium. The latter data also supports the findings of Davis *et al* (2001), who found that RLC phosphorylation in the heart played an important role in determining the amount, timing and rate of force generation across the ventricular wall, modulating systolic ejection. Based on the results of Stelzer *et al* (2006a) and that of Davis *et al* (2001), epicardial myocardium with its higher levels of RLC phosphorylation would produce more force and exhibit accelerated stretch activation with diminished amplitude compared with endocardial myocardium. Therefore, with endocardial fibers arranged in a right-handed helical formation and epicardial fibers in an opposing left-handed helical formation (Streeter *et al.*, 1969), ventricular torsional twist during systole proceeds in the direction of the epicardial fibers (Epstein and Davis, 2006), such that the endocardium is forcibly strained by epicardial fibers to produce delayed stretch activation of the endocardium. Indeed, recent evidence shows that despite being activated first, the endocardium is actively stretched by the epicardium later in systole (Buckberg *et al.*, 2006). Thus, the phosphorylation state of RLC is a determinant of the stretch activation response of myocardium and thereby appears to contribute to work production during ventricular systole. Furthermore, the findings that RLC phosphorylation levels are decreased in end-stage human heart failure suggest that the timing of force generation and work production is disrupted and contributes to depressed systolic function in this disease (Stelzer *et al.*, 2006a)

#### **1.9.3.2 TITIN**

##### **1.9.3.2.1 Phosphorylation of I-band Titin**

PKA-driven phosphorylation of titin increases the functional length of the N2B element (Section 1.6.2), which is expressed only in cardiac muscle titin, resulting in less fractional extension at a given sarcomere

length (Yamasaki *et al.*, 2002). This coincides with a significant decrease in passive tension in skinned rat cardiac myocytes (Yamasaki *et al.*, 2002). These findings were confirmed by Fukuda *et al* (2005), who showed that PKA also phosphorylates N2BA titin, in intact and skinned right ventricular trabeculae treated with isoproterenol. Further, myocardial compliance was also increased (i.e., passive force is decreased) upon  $\beta$ -adrenergic stimulation and the effect was titin isoform dependent (i.e., greater in muscles that express N2B titin at higher levels). Additionally, Yamaski *et al* (2002) reported that  $\beta$ -adrenergic agonists stimulated, whereas antagonists depressed, titin phosphorylation. Thus, the PKA-responsive element of cardiac titin may allow for more rapid and complete cardiac chamber filling during  $\beta$ -adrenergic stimulation, modulating diastolic function (Yamaski *et al.*, 2002). Ultrastructural analysis of a knockout mouse model in which the N2B region of titin was deleted showed that the extension of the remaining spring elements of titin (tandem Ig segments and PEVK region; Section 1.6.2) were increased. These findings, together with reduced sarcomere length and increased passive tension derived from the skinned cardiomyocytes experiments, suggested that the N2B region is important for preventing diastolic dysfunction (Radke *et al.*, 2007).

#### 1.9.3.2.2 Titin kinase

In addition to the N2B sequence of titin, the titin kinase domain (TK) is also phosphorylated by an, as yet, unidentified tyrosine kinase (Mayans *et al.*, 1998). TK is a globular mixed  $\alpha/\beta$  protein with two structural domains, viz. a catalytic domain and a regulatory domain that inhibits the former domain's activity. Unlike other kinases, in which the activation segment undergoes a switch from a “closed” to an “open” conformation after phosphorylation, the activation segment of TK is in an “open” conformation in the autoinhibited structure. The crystal structure of autoinhibited TK (Figure 1.10) shows how a tyrosine (Tyr-170) of the P+1 loop inhibits the active site: The  $\alpha$ R2 helix of the regulatory tail binds to the kinase ATP-binding site in the catalytic domain, thus blocking access of its protein substrate and inhibiting catalysis, while the C-terminus part of the regulatory tail ( $\beta$ R1) forms a  $\beta$ -sheet with  $\beta$ C10 and  $\beta$ C11 of the catalytic domain. Activation of TK is achieved by a dual mechanism; the first step occurs upon phosphorylation of Tyr-170 by an unknown tyrosine kinase. The regulatory C-terminus tail is then removed from the ATP-binding site by  $\text{Ca}^{2+}$ /calmodulin-binding to  $\alpha$ R1 (the N-terminus  $\alpha$ -helix of the regulatory tail), resulting in TK activation. This novel dual autoregulatory mechanism is likely to provide tight control for TK activity during muscle differentiation (Mayans *et al.*, 1998).

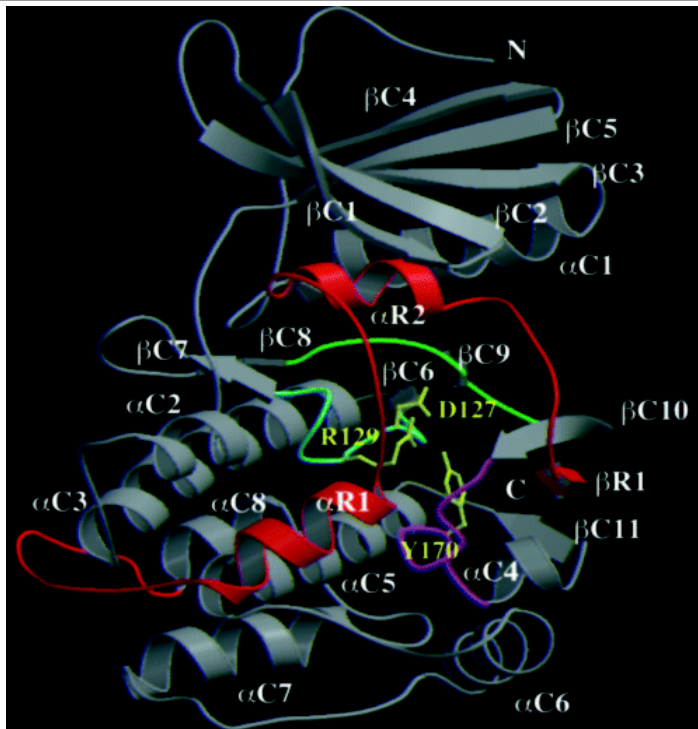


**Figure 1.10.** The three-dimensional ribbon structure of the autoinhibited form of titin kinase. Red, regulatory tail; cyan, catalytic loop; green, activation segment; magenta, P+1 loop. The side chains of residues D127, R129 and Y170 are highlighted in yellow. The autoinhibited TK shows how Tyr-170 of the P+1 loop inhibits the active site. The αR2 helix binds to the kinase ATP-binding site and specifically interacts with the residues involved in catalysis while the C-terminus part of the regulatory tail, βR1, forms a β-sheet with βC10 and βC11. TK activation therefore requires release of autoinhibition, in particular the removal of autoinhibitory tail from the active site upon phosphorylation of Tyr170 and Ca<sup>2+</sup>/calmodulin-binding to the N-terminus αR1 helix (Mayans *et al.*, 1998). Image taken from (Mayans *et al.* 1998).

#### 1.9.3.2.2.1 Function of TK

Titin has been proposed to act as a template for sarcomere assembly and, specifically, the phosphorylation of T-cap by TK in differentiating muscle cells has been shown to influence myofibrillogenesis *in vitro* (Mayans *et al.*, 1998). TK interacts with various proteins involved in muscle gene expression, signalling and ubiquitin-controlled protein turnover (Centner *et al.*, 2001; described in section 1.7.3.1 and 1.6.4) thus, it appears that the TK-associated protein complex may act as a central switchboard where input from various pathways leading to hypertrophy, stress response and protein turnover links the sarcomere to mechanical modulation of muscle gene transcription (Lange *et al.*, 2005).

To elucidate the function of TK in myofibrillogenesis and cardiac function, a number of studies using the gene knockout approach have been performed (Gotthardt *et al.*, 2003; Weinert *et al.*, 2006; Musa *et al.*, 2006; Peng *et al.*, 2007). By conditionally deleting the TK region (exons MEx1 and MEx2) at different stages of embryonic development in a mouse model, Gotthardt *et al* (2003) reported that excision of this region in early cardiac development resulted in embryonic lethality, while postnatal excision lead to the disruption of M-line titin, skeletal muscle weakness and death at ~5 weeks of age. Myopathic changes included pale M-lines devoid of MURF1, and while these sarcomeres incorporated mutant titin, they

eventually disassembled. Thus, the segment of the M-line including TK is crucial for maintaining structural integrity of the sarcomere (Gotthardt *et al.*, 2003). This conclusion was confirmed by another study in mice using a constitutive knockout approach to investigate the role of the same region (Weinert *et al.*, 2006). The TK region of titin was shown to be dispensable for initial sarcomere assembly, but knockout myofibrils failed to grow laterally and eventually disassembled. Unlike in the adult knockout sarcomere, TK-deficient titin did not integrate into the A-band of embryonic knockouts, and thus failed to form a continuous filament system. The failure to cross-link proteins in this region resulted in increased mobility of C-terminus titin, leading to reduced sarcomeric stability and sarcomere disassembly. Titin's M-line region is thus required to form a continuous titin filament and to provide mechanical stability to the embryonic sarcomere (Weinert *et al.*, 2006). The induction of TK deficiency in the hearts of adult mice resulted in cardiac hypertrophy, reduced contractile response to  $\beta$ -adrenergic agonists and extracellular  $\text{Ca}^{2+}$  (Peng *et al.*, 2007). Further, expression analysis showed reduced levels of calmodulin, phospholamban and SERCA2a in knockout mice. The authors speculated that the mechanism underlying the phenotype of the knockout mice involved calmodulin, since it activates TK and also participates in  $\text{Ca}^{2+}$  release of the SR by regulating the activity of SERCA2a and phospholamban through CamK-II ( $\text{Ca}^{2+}$ /calmodulin-dependent kinase). Thus, the TK region directly affects contractile function at the level of intracellular  $\text{Ca}^{2+}$  handling (Peng *et al.*, 2007).

A gene-targeting approach to investigate the role of M-line titin in early sarcomere development by generating heterozygous and homozygous deletions of the entire M-line titin in mouse embryonic cardiac stem cells showed that heterozygous stem cells differentiated into cardiomyocytes, with very little detrimental effect of the Z-disc or M-line organisation, while homozygous stem cells did not differentiate beyond an early stage of myofibrillogenesis. Immunofluorescence assays of undifferentiated cells showed that sarcomeric myosin remained in non-striated structures, Z-disc structures were mainly found in primitive dot-like structures on actin stress fibers and M-line-associated proteins remained punctate. These results showed that the integration of M-line titin is required for myosin filament assembly, M-line formation and maturation of the Z-disc, suggesting that the entire region must be intact for sarcomere assembly (Musa *et al.*, 2006).

### 1.9.3.3 PHOSPHOLAMBAN

The activity of the ATP-driven  $\text{Ca}^{2+}$  pump (SERCA2a) is regulated by phospholamban (PLB; ~25-28 kDa) which, in the dephosphorylated form, decreases the  $\text{Ca}^{2+}$ -affinity of SERCA2a (James *et al.*, 1989). This inhibitory effect is relieved by high cytosolic  $\text{Ca}^{2+}$  and partially relieved by phosphorylation of PLB. PLB is the principal mediator of  $\beta$ -adrenergic responses in the heart and its phosphorylation can increase the SERCA2a pump activity (Matiazzi *et al.*, 2005). PLB is expressed in higher levels in cardiac muscle than smooth and slow-twitch skeletal muscle, while it has not been identified in fast skeletal muscle (Periasamy *et al.*, 2007). PLB has three structural domains (Figure 1.11A): the cytoplasmic domain IA (residues 1-20; which contains the three phosphorylation sites), cytoplasmic domain IB (residues 21-30) and the hydrophobic transmembrane domain II (residues 31-52) (Bhupathy *et al.*, 2007).

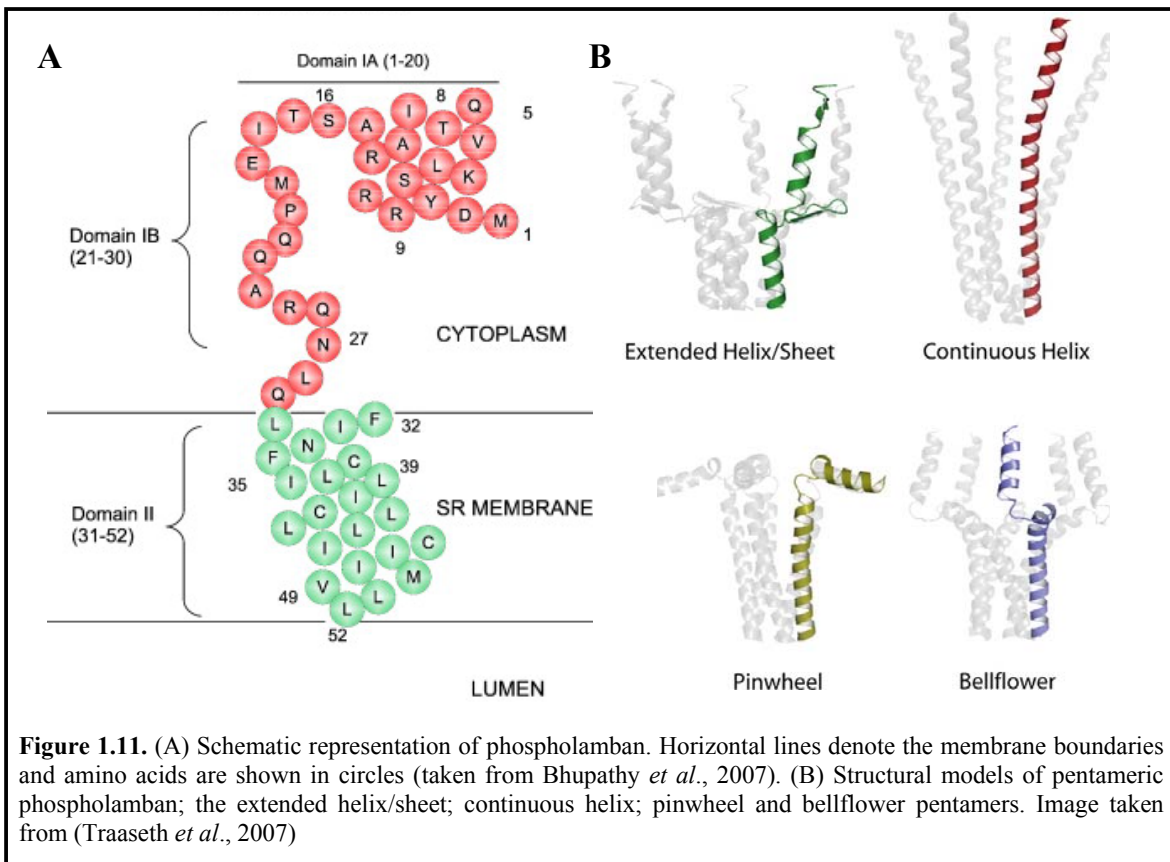


**Figure 1.11.** (A) Schematic representation of phospholamban. Horizontal lines denote the membrane boundaries and amino acids are shown in circles (taken from Bhupathy *et al.*, 2007). (B) Structural models of pentameric phospholamban; the extended helix/sheet; continuous helix; pinwheel and bellflower pentamers. Image taken from (Traaseth *et al.*, 2007)

In the cardiac SR, PLB exists both as pentamers and as monomers. There are four principal proposed structural models of pentameric PLB: an extended helix/sheet model, a continuous model, a pinwheel model and the bellflower model (Figure 1.11B). These models differ primarily in the topology of the dynamic cytoplasmic domain. The predominant conformation of the monomer is L-shaped, with the cytoplasmic domain in contact with the surface of the lipid bilayer (Traaseth *et al.*, 2007). Several studies have shown that equilibrium exists between the monomeric and pentameric states and that phosphorylation shifts the equilibrium in favour of the pentameric form (Kadambi and Kranias, 1997). However, shifting the pentamer/monomer ratio toward the monomer form can increase inhibition of the pump and such an increasing SERCA2a:PLB ratio is associated with depolymerisation of the pentameric PLB. This suggests that it is the monomer form that is the active species, and that the PLB:PLB and PLB:SERCA2a interactions act as inter-dependent, balanced equilibria (Robia *et al.*, 2007). On the other hand, over-expression of a monomeric mutant PLB in the heart of PLB knockout mice led to reduced inhibition of cardiac relaxation compared to a similar level expression of WT PLB, suggesting that pentameric assembly of PLB may enhance the inhibitory effect (Chu *et al.*, 1998). Thus, it remains unclear whether the monomeric or pentameric state of PLB is a more effective inhibitory unit of PLB for SERCA2a (Hagemann and Xiao, 2002).

### **1.9.3.3.1 Phosphorylation of phospholamban**

The flexible N-terminus of cardiac PLB can be phosphorylated at three distinct sites: Ser16 by PKA, Thr17 by CamK-II, and Ser10 by PKC, although phosphorylation at this latter site is not physiologically relevant (Edes and Kranias, 1990). Phosphorylation at the other two sites occurs in a sequential fashion, with phosphorylation at Ser16, which is mainly responsible for the  $\beta$ -adrenergic receptor-mediated cardiac relaxant effect, being a prerequisite for phosphorylation of Thr17. Additionally, Ser16 and Thr17 can be phosphorylated independently. Phosphorylation of Thr17 has been implicated in the frequency-dependent acceleration of relaxation and may act as a cardiac beat-to-beat frequency-decoder (Hagemann and Xiao, 2002). The status of PLB phosphorylation is also dependent on the activity of the type I phosphatase that dephosphorylates PLB, leading to the inhibition of SERCA2a (MacDougall *et al.*, 1991).

The unphosphorylated PLB is believed to interact with and reduce the activity of SERCA2a, thus acting as a “brake” on  $\text{Ca}^{2+}$  re-uptake. Inhibition of this pump, by PLB phosphorylation, disrupts the physical interaction of PLB with SERCA2a and thus stimulates SR  $\text{Ca}^{2+}$  transport by increasing the affinity of the SERCA2a for  $\text{Ca}^{2+}$ , without a significant change in  $V_{\max}$  (Periasamy *et al.*, 2007). This leads to an increase in the velocity of relaxation, SR  $\text{Ca}^{2+}$  load and, as a consequence, subsequent SR  $\text{Ca}^{2+}$  release and myocardial contractility. Thus, the regulation of SERCA2a by PLB is considered to be the primary mechanism for  $\beta$ -adrenergic-mediated response of the heart, and PLB phosphorylation the mechanism for enhanced  $\text{Ca}^{2+}$  transport by the SR (Periasamy *et al.*, 2007).

$\text{Ca}^{2+}$  and PLB phosphorylation may alter the quaternary structure of the SERCA2a-PLB regulatory complex, either by complete dissociation of PLB from the pump or by more subtle structural changes (Robia *et al.*, 2007). PLB is an active inhibitor only if the net charge in domain IA is +1 or +2. The charge in the corresponding interacting sequence of SERCA2a is also important in the interaction. Thus, the reduction of net charge to -2 or less by phosphorylation of Ser16 or Thr17 has a deleterious effect on PLB function. Phosphorylation of Ser16 has been shown to alter the accessibility of PLB to proteinases, implying that conformational change must occur in the cytoplasmic part of PLB. Conformational changes that occur after phosphorylation have been supported by circular dichroism analysis. These conformational changes may also affect the functional interaction between PLB and SERCA2a (Tada, 2003).

### **1.9.3.3.2 Regulation of basal myocardial contractility by PLB**

Phospholamban-deficient mice appeared healthy, grew normally without any developmental defects, and were fertile (Luo *et al.*, 1994). However, they exhibited significantly enhanced myocardial performance compared to WT controls as assessed in work-performing heart preparations. They differed markedly in their contractile parameters, as characterised by significant increases of the maximal rates of pressure development ( $+dP/dt$ ) and shortening in the time to peak pressure and time to half-relaxation. The hyperdynamic state of cardiac function in PLB-deficient mice was closely associated with an increase in the affinity of SERCA2a for  $\text{Ca}^{2+}$ , but was not accompanied by alterations in heart rate or heart weight. These data suggests that PLB is

an important determinant of basal contractility in the mammalian heart (Luo *et al.*, 1994). However, while the loss of PLB in mice is well tolerated, the ablation of PLB in humans by genetic mutations results in dilated cardiomyopathy (DCM) and death (Ha *et al.*, 2007).

The adaptive cellular alterations associated with ablation of the PLB gene and enhanced myocardial contractility in a mouse model included decreased ryanodine receptor levels and metabolic alterations in myocardial energetics (Chu *et al.*, 1996). Histopathological and morphological examinations revealed no abnormalities, and the expression levels of the other SR  $\text{Ca}^{2+}$ -cycling and contractile proteins were similar in knockout and WT hearts. Thus, the augmentation of contractile parameters is mainly due to the "uninhibited" SERCA2a activity as a result of PLB ablation. The down-regulation of the ryanodine receptors indicated a cross-talk between SR  $\text{Ca}^{2+}$  uptake and  $\text{Ca}^{2+}$  release in an attempt to maintain proper  $\text{Ca}^{2+}$  homeostasis in the myocardium, whereas the metabolic alterations indicated a cross-talk between ATP synthesis and utilisation in an attempt to maintain the increased contractile performance (Chu *et al.*, 1996). These findings were substantiated by *in vitro* analyses of isolated ventricular cardiomyocytes from PLB-deficient hearts, which also exhibited enhancement of the rates of re-lengthening, shortening, and  $\text{Ca}^{2+}$  kinetics (Wolska *et al.*, 1996). The enhanced contractile parameters reflected subcellular alterations at the cardiac SR level. SERCA2a affinity for  $\text{Ca}^{2+}$  was significantly increased, and this was associated with increased intra-luminal cardiac SR  $\text{Ca}^{2+}$  content in the PLB-deficient hearts compared with WT hearts (Luo *et al.*, 1994).

Taken together, these studies in genetically altered mice indicate that ablation of the PLB gene leads to enhanced rates of SR  $\text{Ca}^{2+}$  uptake (resulting in increased rates of myocardial relaxation) and consequently larger amounts of SR  $\text{Ca}^{2+}$  available for release (resulting in increased rates of contraction). These findings suggest that PLB is an important determinant of basal contractility in the mammalian heart and that PLB can play a prominent role in mediating the heart's contractile responses to  $\beta$ -adrenergic stimulation (Koss and Kranias, 1996).

#### 1.9.3.4 TROPONINS

##### 1.9.3.4.1 Cardiac Troponin I (cTNI)

Protein-protein interactions inside the troponin complex are controlled not only by  $\text{Ca}^{2+}$ , but are modulated by cTNI phosphorylation as well. The primary phosphorylation sites within human cTNI are Ser23/Ser24, Ser43/Ser45, and Thr144 (Noland *et al.*, 1989). The first two are located in the cardiac-specific N-terminus region and are substrates for PKA and PKC, while Ser43/Ser45 and Thr144 are substrates for PKC. Under *in vitro* conditions, TNI can also be phosphorylated by cGMP-dependent protein kinase (PKG) (Lindhout *et al.*, 2005). PKG is expressed at a low abundance in the heart, can phosphorylate Ser23/24, and although at a 100 times slower rate than PKA, has similar effects to those of PKA (Layland *et al.*, 2005). In addition, phosphorylation of Ser150 by p21-activated kinase 1 induces an increase in  $\text{Ca}^{2+}$ -sensitivity; however the physiological significance of this phosphorylation is poorly understood (Buscemi *et al.*, 2002). As a result, the following sections describe the effect of only PKA and PKC phosphorylation on cTNI.

#### **1.9.3.4.1.1 Phosphorylation by PKA**

In response to  $\beta$ -adrenergic stimulation of the heart (Section 1.9.3), there exists an ordered sequential phosphorylation of Ser23/24 both *in vivo* and *in vitro*; Ser24 may be preferentially phosphorylated, followed by phosphorylation at Ser23 only after phosphorylation at Ser24 is almost completed. It is suggested that Ser24 may be constitutively phosphorylated while the phosphorylation of Ser23 may be functionally more important (Keane *et al.*, 1997). Consistently, the phosphorylation of Ser23 extended and stabilised the C-terminus  $\alpha$ -helix of the NcTNI through electrostatic interactions (Howarth *et al.*, 2007).

Direct interaction between NcTNI and NcTNC influences the conformational exchange in the regulatory domain of cTNI by shifting the equilibrium to favour an “open” conformation that exposes the hydrophobic cleft as described in section 1.9.2 (Li *et al.*, 2004). Phosphorylation of Ser23/24 disrupts the contact between these domains, shifting the conformational equilibrium in NcTNC towards a more “closed” state (Figure 1.12). This hypothesis was confirmed by Sakthivel *et al* (2005), who showed that the  $\text{Ca}^{2+}$ -induced open conformation of NcTNC adopted a partially closed structure in the complex when PKA phosphorylation of cTNI was mimicked (cTNI-PP; Ser23/24; Ser mutated to aspartic acid), and this partially closed conformation became more closed in the presence of both PKA and PKC phosphorylation-mimics of cTNI (cTNI-A//P; Ser23/24, Ser43/45, Thr144; Ser mutated to aspartic acid). However, findings by Dong *et al* (2007), using steady-state and time-resolved fluorescence resonance energy transfer studies, showed that the conformation of NcTNC is not affected by TNI phosphorylation. Rather, cTNI phosphorylation affects the  $\text{Ca}^{2+}$ -sensitivity and modifies the kinetics of the opening and closing of NcTNC (Dong *et al.*, 2007). While the PKA cTNI phosphorylation-induced effect on the conformation of NcTNC is still controversial, there is consensus that cTNI phosphorylation of Ser23/24 results in significant changes in the cTNI structure. Fluorescence resonance energy transfer studies suggested that cTNI adopted a more compact conformation when Ser23/24 were phosphorylated (Dong *et al.*, 1997) and this conclusion has been supported by a surface plasmon resonance study (Reiffert *et al.*, 1998) and nuclear magnetic resonance analyses (Sakthivel *et al.*, 2005).

Further, phosphorylation of cTNI Ser23/24 reportedly weakened interactions with NcTNC and re-positioned the acidic NcTNI for favourable interactions with the basic residues within the inhibitory region of cTNI (Howarth *et al.*, 2007). This acidic NcTNI does not, however, play a direct role in the  $\text{Ca}^{2+}$ -induced transition in the cardiac regulatory or NcTnC but may compete with actin for the inhibitory region of cTNI. Deletion of the acidic N-terminus in TG mice resulted in a decrease in myocardial contractility at baseline and upon  $\beta$ -adrenergic stimulation (Sadayappan *et al.*, 2008). Although the deletion alters conformational states of cTNI and results in decreased contractile function, it is not lethal and does not affect the heart adversely (Sadayappan *et al.*, 2008).

Based on these observations a molecular mechanism for the physiological consequences of PKA phosphorylation at Ser23/24 was proposed (Solaro *et al.*, 2008). The first step involves the N-terminus

interactions between cTNI and cTNC which affects the  $\text{Ca}^{2+}$ -sensitivity. PKA phosphorylation of Ser23/24 of cTNI forms the second step with the weakening of interactions between cTNI and cTNC, resulting in a bending of the acidic NcTNI. The acidic N-terminus then interacts with the inhibitory region of cTNI, weakening the interaction of the inhibitory region with actin and altering crossbridge reactions (Sakthivel *et al.*, 2005). This model can also be extended to provide a molecular understanding of PKC phosphorylation of cTNI at Ser43/45 and Thr144 (Solaro *et al.*, 2008) (Section 1.9.3.4.1.3).

#### 1.9.3.4.1.2 Effect of PKA phosphorylation

The phosphorylation of Ser23/24 by PKA results in a reduction in myofilament  $\text{Ca}^{2+}$ -sensitivity (Abbott *et al.*, 2001; Ward *et al.*, 2002) and an increase in crossbridge cycling rate (Kentish *et al.*, 2001) by reducing the  $\text{Ca}^{2+}$ -binding affinity of cTNC and allowing fine tuning of contractile function (Sakthivel *et al.*, 2005). The decreased myofibrillar  $\text{Ca}^{2+}$ -sensitivity and increased rate at which  $\text{Ca}^{2+}$  dissociates from TNC leads to faster relaxation by increasing the rate of thin filament deactivation (Section 1.9.2). This enhanced relaxation, in conjunction with increased  $\text{Ca}^{2+}$  re-uptake into the sarcoplasmic reticulum, may help maintain proper diastolic function at increased heart rates (Ward *et al.*, 2002).

Findings from animal studies support the hypothesis that phosphorylation of cTNI significantly contributes to the enhanced rate of relaxation during  $\beta$ -adrenergic stimulation. TG mice expressing ssTNI, which cannot be phosphorylated by PKA, showed a significant decrease in the rate of relaxation and depressed effects of  $\beta$ -adrenergic stimulation when compared to hearts expressing cTNI (Fentzke *et al.*, 1999; Peña and Wolska, 2004). Further, Barbato *et al* (2005) showed in isolated working heart experiments that over-expression of N-terminus truncated cTNI (cTNI-ND; residues 1-28 deleted) resulted in significantly faster rate of relaxation and lower left ventricular end diastolic pressure compared with controls. The higher baseline relaxation rate of cTNI-ND hearts were at a level similar to that of WT hearts under  $\beta$ -adrenergic stimulation. The decrease in cardiac output due to lowered preload was significantly smaller for cTNI-ND hearts compared with controls. Thus, deletion of the N-terminus cTNI in the cTNI-ND mice mimicked the effect of the phosphorylated state, indicating that these residues are required to maintain the first step of the phosphorylation switch (Barbato *et al.*, 2005).

Further, mutation of Ser23/24 to express a phosphorylated cTNI mimic (Ser23/24 were mutated to aspartic acid; cTNI-PP) in TG mice showed enhanced diastolic function under basal conditions, augmented relaxation and contraction at higher heart rates compared with non-TG controls (Sakthivel *et al.*, 2005). Takimoto *et al* (2004) also showed that TG mice expressing cTNI-PP showed rate-dependent enhanced basal systolic and diastolic function, and displayed marked augmentation of frequency-dependent inotropy and relaxation. In addition, increased afterload prolonged relaxation in non-TG than cTNI-PP mice. Isoproterenol treatment eliminated the differential force-frequency and after load response between cTNI-PP and controls. These results suggest that cTNI PKA phosphorylation plays a role in the rate-dependent enhancement of systolic and diastolic function *in vivo* and afterload sensitivity of relaxation (Takimoto *et al.*, 2004).

The cross-bridge cycle can also play a major role in determining the intrinsic rate of relaxation as shown by Kentish *et al* (2001). Faster relaxation kinetics are observed from PKA-mediated phosphorylation of TnI as a result of accelerated cross-bridge kinetics, with isolated cardiac muscle showing an almost 2-fold increase in intrinsic relaxation rate after PKA treatment, whereas muscle in which a non-phosphorylatable slow skeletal muscle isoform had partially replaced cTnI were unaffected (Kentish *et al.*, 2001).

Stelzer *et al* (2007) further emphasised the role of phosphorylation of cTNI in the relaxant effect of  $\beta$ -adrenergic stimulation by showing that the primary effect of PKA phosphorylation of cTNI was the reduction of  $\text{Ca}^{2+}$ -sensitivity of force. This function appears to be mediated by the N-terminus as the transfer of an N-terminus-cardiac/slow skeletal-C-terminus TNI fragment into adult rat myocytes was able to decrease the  $\text{Ca}^{2+}$ -sensitivity of tension comparable in magnitude to controls, while the N-terminus-slow skeletal/cardiac-C-terminus TNI fragment did not influence  $\text{Ca}^{2+}$ -activated tension upon PKA phosphorylation (Westfall *et al.*, 2001). Further, Barbato *et al* (2005) showed that over-expression of N-terminus truncated cTNI (cTNI-ND; residues 1-28 deleted) resulted in decreased  $\text{Ca}^{2+}$ -sensitivity of myofibrils in TG mice compared with the controls and similar to the effect of isoproterenol treatment.

Neither the deletion of N-terminus residues of cTNI (Barbato *et al.*, 2005) nor replacement of cTNI with ssTNI (Fentzke *et al.*, 1999) adversely affected the TG mice. Mice in these studies were viable, fertile and exhibited normal ventricular weights and heart rates. These findings contrast the study by Pi *et al* (2002) where the expression of non-phosphorylatable cTNI (in which all five phosphorylation sites were mutated to alanines) in TG mice showed dilated cardiomyopathy, suggesting that the inability of cTNI to be phosphorylated can result in cardiac pathology.

#### 1.9.3.4.1.3 Phosphorylation by PKC

Ser43/45 and Thr144 are substrates mainly for PKC phosphorylation, however, substrate specificity of these sites are not absolute, since PKC can phosphorylate the PKA sites (Noland *et al.*, 1996). The  $\delta$ -isoform of PKC predominantly phosphorylates Ser23/24 (including Ser43/45), the  $\alpha$ - and  $\epsilon$ -isoforms predominantly phosphorylates Ser43/45 of TNI, while the  $\xi$ -isoform phosphorylates TNI poorly (Filatov *et al.*, 1999).

The physiological consequences of PKC phosphorylation was extended from that proposed for PKA phosphorylation (Solaro *et al.*, 2008) (Section 1.9.3.4.1.1). Phosphorylation at Ser43/45 is known to decrease maximal actomyosin ATPase activity and  $\text{Ca}^{2+}$ -sensitivity by stabilising the inactive state of the thin filament (Solaro *et al.*, 2008). The introduction of negative charges at Ser43/45 (by mutating Ser residues to aspartic acid), located on the N-terminus near the interaction site with the C-terminus cTNC, results in an extension and stabilisation of the N-terminus domain helix. This alters the properties at the neighbouring hinge region, required for PKA phosphorylation-dependent bending of NcTNI (Burkart *et al.*, 2003). Thus, PKC phosphorylation at Ser43/45 would decrease mobility of the hinge region of cTNI and have opposite effects on  $\text{Ca}^{2+}$ -sensitivity and crossbridge formation. PKC is also responsible for phosphorylation at Thr144; the

introduction of a negative charge at Thr144, upon phosphorylation, would be predicted to decrease electrostatic interactions between the inhibitory region and both NcTNI and actin. The end result would be the stabilisation of a more extended structure, resulting in an increase in crossbridge kinetics (Solaro *et al.*, 2008). Consistent with this hypothesis, introduction of negative charge at Thr144 (by mutating Thr residue to aspartic acid) appeared to potentiate the effects of PKA phosphorylation at Ser23/24 in a TG mouse model (Sakthivel *et al.*, 2005).

#### **1.9.3.4.1.4. Effect of PKC phosphorylation**

Whereas PKA-mediated phosphorylation is thought to mainly affect the overall  $\text{Ca}^{2+}$ -sensitivity of force development, PKC phosphorylation (Ser43/45) of cTNI inhibits the actomyosin interaction by decreasing maximum tension, ATPase activity (Pi *et al.*, 2003),  $\text{Ca}^{2+}$ -sensitivity and, in concert with Thr144 phosphorylation, reduces thin filament sliding speed (Burkart *et al.*, 2003).

The replacement of approximately 50% endogenous cTNI with non-phosphorylatable cTNI (Ser43/45 phosphorylation sites mutated to alanines) in TG mice did not significantly alter cardiac morphology or function. However, activation of PKC resulted in elevated pressures and a significant delay in the  $\text{Ca}^{2+}$  transient in TG versus WT hearts (MacGowan *et al.*, 2001). The negative inotropic response to agonist-mediated PKC activation in TG mice was also significantly blunted in comparison to WT mice (Montgomery *et al.*, 2002). These results suggested that cTNI phosphorylation by PKC decreases myofilament  $\text{Ca}^{2+}$ -sensitivity and maximum tension. In another TG mouse model, myocytes expressing non-phosphorylatable cTNI (Ser23/24, Ser43/45 and Thr144 mutated to alanine) responded to endothelin treatment by an increase in twitch duration and relaxation time constant compared to WT controls treated with isoproterenol (Pi *et al.*, 2002). These results provide evidence that cTNI phosphorylation by PKC also delays relaxation (Pi *et al.*, 2002).

Further, PKC phosphorylation has been shown to antagonise the effects of PKA-induced cTNI phosphorylation in the whole animal as reported by Sakthivel *et al* (2005). TG mice expressing cTNI with the PKA phosphorylation sites (Ser23/Ser24) mutated to aspartic acid showed enhanced diastolic function under basal conditions, compared to TG mice expressing cTNI mimicking a constant state of complete phosphorylation (cTNI-A//P). There was also a significant decrease in contractility in the cTNI-A//P animals which was not apparent in cTNI-PP. Thus, the primary *in vivo* function of PKC-mediated cTNI phosphorylation is to decrease contractility and to exert an antagonistic role on the ability of PKA to increase relaxation (Sakthivel *et al.*, 2005).

#### **1.9.3.4.2 Cardiac Troponin T (cTNT)**

##### **1.9.3.4.2.1 Phosphorylation by PKC**

TNT is phosphorylated by PKC, not PKA, and *in vitro* studies demonstrate that there are four main sites for PKC-dependent phosphorylation on cTNT in the human sequence (Thr194, Ser198, Thr203 and Thr284)

(Jideama *et al.*, 1996). All of these phosphorylation sites lie within the proposed IT-arm region of the troponin core domain (Section 1.1.3.2), which is postulated to play an important role in  $\text{Ca}^{2+}$  regulation of the troponin regulatory core domain as it undergoes hypothesised conformational changes (Section 1.9.2). Phosphorylation sites within this domain could, therefore, be important for modulating core domain movement in response to  $\text{Ca}^{2+}$  activation (Metzger and Westfall, 2004). Phosphorylation of TNT is proposed to result in the weakening of the interactions of TNT with TM, TNI and possibly TNC, while still allowing full inhibition by TNI of the ATPase activity in the absence of  $\text{Ca}^{2+}$  (Noland and Kuo, 1992). Since TNT bound to Tn-actin is also required for full activation of ATPase activity in the presence of  $\text{Ca}^{2+}$ , weakened interactions of phosphorylated TNT with TNI, TM and TNC would not affect the binding of TNC- $\text{Ca}^{2+}$  to TNI, yet would hinder the detachment of TNI from actin. Thus, full movement of TM into the helical groove of actin would be prevented, leading to attenuation of the  $\text{Ca}^{2+}$ -stimulated ATPase activity or to partial activation. This suggestion is consistent with findings that show that phosphorylated TNT, under a variety of conditions, decrease  $\text{Ca}^{2+}$ -stimulated actomyosin ATPase activity and that, in the absence or presence of TNC and TNI, phosphorylated TNT demonstrated decreased maximal binding to, and affinity for, TM-actin (Noland and Kuo, 1992).

Replacement of half the endogenous cTNT with non-phosphorylatable skeletal TNT in transgenic mice blunted the ability of a phorbol ester analog to reduce maximum tension (Montgomery *et al.*, 2001). This study suggests that PKC-mediated phosphorylation of cTNT acts to inhibit maximum force generation in the myocardium. However, cTNT phosphorylation is considerably lower compared with cTNI phosphorylation (Jideama *et al.*, 1996) and acute activation of PKC by several physiological agonists does not noticeably alter cTNT phosphorylation (Pi *et al.*, 1997). Thus, it may be that cTNT phosphorylation develops during more chronic PKC activation and could play an important role during pathophysiological conditions associated with increased PKC isoform expression, such as myocardial ischaemia (Metzger and Westfall, 2004).

### 1.9.3.5 CARDIAC MYOSIN-BINDING PROTEIN C

#### 1.9.3.5.1 Structure

Myosin-binding protein C (MyBPC) was discovered in the early 1970's (Starr and Offer, 1971), yet more than 30 years later its structural and functional roles are still being solved. MyBPC is a sarcomeric protein associated with the thick filament of striated muscle. It is located in the C-zone of the A-band (Figure 1.1) in a structurally regular pattern of seven to nine, 43nm-apart, transverse stripes (Flashman *et al.*, 2004). The 43nm spacing of these stripes dictates that only every third level of myosin heads in the C-zone is associated with a cMyBPC molecule. This and the number of myosin heads that fall outside the C-zone, limit the number of myosin heads that can interact directly with cMyBPC (Oakley, 2004). Each stripe is composed of two to four MyBPC molecules and represents about two percent of the protein mass in the myofibril. The core structure of MyBPC comprises seven Ig domains and three FNIII domains, numbered from the N-terminus as domains 1-10 (C1-C10) in skeletal muscle (Oakley *et al.*, 2004; Flashman *et al.*, 2004).

#### **1.9.3.5.2 Isoforms**

Three isoforms encoded by three distinct genes, fast skeletal (fsMyBPC; ~128 kDa), slow skeletal (ssMyBPC; originally described as MyBPX; ~128 kDa), and cardiac muscle type (cMyBPC; ~137 kDa) have been identified (Flashman *et al.*, 2004). Myocardial cells were thought to contain only the cardiac isoform throughout development and in the adult (Gautel *et al.*, 1998), but ssMyBPC is also present in moderate amounts in the right atrium and interatrial septum of adult human heart muscle (Dhoot and Perry, 2005). Although the three isoforms share a similar structure consisting of several Ig and FNIII domains and a myosin-binding site in its C-terminus domain, the cardiac isoform has three distinguishing structural differences from the skeletal isoforms. Firstly, the cardiac isoform has an extra 101 amino acid Ig domain at the N-terminus (C0). Secondly, there is a proline-rich insert in the central C5 Ig domain and finally, two additional phosphorylation sites are found in the ~100 amino acid region (the MyBPC motif) that links Ig domains C1 and C2. There is also a cardiac specific LAGGGRRIS loop insertion in the cMyBPC motif which introduces the phosphorylation sites that allows the other sites to then be phosphorylated (Section 1.9.3.5.9.2) The number of phosphorylation sites appears to differ between species, but the cardiac isoform consistently has more sites, usually three (Oakley *et al.*, 2007). The cMyBPC motif had been considered to be unstructured, but recent small-angle X-ray scattering data revealed that the cMyBPC motif in the unphosphorylated state was compact and had dimensions consistent with the Ig superfamily of proteins (Jeffries *et al.*, 2008).

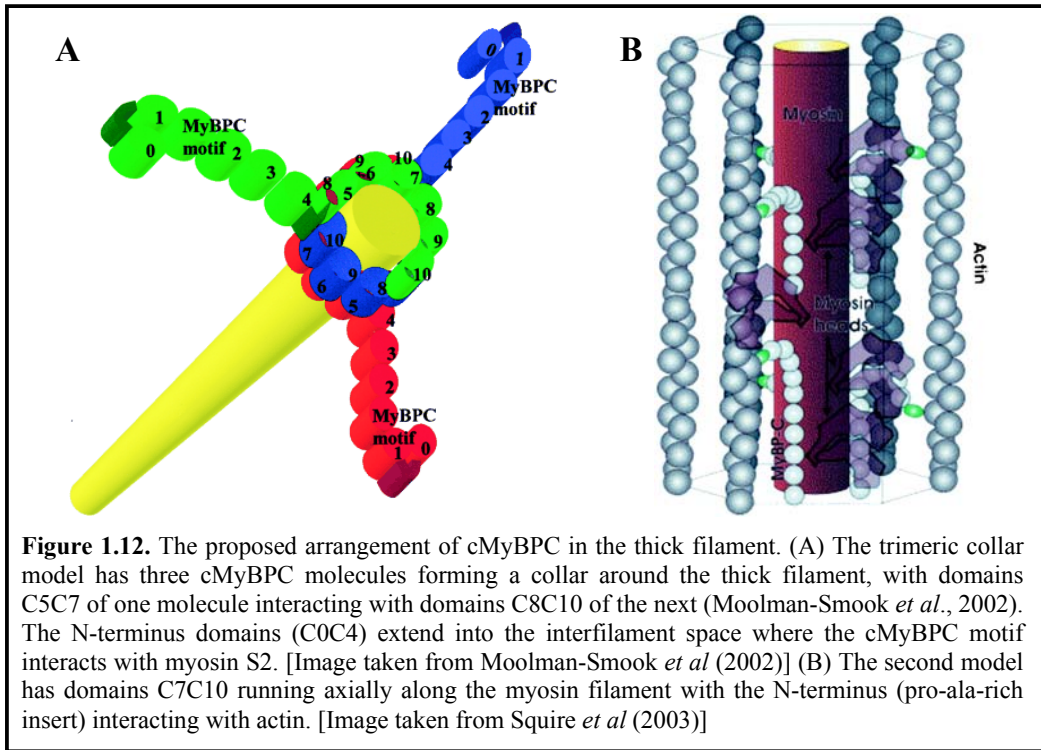
#### **1.9.3.5.3 Other MyBPC's**

MyBPH is located in the A-band of the sarcomere and binds to myosin, restricted to a series of transverse stripes (43nm apart) in the C-and P-zones of the thick filament (Winegrad, 1999). In skeletal muscle, MyBPH is principally associated with fibers of fast twitch muscles, while in cardiac tissue it is restricted to myofibrils of Purkinje fibers. MyBPH is smaller (52 kDa); is encoded by a separate gene from MyBPC and contains only four motifs (two Ig and FNIII). Except for its unique N-terminus sequence of 131 amino acids, MyBPH is quite homologous to MyBPC and the arrangement of its four globular motifs is identical to the last four C-terminus motifs of MyBPC (Gilbert *et al.*, 1998). However, MyBPC can still bind to myosin even if myosin is saturated by MyBPH (Yamamoto, 1984).

#### **1.9.3.5.4 Models of Arrangement**

Two models have been proposed for the arrangement of C-terminus cMyBPC in the sarcomere. The first model, favoured by many researchers (Oakley *et al.*, 2007), was proposed by Moolman-Smook *et al* (2002). The “trimeric collar model” proposes that three staggered MyBPC molecules form a ring/collar around the thick filament (Figure 1.12) which is thought to be stabilised by specific interactions that have been demonstrated between domains C5 and C8, and domains C7 and C10 (Moolman-Smook *et al.*, 2002). This model predicts that domains C0C4, forming the N-terminus of MyBPC, has sufficient length to reach out from the thick filament to interact with the myosin crossbridge (Flavigny *et al.*, 1999; Witt *et al.*, 2001;

Herron *et al.*, 2006), thin filaments (Squire *et al.*, 2003; Kulikovskaya *et al.*, 2003a; Razumova *et al.*, 2006) and/or other, as yet, unidentified interactor(s) (the present study).



The idea that MyBPC molecules form a trimeric collar around the thick filament was initially proposed by Winegrad (1999). This model differed from the Moolman-Smook *et al* model in that the three C-terminus domains (C8C10) of one molecule bound to the three N-terminus domains (C0C2) of the next. While offering no experimental evidence to substantiate this model, Winegrad used it to explain the changes his group had observed in the thick filament (from being tightly packed to being loosely packed with greater order to the myosin heads; Section 1.9.3.5.11.2) upon phosphorylation of the cMyBPC motif (Levine *et al.*, 2001; Winegrad, 1999; Weisberg and Winegrad, 1998). These authors hypothesised that the addition of negative charges upon phosphorylation would disrupt the postulated interaction between C1C2 and C8C9. This disruption would result in a domain shift leading to an interaction between C0 and C10, thus allowing the thick filament to adopt the loose structure with increased diameter as a consequence of an expanded collar (analogous to the buckle on a belt being loosened) (Flashman *et al.*, 2004). This implies that the cMyBPC collar is probably not static, but may have to widen on phosphorylation, and that the collar interactions might have to be abrogated and reformed in a manner compatible with the rate of phosphorylation of the cMyBPC motif. It is not unlikely that such a process, of dynamic tightening and loosening, could also occur among the collar forming domains of the Moolman-Smook *et al* model upon phosphorylation (Moolman-Smook *et al.*, 2002).

The collar model may not be unique to cardiac muscle, as a similar collar of MyBPC may exist in fast skeletal (fs) muscle (Flashman *et al.*, 2008). In an investigation of the interaction between domain C5 and C8

in fast and slow skeletal (ss) isoforms, by Y2H as well as surface plasmon resonance interaction assays, constructs fsC5 and fsC8C10 interacted as strongly as the cardiac types, while the affinity between ssC5 and ssC8C10 was considerably lower. These findings suggested that a similar trimeric collar of MyBPC may exist in fast skeletal muscle (as in the cardiac isoform) but the collar is either not present in slow skeletal muscle or if present, utilises other domains not tested (Flashman *et al.*, 2008).

The second model of the quaternary arrangement of MyBPC in the sarcomere suggests that the C-terminus domains of MyBPC bind axially along the length of the thick filament, and the N-terminus extends perpendicularly toward the thin filament (Squire *et al.*, 2003) (Figure 1.12). Three MyBPC molecules are arranged in this fashion around the same point in the myosin filament. This model has myosin and titin running parallel to each other, along the myosin backbone, accounting for the C8C10 cMyBPC interaction with titin (Freiburg and Gautel, 1996) although a parallel arrangement is not necessarily required to account for these interactions, as titin may bind only one or at most two of the three C-terminus domains of MyBPC (Flashman *et al.*, 2004). The Squire model also does not incorporate the C5:C8 or C7:C10 interaction and apart from X-ray diffraction patterns (Huxley and Brown, 1967; Sjostrom and Squire, 1977), there is no direct experimental evidence that currently supports this model (Oakley *et al.*, 2004).

While the two models differ with regard to the arrangement of the C-terminus domains, both predict that the N-terminus extends into the interfilament space. This arrangement was merely speculative but recent small-angle X-ray scattering data revealed that the N-terminus (C0-C1-cMyBPC motif-C2) in the unphosphorylated state adopted an extended, tandem arrangement in solution that could span interfilament crossbridge distances (Jeffries *et al.*, 2008), consistent with the prediction of both models (Moolman-Smook *et al.*, 2002; Squire *et al.*, 2003).

#### **1.9.3.5.5 N-Terminus Region (Domains C0C2)**

As cMyBPC is a modular protein, its function can be dissected into defined fragments with specific aims (Kunst *et al.*, 2000). As just described, the N-terminus extends into the interfilament space and although the exact function of this region is still a mystery, there is evidence that it plays a role in the regulation of cardiac contractility through phosphorylation of the cMyBPC motif. The next paragraphs describe, briefly, the interactions proposed with this region.

##### **1.9.3.5.5.1 Domain C0 and C0C1 linker**

The function of this cardiac-specific domain remains to be determined. Two Y2H library screens to identify putative interactors of domains C0 and C0C1, performed in the Moolman-Smook lab, yielded no plausible interactors of these domains. It was suggested that these regions, perhaps, interacted with the N-terminus of large proteins that are not represented in a C-terminus primed cDNA library, with average insert sizes between 0.4-4 kb (W.J de Lange, 2004).

Sequence comparison between C0 and myomesin suggested that C0 contained a novel putative LMM-binding site (Flavigny *et al.*, 1999) (Figure 1.13); in addition the pro-ala-rich C0C1 linker was also proposed to interact with myosin (Herron *et al.*, 2006). To further complicate the interpretation of the function of this region, an actin-binding site has also been proposed for C0 (Kulikovskaya *et al.*, 2003a) and the pro-ala-rich C0C1 linker (Squire *et al.*, 2003). It is unlikely that C0 and the C0C1 linker are able to bind to the myosin crossbridge, the myosin backbone and actin simultaneously, therefore it is possible that the N-terminus of MyBPC cycles through different binding partners (Oakley *et al.*, 2004). The conditions which make this possible remain to be determined. These interactions of cMyBPC are described in further detail in sections 1.9.3.5.9.3 and 1.9.3.5.10.

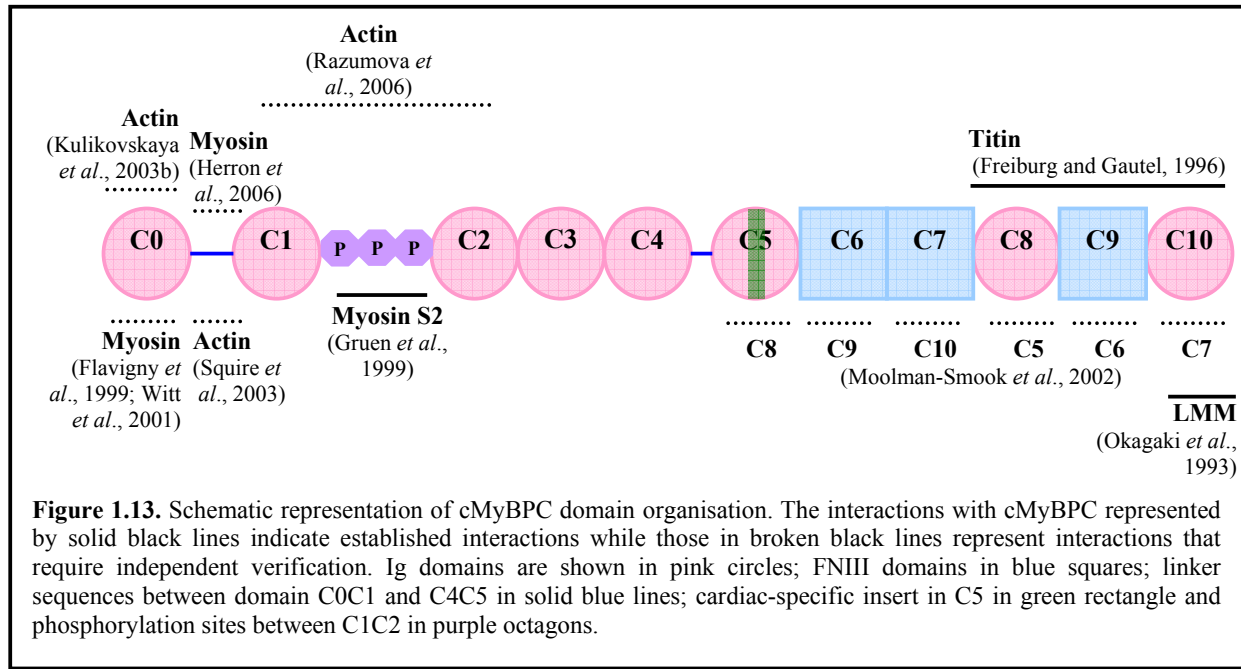


**Figure 1.13.** Schematic representation of cMyBPC domain organisation. The interactions with cMyBPC represented by solid black lines indicate established interactions while those in broken black lines represent interactions that require independent verification. Ig domains are shown in pink circles; FNIII domains in blue squares; linker sequences between domain C0C1 and C4C5 in solid blue lines; cardiac-specific insert in C5 in green rectangle and phosphorylation sites between C1C2 in purple octagons.

### 1.9.3.5.5.2 Domain C1-cMyBPC motif-C2

This region is of particular significance in the cardiac isoform as it houses the phosphorylatable cMyBPC motif which may modulate cardiac contractility by specifically binding to myosin S2 in the absence of phosphorylation (Section 1.9.3.5.9.1) (Gruen *et al.*, 1999a; Gruen *et al.*, 1999b) (Figure 1.13). Trisphosphorylation of the cMyBPC motif releases myosin S2, which is thought to allow the myosin crossbridges to reach out and interact more efficiently with actin, increasing force generation and systolic tension (Kunst *et al.*, 2000; Weisberg and Winegrad, 1996; Kulikovskaya *et al.*, 2003a). Since unphosphorylated C1C2 binds to myosin S2, but phosphorylated C1C2 does not (Kunst *et al.*, 2000), binding partners of the N-terminus of endogenous MyBPC might vary according to the extent of MyBPC phosphorylation (Kulikovskaya *et al.*, 2003a). Accordingly, the C1C2 region has also been shown to interact with actin and possibly other regulatory thin filament proteins (Razumova *et al.*, 2006) (Section 1.9.3.5.10).

### **1.9.3.5.6 Central Domains (C3C6)**

#### **1.9.3.5.6.1 Domains C3 and C4**

An interaction between domain C3 and C10 has been observed by Y2H analyses (W.J de Lange, 2004) and may be explained in terms of the “loosening” collar (Section 1.9.3.5.4). It is possible, upon trisphosphorylation of the cMyBPC motif, when the thick filament diameter increases (Section 1.9.3.5.11.2) that the MyBPC collar loosens and that intermolecular interaction shifts from involving domains C7 and C10 to involving domains C3 and C10. Similarly, as interactions do not necessarily involve perfectly juxtaposed domains, but may involve a staggered association, it is quite possible that an interaction between parts of domain C2 or C4 and C10 exists, depending on the extent of phosphorylation. These interactions have not been tested experimentally and form two of the aims of the present study.

#### **1.9.3.5.6.2 Domain C5**

Domain C5 has a highly dynamic and unstructured cardiac isoform-specific insertion of ~30 amino acids in the CD loop of this domain (Idowu *et al.*, 2003). The function of this proline-rich insert has not yet been determined, but it is proposed to be involved in signalling, forming an SH3-domain recognition sequence, and perhaps binding the CamK-II that co-purifies with cMyBPC (Redwood *et al.*, 1999; Oakley *et al.*, 2004).

In a Y2H screen, using the C5 sequence as “bait”, domain C8 was identified as a preferred binding partner for domain C5 (Moolman-Smook *et al.*, 2002) (Figure 1.13). Data from this study, in conjunction with other biochemical data, led to the proposed “trimeric collar arrangement” for cMyBPC in the sarcomere (Section 1.9.3.5.4). This interaction between domains C5 and C8 is not dependent on the ~30 amino acid cardiac-specific insert in domain C5 and is also relevant in fast skeletal muscle (Flashman *et al.*, 2008; Section 1.9.3.5.4). Thus the function of the insertion sequence remains unclear.

#### **1.9.3.5.6.3 Domain C6**

No specific functions or sarcomeric interactions have, so far, been assigned to domain C6. Based on Y2H protein:protein interaction assays, a peptide encoding domains C5C7 bound to a peptide encoding domains C8C10 with higher affinity than a peptide encoding domain C5 alone (Moolman-Smook *et al.*, 2002) (Figure 1.13). This does not specify that C6 bound to C9, only that additional domain:domain interaction occurred. The interaction between C6 and C9 has not been tested directly as both of these FNIII domains are known to interact promiscuously, likely to complicate the interpretation of data.

#### **1.9.3.5.7 C-Terminus Domains (C7C10)**

Within domains C7C10 of MyBPC, the primary myosin and titin-binding regions are localised to domain C10 and somewhere within domains C8C10, respectively (Okagaki *et al.*, 1993; Freiburg and Gautel, 1996). In the collar model, this region is proposed to interact with other C-terminus cMyBPC molecules to form the collar around the thick filament to aid thick filament stability.

### **1.9.3.5.7.1 Domain C7**

Using C-terminus deletions of MyBPC, Gilbert *et al.* (1996) demonstrated that domains C7C10 are the minimal requirement for the incorporation of the protein into the A-band of the sarcomere, with domain C7 improving the targeting of MyBPC to the C-zone (Gilbert *et al.*, 1999). It is thought that the 11-domain super-repeat of titin dictates cMyBPC's localisation to the C-zone as each super-repeat has a 43nm periodicity like the MyBPC-rich transverse stripes (Flashman *et al.*, 2004). However, MyBPC is not present in every C-zone stripe and therefore additional localisation mechanisms must be present. According to the trimeric collar model, C7 specifically interacts with domain C10 of the next cMyBPC molecule (Moolman-Smook *et al.*, 2002).

### **1.9.3.5.7.2 Domain C8**

Domain C8 has been shown to be the binding partner of domain C5, leading to development of the trimeric collar model (Moolman-Smook *et al.*, 2002). The C8:C5 interaction is also relevant in fast skeletal muscle (Flashman *et al.*, 2008; Section 1.9.3.5.4).

### **1.9.3.5.7.3 Domain C9**

According to the proposed "trimeric collar model" domain C9 is predicted to interact with domain C6. Further, domain C9 may also be significant for titin-binding as it forms part of a Y2H construct (C8C10) that can bind to titin (Moolman-Smook *et al.*, 2002).

### **1.9.3.5.7.4 Domain C10**

Domain C10 of all three isoforms of MyBPC are capable of interacting with LMM and the binding stoichiometry of 0.6-0.7:1 suggests that there is a single binding site for domain C10 on LMM (Alyonycheva *et al.*, 1997). Although domain C10 is necessary, it is not sufficient for maximal binding to myosin. The affinity of MyBPC for myosin increases progressively as the three adjacent modules, C7C9, are added to the C-terminus (Gilbert *et al.*, 1996). The importance of these additional modules in the binding to myosin was also demonstrated by the inability of a peptide encoding domain C10 to displace MyBPC from myosin (Okagaki *et al.*, 1993). Myosin-binding of MyBPH also occurs *via* its C10-homologous C-terminus domain, H4 (Alyonycheva *et al.*, 1997).

### **1.9.3.5.8 C-terminus versus N-terminus**

The C-terminus region of cMyBPC interacts with the LMM portion of myosin, as well as with titin, thus anchoring the protein to the thick filament shaft, specifying its sarcomeric localisation (Gruen and Gautel, 1999) and defining part of its function. *Via* interactions with C-terminus domains of other cMyBPC molecules, cMyBPC also mechanically stabilises the thick filament. The function of the N-terminus and the spectrum of its ligands, on the other hand, are not as clearly defined as the C-terminus. In the following sections, a literature review of what is currently known about the function of the N-terminus cMyBPC is presented.

### **1.9.3.5.9 Interactions with Myosin**

#### **1.9.3.5.9.1 Myosin S2 and cMyBPC**

MyBPC is thought to regulate cardiac contraction, primarily through its N-terminus, *via* the reversible, phosphorylation-dependent (Section 1.9.3.5.9.2) binding of the C1C2 region with myosin S2. When dephosphorylated, the C1C2 region interacts with myosin S2, but upon phosphorylation of the cMyBPC motif, its binding is inhibited. Gruen *et al.* (1999a) mapped the regions of interaction to the proximal 126 amino acid residues of myosin S2 and the ~100 amino acid residues of the cMyBPC motif. Domain C2 residues were also shown to interact with myosin S2 (Ababou *et al.*, 2004) and together with Ser273/Ser282 within the cMyBPC motif they may act synergistically to form an extended myosin S2 “interaction interface” across both domains (Jeffries *et al.*, 2008).

The proximal 126 amino acid residues on myosin S2 immediately follows the head-tail junction and is adjacent to the binding site for the RLC on myosin. This segment of myosin S2 is almost completely identical between all sarcomeric myosin isoforms and vertebrate species (Gruen and Gautel, 1999b). The interaction with MyBPC is hence thought to be independent of the MyBPC or myosin isoform and the MyBPC motifs of both cardiac and ssMyBPCs were demonstrated to bind to the myosin S2 segment with comparable affinities. The interaction with myosin S2 is thought to direct the A-band association of exogenously introduced N-terminus cMyBPC fragments in neonatal rat cardiomyocytes (Gruen and Gautel, 1999).

#### **1.9.3.5.9.2 Phosphorylation of cMyBPC motif**

Four phosphorylation sites designated A-D have been identified, but site-directed mutagenesis studies have shown that putative site D is not phosphorylated as the site may be inaccessible due to folding of the molecule (Gautel *et al.*, 1995). The remaining sites have relative sensitivities to the kinases that are present in the cardiac cell. The CamK-II that co-purifies with cMyBPC, phosphorylates site B only (Flashman *et al.*, 2004; Winegrad, 1999), while PKA is able to phosphorylate the remaining sites. PKC appears to phosphorylate sites A (Ser273) and C (Ser302) only, but investigations in intact heart muscle showed that PKC-mediated phosphorylation is not physiological relevant (Edes and Kranias, 1990). There also appears to exist a hierarchy of phosphorylation between the sites, such that if site B (Ser282; located in the cardiac-specific LAGGGRRIS loop insertion) was mutated or deleted to prevent phosphorylation, the ability of PKA to phosphorylate sites A and C was markedly reduced (Gautel *et al.*, 1995). *In vivo* studies have shown that the first phosphate added to site B by an endogenous CamK-II occurred at a  $\text{Ca}^{2+}$  concentration below that necessary for muscle contraction or for PKA phosphorylation (McClellan *et al.*, 2001). Upon  $\beta$ -adrenergic stimulation, the remaining sites are phosphorylated by PKA. Thus, phosphorylation at site B may function as a conformational switch, rendering other sites on the protein more accessible to the relevant kinase (Gautel *et al.*, 1995).

Further,  $\beta$ -adrenergic agonists cannot cause phosphorylation of cMyBPC in intact cardiac cells, *in vitro*, unless one phosphate (site B) is already present (McClellan *et al.*, 2001). Since this site is phosphorylated by a CamK-II,  $\text{Ca}^{2+}$  plays an important role in cMyBPC phosphorylation. McClellan *et al* (2001) speculated about the critical  $\text{Ca}^{2+}$  concentration required for monophosphorylation (at site B) and proposed that the phosphorylation of site B was either constitutive *in vivo*, could be tied to the normal dynamic flux of  $\text{Ca}^{2+}$  in the myocytes, or requires other specific stimuli. At activating  $\text{Ca}^{2+}$  concentrations, when cMyBPC is fully phosphorylated, increased maximum force has been observed (McClellan *et al.*, 2001). These results suggest that cMyBPC phosphorylation, regulated by intracellular  $\text{Ca}^{2+}$  levels (to activate CamK-II) and  $\beta$ -adrenergic stimulation (to activate PKA), determines the state of interaction of cMyBPC with myosin S2 (McClellan *et al.*, 2001).

Fast and ssMyBPC are not phosphorylated to any great extent by PKA (Lim and Walsh, 1986; Gruen *et al.*, 1999a) and since these isoforms do not have the LAGGGRRIS insertion in the cMyBPC motif, which contains site B, it is also unlikely that they are phosphorylated by the CamK-II. This isoform difference may signify a more stringent regulation of cardiac contraction (Oakley *et al.*, 2004).

Dephosphorylation of cMyBPC occurs in response to cholinergic agonists such as acetylcholine (Hartzell and Titus, 1982). *In vitro* studies in chicken have shown that this occurs predominantly *via* protein phosphatase 2A, which is involved in the dephosphorylation of other sarcomeric proteins and has been shown to co-purify with cMyBPC (Schlender and Bean, 1990). It is not known whether there is a specific order for cMyBPC dephosphorylation.

#### 1.9.3.5.9.3 Other myosin interactions with cMyBPC

The interactions of LMM with domain C10 (Section 1.9.3.5.7.4) and myosin S2 with the cMyBPC motif (Section 1.9.3.5.9.1) are well recognised, however, several other interactions between myosin and N-terminus cMyBPC have been proposed but require further verification.

A myosin-binding site within domains C0C1 was proposed based on findings that N-terminus truncated cMyBPC fragments (C0C1, C0C3 and C0C4; all containing domain C0C1) transfected into foetal rat cardiomyocytes showed A-band localisation in 10% of expressing cardiomyocytes (Flavigny *et al.*, 1999). Sequence analysis of C0C1 indicated that there was a region of homology between domain C0 of human cMyBPC and the myosin-binding My1 domain of myomesin (Section 1.4.1), thus C0 might possess myosin-binding capabilities (Flavigny *et al.*, 1999). The authors did not explain the diffuse localisation (90%) of the truncated cMyBPCs, only stating that their observation was consistent with previous studies obtained with expressed truncated cTNT or cMyBPC. It is possible that the diffuse localisation of fragments containing C0C1 is due to interaction of C0/pro-ala-rich linker/C1 with a thin filament component as suggested by others (Section 1.9.3.5.10). Since the C-zone (which also contains thin filaments) cannot be distinguished within the A-band by confocal microscopy, it is possible that C0C1 may have interacted with a thin filament

component. This suggestion however seems unlikely in light of a study by Herron *et al* (2006), which showed that exogenously added C0C1 or C0C2 fragments were predominantly localised to the A-band with no evidence for binding to the I-band (thin filaments) in human and rodent skinned cardiac myocytes. These results thus suggested a novel interaction between N-terminus cMyBPC and an A-band protein (almost certainly a myosin component). Further, the addition of exogenous C0C1 or C0C2 (>10umol/L) recombinant fragments to the cardiac myocytes resulted in the activation of force production in the absence of  $\text{Ca}^{2+}$ , while addition of fragments C0 or C1C2 did not produce similar effects (Herron *et al.*, 2006). Deletion mapping determined that the activating effect of C0C1 or C0C2 resulted from the binding of the pro-ala-rich linker to an unknown sarcomeric component, rather than domain C0 (Herron *et al.*, 2006). These results suggested that C0C1/C0C2 was able to switch on the thin filament by a mechanism different from that of  $\text{Ca}^{2+}$  (Section 1.9.1). This action has not been seen in previous studies using N-terminus fragments of cMyBPC, but these earlier studies used fragments containing either C0 (Kulikovskaya *et al.*, 2003a) or C1C2 (Harris *et al.*, 2004), neither of which exhibit this  $\text{Ca}^{2+}$ -independent activation. The precise mechanism for the activating effect of C0C1/C0C2 on force production and crossbridge cycling remains to be established (Herron *et al.*, 2006).

In contrast to the studies which showed that the C1C2 fragment activated neither force nor crossbridge cycling (Herron *et al.*, 2006; Harris *et al.*, 2004), Razumova *et al* (2006) showed that in an *in vitro* motility assay using heavy meromyosin and F-actin, a cMyBPC fragment (C1C2) reduced actin filament velocity at high  $\text{Ca}^{2+}$  concentrations (in the presence or absence of troponin and tropomyosin) but increased filament speed at low  $\text{Ca}^{2+}$  concentration in the presence of troponin and tropomyosin. These effects were attributed to an interaction, demonstrated by cosedimentation, between C1C2 and actin (described further in section 1.9.3.5.10). Since myosin S2 was also present in the HMM fragment, the dual effect of the C1C2 fragment could have been attributed to an interaction between myosin S2 as the MyBPC motif as fragments lacking this region (C0C1 and C2C4) did not produce similar effects. In a follow-up study, the extent to which interactions with myosin S2 contributed to effects of C1C2 was investigated by using myosin S1 motor domains (lacking S2) to generate movement (Shaffer *et al.*, 2007). Surprisingly, the results are similar to the previous study suggesting that myosin S2 was not required for the effects of C1C2 on motility and instead suggested that C1C2 interacted with actin and/or myosin S1 to affect crossbridge kinetics (Shaffer *et al.*, 2007). But, a direct interaction with myosin S1 is doubtful, as previous studies reported that myosin S1 alone did not compete for C1C2-binding in separate cosedimentation experiments, suggesting that C1C2 bound weakly or not at all to myosin S1 (Gruen *et al.*, 1999a). Further, the finding that C1C2 inhibited actin-activated S1 ATPase rates in solution but not intrinsic ATPase rates suggested that the effects of C1C2 in motility assays are due primarily to the interaction with actin and not myosin (Shaffer *et al.*, 2007).

#### 1.9.3.5.10 Interaction with Actin

Early studies have shown that MyBPC interacted with actin in both regulated and unregulated filaments (Moos *et al.*, 1978; Yamamoto, 1986), and that actin had a low affinity for all isoforms of MyBPC

(Yamamoto and Moos, 1983), suggesting that the region of interaction was unlikely to be cardiac-specific. Also, MyBPC increased actin-activated myosin ATPase in solution by producing links between actin and myosin to form aggregates of the two contractile proteins (Moos *et al.*, 1978; Moos and Feng, 1980), an effect that varied depending on the ionic strength and molar ratio of actin and myosin, suggesting that MyBPC may facilitate positioning of myosin and actin for interaction (Korte *et al.*, 2003).

The pro-ala-rich linker preceding domain C1 has been identified, by homology modelling, as a likely candidate for actin-binding (Squire *et al.*, 2003). This N-terminus MyBPC region shares homology with the N-terminus extension of ELC (Section 1.3.2) and the PEVK region of titin (Section 1.6.2), both of which interact with actin (Timson *et al.*, 1998; Linke *et al.*, 2002). Further, *in vitro* immunoprecipitation assays showed that fragments of cMyBPC containing domain C0 (C0, C0C1, C0C2) were able to bind actin while C1C2 could not (Kulikovskaya *et al.*, 2003a). Also, phosphorylation of the cMyBPC motif in these fragments (C1C2 and C0C2) did not alter actin-binding. The interaction of C0C1 or C0C2 with actin was stronger than with C0 alone suggesting that the region of interaction may extend to the pro-ala-rich linker.

Additionally, to evaluate the relationship between the binding of C0-containing fragments to actin and binding of C1C2 to myosin, MyBPC fragments (C0C1, C1C2 or C0C2) were incubated with cardiac trabeculae that contained either unphosphorylated or phosphorylated MyBPC (Kulikovskaya *et al.*, 2003a). In trabeculae with primarily unphosphorylated MyBPC (and therefore a high degree of endogenous C1C2 binding to myosin), exogenously added C1C2 did not bind to the trabeculae, however a substantial amount of exogenously added C0C1 bound to the trabeculae. Conversely, in trabeculae where there was a high degree of phosphorylated endogenous MyBPC, a substantial amount of C1C2 bound, but no C0C1 bound to the trabeculae. Exogenous C0C2 bound to trabeculae with primarily phosphorylated MyBPC and to a lesser degree to trabeculae with primarily unphosphorylated MyBPC. These findings suggested that in the presence of unphosphorylated MyBPC, myosin S2 was bound to endogenous cMyBPC C1C2 and therefore exogenous added C1C2 or C0C2 could not bind. On the other hand, in the virtual absence of unphosphorylated endogenous MyBPC, myosin S2 was free to interact with exogenous C1C2 or C0C2 (Kulikovskaya *et al.*, 2003a).

In these experiments exogenous C0C1 bound to trabeculae when endogenous MyBPC was unphosphorylated (C1C2 interacting with myosin S2, thus keeping the myosin head away from actin) and actin was available to bind exogenous C0C1. But when MyBPC was phosphorylated (and C1C2 released myosin S2), actin was no longer available to bind exogenous C0C1. This suggested that endogenous C0 bound to actin when cMyBPC was phosphorylated (Kulikovskaya *et al.*, 2003a). The authors suggested that this interaction between domain C0 and actin provided an internal load during contraction similar to the model proposed by Hofmann *et al* (1991a) (Section 1.9.3.5.11.4 and 1.9.3.5.11.6). The effect of cMyBPC to slow the rates of crossbridge cycling may appear to be deleterious to contractile function, however slowed rates of crossbridge cycling

may be beneficial *in vivo* by prolonging systolic ejection and perhaps increasing contractile efficiency by minimising ATP utilisation (Kulikovskaya *et al.*, 2003a).

Shaffer *et al* (2007) speculated whether the actin-binding region on cMyBPC extended beyond domain C0 and the pro-ala-rich linker to include domains C1C2. The answer lay in whether the cMyBPC motif plus two flanking domains, C1 and C2, had sufficient length to span the interfilament distance, allowing interaction with both myosin S2 and the thin filament. NMR studies have shown that a portion of the myosin S2-binding site was located near the C-terminus of C2 (Ababou *et al.*, 2004; Ababou *et al.*, 2006), while small-angle X-ray scattering revealed that the N-terminus of cMyBPC (C0-C1-cMyBPC motif-C2) adopted an extended, tandem arrangement in solution that could span interfilament crossbridge distances (Jeffries *et al.*, 2008). Thus, it is most plausible that N-terminus domains of cMyBPC interacts with both thick and thin filaments and can therefore modulate actomyosin interactions through direct interaction (Shaffer *et al.*, 2007).

Using N-terminus cMyBPC fragments (C0C1, C1C2, C0C2 and C2C4), Razumova *et al* (2006) showed that C1C2 dramatically increased filament sliding speeds at low  $\text{Ca}^{2+}$  concentrations (only in the presence of troponin and tropomyosin), but reduced speeds at high  $\text{Ca}^{2+}$  concentrations (with or without thin filament regulatory proteins) in an *in vitro* motility assay. In contrast to C1C2, C0C1 and C2C4 had no effect on filament mobility, while C0C2 (cMyBPC motif present) had a qualitatively similar effect to that of C1C2. Further, C1C2 could crosslink F-actin; an interaction that persisted at physiological ionic strength, mediated primarily by relatively weak electrostatic interactions (Razumova *et al.*, 2006). The role of troponin and tropomyosin on the activating effect of C1C2 at low  $\text{Ca}^{2+}$  concentrations was not explored in this experiment; considering that C1C2 also cosedimented with Tn and TM, the activating effect of C1C2 may also involve these components and not just actin.

#### **1.9.3.5.11 Function of cMyBPC**

The early appearance of cMyBPC during the assembly of the thick filaments was taken as a suggestion that their main function was in the regulation of myosin filament assembly in sarcomerogenesis (Lin *et al.*, 1994). However, the discovery that the cardiac isoform can be phosphorylated by PKA and detection of an associated CamK-II suggested a role for cMyBPC in the regulation of muscle contraction (Gruen and Gautel, 1999a). The effects of cMyBPC phosphorylation on a number of parameters are described in the following sections. Further, understanding the function of cMyBPC is clinically relevant, as *MYBPC3* mutations are widely recognised to cause familial hypertrophic cardiomyopathy (Section 1.10.1).

##### **1.9.3.5.11.1 Thick filament stability and cardiac function**

###### **Thick filament formation**

*In vitro* evidence suggests that MyBPC plays an important role in the formation of myofibrils in skeletal and cardiac muscle (Flashman *et al.*, 2004). Purified myosin can self-assemble into thick filaments in the absence of MyBPC; however, the addition of physiological ratios of MyBPC resulted in increased filament length,

improved structure and compactness of filament, and a clearly distinguishable central bare-zone (Maw and Rowe, 1986). In COS cells, MyBPC modified the assembly of MHC molecules by compacting them at the periphery of the nucleus into cable-like structures. When a C-terminus truncated MyBPC (C4C10 deleted) is co-expressed, the MHC filaments are neither dispersed throughout the cytoplasm, similar to when MHC is expressed alone, nor compacted to the perinuclear region as when it is co-expressed with WT MyBPC. The truncated MyBPC alters the normal MHC assembly and results in a heterogeneous distribution of MHC (Sébillon *et al.*, 2001; Flashman *et al.*, 2004).

### **Thick filament stability**

The addition of exogenous C5 to isolated skinned cardiac trabeculae resulted in the loss of MyBPC and MHC (to a smaller extent). These findings suggest that exogenous C5 competed with endogenous C5 and disrupted the normal interactions of endogenous C5 as well as thick filament composition (McClellan *et al.*, 2004). The normal interaction of C5, according to the trimeric collar model (Section 1.9.3.5.4), would be with domain C8, thus the disruption of this interaction (in this model) would be expected to lead to an unstable collar, resulting in the cleavage of endogenous cMyBPC and perhaps to unstable MHC filaments (McClellan *et al.*, 2004).

In a study using chemically skinned trabeculae from WT rat hearts, cMyBPC was shown to exist in two different forms that produced either stable or unstable thick filaments (Kulikovskaya *et al.*, 2007). The stable form had well-ordered myosin heads and required cMyBPC phosphorylation while the unstable form was associated with disordered myosin heads and unphosphorylated cMyBPC. In tissue with intact cardiac cells, the unphosphorylated cMyBPC was more easily proteolysed, causing cMyBPC and myosin to be released. Antibody staining of the cMyBPC proteolytic fragments showed that the C5C10 region underwent proteolysis as anti-C5 or anti-C8C9 could not stain these fragments (Kulikovskaya *et al.*, 2007). Filaments deficient in phosphorylated cMyBPC are fragmented by shear force that is well tolerated by the stable form (Kulikovskaya *et al.*, 2007). Thus, findings from the two studies described here suggest that the “trimeric collar” and cMyBPC phosphorylation function to provide thick filament stability.

### **Sarcomere formation and cardiac function**

While *in vitro* experiments indicated that MyBPC may play a role in thick filament formation, murine knockout models of cMyBPC do not show a lack of sarcomere formation (Harris *et al.*, 2002; McConnell *et al.*, 1999). Homozygous mutant MyBPC mice (cardiac myosin heavy chain-binding and titin-binding domains truncated; MyBPC<sup>t/t</sup>) expressed less than 10% truncated protein, which were located in M-lines of otherwise normal sarcomeres (McConnell *et al.*, 1999). These findings were confirmed by another study which showed that cMyBPC homozygous-null (cMyBPC<sup>-/-</sup>) mice were viable and that regular sarcomere striations such as the Z-line, A-band and M-line were distinguishable, although frequently misaligned (Harris *et al.*, 2002). This suggested that either MyBPC played a minor role in sarcomere assembly or that this important function had been taken over by some, as yet, unidentified mechanism. The expression of skeletal

MyBPC did not increase to compensate for the lack of cMyBPC, although the possible up-regulation of other myosin-binding proteins was not examined (Harris *et al.*, 2002). Sarcomeric structures were also observed in cMyBPC TG mice where the phosphorylatable Ser residues in the cMyBPC motif were either mutated to non-phosphorylatable alanines (Sadayappan *et al.*, 2005) or to aspartic acid, to mimic constitutive phosphorylation (Sadayappan *et al.*, 2006). These TG mouse studies conflict with previous suggestions that cMyBPC performed essential structural roles during sarcomere assembly and myofibrillogenesis; however, these earlier proposals were based on observations that MyBPC affected thick filament assembly *in vitro* (Section 1.9.3.5.11.1; thick filament formation) and that MyBPC expression coincided with myosin and myofibril assembly during development (Gautel *et al.*, 1998; Schulteiss *et al.*, 1990). It is possible that in the native myofilament, other factors besides MyBPC contribute to sarcomere assembly (Flashman *et al.*, 2004).

While the presence of cMyBPC is not required for sarcomere formation, the lack of cMyBPC (Stelzer *et al.*, 2006b, c; Harris *et al.*, 2002; Palmer *et al.*, 2004a; Stelzer *et al.*, 2007) and decreased levels of cMyBPC phosphorylation (Sadayappan *et al.*, 2005) in the myocardium have been implicated in both systolic and diastolic dysfunction. The findings from these studies are summarised in the following paragraphs.

Homozygous mice expressing a C8C10 truncated cMyBPC ( $cMyBPC^{t/t}$ ), analogous to that found in human HCM, exhibited neonatal onset of dilated cardiomyopathy with prominent histopathology of myocyte hypertrophy, myofibrillar disarray, fibrosis, dystrophic calcification, left ventricular (LV) dilation and reduced contractile function, which manifested in depressed systolic contractility with diastolic dysfunction (McConnell *et al.*, 1999). Using this model, Palmer *et al* (2004a) showed that systolic LV chamber stiffness was also reduced. The authors attributed reduced stiffness to the lack of cMyBPC, which, if present, would have provided structural support *via* its strong interactions with myosin and titin. The structural integrity afforded by these interactions may be responsible for as much as 50% of the normal longitudinal stiffness between crossbridges and the M-line. Functionally, the overly compliant cMyBPC-deficient myocardium of these TG mice may not be able to provide the requisite transmural wall stress at normal LV chamber dimensions to accommodate normal LV pressure and would therefore be expected to dilate (Palmer *et al.*, 2004a).

In addition, Palmer *et al* (2004b) showed that cMyBPC appeared less important for initiating force development than for sustaining force and muscle stiffening so that systole could extend normally throughout ejection. Without it, chambers can only eject for a very short duration thereby depressing cardiac output. This was expressed by the abbreviation of the time to peak elastance, with premature relaxation starting shortly after ejection was initiated in  $cMyBPC^{t/t}$  mice. The reduced elastance appeared to be fairly specific to cMyBPC-deficient hearts, as it was not mimicked in other models of cardiac dysfunction such as autoimmune myocarditis and myocardial stunning. These findings (Palmer *et al.*, 2004a; Palmer *et al.*, 2004b) suggested that cMyBPC provided mechanical stability to the myofilament lattice in such a manner as to significantly influence the transmission of force across the sarcomere and sustain systolic stiffening. A

deficient incorporation of cMyBPC therefore may reduce tension and stiffness of sarcomeres to a degree that would lead to the disruption of myocytes and trigger a progression to dilated cardiomyopathy (Palmer *et al.*, 2004b).

Further animal studies showed that homozygous ( $cMyBPC^{-/-}$ ) and heterozygous ( $cMyBPC^{+/-}$ )  $cMyBPC$ -null mice exhibited different cardiac disorders (Carrier *et al.*, 2004). Heterozygous mice developed asymmetric septal hypertrophy associated with fibrosis at ten to eleven months of age, without impairment of left ventricular function. This type of hypertrophy, although without myofiber disarray, is similar to human HCM. Homozygous mice showed eccentric left ventricular hypertrophy with decreased fractional shortening at three to four months of age and developed impaired diastolic relaxation. This phenotype shows more resemblance to human dilated cardiomyopathy following cardiac hypertrophy (Carrier *et al.*, 2004). Using this mouse model, Eijssen *et al* (2008) explored how the difference in the amount of mutant sarcomeric protein caused the markedly different phenotypes. Nine week old homozygous mice already showing signs of hypertrophy and heterozygous mice still in the prehypertrophic stage were used to identify processes and/or pathways that were dis-regulated as a consequence of the mutant protein. Despite the striking difference in phenotype, the number of differentially expressed cardiac genes did not differ substantially between  $cMyBPC^{+/-}$  and  $cMyBPC^{-/-}$  animals with changes in gene expression indicating an increased energy demand, activation of the Jun N-terminus kinase (JNK) and p38 subsystems of the mitogen-activated protein kinase (MAPK) signalling pathway and the deactivation of extracellular signal-regulated kinase 1/2 (ERK) signalling. The JNK, p38 and ERK subsystems are known to be involved in cardiac hypertrophy. Further, the induction of the apoptotic process suggested that unfavourable changes at the gene expression level were initiated even before overt hypertrophy occurred (in  $cMyBPC^{+/-}$  mice) and persisted after hypertrophy had been fully established (in  $cMyBPC^{-/-}$  mice), in this model. Changes in gene expression encoding structural and contractile protein genes were less prominently present, most likely because hypertrophy was either not yet present ( $cMyBPC^{+/-}$ ) or already completed ( $cMyBPC^{-/-}$ ). In addition, altered protein turnover was also observed in these hearts as changes in cardiac structures require the formation and degradation of an adapted spectrum of proteins. In general, changes were more pronounced in the  $cMyBPC^{-/-}$  mice corresponding to the early hypertrophic condition and the development of a more severe phenotype in these mice (Eijssen *et al.*, 2008).

The mechanism by which mutant  $cMyBPC$  protein causes dysfunction either *via* haploinsufficiency or “poison” peptide has also been investigated. Yang *et al* (1999) showed that mutant  $cMyBPC$  (lacking only the myosin-binding domain) was stably expressed and, although it was incorporated into the sarcomere, it was not restricted to the A-band. Immunofluorescence showed reactivity in the I-band and Z-disc, as well as being diffuse in the cytoplasm. The findings contradict a previous study where mutant  $cMyBPC$  protein lacking both the myosin and titin-binding domains (C8C10) was not detected in TG mice (Yang *et al.*, 1998).  $cMyBPC$  mRNA levels were comparable between both models although the proteins levels were not. The authors hypothesised that TG mRNA was translated efficiently but only a very small portion was

incorporated into the sarcomere, with the unincorporated protein being degraded rapidly (James *et al.*, 1999). This was also observed in another truncated mouse model (cMyBPC<sup>t/t</sup>; domains C8C10 truncated), where no truncated cMyBPC was detected in the myocardium, although the level of transcription for this truncated MyBPC has been reported to be ~14% compared to WT (McConnell *et al.*, 1999; Palmer *et al.*, 2004a). The absence of cMyBPC protein in some of these models precludes the possibility that the truncated MyBPC acted as a “poison” peptide and the cardiomyopathy observed must therefore be due to the mechanical consequences of the absence or insufficient levels of cMyBPC (Palmer *et al.*, 2004a).

In a long-term follow-up study of the TG mice expressing truncated cMyBPC from two studies (Yang *et al.*, 1998 [lacking both the myosin and titin-binding domains (C8C10)]; Yang *et al.*, 1999 [lacking only the myosin-binding domain]), cardiac hypertrophy was observed in adults older than one year (Yang *et al.*, 2001a). TG animals stressed either by physical exercise or chronic β-adrenergic stimulation showed bradycardia and sudden death was observed, while unstressed TG animals had a normal life span. Findings from this study showed that while an unstressed heart was able to compensate effectively for the intrinsic mechanical and kinetic deficits resulting from *MYBPC3* mutation, functional deficits present at the whole organ level upon exposure to stress. These findings are similar to what has been observed in human subjects, where *MYBPC3* mutations are often, but not always, associated with late onset and benign phenotype (Yang *et al.*, 2001a). Further, truncated proteins resulting from different *MYBPC3* gene mutations are unstable in myocardial tissue of patients (Rottbauer *et al.*, 1997; Moolman *et al.*, 2000; Vignier *et al.*, 2001) comparable to that seen in mouse models of HCM/DCM (Yang *et al.*, 1999; Palmer *et al.*, 2004a). This suggests that the “null allele” mechanism leading to protein haploinsufficiency could be involved in the pathogenesis of at least some cases of *MYBPC3*-associated human HCM.

The phosphorylation patterns of cMyBPC have also been shown to have a significant effect on the whole-heart function and cardiac haemodynamics (Sadayappan *et al.*, 2005). In various mouse models of cardiac stress, cMyBPC was extensively phosphorylated under basal conditions and became dephosphorylated during the development of heart failure or pathological hypertrophy, with the trisphosphorylated form largely or completely absent in the advanced stages of heart failure (Sadayappan *et al.*, 2005). This phenomenon appeared to be independent of the type of cardiac stress, as pressure overload, ischemic-reperfusion injury, and various genetic alterations in the cardiac machinery all resulted in significantly decreased phosphorylation. To investigate whether the dephosphorylated form of cMyBPC was able to cause disease, a TG mouse that expressed a non-phosphorylatable cMyBPC (MyBPC<sup>AIP-</sup>; Ser residues in the MyBPC motif were mutated to alanines) was generated (Sadayappan *et al.*, 2005). Mice in which approximately 40% of the endogenous cMyBPC was replaced with MyBPC<sup>AIP-</sup> appeared overtly normal with no cardiac hypertrophy and/or dilation. However, the mice displayed an ill-defined sarcomeric pattern (altered H-zones and M-lines), upregulation of genes associated with a hypertrophic response (such as atrial-natriuretic factor, β-MHC, brain natriuretic peptide, and skeletal α-actin, part of the so called foetal gene program), and contraction and relaxation were significantly decreased. Further, the inability of MyBPC<sup>AIP-</sup> to rescue a

cMyBPC<sup>t/t</sup> phenotype (domains C8 to C10 deleted) is consistent with the hypothesis that cMyBPC phosphorylation is essential for normal cardiac function. In contrast, equivalent TG expression of WT cMyBPC effectively rescued the cMyBPC<sup>t/t</sup> mice, resulting in restoration of normal cardiac morphology, preventing activation of the foetal gene program, and resulting in normal cardiac haemodynamics. Both MyBPC<sup>AIP-</sup> and WT MyBPC appear to incorporate normally into the sarcomere, yet only the phosphorylatable form is effective in suppressing the cMyBPC<sup>t/t</sup> phenotype (Sadayappan *et al.*, 2005). Thus, it is not absolutely clear that dephosphorylated cMyBPC directly causes cardiac disease or whether it is an effect of the disease condition on the capacity of the kinases as reduced cMyBPC phosphorylation has been reported in human atrial fibrillation (El-Armouche *et al.*, 2006) and in failing human hearts (El-Armouche *et al.*, 2007). This finding during heart failure is in agreement with attenuated  $\beta$ -adrenergic responsiveness (desensitisation) mainly as a result of decreased  $\beta_1$ -adrenoreceptor number and function and thus attenuated PKA activity (Vatner *et al.*, 1996; Lohse *et al.*, 2003). A reduction in the level of PLB and cTNI phosphorylation measured in several studies in human and dog heart failure have also been observed (El-Armouche *et al.*, 2007).

While dephosphorylated cMyBPC may be associated with disease either as cause or consequence, cMyBPC phosphorylation can actually protect the myocardium from ischaemic injury (Sadayappan *et al.*, 2006). TG mice that expressed a constitutively phosphorylated cMyBPC (cMyBPC<sup>AIP+</sup>; Ser in the MyBPC motif mutated to aspartic acid) were able to restore normal cardiac function to cMyBPC<sup>t/t</sup> mice; furthermore, these hearts were resistant to ischaemia-reperfusion injury (Sadayappan *et al.*, 2006).

Taken together, these studies show that while cMyBPC is not absolutely essential for sarcomere formation, it is necessary for the integrity of sarcomere structure and its phosphorylation is crucial for normal cardiac function, both systolic and diastolic.

#### **1.9.3.5.11.2 Structure of the thick filament and effect on crossbridges**

Myosin crossbridges showed a series of structural changes observed by electron microscopy and optical diffraction upon cMyBPC phosphorylation by PKA, which depended on the isoform of myosin present (Weisberg and Winegrad, 1998). Phosphorylation of cMyBPC in thick filaments containing  $\alpha$ -MHC led to decreased flexibility of crossbridges (with increased order of the crossbridges), looser packing of the backbone of the thick filament, and extension of the crossbridge to what would be the surface of a thin filament in the intact filament lattice. In contrast, the flexibility of the crossbridges containing  $\beta$ -MHC was greater with cMyBPC unphosphorylated than those with  $\alpha$ -MHC, and treatment with PKA did not extend the crossbridges nor change their flexibility (Weisberg and Winegrad, 1998). These authors suggested that the rates of attachment and detachment of the crossbridges to actin must be modified by the change in position of the crossbridge (Weisberg and Winegrad, 1996). Thus, it appears that phosphorylation of cMyBPC may play an important role in regulating the position of the myosin head with respect to the thin filament.

Thick filament structural changes have also been observed, upon MyBPC phosphorylation, by electron microscopy. PKA-mediated phosphorylation increased optical diffraction and filament thickness in the C-zone (Levine *et al.*, 2001). Different degrees of cMyBPC phosphorylation resulted in distinct changes in isolated thick filaments. In the absence of cMyBPC phosphorylation, the thick filament had a disordered structure (myosin heads extending at different angles from the backbone). The addition of the first phosphate to cMyBPC (at site B) induced a change from the disordered structure to a tight structure (myosin heads lying along the backbone). With the addition of the second and third phosphates, by PKA, to sites A and C (di- and triphosphorylated cMyBPC) greater order of myosin heads and looser packing of myosin was observed (Levine *et al.*, 2001). There is no significant difference in the structure of the thick filament produced by the increase in phosphorylation from two to three, and therefore these two states can be lumped together. In this fully phosphorylated state, the myosin heads appeared extended from the thick filament backbone, closer to the thin filament surface, favouring interaction between the thick and thin filament. Thus, electron microscopy of isolated thick filaments confirmed that phosphorylation of cMyBPC initiates crossbridge movement away from the thick filament backbone (Levine *et al.*, 2001).

Disordering of the arrangement of surface myosin heads and declining contractility are coincident with dephosphorylation of MyBPC, while rephosphorylation leads to recovery of both contractility and order (Levine *et al.*, 2001). It is possible that thick filaments have as many as three (or even four) stable structures resulting from the addition of 0, 1, 2 or 3 phosphates. *In vivo*, the relative amounts of each of these three structural states should depend on the level of rhythmic activation of contraction and presumably the time-averaged intracellular  $\text{Ca}^{2+}$  concentration (McClellan *et al.*, 2001).

Thus, the packing of myosin filaments and their heads are intimately linked to the state of cMyBPC phosphorylation, where the extent of phosphorylation correlates with an increased ability of myosin heads to interact with the thin filament. Phosphorylation of cMyBPC also produces a change in flexibility of the crossbridges, probably by changes in the hinge region between the head and the rod portions of the myosin molecule. It is not yet clear how this occurs, but changes in flexibility of the crossbridges could modulate crossbridge detachment rate, and changes in distance from its actin-binding sites as a result of altered packing of myosin rods modulate the attachment rate (Winegrad, 1999).

Kunst *et al* (2000) showed that the properties of the crossbridges can also be modified by the binding of C1C2 to myosin near its hinge region. MyBPC fragments were examined for their effects on the contractile property of skeletal muscle, where phosphorylation of endogenous MyBPC does not occur. Of particular interest were the results with fragments C1C2, where unphosphorylated C1C2 bound to the skinned slow skeletal fibers and reduced  $F_{\max}$  by 50%. The binding changed some of the physical properties of fibers, such as stiffness of crossbridges (Kunst *et al.*, 2000). Thus, collectively these studies suggest that cMyBPC phosphorylation alters the structure of the thick filament (Levine *et al.*, 2001), may modify the kinetics of

crossbridge cycling (Weisberg and Winegrad, 1998) and may also alter the mechanical properties of the hinge region of myosin (Kunst *et al.*, 2000).

#### **1.9.3.5.11.3 Actomyosin ATPase Activity**

Of the myofilament proteins that are phosphorylated (cMyBPC, TNI and RLC), only cMyBPC phosphorylation had a clear correlation with the direction and magnitude of the change in ATPase activity (McClellan *et al.*, 1994). The phosphorylation of cTNI does not increase  $F_{max}$ , and PKA does not phosphorylate RLC (McClellan *et al.*, 2001). Also, a significant increase in maximal ATPase activity and contractility, with a decrease in PKA-dependent phosphorylation, was reported in a mouse model where 30-40% of endogenous cMyBPC was substituted with a construct having a deletion of the cMyBPC LAGGGRRIS insertion (Section 1.9.3.5.1; Yang *et al.*, 2001b). Further, PKA-mediated phosphorylation of cMyBPC has different effects on actomyosin ATPase activity depending on the isoform of MHC present. In rat hearts, PKA-mediated phosphorylation of cMyBPC increased ATPase activity of crossbridges with  $\alpha$ -MHC, but not with  $\beta$ -MHC (Weisberg and Winegrad, 1996).

Contrasting the above data, no change in the ATPase activity was reported upon the removal of unphosphorylated cMyBPC from reconstituted regulated actomyosin systems and its replacement with phosphorylated cMyBPC (Garvey *et al.*, 1988). This study and others (Hofmann *et al.*, 1994; Wattanapermpool *et al.*, 1995) performed in reconstituted contractile protein systems argue against a role for cMyBPC phosphorylation in the regulation of cardiac contractility. But, these apparent inconsistencies can be resolved if the effect of cMyBPC phosphorylation on contractility occurs as a result of changes in the structure of the thick filament (Levine *et al.*, 2001). Reconstituted protein systems do not reproduce the normal thick filament structure nor the steric arrangement of contractile proteins in a filament lattice; therefore, it is very unlikely that the normal strain developed within crossbridges attached to actin in the normal intact contractile filament lattice is reproduced in reconstituted systems (Weisberg and Winegrad, 1998).

#### **1.9.3.5.11.4 Effect on force and kinetics of force production**

##### **Ca<sup>2+</sup>-activated force ( $F_{max}$ )**

Maximum Ca<sup>2+</sup>-activated force ( $F_{max}$ ) is essentially equal to the maximum force developed, measured during contraction of intact and skinned ventricular myocardium (McClellan *et al.*, 2001). Variable effects on  $F_{max}$  have been observed upon cMyBPC phosphorylation, chemical extraction or genetic ablation of cMyBPC (Hofmann *et al.*, 1991b; Kunst *et al.*, 2000; McClellan *et al.*, 2001; Kulikovskaya *et al.*, 2003b; Harris *et al.*, 2004; Herron *et al.*, 2001). McClellan *et al* (2001) showed that a direct relationship existed between the percentage of phosphorylated cMyBPC and  $F_{max}$ , suggesting that in the total absence of phosphorylation, little force is generated. These findings were consistent with those of another study which showed that the unphosphorylated C1C2 fragment reduced  $F_{max}$  in skinned skeletal muscle by 50%, a finding that was reversed upon trisphosphorylation (Kunst *et al.*, 2000). Similarly, Herron *et al* (2001) showed that  $F_{max}$  was

significantly greater after PKA treatment of skinned rat cardiac myocytes. Since endogenous cMyBPC was still present in the Kunst *et al* (2000) study, it was possible that the effects observed were due to competition of added C1C2 with native cMyBPC for binding to S2. Thus, Harris *et al* (2004) repeated this study using cardiac myocytes from cMyBPC-deficient mice, but the addition of unphosphorylated C1C2 to these or WT cardiac myocytes did not alter  $F_{max}$ . Reasons for the discrepancy between effects of C1C2 peptides were unclear, and could be related to myosin isoform type or other fiber differences (Harris *et al.*, 2004).

Further discrepancies around the effect of cMyBPC on force is evident from a study by Hofmann *et al* (1991b), who showed that the chemical extraction of 60-70% of cMyBPC did not alter  $F_{max}$ . In contrast, Kulikovskaya *et al* (2003b) showed that this extraction reduced  $F_{max}$  to 74% its original value, which was reversible by the addition of purified cMyBPC to the relaxing solution. Previous findings from Levine *et al* (2001) and McClellan *et al* (1994) led Kulikovskaya *et al* (2003b) to conclude that the changes in  $F_{max}$  were as a result of structural changes in the thick filament and not as a direct effect of cMyBPC on the force generating interactions. Before cMyBPC extraction, the myosin heads in the majority of thick filaments were well ordered, but after extraction the majority of thick filaments had disordered myosin heads. Order was restored after incubation with cMyBPC, which also increased  $F_{max}$ . Thick filaments with disordered myosin heads have been associated with low  $F_{max}$ , particularly in the presence of a reduced level of phosphorylation of cMyBPC (Levine *et al.*, 2001; McClellan *et al.*, 1994). These correlations suggested that the mechanism by which  $F_{max}$  was reduced with extraction of cMyBPC was a change in the structure of the thick filament that affected the relationship of the myosin heads to the backbone of the filament and presumably to the interactive sites on actin. It was proposed that cMyBPC likely exerted at least part of its effect on contractility by altering overall structure of thick filaments (Kulikovskaya *et al.*, 2003b).

McClellan *et al* (2001) further showed that there are two different  $Ca^{2+}$ -sensitive reactions that could modify  $F_{max}$ . One was regulated by  $Ca^{2+}$  concentrations below the threshold for activation of force and the second by  $Ca^{2+}$  in the same concentration range as force development. The changes in  $F_{max}$  that occur entirely within the range of  $Ca^{2+}$  concentration below contraction threshold are correlated with changes in the phosphorylation of MyBPC (McClellan *et al.*, 2001).

### Power Output

Peak absolute power and peak normalised power were all significantly greater after PKA treatment of skinned rat cardiomyocytes (Herron *et al.*, 2001). PKA increased peak normalised power output more during submaximal  $Ca^{2+}$ -activations than during maximal  $Ca^{2+}$ -activations. These findings were similar in a cMyBPC-deficient mouse model (Korte *et al.*, 2003). In addition, the rate of force redevelopment during half-maximal  $Ca^{2+}$ -activation in skinned mouse cardiomyocytes was also increased (Korte *et al.*, 2003; Stelzer *et al.*, 2006b). The accelerated rate of force development and increased power output at submaximal levels of activation in the cMyBPC-deficient myocardium suggested that cMyBPC is an important regulator

of myocardial work capacity, whereby unphosphorylated cMyBPC acts to limit power output (Korte *et al.*, 2003).

### **Contractile efficiency, work and rate of force decay**

In cMyBPC-deficient mouse models, contractile efficiency was significantly enhanced, maximum oscillatory work occurred at higher frequencies and under rigor conditions, and the internal viscous load was significantly lower compared to WT mice (Palmer *et al.*, 2004c). In addition, the rate of force decay and the delayed force transient were also accelerated in cMyBPC-deficient myocardium compared to WT controls (Stelzer *et al.*, 2006c). Contractile efficiency was enhanced in cMyBPC-deficient myocardium, probably through a reduced loss of mechanical energy normally brought about by a viscous load provided by cMyBPC (Palmer *et al.*, 2004c). The latter findings also suggested that cMyBPC normally constrains the spatial position of myosin crossbridges, which in turn, limits both the rate and extent of interaction of crossbridges with actin. Ablation of cMyBPC removed this constraint, increased the likelihood of crossbridge-binding to actin, and speeded the rate of delayed force development following stretch (Stelzer *et al.*, 2006c). These effects are similar to that of cMyBPC phosphorylation, i.e., an increase in the proximity of myosin heads to actin caused the disruption of cMyBPC binding to myosin S2, which increased the probability of crossbridge binding.

Further, cMyBPC modulates contraction by limiting actomyosin interactions so that crossbridge cycling is slower in the presence of unphosphorylated cMyBPC (when attached to myosin S2) than in its absence (Stelzer *et al.*, 2006b, c). Slowing of the crossbridge kinetics by cMyBPC may account for the dramatic accelerations observed in the time courses of stretch activation in myocytes from cMyBPC null mice (Stelzer *et al.*, 2006c) and in normalised elastance of hearts from cMyBPC-deficient mice (Palmer *et al.*, 2004c). Hypotheses for how MyBPC slows actomyosin interactions include a “tether” model described in the next section and section 1.9.3.5.11.6.

### **Maximal shortening velocity ( $V_{\max}$ )**

The maximal shortening velocity ( $V_{\max}$ ) was increased in the low velocity phase at submaximal  $\text{Ca}^{2+}$  in skinned fibres from rabbit psoas muscles partially depleted of MyBPC (Hofmann *et al.*, 1991a). These findings are consistent with a truncated cMyBPC mouse model (cMyBPC<sup>trt</sup>; lacking domains C8C10) that also showed an enhanced  $V_{\max}$  compared to WT (Palmer *et al.*, 2004b).  $V_{\max}$  of a muscle fibre is directly related to the rate of crossbridge cycling and is thought to be limited by the rate of detachment of crossbridges compressed as a result of relative sliding of thick and thin filaments (Huxley, 1957). Hofmann *et al* (1991a) proposed a model in which an internal load slowed  $V_{\max}$  at low levels of activation once a given amount of active shortening had occurred. cMyBPC may contribute to this internal load by either binding to actin and/or myosin or by influencing mechanical properties of myosin crossbridges. It is proposed that cMyBPC slows shortening velocity at low levels of activation by a direct effect upon the mechanical properties of myosin S2. It is suggested that cMyBPC tethers S2 to the thick filament backbone, resulting in

an internal load due to buckling of S2 at the tether point and subsequent straining of crossbridges as shortening proceeds. The effect on low-velocity phase may be due to an internal load arising from buckling of long-lived crossbridges (a population of slowly cycling crossbridges), which are then strained in a direction that opposes further shortening. cMyBPC binding to S2 contributes to this internal load by placing a structural constraint on these long-lived crossbridges. At low levels of activation, all bound crossbridges initially aid shortening, but as shortening proceeds, S2 is compressively strained giving rise to a force that opposes shortening and ultimately limits high velocity  $V_{max}$  (Hofmann *et al.*, 1991a).

A number of studies have shown that myosin S2-binding is sufficient to tether the myosin heads near the thick filament backbone independent of the LMM myosin-binding sites of cMyBPC (Kunst *et al.*, 2000; Harris *et al.*, 2001). The addition of a recombinant protein containing the S2-binding site (i.e. C1C2) increased  $Ca^{2+}$ -sensitivity of tension in permeabilised myocytes that lacked endogenous cMyBPC (and therefore lack the second LMM-binding site) (Harris *et al.*, 2004). Further, Kunst *et al* (2000) showed that cMyBPC peptides containing the S2-binding domain increased contractility in skinned skeletal muscle fibers concluding that binding of cMyBPC to myosin S2 directly affected contraction independent of binding to LMM. Data from more recent studies suggested that even myosin S2 may not be required for the effects of C1C2 and there may exist a novel mechanism whereby interactions of C1C2 with myosin S1 or the thin filament may affect crossbridge kinetics and contractility (Razumova *et al.*, 2006; Shaffer *et al.*, 2007) (Section 1.9.3.5.9.3 and 1.9.3.5.10).

#### 1.9.3.5.11.5 Effect on $Ca^{2+}$ -sensitivity

Intracellular  $Ca^{2+}$  levels can influence the response of the contractile system to  $\beta$ -adrenergic activity. Sufficient reduction of intracellular  $Ca^{2+}$  blocks the ability of PKA to phosphorylate cMyBPC in intact cells, as  $Ca^{2+}$  is required to activate the CamK-II that adds the first phosphate to site B, before PKA can phosphorylate the remaining sites (McClellan *et al.*, 2001).  $Ca^{2+}$ -regulated changes in thick filament structure that modulate the maximum level of force production and  $Ca^{2+}$ -sensitivity of contraction fit well with changes in contractile activity that occur from alterations in excitation-contraction coupling. An increase in cytoplasmic  $Ca^{2+}$  not only leads to greater  $Ca^{2+}$ -binding to TNC and greater thin filament activation, but also increases the probability of myosin heads forming bonds with actin (McClellan *et al.*, 2001). The increase in cytoplasmic  $Ca^{2+}$  also alters thick filament structure to produce a more rapid rate of crossbridge attachment and greater force production as a result of an enhanced contraction. Lowering cytoplasmic  $Ca^{2+}$  moves crossbridges away from the thin filament, decreasing the probability of formation of the weakly-binding state (Levine *et al.*, 2001).

The effect of cMyBPC on  $Ca^{2+}$ -sensitivity is still controversial, since studies showing that extraction, truncation or knockout of cMyBPC resulted in different effects. A regulatory role was indicated by an increase in the  $Ca^{2+}$ -sensitivity of tension following extraction of the majority of the cMyBPC from skinned cardiac myocytes (Hofmann *et al.*, 1991b), in skinned cardiac muscle from TG expressing C-terminally

truncated cMyBPC (lacking domains C8C10) (Yang *et al.*, 1998; Palmer *et al.*, 2004a), and in skinned skeletal muscle exposed to exogenous soluble N-terminus fragments of cMyBPC (Kunst *et al.*, 2000). A similar increase in  $\text{Ca}^{2+}$ -sensitivity has been observed in a knock-in mouse model with an N-terminus truncation (C0C1 linker and C1 removed) (Witt *et al.*, 2001), while no change (Palmer *et al.*, 2004b) or a decrease (Korte *et al.*, 2003; Harris *et al.*, 2002) in  $\text{Ca}^{2+}$ -sensitivity was found in other studies. *In vitro* contractile protein reconstitution studies demonstrated that the decrease in  $\text{Ca}^{2+}$ -sensitivity associated with PKA phosphorylation is not altered by myofibrils lacking MyBPC (Wattanapermpool *et al.*, 1995). Discrepancies such as these highlight the current difficulty in understanding the means by which cMyBPC and its phosphorylation regulate cardiac contractility.

The knock-in mouse model that carried an N-terminus truncated cMyBPC (C0C1 linker and C1 removed) showed that left ventricular fibers from homozygous mutant mice exhibited an increased  $\text{Ca}^{2+}$ -sensitivity of force development, particularly at lower  $\text{Ca}^{2+}$  concentrations. The findings suggested that at least part of the change in  $\text{Ca}^{2+}$ -sensitivity of cardiac sarcomeres may be related to a functional role of the N-terminus cMyBPC domains (Witt *et al.*, 2001). Additionally, Harris *et al* (2004) showed that the addition of exogenous unphosphorylated C1C2 protein to WT myocytes reversibly increased myofilament  $\text{Ca}^{2+}$ -sensitivity of tension, results which were also observed in myocytes isolated from cMyBPC knockout mice. However, phosphorylation of these exogenous C1C2 peptides by PKA reduced the ability to increase  $\text{Ca}^{2+}$ -sensitivity. These results demonstrated that binding of the C1C2 peptide to S2 alone was sufficient to affect myosin contractile function and suggested that binding of cMyBPC to myosin S2, regulated by cMyBPC phosphorylation, directly influences myofilament  $\text{Ca}^{2+}$ -sensitivity (Harris *et al.*, 2004). Kunst *et al* (2000) reached a similar conclusion based on the observation that exogenously added unphosphorylated C1C2 peptide increased  $\text{Ca}^{2+}$ -sensitivity of tension in permeabilised skeletal muscle fibers.

Further, Calaghan *et al* (2000) found that the addition of purified S2 to permeabilised myocytes increased  $\text{Ca}^{2+}$ -sensitivity, presumably by competing with endogenous S2 for binding to cMyBPC. The changes in the kinetics of contraction and  $\text{Ca}^{2+}$  transient are similar to those seen when myofilament sensitivity is increased through an increase in the affinity of TNC for  $\text{Ca}^{2+}$  (Calaghan *et al.*, 2000) due to a change in crossbridge cycling. If myosin heads spend a greater fraction of their cycle attached to actin, an increase in TNC affinity for  $\text{Ca}^{2+}$  would be expected, as strong-binding myosin heads increase TNC- $\text{Ca}^{2+}$  affinity (Rice *et al.*, 1999). This would result from changes in troponin conformation brought about by movement of tropomyosin that is induced by strong-binding crossbridges (Vibert *et al.*, 1997). This may also be the mechanism by which myofilament  $\text{Ca}^{2+}$ -sensitivity is increased in the cardiac myocytes when cMyBPC is phosphorylated (Calaghan *et al.*, 2000). The converse may apply in the numerous studies that have shown a decrease in the slope of the tension- $p\text{Ca}^{2+}$  curve (reflecting a decrease in co-operativity in myosin head attachment) that results from a lack of cMyBPC (Hofmann *et al.*, 1991b; Witt *et al.*, 2001; Cazorla *et al.*, 2006; Pohlmann *et al.*, 2007).

The increased myofilament  $\text{Ca}^{2+}$ -sensitivity seen in ventricular cardiomyocytes isolated from cMyBPC knockout mice was accompanied by a lower diastolic sarcomere length, which could be abolished by actin-myosin inhibitors, indicating that even during diastole residual bonds remain between actin and myosin (Pohlmann *et al.*, 2007). The relationship between  $\text{Ca}^{2+}$  and sarcomere length showed that cMyBPC-deficient cells started to contract at lower  $\text{Ca}^{2+}$  concentrations and that sarcomere shortening and the  $\text{Ca}^{2+}$  transient were also prolonged in these cells. Cardiac myocytes isolated from the left atria of these mice showed an increased sensitivity to external  $\text{Ca}^{2+}$  and, in contrast to WT cells, continued to develop twitch force at low micromolar  $\text{Ca}^{2+}$ . Thus, removal of cMyBPC results in defective diastolic relaxation and a smaller dynamic range of cell shortening, as a consequence of increased myofilament  $\text{Ca}^{2+}$ -sensitivity. cMyBPC therefore functions as a restraint on myosin-actin interaction at low  $\text{Ca}^{2+}$  and short sarcomere length to allow complete relaxation during diastole (Pohlmann *et al.*, 2007). These findings are consistent with an earlier study (Cazorla *et al.*, 2006) where  $\text{Ca}^{2+}$ -sensitivity of myofilaments was higher in skinned ventricular myocytes from cMyBPC knockout mice than in WT cells at short sarcomere length, but the difference disappeared at longer sarcomere length. The increase in  $\text{Ca}^{2+}$ -sensitivity at the shorter sarcomere length in the cMyBPC knockout cells was accompanied by a significant decrease in the slope of the tension- $p\text{Ca}^{2+}$  curve, reflecting a decrease in co-operativity in myosin head attachment (Cazorla *et al.*, 2006).

Crossbridge cycling at low diastolic  $\text{Ca}^{2+}$  (Pohlmann *et al.*, 2007) in cardiomyocytes isolated from cMyBPC knockout mice may be explained by the findings from a recent study describing the radial displacement of crossbridges away from the thick filament in the absence of  $\text{Ca}^{2+}$  in relaxed myocardium depleted of cMyBPC (Colson *et al.*, 2007). These results are consistent with a model in which cMyBPC normally acts to tether myosin crossbridges nearer to the thick filament backbone, thereby reducing the likelihood of crossbridge-binding to actin under low  $\text{Ca}^{2+}$  concentrations (Pohlmann *et al.*, 2007).

#### 1.9.3.5.11.6 cMyBPC as an internal load

Various studies support the hypothesis that cMyBPC modulates cardiac contraction by limiting actomyosin interaction so that crossbridge cycling is slower in the presence of unphosphorylated cMyBPC than in its absence or when it is phosphorylated (Korte *et al.*, 2003; Stelzer *et al.*, 2006b, c). Hofmann *et al* (1991a) proposed the “tether” model which describes how cMyBPC acts as an internal load within the thick filament that opposes shortening. According to this model, cMyBPC could give rise to an internal load by tethering myosin S2 to the thick filament, thereby limiting myosin head position and/or mobility. A similar hypothesis is proposed by the trimeric collar model, whereby C-terminus cMyBPC molecules form a collar around the thick filament, and with N-terminus regions binding to S2, thus limiting crossbridge formation (Moolman-Smook *et al.*, 2002). Kulikovskaya *et al* (2003a) also proposed that cMyBPC provides an internal load *via* its interaction with actin when cMyBPC is phosphorylated. Such a load could serve a useful function if cMyBPC was able to store some of the energy generated during systole to assist in the filling of the heart during diastole (Kulikovskaya *et al.*, 2003a). The rate of filling of the ventricles becomes progressively more important during diastole, as  $\beta$ -adrenergic stimulation which increases heart rate also increases

phosphorylation of MyBPC. For cMyBPC to store energy effectively during systole, it must not detach and reattach to actin during the contraction because detachment and reattachment would dissipate the stored energy as heat (Kulikovskaya *et al.*, 2003a).

Removal of this constraint, in which ever model, would increase myosin head flexibility and bring the head in closer proximity to actin, thereby enhancing the probability of crossbridge formation. This hypothesis is supported by numerous studies where increased power output (Herron *et al.*, 2001), enhanced contractility (Palmer *et al.*, 2004c), lower viscous load (Palmer *et al.*, 2004c) and increased  $V_{max}$  (Hofmann *et al.*, 1991a) have been observed upon either cMyBPC phosphorylation or deficiency.

## **1.10 CARDIOMYOPATHY**

The importance of RLC, titin, cTNI, TNT, PLB and cMyBPC in cardiac function is evident from findings that mutations in the genes that encode these proteins underlie some cases of hypertrophic cardiomyopathy (HCM) and/or dilated cardiomyopathy (DCM).

### **1.10.1 Hypertrophic Cardiomyopathy**

HCM is a primary myocardial disorder with an autosomal dominant pattern of inheritance that is characterised by ventricular hypertrophy, with histological features of myocyte hypertrophy, myofibrillar disarray and interstitial fibrosis (Maron *et al.*, 1997). HCM is one of the most common inherited cardiac disorders, with prevalence of 1 in 500 in young adults (Maron *et al.*, 1995). In addition, it is a frequent cause of sudden death, particularly in young individuals and competitive athletes with a prevalence ranging from <1% in the general community (Fatkin and Graham, 2002).

HCM is a genetically heterogeneous disorder with disease-causing mutations being identified in genes encoding protein components of the cardiac sarcomere. Thus far, mutations in the genes that encode  $\beta$ -MHC, ELC, RLC, cMyBPC, cardiac actin, cTNT, cTNI, cTNC, TM and titin have been reported (Bashyam *et al.*, 2003). Mutations in genes encoding non-sarcomeric proteins have also been reported to cause HCM (Geier *et al.*, 2008). For each of the disease genes, a variety of different mutations have been reported. In some cases, the encoded protein is of normal size, while in other cases the mutation may result in a premature termination codon or cause a shift of the reading frame with truncation of the encoded protein. Mutations in the known disease genes account for ~50-70% of all cases of HCM. It is possible that a significant number of novel genes may remain to be identified. Despite intensive research, the mechanisms by which disease-causing mutations impair cardiac function and result in left ventricular hypertrophy remain controversial (Fatkin and Graham, 2002).

### **1.10.2 Dilated Cardiomyopathy**

DCM is a myocardial disease characterised by dilatation and impaired contraction of the left ventricle or both ventricles that results in progressive heart failure and sudden cardiac death from ventricular arrhythmia.

DCM has been identified as a relatively common disease, affecting about 40-50 cases per 100000 people (Codd *et al.*, 1989), of which 25-30% are familial DCM. Histologically, DCM is characterised by myocyte hypertrophy, fibrosis of the extracellular matrix and myocardial disarray. The hallmark of DCM is left ventricular enlargement with a reduction of ejection fraction and cardiac output (Franz *et al.*, 2001). Mutations associated with DCM have been identified in genes encoding proteins of the sarcomere, cytoskeleton and the sarcolemma. Although in most diseased hearts, only single mutations are identified, the various mutations all lead to the same disease phenotype, characteristic of DCM. To date, mutations in the genes that encode  $\beta$ -MHC, cMyBPC, actin,  $\alpha$ -TM, TNT, TNI, TNC, titin, T-cap, desmin, vinculin,  $\delta$ -sarcoglycan and MLP have been identified (Chang and Potter, 2005). Like HCM, the mechanisms by which mutations in these genes cause disease remain elusive.

### 1.11 IN THE PRESENT STUDY

Based on the literature review, it is evident that the N-terminus of cMyBPC plays a crucial role in various aspects of structural integrity (thick filament and the sarcomere), cardiac function, in addition to modulating cardiac contractility *via* phosphorylation of the cMyBPC motif (Oakley *et al.*, 2007). The quaternary arrangement of cMyBPC, in the sarcomere, is central to the means by which it achieves these functions. The C-terminus domains are proposed to form a trimeric collar around the thick filament (Moolman-Smook *et al.*, 2002), which is hypothesised to dynamically form and release upon phosphorylation of the MyBPC motif, accommodating or facilitating the changes in the thick filament backbone diameter and affecting crossbridge formation. The N-terminus domains are thought to modulate cardiac contractility by extending into the interfilament space where they may cycle between binding partners dependent perhaps on the phosphorylation status of the MyBPC motif (Kulikovskaya *et al.*, 2003a). Considering the importance of this region, this project focused on the identification of interactors of the N-terminus, using Y2H library screening and adjunctive confirmatory techniques. Previous, library screens using domains C0 and C0C1 as “bait” had yielded no plausible interactors and the reasons for this have been discussed earlier (Section 1.9.3.5.5.1). The present study aimed to identify interactors of domains C1C2, under conditions mimicking the various phosphorylation states of the cMyBPC motif. C1C2 bait constructs mimicking the native, monophosphorylated, trisphosphorylated and dephosphorylated conditions of the cMyBPC motif were used to screen cardiac cDNA libraries, in separate yeast two-hybrid library screens. Putative C1C2 interactors were subject to *in vitro* co-immunoprecipitation (Co-IP), and three-dimensional *in vivo* co-localisation or bioluminescence resonance energy transfer (BRET) analyses to verify interaction with N-terminus cMyBPC. Additionally, the ability of the cardiac-specific region N-terminus of C1 to autoregulate the interactions of the C1C2 region, analogous to the regulatory role of the titin kinase tail (Section 1.9.3.2.2), was also tested by Y2H direct protein-protein interaction assays. Further, the previously observed interaction between domain C3 and C10, (Section 1.9.3.5.6.1) and the hypothesised interaction between domain C2 and C10 was also tested by BRET analysis.

## CHAPTER TWO: MATERIALS AND METHODS

INDEX	PAGE
<b>2.1 DNA EXTRACTION</b>	72
<b>2.1.1 Bacterial plasmid purification</b>	72
<b>2.1.2 Bacterial plasmid purification using Wizard® Purefection Plasmid DNA purification kit</b>	72
<b>2.1.3 Yeast plasmid purification</b>	73
<b>2.1.4 DNA purification using the GFX™ PCR DNA Purification Kit</b>	73
<b>2.2 POLYMERASE CHAIN REACTION</b>	73
<b>2.2.1 Oligonucleotide primer design and synthesis</b>	73
<b>2.2.1.1 Primers for generation of insert for Y2H cloning</b>	73
<b>2.2.1.2 Primers for Y2H insert screening</b>	75
<b>2.2.1.3 Primers for <i>in vitro</i> transcription and translation</b>	76
<b>2.2.1.4 Primers for Bioluminescence Resonance Energy Transfer assays (BRET)</b>	76
<b>2.2.1.5 Primers for <i>in vivo</i> co-localisation experiments</b>	77
<b>2.2.1.6 Primers for In-Fusion™ 2.0 Dry-Down PCR Cloning kit</b>	77
<b>2.2.1.7 Primers for Co-localisation and BRET assay insert screening</b>	78
<b>2.2.2 High Fidelity PCR</b>	79
<b>2.2.3 Site-directed mutagenesis PCR</b>	79
<b>2.2.4 Bacterial colony PCR</b>	82
<b>2.2.5 PCR amplification for <i>in vitro</i> transcription and translation</b>	82
<b>2.3 GEL ELECTROPHORESIS</b>	83
<b>2.3.1 Agarose gel electrophoresis</b>	83
<b>2.3.1.1 Agarose gel electrophoresis for the visualisation of PCR amplified products plasmid DNA isolated from <i>E.coli</i></b>	83
<b>2.3.2 Sodium dodecyl sulphate polyacrylamide gel electrophoresis (SDS-PAGE)</b>	83
<b>2.4 AUTORADIOGRAPHY OF SDS POLYACRYLAMIDE GELS</b>	83
<b>2.5 AUTOMATED DNA SEQUENCING</b>	84
<b>2.6 SEQUENCE ANALYSIS</b>	84
<b>2.6.1 DNA sequence analysis</b>	84
<b>2.6.2 Protein sequence analysis</b>	84
<b>2.7 Y2H prey identification</b>	84
<b>2.8 RESTRICTION ENZYME DIGESTION</b>	85
<b>2.8.1 Restriction enzyme digests for cloning inserts</b>	85
<b>2.9 GENERATION OF CONSTRUCTS</b>	86
<b>2.9.1 Generation of Y2H constructs</b>	86

<b>2.9.2 Generation of constructs for BRET analyses</b>	<b>86</b>
<b>2.9.3 Generation of constructs for <i>in vivo</i> co-localisation assays</b>	<b>86</b>
<b>2.9.4 Alkaline phosphatase treatment of vector</b>	<b>86</b>
<b>2.9.5 DNA ligation</b>	<b>87</b>
<b>2.9.6 Cloning constructs using the In-Fusion™ 2.0 Dry-Down PCR Cloning Kit: Preparation of inserts and vectors, and cloning procedure</b>	<b>87</b>
<b>2.10 BACTERIAL STRAINS, YEAST STRAINS AND CELL LINES</b>	<b>87</b>
<b>2.10.1 Bacterial strains</b>	<b>87</b>
<b>2.10.2 Yeast strains</b>	<b>87</b>
<b>2.10.3 Cell lines</b>	<b>88</b>
<b>2.11 GENERATION OF <i>E.coli</i> DH5<math>\alpha</math> COMPETENT CELLS</b>	<b>88</b>
<b>2.12 CULTURING OF CELL LINES</b>	<b>88</b>
<b>2.12.1 Culture of cells from frozen stocks</b>	<b>88</b>
<b>2.12.1.1 Thawing the cells</b>	<b>88</b>
<b>2.12.1.2 Removing Dimethyl sulphoxide (DMSO) from stocks and culturing cells</b>	<b>88</b>
<b>2.12.2 Splitting of cell cultures</b>	<b>89</b>
<b>2.13 TRANSFORMATION AND TRANSFECTION OF PLASMIDS INTO PROCARYOTE AND EUKARYOTE CELLS</b>	<b>89</b>
<b>2.13.1 Bacterial plasmid transformations</b>	<b>89</b>
<b>2.13.2 Yeast plasmid transformation</b>	<b>89</b>
<b>2.13.3 Transfection of H9C2 cells</b>	<b>90</b>
<b>2.13.4 Differentiation of H9C2 cells</b>	<b>91</b>
<b>2.14 ASSESSMENT OF Y2H CONSTRUCTS</b>	<b>92</b>
<b>2.14.1 Phenotypic assessment of yeast strains</b>	<b>92</b>
<b>2.14.2 Toxicity tests of transformed yeast cells</b>	<b>92</b>
<b>2.14.3 Testing of mating efficiency</b>	<b>92</b>
<b>2.15 Y2H ANALYSIS</b>	<b>93</b>
<b>2.15.1 Cardiac cDNA library</b>	<b>93</b>
<b>2.15.2 Establishment of bait culture</b>	<b>93</b>
<b>2.15.3 Library mating</b>	<b>94</b>
<b>2.15.4 Establishing a library titre</b>	<b>94</b>
<b>2.15.5 Detection of activation of nutritional and reporter genes</b>	<b>94</b>
<b>2.15.5.1 Selection of transformant yeast colonies</b>	<b>94</b>
<b>2.15.5.2 Selection of diploid yeast colonies containing putative interactor peptides</b>	<b>95</b>
<b>2.15.6 Detection of activation of colourimetric reporter genes</b>	<b>95</b>
<b>2.15.6.1 X-<math>\alpha</math>-Galactosidase assay</b>	<b>95</b>

<b>2.15.7 Rescuing prey plasmids from diploid colonies</b>	<b>95</b>
<b>2.15.8 Interaction specificity test</b>	<b>96</b>
<b>2.15.9 Direct Y2H protein-protein interaction assays</b>	<b>96</b>
<b>2.16 CO-IMMUNOPRECIPITATION (Co-IP)</b>	<b>97</b>
<b>2.16.1 Creating an RNase-free experimental environment</b>	<b>97</b>
<b>2.16.2 Transcription and translation of baits and preys</b>	<b>97</b>
<b>2.16.3 Co-IP of translated PCR products</b>	<b>98</b>
<b>2.17 IN VIVO CO-LOCALISATION</b>	<b>100</b>
<b>2.17.1 Co-localisation assay</b>	<b>100</b>
<b>2.18 BIOLUMINESCENCE RESONANCE ENERGY TRANSFER (BRET)</b>	<b>101</b>
<b>2.18.1 BRET assay</b>	<b>102</b>
<b>2.18.2 Statistical Analysis</b>	<b>102</b>

## **2.1 DNA EXTRACTION**

### **2.1.1 Bacterial plasmid purification**

One *Escherichia coli* (*Ecoli*) colony containing the plasmid of interest was picked from an appropriate selection plate and inoculated into 10ml of Luria-Bertani Broth (LB) (Appendix I), supplemented with the appropriate antibiotic, in a 50ml polypropylene tube. The culture was then incubated at 37°C overnight, while shaking at 250rpm in a YIH DER model LM-530 shaking incubator.

The culture was centrifuged, the next day, for 10 minutes at 3000rpm in a Beckman model TJ-6 centrifuge, after which the supernatant was discarded and the pellet resuspended in 1ml of cell suspension solution (Appendix I) by gentle pipetting. Two millilitres of cell lysis solution (Appendix I) was added and the contents were mixed by gentle inversion of the tube, which was then incubated at room temperature for 5 minutes. Two millilitres of neutralisation solution (Appendix I) was added to the tube and the contents were once again mixed by gentle inversion and incubated at room temperature for 5 minutes. Following this incubation, 5ml of phenol/chloroform/isoamyl alcohol (25:24:1 [PCI]) (Sigma, St Louis, MO, USA) was added to the tube and the contents mixed by gentle inversion, followed by centrifugation at 3000rpm for 15 minutes at 4°C in a Multex centrifuge (MSE Scientific Instruments, Sussex, UK), in order to allow for phase separation.

The upper clear plasmid-containing (aqueous) phase was transferred to a new sterile 50ml polypropylene tube and approximately 0.7X volume 100% isopropanol (Merck, Darmstadt, Germany) was added to the tube, which was mixed well by gentle inversion. This was followed by centrifugation at 4°C for 45 minutes in a Multex centrifuge at 10000rpm. After centrifugation, the supernatant was discarded and the pellet was washed twice with 2ml ice cold 70% ethanol and then air-dried. The dried pellet was resuspended in 100µl sterile water and subsequently 3µl of this plasmid was resolved on a 1% SB agarose gel (Appendix I) for verification (Section 2.3.1.1).

### **2.1.2 Bacterial plasmid purification using Wizard® Purefection Plasmid DNA purification kit**

The Wizard® Purefection Plasmid DNA purification kit (Wizard® Purefection Plasmid DNA purification kit, Promega Corp. Madison Wisconsin, USA) was used to isolate plasmid DNA, free of endotoxins, which was used to transfect H9C2 cells for bioluminescence resonance energy transfer (BRET) (Section 2.18) and *in vivo* co-localisation assays (Section 2.17).

Twenty microlitres of a bacterial glycerol stock, of the appropriate vector, was inoculated into 10ml LB media (supplemented with the appropriate antibiotic) in separate 50ml polypropylene tubes. The cultures were incubated at 37°C overnight, while shaking at 250rpm in a YIH DER model LM-530 shaking incubator. The next day, the cultures were centrifuged for 10 minutes at 3000rpm in a Beckman model TJ-6 centrifuge. The supernatant was then discarded and the plasmid DNA was extracted using the Wizard® kit, as per manufacturer's instructions. Following extraction, the DNA was resuspended in 50µl sterile water and the

concentration visually determined by electrophoresing an aliquot of the DNA on a 1% SB agarose gel (Appendix I) (Section 2.3.1.1).

### **2.1.3 Yeast plasmid purification**

In order to isolate the plasmid of interest from yeast cells, a loop-full (~10µl) of these cells growing on the appropriate solid media was inoculated into 1ml synthetic dropout (SD) medium containing the appropriate dropout supplement (BD Bioscience, Clontech, Paulo Alto, CA, USA) and incubated overnight at 30°C in a shaking incubator (SCILAB Instrument Co. Ltd, Taipei, Taiwan) at 250rpm. Four millilitres of YPDA media (Appendix I) was added to the culture the next morning, and the culture incubated for an additional 4 hours at 30°C. Thereafter, the culture was centrifuged at 3000rpm for 5 minutes. The pellet was resuspended in 200µl of yeast lysis buffer (Appendix I), to which 200µl PCI and 0.3g 450-600µm glass beads (Sigma) were added. The yeast cells were milled by vortexing this mixture for 2.5 minutes using a Snijders model 34524 press-to-mix vortex, followed by centrifugation at 14000rpm for 5 minutes at room temperature in a Beckman Microfuge Lite. The aqueous phase was transferred to a new, sterile 1.5ml microcentrifuge tube and 100µl of this solution was purified using the GFX™ PCR DNA purification kit (Section 2.1.4). The purified DNA was eluted in 30µl sterile water, and this solution was used to transform DH5α *Ecoli* cells (Section 2.13.1).

### **2.1.4 DNA purification using the GFX™ PCR DNA Purification Kit**

Purification of bacterial plasmid preparations (Section 2.1.1 and Section 2.1.3) and PCR-amplified DNA products (Section 2.2) were performed, using the GFX™ PCR DNA Purification Kit (GE Healthcare, Buckinghamshire, UK) as per manufacturer's instructions, to obtain purified products suitable for nucleotide sequencing (Section 2.5) and cloning reactions (Section 2.9).

## **2.2 POLYMERASE CHAIN REACTION**

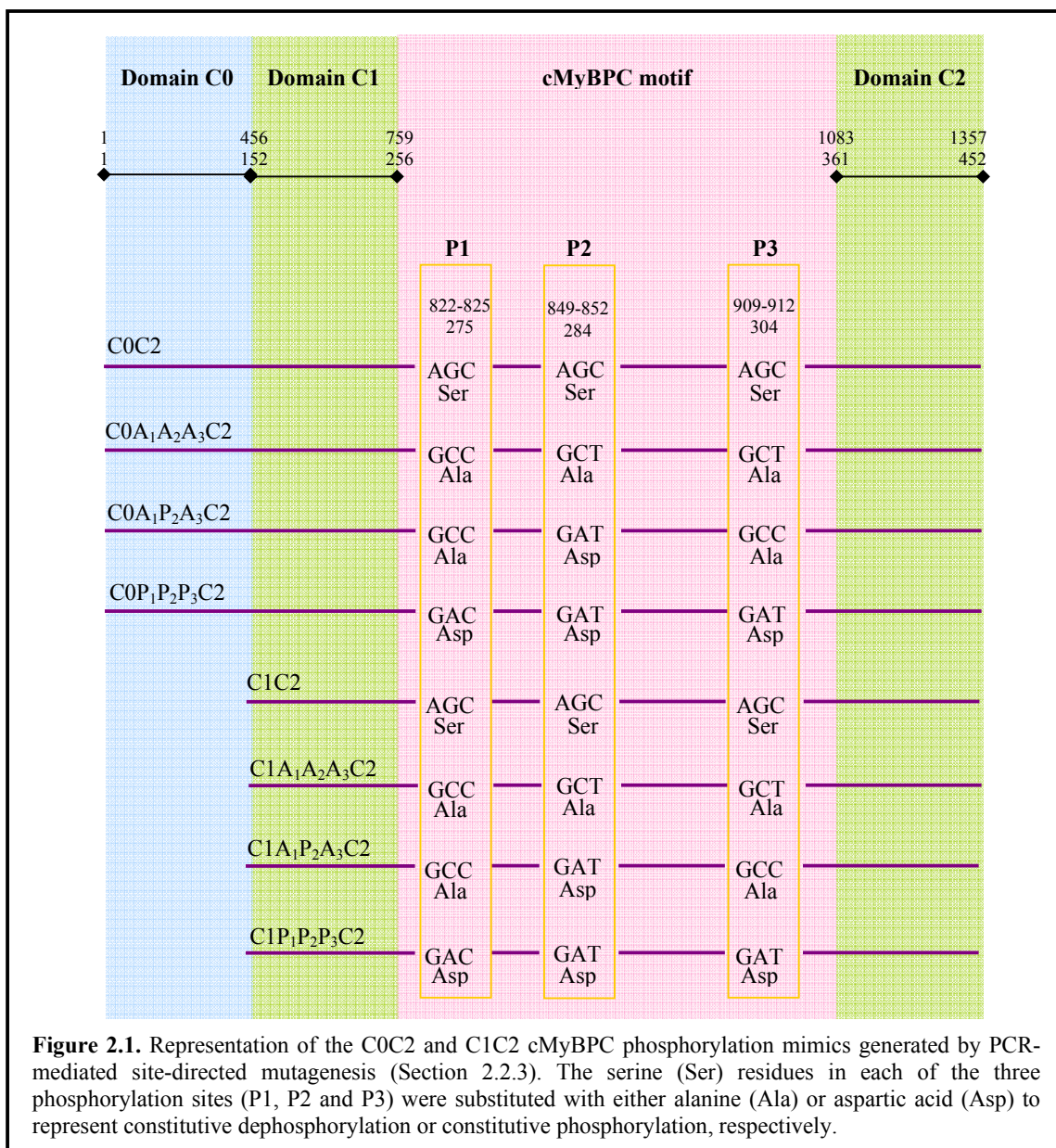
### **2.2.1 Oligonucleotide primer design and synthesis**

Primers were designed using sequence data from the Genbank database (<http://www.ncbi.nlm.nih.gov/Entrez>). Before synthesis, each primer set was analysed for self-complimentarity, primer-primer complimentarity, and compatibility of melting temperatures using DNAMan™ version 4 software (Lynnion Biosoft Corp©). All primers used in this study were synthesised at the University of Cape Town DNA synthesis Laboratory (University of Cape Town, Cape Town, RSA).

#### **2.2.1.1 Primers for generation of insert for Y2H cloning**

To generate PCR-amplified fragments of the C0C2 and C1C2 region representing the various phosphorylation states of the cMyBPC motif, outer forward and reverse primers, in addition to various sets of complimentary site-directed mutagenesis primers, were designed using the *MYBPC3* mRNA sequence (GenBank: <http://www.ncbi.nlm.nih.gov/Entrez>; sequence accession number: NM\_000256). To mimic the various phosphorylation states of the cMyBPC motif, the serine residues in each of the three phosphorylation

sites were substituted with either aspartic acid, to represent constitutive phosphorylation, or alanine, to represent constitutive dephosphorylation, by PCR-mediated site-directed mutagenesis (Figure 2.1) (Section 2.2.3). These phosphorylation mimics have been successfully used in other studies (Sadayappan *et al.*, 2005; Sadayapan *et al.*, 2006). Since the serine residues in the first and second phosphorylation sites were 8 amino acids apart, one set of complimentary mutagenesis primers was designed to allow generation of mimics of each of the phosphorylation state-combinations at these two sites. A separate set of primers were designed to substitute the serine in the third phosphorylation site, 19 amino acids away from the second phosphorylatable serine in the cMyBPC motif. To generate the full length C1C2 phosphorylation mimics, outer primers C1-F and C2-R were designed, while for the C0C2 phosphorylation mimics, C0-F was designed to be used in conjunction with C2-R (Table 2.1).



The subsequent cloning of these PCR-amplified fragments was facilitated by the addition of a unique restriction enzyme site to the 5' end of both the outer forward (C1-F and C0-F) and reverse (C2-R) primers. In addition, the 5' end contained additional ‘overhang’ nucleotides to allow restriction enzyme digestion, while a transcription termination codon was added to the 5' tag of the reverse primer.

**Table 2.1.** Nucleotide sequences of primers used for the amplification of the C1C2 and C0C2 PCR products, representing the different phosphorylation states of the cMyBPC motif

Primer	Sequence
C1-F <sup>Nde I</sup>	5'- <b>A</b> CTGCAGAAC <b>C</b> ATATGCCCATTGGCCTTTCGTGA-3'
C2-R <sup>EcoR I</sup>	5'- <b>A</b> CTGCAGAAC <b>G</b> AATT <b>C</b> TAGGGCTCTTCACAAAGAGCT-3'
C0-F <sup>Nde I</sup>	5'- <b>A</b> CTGCAGAAC <b>C</b> ATATGATGCCCTGAGCCGGGAAG-3'
C1P <sub>1</sub> P <sub>2</sub> -F	5'-GCCGCACG <b>G</b> A CCTGGCTGGAGGTGGTCGGCGGATC <b>G</b> ATGATAGCC-3'
C1P <sub>1</sub> P <sub>2</sub> -R	5'-GGCTATCA <b>T</b> CGATCCGCCGACCACCTCCAGCCAGG <b>T</b> CCGGCGGC-3'
C1P <sub>3</sub> -F	5-GAGAGAC <b>G</b> ATTCCGGACC-3'
C1P <sub>3</sub> -R	5-GGTCCGGAA <b>A</b> TCGTCTCTC-3'
C1A <sub>1</sub> A <sub>2</sub> -F	5'-GCCGCACG <b>G</b> CCCTGGCTGGAGGTGGTCGGCGGATC <b>G</b> CTGATAGCC-3'
C1A <sub>1</sub> A <sub>2</sub> -R	5'-GGCTATCA <b>G</b> C GATCCGCCGACCACCTCCAGCCAGG <b>G</b> CCGTGCGGC-3'
C1A <sub>3</sub> -F	5-GAGAGAC <b>G</b> CTTCCGGACC-3'
C1A <sub>3</sub> -R	5-GGTCCGGAA <b>A</b> GC GTCTCTC-3'
C1A <sub>1</sub> P <sub>2</sub> -F	5'-GCCGCACG <b>G</b> CCCTGGCTGGAGGTGGTCGGCGGATC <b>G</b> ATGATAGCC-3'
C1A <sub>1</sub> P <sub>2</sub> -R	5'-GGCTATCA <b>T</b> CGATCCGCCGACCACCTCCAGCCAGG <b>G</b> CCGTGCGGC-3'

The nucleotide sequence in black font represents the sequence of the primer that anneals to the DNA in the PCR reaction. An “overhang” tag to facilitate restriction enzyme digestion is represented in blue font, while the sequence in bold red font represents the different restriction enzyme sites. The nucleotides in bold orange represents that the bases that were mutated: AG→GA substitution to alter serines to glutamic acids for the phosphorylated mimic and AG→GC substitution to alter serines to alanines for the dephosphorylated mimic. Abbreviations: °C, degrees Celsius; Ta, annealing temperature

### 2.2.1.2 Primers for Y2H insert screening

Vector-specific primers, flanking the multiple cloning site (MCS) of pGBKT7 (BD Bioscience, Clontech) (Appendix V) and pACT2 (BD Bioscience, Clontech) (Appendix V), were designed to amplify inserts cloned into these vectors. The vector sequences used in the design of these primers were obtained from the Clontech Matchmaker™ vector handbook ([www.clontech.com](http://www.clontech.com)) and are shown in Table 2.2.

**Table 2.2.** Primer sequences and annealing temperatures used for the amplification of inserts from Y2H cloning vectors

Name	Sequence	Ta (°C)
pGBKT7-F	5'-TCATCGGAAGAGAGTAG-3'	45
pGBKT7-R	5'-TCACTTAAAATTTGTATACA-3'	
pACT2-F	5'-CTATTCGATGATGAAGATACCCCACCAAACC-3'	57
pACT2-R	5'-GTGAACTTGCAGGGTTTCAGTATCTACGA-3'	

Abbreviations: °C, degrees Celsius; Ta, annealing temperature

### 2.2.1.3 Primers for *in vitro* transcription and translation

In order to generate PCR-amplified products to be used in *in vitro* transcription and translation experiments (Section 2.16.2), primers were designed using pGBK7 and pACT2 vector sequences obtained from Clontech™ Matchmaker™ vector handbook ([www.clontech.com](http://www.clontech.com)). The primer sequences and annealing temperatures are shown in Table 2.3.

**Table 2.3.** Primers for the generation of products used in *in vitro* transcription and translation experiments

Name	Sequence	Ta(°C)
BK-Myc-F	5'-AAATAAAATTGTAATACGACTCACTATAGGGCGAGCCGCCACCATGGAGGAGCAG AAGCTGATGTCA-3'	49
BK-R	5'-TCACTTTAAAATTGTATACAC-3'	
ADHA-F	5'-AAATAAAATTGTAATACGACTCACTATAGGGCGAGCCGCCACCATGTACCCATAC GACGTTCCAGAT-3'	42
ADHA-R	5'-GGGGTTTTTCAGTATCTACGAT-3'	

Abbreviations: °C, degrees Celsius; Ta, annealing temperature

### 2.2.1.4 Primers for Bioluminescence Resonance Energy Transfer assays (BRET)

Sequence-specific primers were designed to PCR amplify inserts [C1C10 (pRluc-C1), C3C10 (pRluc-C1), C7C10 (pRluc-C1), C3C10 (GFP<sup>2</sup>-MCS-Rluc), C7C10 (GFP<sup>2</sup>-MCS-Rluc), actin (ACTC1) (pGFP<sup>2</sup>-C3) and cTNI (pGFP<sup>2</sup>-C3)] and clone them into the appropriate vectors (Perkin Elmer, Massachusetts, USA) (Appendix V). To facilitate the subsequent cloning of these PCR-amplified fragments, the 5' ends of both the forward and reverse primers contained a unique restriction enzyme recognition site. The 5'-ends also contained additional ‘overhang’ nucleotides to allow restriction enzyme digestion. At least one transcription termination codon was added to the 5'-tag of the reverse primer. The nucleotide sequences and annealing temperatures of the primers are shown in Table 2.4. To generate the cMyBPC inserts, the cMyBPC cDNA construct was used as template in the PCR reaction, while cardiac cDNA from a cDNA library (MATCHMAKER, Clontech) was used to amplify ACTC1 and cTNI.

**Table 2.4.** Primers for the generation of products used for BRET assays

Name	Accession No. Base pairs	Sequence	Ta( <sup>0</sup> C)
cTNI-F <sup>EcoRI</sup>	NM_000363	5'- <b>ACTGCAGAA</b> <b>GAATTC</b> ATGGCGGATGGGAGCAGCG-3'	
cTNI-R <sup>KpnI</sup>	1-633	5'- <b>ACTGCAGAA</b> <b>GGTAC</b> CTCAGCTCTCAAACCTTTCTTGC-3'	50
ACTC1-F <sup>EcoRI</sup>	NM_005159	5'- <b>ACTGCAGAA</b> <b>GAATTC</b> GGATGTGTGACGACGAGGAGAC-3'	
ACTC1-R <sup>KpnI</sup>	1-1134	5'- <b>ACTGCAGAA</b> <b>GGTAC</b> CTTAGAAGCATTGCGGTGGAC-3'	52
C1C10-F <sup>EcoRV</sup>	NM_000256	5'- <b>ACTGCAGAA</b> <b>GATATC</b> CCCATTGGCCTCTCGTGA-3'	
C1C10-R <sup>BamHI</sup>	457-3825	5'- <b>ACTGCAGAA</b> <b>GGATTC</b> TTATCACTGAGGCACTCGCA-3'	50
C3-F <sup>KpnI</sup>	NM_000256; 1359	5'- <b>ACTGCAGAA</b> <b>GGTAC</b> CCCTGTGCTCATCACGCGCCC-3'	
C10-R <sup>XbaI</sup>	NM_000256	5'- <b>ATCACAGCA</b> <b>TCTAGA</b> CTATCACTGAGGCACTCGCA-3'	55
C7-F <sup>KpnI</sup>	NM_000256; 3604	5'- <b>ACTGCAGAA</b> <b>GGTAC</b> GGTCCCCCAGCGAACCC-3'	55

Abbreviations: <sup>0</sup>C, degrees Celsius; Ta, annealing temperature. The nucleotide sequence in black font represents the sequence of the primer that anneals to the DNA in the PCR reaction. An “overhang” tag to facilitate restriction enzyme digestion is represented in blue font, while the sequence in bold red font represents the different restriction enzyme sites.

### 2.2.1.5 Primers for *in vivo* co-localisation experiments

In order to PCR amplify domains C1C10 cMyBPC from a cMyBPC construct and clone it into the pGFP<sup>2</sup>-C3 vector, sequence-specific primers were designed. To facilitate the subsequent cloning of the PCR-amplified fragments, the same procedure as that described in section 2.2.1.4 was performed. The nucleotide sequence and annealing temperature of this primer set is shown in Table 2.5.

**Table 2.5.** Primers for the generation of products used in *in vivo* co-localisation experiments

Name	Sequence	Ta( <sup>0</sup> C)
C1C10-F <sup>EcoRV</sup>	5'- <b>ACTGCAGAA</b> <b>GATATC</b> CCCATTGGCCTCTCGTGA-3'	
C1C10-R <sup>BamHI</sup>	5'- <b>ACTGCAGAA</b> <b>GGATTC</b> TTATCACTGAGGCACTCGCA-3'	50

Abbreviations: <sup>0</sup>C, degrees Celsius; Ta, annealing temperature. The nucleotide sequence in black font represents the sequence of the primer that anneals to the DNA in the PCR reaction. An “overhang” tag to facilitate restriction enzyme digestion is represented in blue font, while the sequence in bold red font represents the different restriction enzyme sites.

### 2.2.1.6 Primers for In-Fusion™ 2.0 Dry-Down PCR Cloning kit

Since the cloning of cMyBPC domains C2C10 into vectors pRLuc-C1 and GFP<sup>2</sup>-MCS-Rluc proved difficult *via* traditional cloning methods, the In-Fusion™ 2.0 Dry-Down PCR Cloning kit (BD Bioscience, Clontech) was used. For successful cloning, the PCR generated fragment to be cloned must share at least 15 base pairs of homology at each end with the linearisation site of the vector. Sequence-specific primers were therefore designed to PCR amplify domains C2C10 of cMyBPC, with 5'-overhangs that had appropriate homology to the cloning vector (Table 2.6). In addition, the cloning of inserts into the DsRed-Monomer-C1 (Appendix V) (Clontech) vector for *in vivo* co-localisation was also performed using this method. The primer sequences are shown in Table 2.6.

Restriction enzyme sites and overhang nucleotides did not need to be built into the primers as the kit did not employ traditional cloning methods.

**Table 2.6.** Primers for the generation of products used for In-Fusion™ cloning

Name	Accession No Base pairs	Sequence	Ta (°C)
C2C10-	NM_000256	5'- <b>TCTCACCGTCTGCAGGATATCAA</b> AGCACAGCCTTCAGAAGAAG-3'	
RC1-F	1069-3826		55
C2C10-		5'- <b>GGTGGATCCCGGGCCGCGG</b> TTCACTGAGGCACTCGCAC-3'	
RC1-R			
C2C10-	NM_000256	5'- <b>GGATCAAGCTTGACCGGTACC</b> AGCACAGCCTTCAGAAG AAG-3'	
MCS-F	1069-3825		55
C2C10-		5'- <b>GCTGGTCATGGTGGCTCTAGA</b> CTGAGGCACTCGCAC-3'	
MCS-R			
HSPB7-F	NM_014424	5'- <b>TCCGGACTCAGATCTCGAGCT</b> GCCCAGGACCCGCCATGGAG-3'	
	1-513	5'-	
HSPB7-R		<b>CCGGGCCCGCGGTACCGTCGACT</b> CAGATTGATCTCCGTCCGGAAGG	57
		TCA-3'	
ENO3-F	NM_053013	5'- <b>TCCGGACTCAGATCTCGAGCT</b> ATGGCCATGCAGAAAATCTTG-3'	
ENO3-R	1-1305	5'- <b>CCGGGCCCGCGGTACCGTCGACT</b> CACTTGGCCTTCGGGTTAC-3'	48

Abbreviations: °C, degrees Celsius; Ta, annealing temperature. The nucleotide sequence in bold blue font represents the region of vector homology (for cloning by the In-Fusion™ method) while the black font shows the insert-specific sequence that anneals to the DNA in the PCR reaction.

#### 2.2.1.7 Primers for Co-localisation and BRET assay insert screening

Vector-specific forward and reverse primers, flanking the multiple cloning site (MCS) of GFP<sup>2</sup>-C3 (Appendix V), GFP<sup>2</sup>-MCS-Rluc (Appendix V) and Rluc-C1 (Appendix V), were designed to amplify inserts cloned into these vectors. The vector sequences used in the design of these primers were obtained from the BRET<sup>2</sup>™ technical data sheet ([www.perkinelmer.com](http://www.perkinelmer.com)) and are shown in Table 2.7.

**Table 2.7.** Primers for Co-localisation and BRET assay insert screening

Name	Sequence	Ta(°C)
GFP <sup>2</sup> -C3-F	5'-CTGCTGGAGTTCGTGACC-3'	
GFP <sup>2</sup> -C3-R	5'-TTTATGTTTCAGGTTCAAGG-3'	44
Rluc-C1-F	5'- GAACAACGGGCCGGGATC-3'	
Rluc-C1-R	5'-CAAGTAAACCTCTACAAATGTGGTAT-3'	55
GFP <sup>2</sup> -MCS-Rluc-F	5'-ATCACTCTCGGCATGGAC-3'	
GFP <sup>2</sup> -MCS-Rluc-R	5'- GTCATGGTGGCTCTAGAG G-3'	55
DsRed-F	5'- TACGAGCACGCCGAGGCC-3'	
DsRed-R	5'- CAAGTAAACCTCTACAAATGTGGTATGGC-3'	55

Abbreviations: °C, degrees Celsius; Ta, annealing temperature

## 2.2.2 High Fidelity PCR

High fidelity PCR was used to amplify overlapping segments to generate the C1C2 and C0C2 cMyBPC PCR fragments mimicking the different phosphorylation states of the cMyBPC motif (Section 2.2.3). The phosphorylation mimics were subsequently cloned into the Y2H bait vector, pGBT7 (Section 2.9.1) (Appendix V). In addition, high fidelity PCR was used to amplify inserts for BRET (Section 2.18) and *in vivo* co-localisation (Section 2.17) assays.

For the amplification, 50ng of cMyBPC cDNA, plasmid DNA (Section 2.1.1) or PCR template (Section 2.2.3) was used in a reaction performed in a 50 $\mu$ l volume containing: 150ng of each primer (Table 2.1-2.6), 1.5 $\mu$ l of an equimolar dNTP solution (2.5mM of each dATP, dCTP, dTTP and dGTP) (TaKaRa Shuzo Co. Ltd, Shiga, Japan), 5 $\mu$ l of 10X Ex Taq<sup>TM</sup> Mg<sup>2+</sup>-containing reaction buffer (TaKaRa Shuzo Co. Ltd), 1.5U Ex Taq<sup>TM</sup> (TaKaRa Shuzo Co. Ltd) and sterile water to a final volume of 50 $\mu$ l. Thermal cycling was performed in a Mastercycler® ep PCR system (Eppendorf, Hamburg, Germany). Thermal cycling parameters consisted of a single denaturing cycle of 94°C for 2 minutes followed by 30 cycles of 94°C for 30 seconds, annealing temperature (Ta; Table 2.1-2.6) for 30 seconds and 72°C for 1 minute. A final elongation step was performed at 72°C for 5 minutes. The amplification products were subsequently visualised by gel electrophoresis on a 1% SB agarose gel for verification (Section 2.3.1).

## 2.2.3 Site-directed mutagenesis PCR

*In vitro* site-directed mutagenesis PCR was used to generate the C0C2 and C1C2 PCR products, representing the different phosphorylation states of the MyBPC motif, respectively (Section 2.1.1.1). The PCR products generated represented the native C1C2 fragment (C1C2), a monophosphorylated (C1A<sub>1</sub>P<sub>2</sub>A<sub>3</sub>C2), trisphosphorylated (C1P<sub>1</sub>P<sub>2</sub>P<sub>3</sub>C2), as well as a dephosphorylated (C1A<sub>1</sub>A<sub>2</sub>A<sub>3</sub>C2) fragment. The C0C2 fragments represented the same phosphorylation states as the C1C2 mimics, with the addition of the C0 domain and the pro-alanine-rich linker sequence between C0 and C1. The primer sequences and primer pairs used to generate these PCR fragments are shown in Table 2.1 and Table 2.8.

PCR mediated site-directed mutagenesis for the C0C2-dephosphorylated (C0A<sub>1</sub>A<sub>2</sub>A<sub>3</sub>C2) bait fragment is described; other phosphorylation mimic fragments were generated in an analogous manner. The first set of PCR reactions involved generating two overlapping PCR segments in which the serine residues in the first two phosphorylation sites have been mutated to alanine residues. Two complimentary mutagenesis primers (C1A<sub>1</sub>A<sub>2</sub>-F and C1A<sub>1</sub>A<sub>2</sub>-R; Table 2.1 and Table 2.8), were used in conjunction with the outer primers C0-F and C2-R, respectively, in two separate high-fidelity PCR reactions (Figure 2.2, Step A). In both these PCR reactions, 50ng of MyBPC cDNA was used as template and thermal cycling was performed in a Mastercycler® ep PCR system for 30 cycles with cycling profiles consisting of 30 seconds at 94°C, 30 seconds at 55°C, and 1 minute at 72°C for extension. Five microlitres of the overlapping segments that were generated by this initial PCR were separated on a 2% SB agarose gel to confirm that the sizes of the products were appropriate (Section 2.3.1.1).

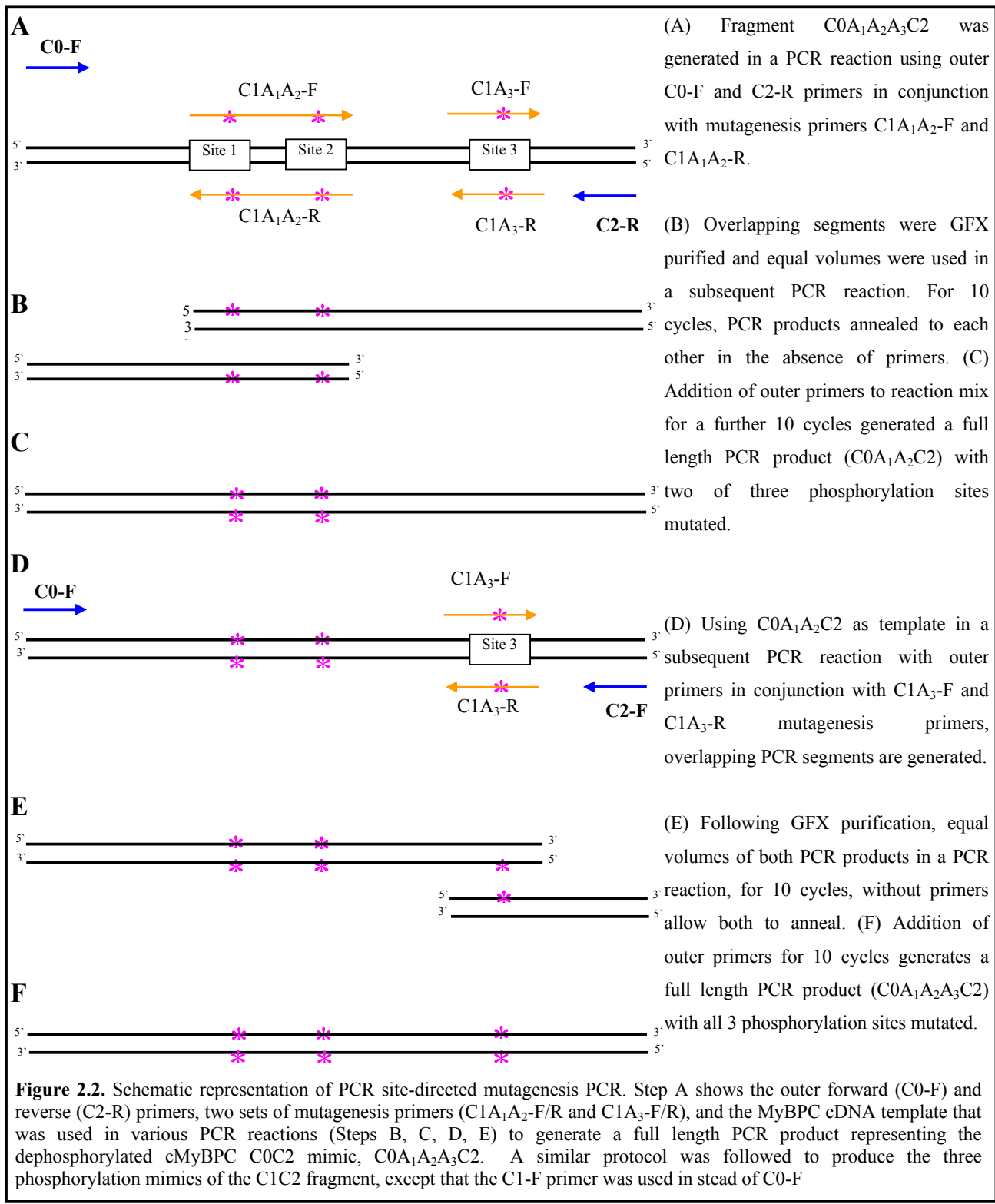
Following GFXTM purification of these PCR products (Section 2.1.4) (Figure 2.2, Step B) to remove the primers, a 4 $\mu$ l aliquot of each product was added to the second PCR reaction mix consisting of: 1.5 $\mu$ l of an equimolar dNTP solution (consisting of 2.5mM each of dATP, dCTP, dTTP and dGTP), 5 $\mu$ l of 10X Ex TaqTM Mg<sup>2+</sup>-containing reaction buffer, 1.5U Ex TaqTM and sterile water to a final volume of 46.5 $\mu$ l. This mixture was subjected to 10 cycles of thermal cycling identical to that described above; during this step, annealing of the overlapping regions of the mutagenesis primers allowed filling-in of the full-length product.

**Table 2.8.** Primer pairs and annealing temperatures used for the amplification of C1C2 and C0C2 PCR products, representing the different phosphorylation states of the cMyBPC motif

PCR Fragment	PCR 1	PCR 2	PCR 3	PCR 4	Ta (°C)
C1P <sub>1</sub> P <sub>2</sub> P <sub>3</sub> C2	C1-F & C1P <sub>1</sub> P <sub>2</sub> -R	C1-F & C2-R	C1-F & C1P <sub>3</sub> -R	C1-F & C2-R	55
	C1P <sub>1</sub> P <sub>2</sub> -F & C2-R		C1P <sub>3</sub> -F & C2-R		
C1A <sub>1</sub> P <sub>2</sub> A <sub>3</sub> C2	C1-F & C1A <sub>1</sub> P <sub>2</sub> -R	C1-F & C2-R	C1-F & C1A <sub>3</sub> -R	C1-F & C2-R	55
	C1A <sub>1</sub> P <sub>2</sub> -F & C2-R		C1A <sub>3</sub> -F & C2-R		
C1A <sub>1</sub> A <sub>2</sub> A <sub>3</sub> C2	C1-F & C1A <sub>1</sub> A <sub>2</sub> -R	C1-F & C2-R	C1-F & C1A <sub>3</sub> -R	C1-F & C2-R	55
	C1A <sub>1</sub> A <sub>2</sub> -F & C2-R		C1A <sub>3</sub> -F & C2-R		
C0P <sub>1</sub> P <sub>2</sub> P <sub>3</sub> C2	C0-F & C1P <sub>1</sub> P <sub>2</sub> -R	C0-F & C2-R	C0-F & C1P <sub>3</sub> -R	C0-F & C2-R	55
	C1P <sub>1</sub> P <sub>2</sub> -F & C2-R		C1P <sub>3</sub> -F & C2-R		
C0A <sub>1</sub> P <sub>2</sub> A <sub>3</sub> C2	C0-F & C1A <sub>1</sub> P <sub>2</sub> -R	C0-F & C2-R	C0-F & C1A <sub>3</sub> -R	C0-F & C2-R	55
	C1A <sub>1</sub> P <sub>2</sub> -F & C2-R		C1A <sub>3</sub> -F & C2-R		
C0A <sub>1</sub> A <sub>2</sub> A <sub>3</sub> C2	C0-F & C1A <sub>1</sub> A <sub>2</sub> -R	C0-F & C2-R	C0-F & C1A <sub>3</sub> -R	C0-F & C2-R	55
	C1A <sub>1</sub> A <sub>2</sub> -F & C2-R		C1A <sub>3</sub> -F & C2-R		

Following this step, 1 $\mu$ l of 150ng each of the outer forward and reverse primers (C0-F and C2-R), formamide to a final concentration of 5% and an additional 1.5U Takara Ex TaqTM were added to these tubes, to a final volume of 50 $\mu$ l. This was followed by a further 10 thermal cycles under the same conditions in order to amplify the filled-in product. The full-length PCR product thus obtained, with two phosphorylation sites mutated (Figure 2.2, Step C), was visualised on a 2% SB agarose gel (Section 2.3.1.1). The C0A<sub>1</sub>A<sub>2</sub>C2 PCR

product was GFXTM purified (Section 2.1.4) prior to it being used as template in subsequent PCR reactions. To mutate the third phosphorylation site, a second set of complimentary mutagenesis primers (C1A<sub>3</sub>-F and C1A<sub>3</sub>-R; Table 2.1 and Table 2.8), were used in conjunction with the outer primers C2-R and C0-F, respectively, in a third high-fidelity PCR reaction (Section 2.2.2) (Figure 2.2, Step D). Fifty nanograms of the C0A<sub>1</sub>A<sub>2</sub>C2 PCR product, generated as described above, was used as template in both these PCR reactions.



The thermal cycling conditions and PCR mix was the same as described above, to generate overlapping PCR segments. Five microlitres of the overlapping segments that were generated were separated on a 2% SB agarose gel to confirm the size of the products (Section 2.3.1.1). Following GFXTM purification of these PCR products (Section 2.1.4) (Figure 2.2, Step E) they were used as template in the fourth PCR reaction to generate a full length product representing a dephosphorylated C0C2 mimic, C0A<sub>1</sub>A<sub>2</sub>A<sub>3</sub>C2 (Figure 2.2, Step F). The thermal cycling conditions and PCR mix were the same as described for generating the C0A<sub>1</sub>A<sub>2</sub>C2 PCR product.

The native C1C2 and C0C2 mimics were generated by two high fidelity PCR reactions using the outer primers, C1-F & C2-R and C0-F & C2-R, respectively. The PCR reaction mix and cycling conditions were as described before (Section 2.2.2).

#### **2.2.4 Bacterial colony PCR**

Bacterial colony PCRs were performed to identify the bacterial colonies harbouring the desired recombinant plasmid to be used in Y2H (Section 2.15), BRET (Section 2.18) and *in vivo* co-localisation (Section 2.17) analyses. In these PCR reactions, instead of using 100ng of genomic DNA as template, an amount from an individual bacterial colony was picked from an agar plate containing the appropriate antibiotic and used as template. In addition, vector-specific primers were used for these amplifications [Y2H (Table 2.2), *in vivo* co-localisation (Table 2.7) and BRET (Table 2.7)]. The 50μl reaction contained 75μM of each of dATP, dCTP, dGTP and dTTP (Promega Corp.), 5μl of a 10X Taq DNA polymerase buffer (Bioline UK Ltd, London, UK), 1.5mM magnesium chloride (Bioline UK Ltd), 150ng of each primer, 0.5U Taq DNA polymerase (Bioline UK Ltd) and sterile water. Amplification was performed in a Mastercycler® ep PCR system. The cycling parameters consisted of a single denaturing cycle of 94°C for 2 minutes followed by 30 cycles of 94°C for 30 seconds, Ta (Table 2.2 or Table 2.7) for 30 seconds and 72°C for 1 minute. A final elongation step was performed at 72°C for 5 minutes. The amplification products were subsequently visualised by gel electrophoresis on a 1% SB agarose gel for verification (Section 2.3.1.1).

#### **2.2.5 PCR amplification for *in vitro* transcription and translation**

For the amplification of inserts for *in vitro* transcription and translation reactions (Section 2.16.2), the MyBPC phosphorylation mimics in bait vector pGBK7 and prey clones in vector pACT2, isolated during the Y2H library screens, were used as template. The amplification reaction mix and thermal cycling conditions were the same as in section 2.2.2. The primer pairs (BK-Myc-F/R and ADHA-F/R) and Ta are shown in Table 2.3. The amplification products were subsequently visualised by gel electrophoresis on a 1% SB agarose gel for verification (Section 2.3.1.1).

## **2.3 GEL ELECTROPHORESIS**

### **2.3.1 Agarose gel electrophoresis**

Agarose gel electrophoresis was used, in this study, to either visualise PCR-amplified fragments (Section 2.2) or plasmid preparations (Section 2.1.1 or Section 2.1.2) for verification of the reaction.

#### **2.3.1.1 Agarose gel electrophoresis for the visualisation of PCR amplified products plasmid DNA isolated from *E.coli***

To verify that the PCR amplifications were successful, the amplification products were electrophoresed as follows: 8 $\mu$ l PCR product was mixed with 1 $\mu$ l bromophenol blue loading dye (Appendix I). Each sample was then loaded into separate wells of a 1-2% (depending on the size of the amplified fragment) horizontal agarose gel of 7x9x1cm dimensions, containing 1 $\mu$ g/ml ethidium bromide (Appendix I) and 1X SB buffer (Appendix I). A molecular size marker, viz. a 100 base pair ladder (Promega Corp.), was co-electrophoresed with all the PCR amplified products. Electrophoresis was performed at 10V/cm for 20 minutes in 1X SB running buffer (Appendix I). Following electrophoresis, the DNA fragments were visualised on a long wave 3UV trans-illuminator (UVP, Inc. Upland, CA, USA) and photographs were obtained using an ITC Polaroid camera and Sony video-graphic printer (Sony Corporation, Shinagawa-ku, Tokyo, Japan).

One to five microlitres of plasmid DNA isolated from *E.coli* (Section 2.1.1 and 2.1.2) was electrophoresed in the same manner as described above, but on a 1% horizontal agarose gel. A  $\lambda$ PstI (Appendix I) size marker was co-electrophoresed with the purified plasmids.

### **2.3.2 Sodium dodecyl sulphate polyacrylamide gel electrophoresis (SDS-PAGE)**

Protein products, derived by coupled transcription/translation reactions from PCR products (Section 2.16.2), as well as from co-immunoprecipitation (Co-IP) reactions (Section 2.16.3), were electrophoresed in 200x200x0.5mm, 15-20% polyacrylamide gels containing 1% sodium dodecyl sulphate (SDS) (Appendix I). Typically, 15 $\mu$ l of SDS loading buffer (Appendix I) was mixed with 2 $\mu$ l of translated protein or 15 $\mu$ l Co-IP reaction products and incubated at 95 $^{\circ}$ C for 5 minutes. The samples were then loaded onto the vertical gel, electrophoresed at 230V for 4-6 hours in 1X SDS running buffer (Appendix I). The bands were visualised by autoradiography (Section 2.4).

## **2.4 AUTORADIOGRAPHY OF SDS POLYACRYLAMIDE GELS**

Following SDS-PAGE (Section 2.3.2), the electrophoresis apparatus was dismantled and the gel transferred to Whatman 3M paper (Whatman International Lt, Maidstone, England). The gel on the Whatman paper was subsequently heat and vacuum-dried on a Drygel Sr<sup>TM</sup> slab gel drier (Hoeffer Scientific Instruments, San Francisco, CA, USA) for one hour. When the gel had completely dried, it was exposed to an appropriately sized piece of autoradiography film [Kodak (Eastman Kodak Company, Rochester, New York, USA) inside an autoradiography cassette, for 1-7 days (depending on the strength of the radioactive signal and

concentration of proteins), after which it was developed in a Hyperprocessor™ automatic autoradiography film processor (Amersham Pharmacia Biotech UK Ltd., Little Chalfont, Bucks, UK).

## **2.5 AUTOMATED DNA SEQUENCING**

Bidirectional automated DNA sequencing of cloned inserts was performed at the Core Sequencing Facility of the Department of Genetics at the University of Stellenbosch, RSA, on an ABI Prism™ 377 or an ABI Prism™ 3100 automated sequencer (P.E. Applied Biosystems, Forster City, CA, USA). The vector-specific primers were used for the sequencing reactions of constructs [Y2H (Table 2.2), *in vivo* co-localisation (Table 2.7) and BRET assay (Table 2.7)].

## **2.6 SEQUENCE ANALYSIS**

### **2.6.1 DNA sequence analysis**

DNA sequence analysis was performed using the ChromasPro computer program (Techelysium Pty Lmt, Helensvale, Queensland, Australia) to verify the sequence integrity and reading frame of the bait fragments generated by PCR-amplification (Section 2.9.1), the putative positive prey clones isolated during the Y2H library screening (Section 2.15) as well as the inserts cloned for *in vivo* co-localisation (Section 2.17) and BRET analyses (Section 2.18).

The nucleotide sequence of the baits, as determined by automated sequencing, was compared to the *MyBPC3* cDNA sequence obtained from the Genbank database ([www.ncbi.nlm.nih.gov/Entrez](http://www.ncbi.nlm.nih.gov/Entrez)). Particular attention was paid to ensure that the correct base pairs were substituted in the C0C2 and C1C2 phosphorylation mimics.

### **2.6.2 Protein sequence analysis**

To compare the secondary structure of putative preys with the  $\alpha$ -helical coiled-coil structure of myosin S2, protein sequence analysis was performed. Briefly, the protein sequence of myosin S2 was aligned with each of the putative prey proteins using Clustal W online software (<http://align.genome.jp/>). The alignment was subsequently compared to the Homologous Structure Alignment Database (HOMSTRAD: a curated database of structure-based alignments for homologous protein families) (Mizuguchi *et al.*, 1998) using Fugue (<http://tardis.nibio.go.jp/fugue/prfsearch.html>), which annotated the structural alignment. A z-score of  $\geq 3.0$  and confidence level of  $\geq 90\%$  indicated that an evolutionary relationship and/or common secondary structure exists between the aligned proteins.

## **2.7 Y2H prey identification**

In order to assign identity to the Y2H putative positive preys, nucleotide sequences obtained through automated sequencing (Section 2.6.1) were BLASTed against the Genbank database using BLASTN (<http://www.ncbi.nlm.nih.gov/BLAST/>). To determine whether the prey insert encoded for an in-frame protein, the nucleotide sequence of the prey insert sequence only (i.e. in the absence of vector or GAL4

domain sequences) was translated in DNAMan, following which a BLASTP search of the translated sequence was performed against public protein databases. The subcellular localisation of the prey protein was determined using Proteome Analyst (<http://pa.cs.ualberta.ca:8080/pa/pa/index.html>) and ESLpred (<http://www.imtech.res.in/raghava/eslpred>).

The size of the peptides encoded by the individual inserts was determined by aligning the nucleotide sequence of the insert to the reference sequence identified in the online database. The nucleotide sequence from the point at which the 5' end of the insert sequence aligned with the reference sequence until the stop codon in the reference sequence, was translated using DNAMAN. The amino acid sequence of the translated peptide, encoded by the insert, was then BLASTed (BLASTP) against protein databases to determine whether such a peptide was represented in protein databases, to determine its identity and whether it encoded particular protein domains.

## 2.8 RESTRICTION ENZYME DIGESTION

### 2.8.1 Restriction enzyme digests for cloning inserts

To clone the PCR-generated fragments into the appropriate vectors, both the insert and vector were sequentially double-digested. These included cloning of bait fragments (Section 2.2.3) into bait vector pGBKT7 (Appendix V) for Y2H analyses, cMyBPC inserts into pRLuc-C1 (Appendix V) and GFP<sup>2</sup>-C3 (Appendix V) for BRET (Section 2.18) and co-localisation assays (Section 2.17), respectively, and prey inserts into GFP<sup>2</sup>-C3 for co-localisation assays (Section 2.17). For the respective cloning of C2C10 into pRLuc-C1 and GFP<sup>2</sup>-MCS-Rluc (Appendix V), and prey inserts into DsRed-Monomer-C1 (Appendix V) vector (using the In-fusion cloning method), only the vectors were sequentially double-digested.

The digests were prepared in a 100µl reaction volume as follows: 50µl insert PCR product or vector DNA was mixed with 5µl of the 5' restriction enzyme (Table 2.1, Table 2.4 or Table 2.5), 10µl restriction enzyme buffer and 35µl of sterile water. The mixes were incubated at 37°C for 2 hours. Following this incubation, the samples were heat inactivated in a waterbath (Memmert®, Schwabach, Germany) at 65°C for 20 minutes, then purified using the GFX™ DNA purification kit (Section 2.1.4). The samples were subsequently eluted in 50µl sterile water, to which 5µl of the 3' restriction enzyme (Table 2.1, Table 2.4 or Table 2.5), 10µl restriction enzyme buffer and 35µl sterile water were added. The samples were incubated again at 37°C for 2 hours; inactivated and then purified using the GFX™ DNA purification kit (Section 2.1.4). The double-digested vector (pGBKT7, pRLuc-C1, GFP<sup>2</sup>-C3, GFP<sup>2</sup>-MCS-Rluc or DsRed-Monomer-C1) was subsequently treated with *Calf Intestinal Alkaline Phosphatase (CIAP)* (Section 2.9.4), prior to being used in the ligation reactions (Section 2.9.5), to prevent the vector from annealing to itself, while the purified, double-digested insert was used directly in the ligation reactions.

## **2.9 GENERATION OF CONSTRUCTS**

### **2.9.1 Generation of Y2H constructs**

The Y2H bait-inserts (C1C2, C1P<sub>1</sub>P<sub>2</sub>P<sub>3</sub>C2, C1A<sub>1</sub>P<sub>2</sub>A<sub>3</sub>C2, C1A<sub>1</sub>A<sub>2</sub>A<sub>3</sub>C2, C0C2, C0P<sub>1</sub>P<sub>2</sub>P<sub>3</sub>C2, C0A<sub>1</sub>P<sub>2</sub>A<sub>3</sub>C2, and C0A<sub>1</sub>A<sub>2</sub>A<sub>3</sub>C2) were cloned individually into the pGBKT7 bait-vector (Appendix V) and, after verification of the integrity of the sequence and conservation of the GAL4 DNA-BD reading frame by automated sequencing (Section 2.5), were transformed individually into the yeast strain AH109 (Section 2.13.2). In this study, the C1A<sub>1</sub>P<sub>2</sub>A<sub>3</sub>C2 (monophosphorylated mimic) and the C1A<sub>1</sub>A<sub>2</sub>A<sub>3</sub>C2 (dephosphorylated mimic) constructs were used by the author, in separate experiments, to screen a Clontech MATCHMAKER pre-transformed cardiac cDNA library (BD Bioscience, Clontech) (Section 2.15.1), while the native C1C2 bait as well as the C1P<sub>1</sub>P<sub>2</sub>P<sub>3</sub>C2 bait had been used to perform similar screens previously (by JC Moolman-Smook and LJ Korkie). In each case, the library was comprised of cardiac cDNAs cloned into the pACT2 prey-vector (Appendix V) and pretransformed into yeast strain Y187.

### **2.9.2 Generation of constructs for BRET analyses**

Bait PCR fragments representing domains C1C10 (pRluc-C1; Appendix V), C2C10 (pRluc-C1 and GFP<sup>2</sup>-MCS-Rluc; Appendix V), C3C10 (pRluc-C1 and GFP<sup>2</sup>-MCS-Rluc) and C7C10 (pRluc-C1 and GFP<sup>2</sup>-MCS-Rluc) of cMyBPC were cloned into the appropriate vectors, while prey inserts ACTC1 and cTNI were cloned into pGFP<sup>2</sup>-C3 (Appendix V), respectively. The integrity of the sequence and the reading frame was verified by automated sequencing (Section 2.5).

### **2.9.3 Generation of constructs for *in vivo* co-localisation assays**

For *in vivo* co-localisation, the PCR fragment representing domains C1C10 of cMyBPC was cloned into vector pGFP<sup>2</sup>-C3, while the prey inserts were cloned into the DsRed-Monomer-C1 vector (Appendix V). The integrity of the sequence and the reading frame was verified by automated sequencing (Section 2.5). The PDE4DIP- and COMMD4-tagged YFP (yellow fluorescent protein) constructs, in vector pdEYFP-C1amp (Appendix V), were purchased from the German Resource Center for Genome Research (RZPD, Berlin, Germany)

### **2.9.4 Alkaline phosphatase treatment of vector**

Following double restriction enzyme digestion (Section 2.8), the ends of the linearised plasmid were *CIAP*-treated (to remove the phosphate groups), to prevent the vector re-circularising by self-ligation. The reaction mix consisting 50µl of the digested vector, 1µl *CIAP* (Promega Corp.), 10µl *CIAP* buffer and 38µl sterile water. The reaction mix was incubated for 2 cycles of 15 minutes each, at 37°C and 56°C, respectively. Between the cycles a further 1µl *CIAP* enzyme was added to the reaction mix. The *CIAP*-ed vector was subsequently purified using the GFX™ DNA purification kit (Section 2.1.4) and used in the appropriate ligation reaction (Section 2.9.5).

### **2.9.5 DNA ligation**

DNA ligation reactions were performed to generate constructs used in the Y2H analyses (Section 2.15), BRET (Section 2.18) and *in vivo* co-localisation assays (Section 2.17). The reaction mix consisted of 2µl of the double-digested insert, 1µl of *CIAP*-treated, double-digested vector (Section 2.9.4), 5µl 2x T4 DNA ligase buffer (Promega Corp.), 5U T4 DNA ligase and sterile water to a final volume of 10µl. The sample was then incubated overnight at 4°C. Following incubation, 5µl of the sample was transformed into the *Ecoli* DH5α (Section 2.13.1). The transformed cultures were then plated on LB agar plates (Appendix I) containing the appropriate antibiotic. After incubation of the plates, successful ligation reactions were confirmed by bacterial colony PCRs (Section 2.2.4) as vectors did not allow blue-white selection of colonies containing recombined plasmids.

### **2.9.6 Cloning constructs using the In-Fusion™ 2.0 Dry-Down PCR Cloning Kit: Preparation of inserts and vectors, and cloning procedure**

The In-Fusion™ 2.0 Dry-Down PCR Cloning Kit (BD Bioscience, Clontech) was used to clone inserts into vectors that proved intractable to cloning using traditional methods. Briefly, the PCR products to be cloned were analysed by agarose gel electrophoresis (Section 2.3.1.1) to confirm that a single DNA fragment had been generated and to estimate the concentration of the PCR product by measuring against a molecular weight ladder run on the same gel. For successful In-Fusion cloning, the cloning vector (GFP<sup>2</sup>-MCS-Rluc, pRluc-C1 and DsRed-Monomer-C1) was double restriction enzyme digested, viz. at two unique sites between the regions of homology included in the PCR primers (Table 2.6), in the same manner as described previously (Section 2.8.1). The subsequent steps of the cloning procedure were performed as per manufacturers' instructions. The reaction mix (5µl) was then used to transform DH5α *Ecoli* cells (Section 2.13.1).

## **2.10 BACTERIAL STRAINS, YEAST STRAINS AND CELL LINES**

### **2.10.1 Bacterial strains**

To facilitate the selection and purification of constructs used in the various analyses, ligation reaction mixtures were used to transform *E.coli* DH5α cells. Transformed bacterial colonies were selected on the basis of their ability to grow on LB agar plates containing selection antibiotics, and recombined plasmids identified by colony PCR (Section 2.2.4). When selecting for pGBKT7, DsRed-Monomer-C1 and pRluc-C1 recombinants, kanamycin was used as a selection antibiotic, while pACT2 recombinants were selected using ampicillin and, pGFP<sup>2</sup>-C3 and GFP<sup>2</sup>-MCS-Rluc recombinants were selected using Zeocin™.

### **2.10.2 Yeast strains**

The pGBKT7 bait constructs (C1C2, C1P<sub>1</sub>P<sub>2</sub>P<sub>3</sub>C2, C1A<sub>1</sub>P<sub>2</sub>A<sub>3</sub>C2, C1A<sub>1</sub>A<sub>2</sub>A<sub>3</sub>C2, C0C2, C0P<sub>1</sub>P<sub>2</sub>P<sub>3</sub>C2, C0A<sub>1</sub>P<sub>2</sub>A<sub>3</sub>C2, and C0A<sub>1</sub>A<sub>2</sub>A<sub>3</sub>C2) were used to transform the yeast strain AH109 (Section 2.13.2). The clones present in the pre-transformed Clontech cDNA library (Section 2.15.1) used in the Y2H analysis had been transformed into the yeast strain Y187 by the manufacturer.

### **2.10.3 Cell lines**

For the *in vivo* co-localisation (Section 2.17) and BRET assays (Section 2.18), the appropriate combinations of vectors were co-transfected into cardiac myocytes, H9C2 (Section 2.13.3).

## **2.11 GENERATION OF *E.coli* DH5 $\alpha$ COMPETENT CELLS**

A 20 $\mu$ l aliquot of an *E.coli* DH5 $\alpha$  (-70°C) glycerol stock was inoculated into 10ml LB-media and incubated overnight at 37°C in a YIH DER model LM-530 shaking incubator at approximately 200rpm. Following incubation, a 300 $\mu$ l aliquot of this preculture was inoculated into a 2l Erlenmeyer flask containing 200ml LB media. This culture was then incubated at room temperature for 24 hours, while shaking at 70rpm, to mid-log phase ( $OD_{600nm}=0.6$ ) on a Labcon orbital shaker (Labcon Pty, Ltd, Maraisburg, RSA). At this optical density, the culture was decanted into 4x50ml polypropylene tubes, which were centrifuged at 3000rpm for 15 minutes at 4°C in a Multitex centrifuge. The supernatant was removed and 8ml of ice-cold CAP buffer (Appendix I) was used to resuspend the pellet. The cells were re-pelleted by centrifugation at 3000rpm at 4°C in a Multitex centrifuge. The supernatant was discarded and the pellet was resuspended in 4ml of ice-cold CAP buffer. The suspended cells were then transferred into 2ml microcentrifuge tubes in 200 $\mu$ l aliquots and stored at -70°C until they were needed.

## **2.12 CULTURING OF CELL LINES**

### **2.12.1 Culture of cells from frozen stocks**

#### **2.12.1.1 Thawing the cells**

*Rattus norvegicus* (rat) cardiac (atrial) myocytes, H9C2 were purchased from the American Type Culture Collection (ATCC, Manassas, VA, USA). The frozen stock was thawed rapidly by immersion in a 37°C water bath for 10 minutes. Once the cells were thawed, the outside of the vial was immediately sterilised with 70% ethanol.

#### **2.12.1.2 Removing Dimethyl sulphoxide (DMSO) from stocks and culturing cells**

To ensure maximum viability of the cells upon plating, it was necessary to remove the DMSO from the frozen stock. The following method was used: 1ml of growth media (Appendix I), prewarmed to 37°C was added to the thawed stock and mixed by gentle pipetting. The mixture was transferred to a 12ml Greiner tube (Greiner Bio-one, Frickenhausen, Germany) and another 5ml growth media was added. The cells were then pelleted by centrifugation at 1000rpm for 3 minutes using a Sorval® GLC-4 General Laboratory centrifuge (Separations Scientific, Johannesburg, RSA), followed by removal of the supernatant. The pellet was resuspended in another 5ml growth media and the cells were once again centrifuged at 1000rpm for 3 minutes using a Sorval® GLC-4 General Laboratory centrifuge. Following this, the cells were resuspended in 10ml growth media and transferred into a T25 culture flask. The flask was gently swirled in order to distribute the cells evenly over the growth surface of the flask. The flask was then incubated at 37°C in a Farma-thermosteril-cycle 5% carbon dioxide humidified incubator (Farma International, Miami, Florida, USA).

## **2.12.2 Splitting of cell cultures**

Pre-confluent cultures (approximately 80-90% confluence) were split every 2-4 days. Briefly, the growth media was removed from the flask, and the cells were washed with sterile phosphate buffered saline (PBS) containing no calcium or magnesium (Cambrex, Walkersville, MD, USA). To facilitate the detachment of the cells from the growth surface of the flask, 2ml of trypsin (Highveld Biological, Lyndhurst, RSA) was added. After 5 minutes, 5ml growth media was added and the cells gently resuspended. The resuspended cells were transferred to a 12ml Greiner tube and the cells pelleted by centrifugation at 1000rpm for 3 minutes using a Sorval® GLC-4 General Laboratory centrifuge. Following this, the cells were resuspended in 10ml growth media and transferred to 4 flasks each containing 10ml growth media.

## **2.13 TRANSFORMATION AND TRANSFECTION OF PLASMIDS INTO PROCARYOTE AND EUKARYOTE CELLS**

### **2.13.1 Bacterial plasmid transformations**

An aliquot of competent *E.coli* DH5 $\alpha$  cells (Section 2.11) was removed from the -70°C freezer and allowed to thaw on ice for 20 minutes, prior to the transformation. Once the cells had thawed, 1 $\mu$ l of the plasmid preparation (Section 2.1.1), or 3-5 $\mu$ l of the ligation reaction (Section 2.9.5) was added and the mixture was then incubated on ice for 20 minutes. After this incubation, the sample was placed in a water bath at 42°C for exactly 45 seconds. The sample was then removed from the water bath and allowed to rest for 2 minutes at room temperature. Next, 1ml of LB media was added to the mixture and the sample was incubated for 1 hour at 37°C, while shaking at 200rpm in a YIH DER model LM-530 shaking incubator. Subsequently, 200 $\mu$ l of the sample was plated onto LB agar plates (Appendix I) containing the appropriate selection antibiotic. The remaining transformation mixture was centrifuged at 13000rpm for 1 minute in a Beckman Microfuge Lite, the supernatant discarded and the pellet resuspended in 200 $\mu$ l LB media. This was then also plated onto the appropriate LB agar plates. All the plates were incubated, inverted, overnight at 37°C in a model 329 stationary C0<sub>2</sub> incubator (Former Scientific, Marietta, Ohio, USA).

### **2.13.2 Yeast plasmid transformation**

Ten microlitre aliquots of the yeast strain to be transformed (AH109 or Y187) were streaked from frozen stocks onto YPDA agar plates (Appendix I). These plates were then incubated inverted at 30°C for 2-3 days in a Sanyo MIR262 stationary ventilated incubator (Sanyo Electronic Company Ltd, Ora-Gun, Japan). Following incubation, a volume representing 20-50 $\mu$ l of yeast cells was picked and resuspended in 1ml sterile water in a sterile 2ml microcentrifuge tube. The cells were then pelleted by centrifugation at 13000rpm for 30 seconds in a Beckman Microfuge Lite. The supernatant was removed and the pellet was resuspended in 1ml 100mM lithium acetate (Appendix I) and incubated for 5 minutes at 30°C in a MIR262 stationary ventilated incubator. The cells were pelleted again by centrifugation at 13000rpm for 20 seconds in a Beckman Microfuge Lite and all the lithium acetate was removed. Next, 240 $\mu$ l of 50% polyethylene glycol (PEG) (Appendix I), 36 $\mu$ l 1M lithium acetate (Appendix I), 25 $\mu$ l of 2mg/ml heat denatured and snap-cooled sonicated herring sperm DNA (Promega Corp.), 10-20 $\mu$ l plasmid preparation (Section 2.1.1 and

2.1.3) and sterile water were added to a final volume of 350 $\mu$ l. The sample was then mixed by vortexing using a Snijders model 34524 press-to-mix vortex for at least 1 minute and incubated at 42°C for 20-30 minutes in a water bath. Following incubation, the cells were pelleted by centrifugation at 13000rpm in a Beckman Microfuge Lite and all the supernatant was removed. The cells were resuspended in 250 $\mu$ l sterile water, plated onto the appropriate selection plates (Appendix I) and incubated upside down at 30°C for 2-5 days in a Sanyo MIR262 stationary ventilated incubator.

### 2.13.3 Transfection of H9C2 cells

For the BRET assays, approximately 1-3x10<sup>5</sup> cells/well were seeded in 6-well tissue culture plates while 1x10<sup>4</sup> cells/well were seeded for the co-localisation assay in borosilicate coverglass chambers (Nunc, New York, USA) in complete growth media (Appendix I) and incubated at 37°C in a Farma-thermoster-i-cycle 5% carbon dioxide humidified incubator. After forty-eight hours, the cells were visualised using a Nikon TMS light microscope (housed at the Department of Physiology, University of Stellenbosch) to determine the level of confluence. Cells were transfected once they reached approximately 70-80% confluency. For each transfection performed (BRET and co-localisation assays), 100 $\mu$ l of serum-free medium (Appendix I) was aliquoted into sterile 1.5ml microcentrifuge tubes and 6 $\mu$ l of Genejuice® (Novagen, Darmstadt, Germany) was added to each tube. This mixture was thoroughly vortexed using a Snijders model 34524 press-to-mix vortex and incubated at room temperature for 5 minutes. A total of 3 $\mu$ g of the appropriate combination of plasmids (Section 2.1.2) for the BRET assay (pGFP<sup>2</sup>-C3:pRluc-C1; 3:1) (Section 2.18; Table 2.9-10) and 1 $\mu$ g of vector DNA for the co-localisation assay (pGFP<sup>2</sup>-C3:YFP and pGFP<sup>2</sup>-C3:DsRed-Monomer-C1; 1:1) (Section 2.17; Table 2.11) was added to the mixture and mixed by gentle pipetting. The Genejuice/DNA/medium mixture was incubated at room temperature for 30 minutes. This mixture was then added drop-wise to the cells in the growth media while the culture plates were gently rocked back and forth in order to evenly distribute the drops across the surface of the plate. The cells were incubated at 37°C in a Farma-thermoster-i-cycle 5% carbon dioxide humidified incubator for 48 hours. Following this incubation the cells were then differentiated into cardiac myotubes (Section 2.13.4).

**Table 2.9.** Transfection experiment layout for BRET assay

Transfection (1:3*)	pRluc-C1 construct	pGFP <sup>2</sup> -C3 construct
C1C10/C2C10 bait control	C1C10 cMyBPC/C2C10	Empty pGFP <sup>2</sup> -C3
TNNI control	Empty pRluc-C1	cTNI
ACTC1 control	Empty pRluc-C1	ACTC1
Test 1	C1C10 cMyBPC/C2C10	cTNI
Test 2	C1C10 cMyBPC/C2C10	ACTC1
Gene Juice control	-	-
Untransfected control	-	-

\*Ratio to a total of 3 $\mu$ g

**Table 2.10.** Transfection experiment layout for MCS BRET assay

Transfection (1:1*)	pRLuc-C1 construct	pGFP <sup>2</sup> -C3 construct	MCS construct
Control 1	C2C10 cMyBPC	Empty pGFP <sup>2</sup> -C3	-
Control 2	C3C10 cMyBPC	Empty pGFP <sup>2</sup> -C3	-
Control 3	C7C10 cMyBPC	Empty pGFP <sup>2</sup> -C3	-
Test 1	-	-	C2C10 MCS
Test 2	-	-	C3C10 MCS
Test 3	-	-	C7C10 MCS
Gene Juice control	-	-	-
Untransfected control	-	-	-

\*Ratio to a total of 3µg

**Table 2.11.** Transfection experiment layout for *in vivo* co-localisation assay

Transfection (1:1*)	pGFP <sup>2</sup> construct	EYFP construct	DsRed construct
Control 1	C1C10 cMyBPC	-	-
Control 2	-	PDE4DIP	-
Control 3	-	COMMD4	-
Test 1	C1C10 cMyBPC	PDE4DIP	-
Test 2	C1C10 cMyBPC	COMMD4	-
Test 3	C1C10 cMyBPC	-	HSPB7
Test 4	C1C10 cMyBPC	-	ENO3
Gene Juice control	-	-	-
Untransfected control	-	-	-

\*Ratio to a total of 1µg

For the GFP:YFP co-localisations, the pGFP<sup>2</sup>-C3 construct (C1C10 cMyBPC) and each of the YFP constructs (COMMD4 and PDE4DIP) were transfected separately (Control 1-3, Table 2.11), to allow the capture of reference images for spectral unmixing (Section 2.17) of the images during analysis. Spectral unmixing was not necessary for the GFP:DsRed co-localisations.

#### 2.13.4 Differentiation of H9C2 cells

In order to differentiate cardiac myocytes into myotubes, the growth medium was changed 48 hours after transfection. Briefly, the growth media was removed, the cells washed with sterile PBS (containing no calcium or magnesium) and 3ml of differentiating growth medium (Appendix I) was added. The cells were incubated at 37°C in a Farma-thermosteril-cycle 5% carbon dioxide humidified incubator for seven days. On day four, the cells were washed again and fresh differentiating media was added. On day seven, the cells were visualised using an Olympus IX 81 motorised inverted microscope (Olympus, Hamburg, Germany) to confirm that the cells were differentiated. The cells were subsequently photographed for co-localisation (Section 2.17) or the BRET assay (Section 2.18) was performed.

## **2.14 ASSESSMENT OF Y2H CONSTRUCTS**

### **2.14.1 Phenotypic assessment of yeast strains**

Phenotypic assessment of each of the yeast strains used in the Y2H analysis was performed prior to transformation reactions. Strains AH109 and Y187 were plated onto agar plates lacking particular essential amino acids (Appendix I), viz. SD<sup>-Ade</sup>, SD<sup>-Trp</sup> (SD<sup>-W</sup>) SD<sup>-His</sup>, SD<sup>-Leu</sup> (SD<sup>-L</sup>) and SD<sup>-Ura</sup>. Non-transformed yeast cells that were unable to grow on SD<sup>-Ade</sup>, SD<sup>-W</sup>, SD<sup>-His</sup> and SD<sup>-L</sup> but were able to grow on SD<sup>-Ura</sup> were considered to reflect the original phenotype of this yeast strain, and were used for the transformation and subsequent Y2H analysis. Following transformation (Section 2.13.2) of the bait constructs into AH109, the transformed yeast was again streaked onto the respective agar plates SD<sup>-Ade</sup>, SD<sup>-W</sup>, SD<sup>-His</sup>, SD<sup>-L</sup> and SD<sup>-Ura</sup>. This was performed to test whether the AH109 transformed with the bait construct was able to autonomously activate transcription of reporter genes, as well as to monitor phenotypic integrity of the yeast strain after manipulation. AH109 yeast containing the bait construct should only be able to grow on SD<sup>-W</sup> and SD<sup>-Ura</sup> plates.

### **2.14.2 Toxicity tests of transformed yeast cells**

Prior to performing the library mating (Section 2.15.3), it was important to establish whether the bait-constructs had any toxic effect on its host strain, AH109. Linearised growth curves of AH109 singly transformed with the pGBKT7-baits (C1C2, C1P<sub>1</sub>P<sub>2</sub>P<sub>3</sub>C2, C1A<sub>1</sub>P<sub>2</sub>A<sub>3</sub>C2, C1A<sub>1</sub>A<sub>2</sub>A<sub>3</sub>C2, C0C2, C0P<sub>1</sub>P<sub>2</sub>P<sub>3</sub>C2, C0A<sub>1</sub>P<sub>2</sub>A<sub>3</sub>C2, and C0A<sub>1</sub>A<sub>2</sub>A<sub>3</sub>C2) constructs were generated and subsequently compared to a growth curve of AH109 yeast transformed with non-recombinant pGBKT7. These growth curves were set up concurrently under the same experimental conditions.

The growth curves were generated by growing each of the transformed yeast strains to stationary phase in SD<sup>-W</sup> media (Appendix I) in a 50ml polypropylene tube at 30°C in a YIH DER model LM-530 shaking incubator shaking at 200rpm. Following this incubation, a 1:10 dilution of each primary culture was made in SD<sup>-W</sup> and incubated for an additional 24 hours in a 50ml polypropylene tube at 30°C in a YIH DER model LM-530 shaking incubator with shaking at 200rpm. Every two hours, over a period of eight hours during this incubation, a 1ml aliquot of the culture was taken and its OD<sub>600nm</sub> was measured. A reading of the culture after overnight (24 hours) growth was also taken. A linearised graph of the log of these OD<sub>600nm</sub> readings versus time was constructed and the slopes of the graphs generated for the recombinant and non-recombinant transformants were compared.

### **2.14.3 Testing of mating efficiency**

Small-scale yeast matings were performed to determine the effect the bait constructs had on the mating efficiency of AH109. In these mating experiments, the AH109 singly transformed with pGBKT7 bait constructs (C1C2, C1P<sub>1</sub>P<sub>2</sub>P<sub>3</sub>C2, C1A<sub>1</sub>P<sub>2</sub>A<sub>3</sub>C2, C1A<sub>1</sub>A<sub>2</sub>A<sub>3</sub>C2, C0C2, C0P<sub>1</sub>P<sub>2</sub>P<sub>3</sub>C2, C0A<sub>1</sub>P<sub>2</sub>A<sub>3</sub>C2, and C0A<sub>1</sub>A<sub>2</sub>A<sub>3</sub>C2) were mated with the prey host strain, Y187, transformed with the non-recombinant prey vector pACT2 or the control prey vector, pTD1.1, supplied by the manufacturer (BD Bioscience, Clontech),

respectively. Concurrently, control matings were also performed where yeast strain AH109 transformed with non-recombinant pGBKT7 or the control pGBKT7-53 vector supplied by the manufacturer (BD Bioscience, Clontech) was mated with the prey host strain, Y187 transformed with the non-recombinant prey vectors pACT2 or the pTD1.1 control vector. The experimental procedure was as follows:

Each of the yeast strains used in the mating efficiency experiments was plated onto the appropriate nutritional selection plates (AH109 pGBKT7-C1C2, AH109 pGBKT7-C1P<sub>1</sub>P<sub>2</sub>P<sub>3</sub>C2, AH109 pGBKT7-C1A<sub>1</sub>P<sub>2</sub>A<sub>3</sub>C2, AH109 pGBKT7-C1A<sub>1</sub>A<sub>2</sub>A<sub>3</sub>C2, AH109 pGBKT7-C0C2, AH109 pGBKT7-C0P<sub>1</sub>P<sub>2</sub>P<sub>3</sub>C2, AH109 pGBKT7-C0A<sub>1</sub>P<sub>2</sub>A<sub>3</sub>C2, AH109 pGBKT7-C0A<sub>1</sub>A<sub>2</sub>A<sub>3</sub>C2, AH109 pGBKT7 and AH109 pGBKT7-53 on SD<sup>-W</sup> plates; Y187 pACT2 and Y187 pTD1.1 on SD<sup>-L</sup> plates). These plates were incubated for 2-5 days in a Sanyo MIR262 stationary ventilated incubator. A single colony from these agar plates were used for each test mating experiment, which was performed in 1ml YPDA media (Appendix I) in a 2ml microcentrifuge tube. The matings were incubated overnight at 30°C, shaking at 200rpm, in a YIH DER model LM-530 shaking incubator. Following the overnight incubation, serial dilutions (1:10, 1:100, 1:1000 and 1:10000) of the mating cultures were plated onto SD<sup>-L</sup>, SD<sup>-W</sup>, SD<sup>-L-W</sup> agar plates (Appendix I) and incubated for 4-5 days at 30°C in a Sanyo MIR262 stationary ventilated incubator. After the incubation period, the colonies on each plate were counted and used to calculate the mating efficiency (Appendix II).

## 2.15 Y2H ANALYSIS

### 2.15.1 Cardiac cDNA library

A pre-transformed human MATCHMAKER cardiac cDNA library (BD Bioscience, Clontech) consisting of *S.cerevisiae* Y187 transformed with a cardiac cDNA library constructed in pACT2 was used in the Y2H library assay. The library consisted of normal, whole hearts pooled from 3 male Caucasians aged between 28 and 47 years. The library was *Xho*I-(dT)<sub>15</sub> primed and contained approximately 3.5x10<sup>6</sup> independent clones inserted into the pACT2 vector between *Xho*I and *Eco*RI sites. The average insert size for this library is 2.0kb, with a range of between 0.4 and 4.0Kb.

### 2.15.2 Establishment of bait culture

An aliquot of AH109 transformed with either pGBKT7-C1A<sub>1</sub>P<sub>2</sub>A<sub>3</sub>C2 or pGBKT7-C1A<sub>1</sub>A<sub>2</sub>A<sub>3</sub>C2, from a glycerol stock, was streaked out onto SD<sup>-W</sup> plates. The plates were placed upside down and incubated for 4 days at 30°C in a Sanyo MIR262 stationary ventilated incubator. In separate experiments, a single yeast colony was inoculated into 1ml SD<sup>-W</sup> liquid media, in a 2ml microcentrifuge tube, and incubated at 30°C overnight, while shaking at 200rpm in a YIH DER model LM-530 shaking incubator. Following incubation, the preculture was split and inoculated into four separate 500ml Erlenmeyer flasks, each containing 50ml SD<sup>-W</sup> media. The reason for producing four bait cultures was to facilitate a final bait culture with a titre of at least 1x10<sup>10</sup>, i.e. 100-fold excess of bait to prey to facilitate high mating efficiency, by pooling of the initial cultures. The four cultures were incubated at 30°C overnight, while shaking at 200rpm in a YIH DER model LM-530 shaking incubator. Following overnight incubation, the titre of the bait culture was estimated by

measuring the OD<sub>600nm</sub> of a 1ml aliquot of the bait culture. This estimation was subsequently confirmed by means of a haemocytometric cell count (Appendix II).

### **2.15.3 Library mating**

Prior to library mating, a 1ml aliquot of the pre-transformed cardiac cDNA library (Section 2.15.1) was removed from the -70°C freezer and thawed on ice. Once thawed, the library aliquot was vortexed using a Snijders model 34524 press-to-mix vortex and 10µl was aliquoted into a sterile 1.5ml microcentrifuge tube for library titering (Section 2.15.4). The bait pellet (AH109 pGBKT7-C1A<sub>1</sub>P<sub>2</sub>A<sub>3</sub>C<sub>2</sub> or AH109 pGBKT7-C1A<sub>1</sub>A<sub>2</sub>A<sub>3</sub>C<sub>2</sub> (Section 2.15.2) was resuspended in 45ml 2x YPDA media (Appendix I) supplemented with 10µg/ml kanamycin in a 2L Erlenmeyer flask. The remaining 990µl of the library culture was added to this Erlenmeyer flask, which was then incubated at 30°C for 24 hours, while shaking at 50rpm in a YIH DER model LM-530 shaking incubator.

Following this incubation, the entire mating culture was transferred to a sterile 50ml polypropylene microcentrifuge tube, the cells pelleted by centrifugation at 3000rpm for 5 minutes in a Multex centrifuge, and the supernatant subsequently removed. The Erlenmeyer flask in which the library mating was performed was rinsed twice with 40ml 2X YPDA containing 10µg/ml kanamycin. Each time the flask was rinsed, this 2X YPDA rinsing media was used to resuspend the cell pellet and the cells then re-pelleted by centrifugation at 3000rpm for 10 minutes at room temperature in a Multex centrifuge. Following the final centrifugation step, the supernatant was removed and the pellet resuspended in 15ml 0.5X YPDA (Appendix I) containing 10µg/ml kanamycin.

In order to determine the library mating efficiency 100µl aliquots of a serial dilution (1:10; 1:100; 1:1000; and 1:10000) of the mating mix was plated onto 90mm SD<sup>-L</sup>, SD<sup>-W</sup> and SD<sup>-L-W</sup> agar plates. Two hundred and fifty microlitre aliquots of the remaining culture was plated onto each of 60 140mm TDO (media lacking leucine, tryptophan and histidine) (Appendix I) plates. The TDO plates were incubated, upside-down, for 3 weeks in a Sanyo MIR262 stationary ventilated incubator.

### **2.15.4 Establishing a library titre**

The serial dilutions of the library culture (Section 2.15.3) was plated onto 90mm SD<sup>-L</sup> agar plates (Appendix I) and incubated in a Sanyo MIR262 stationary ventilated incubator for 4 days. Colony counts were performed on the plates, after the 4 day incubation, in order to calculate the number of library plasmids screened (Appendix II).

### **2.15.5 Detection of activation of nutritional and reporter genes**

#### **2.15.5.1 Selection of transformant yeast colonies**

Yeast transformed with the bait constructs (pGBKT7-C1C2, pGBKT7-C1P<sub>1</sub>P<sub>2</sub>P<sub>3</sub>C<sub>2</sub>, pGBKT7-C1A<sub>1</sub>P<sub>2</sub>A<sub>3</sub>C<sub>2</sub>, pGBKT7-C1A<sub>1</sub>A<sub>2</sub>A<sub>3</sub>C<sub>2</sub>, pGBKT7-C0C2, pGBKT7-C0P<sub>1</sub>P<sub>2</sub>P<sub>3</sub>C<sub>2</sub>, pGBKT7-C0A<sub>1</sub>P<sub>2</sub>A<sub>3</sub>C<sub>2</sub>, and pGBKT7-

C0A<sub>1</sub>A<sub>2</sub>A<sub>3</sub>C2) (Section 2.13.2) to be used in Y2H analysis was plated onto SD<sup>-W</sup> agar plates. Following incubation for 4-6 days in a Sanyo MIR262 stationary ventilated incubator, transformed yeast colonies were picked and used in either small or large scale bait cultures (Section 2.15.2), interaction specificity tests (Section 2.15.8) or direct Y2H protein-protein interaction assays (Section 2.15.9). Yeast transformed with prey plasmids (Section 2.15.7) to be used in interaction specificity tests (Section 2.15.8) were plated onto SD<sup>-L</sup> agar plates and allowed to grow under the same conditions described above.

#### **2.15.5.2 Selection of diploid yeast colonies containing putative interactor peptides**

Diploid yeast colonies generated by small-scale or library matings were first plated onto TDO (Section 2.15.3), and then restreaked onto QDO (media lacking leucine, histidine, tryptophan and adenine) (Appendix I) plates, in order to identify yeast colonies in which an interaction between the bait and prey peptides had taken place. Growth of the yeast cells on TDO plates signified the transcriptional activation of the *HIS3* nutritional gene, while growth on QDO plates indicated transcriptional activation of both the *HIS3* and *ADE2* nutritional genes. The activation of these genes in diploid yeast cells is indicative of an interaction between the bait and prey peptides.

After plating the library mating culture onto TDO agar plates, growth of yeast colonies were monitored every seven days. Colonies (with a diameter >2mm) were picked and simultaneously restreaked onto TDO and QDO plates. These plates were incubated for four days at 30<sup>0</sup>C in a Sanyo MIR262 stationary ventilated incubator. Those colonies growing on these initial QDO plates were then picked and restreaked onto fresh QDO plates which were then incubated for four days at 30<sup>0</sup>C prior to being used for the X- $\alpha$ -galactosidase assay (Section 2.15.6.1) to assess the activation of the *MEL1* gene.

#### **2.15.6 Detection of activation of colourimetric reporter genes**

##### **2.15.6.1 X- $\alpha$ -Galactosidase assay**

This assay was performed to test for the activation of the *MEL1* reporter gene by the interaction between bait and prey peptides (Section 2.15.5.2). Briefly, yeast colonies in which the *HIS3* and *ADE2* reporter genes have been activated, as determined by their growth on QDO agar plates, were replicated from QDO plates onto Hybond N<sup>+</sup> nylon membranes (Amersham Pharmacia Biotech UK Ltd.). These membranes were subsequently placed colony-side up onto a fresh QDO plate impregnated with 5mg/ml X- $\alpha$ -Gal solution (Appendix I) (BD Bioscience, Clontech). The plates were subsequently incubated at 30<sup>0</sup>C in a Sanyo MIR262 stationary ventilated incubator for 16-48 hours. Following incubation for 16-48 hours, the intensity of the blue colour of the yeast colonies that had activated the *MEL1* reporter gene was assessed.

#### **2.15.7 Rescuing prey plasmids from diploid colonies**

To facilitate identification of the interactor proteins, each individual prey needed to be isolated from diploid colonies which had shown transcription of the *HIS3*, *ADE2* and *MEL1* reporter genes. Plasmid DNA, containing both bait and prey plasmids, was isolated from each of the diploid cells (Section 2.1.3) and

transformed into *E.coli* strain DH5 $\alpha$  as described in section 2.13.1. The transformants were plated onto LBamp plates, which only allow growth of transformants containing the prey constructs, and thus selection of these bacteria over those containing bait constructs. These prey construct-containing colonies were subsequently transformed into the yeast strain Y187 (Section 2.13.2) for interaction specificity tests (Section 2.15.8).

### 2.15.8 Interaction specificity test

To assess the specificity of interactions between either pGBKT7-C1A<sub>1</sub>P<sub>2</sub>A<sub>3</sub>C<sub>2</sub> or pGBKT7-C1A<sub>1</sub>A<sub>2</sub>A<sub>3</sub>C<sub>2</sub> bait and its putative preys, respectively, interaction-specificity tests were performed following nutritional (Section 2.15.5.2) and colourimetric selection tests (Section 2.15.6.1). Y187 colonies expressing distinct prey peptides were mated individually with the yeast strain AH109, transformed with either the pGBKT7-C1A<sub>1</sub>P<sub>2</sub>A<sub>3</sub>C<sub>2</sub> or -C1A<sub>1</sub>A<sub>2</sub>A<sub>3</sub>C<sub>2</sub> construct, AH109 transformed with non-recombinant pGBKT7, AH109 transformed with the pGBKT7-53 control bait-plasmid, encoding murine p53, supplied by the manufacturer (BD Bioscience, Clontech), AH109 transformed with the Reeler domain or AH109 transformed with PKDd10. After the resulting diploid colonies were selected, these clones were streaked onto TDO and QDO selection plated to test for activation of nutritional genes, thereby testing whether the prey-peptides were able to interact with these heterologous baits as well as with the AH109 pGBKT7-C1A<sub>1</sub>P<sub>2</sub>A<sub>3</sub>C<sub>2</sub> or AH109 pGBKT7-C1A<sub>1</sub>A<sub>2</sub>A<sub>3</sub>C<sub>2</sub> bait.

Prey clones that interacted specifically with either the AH109 pGBKT7-C1A<sub>1</sub>P<sub>2</sub>A<sub>3</sub>C<sub>2</sub> or AH109 pGBKT7-C1A<sub>1</sub>A<sub>2</sub>A<sub>3</sub>C<sub>2</sub> bait, as determined by the interaction specificity test were considered putative true interactors. The inserts of these putative interactors were then nucleotide sequenced (Section 2.5) to determine their identities.

### 2.15.9 Direct Y2H protein-protein interaction assays

Small scale yeast mating was performed to determine whether bait-prey interaction identified by Y2H was driven by domains C1 or C2, or whether it was specific to a particular phosphorylation state of the MyBPC-motif. In these mating experiments, the AH109-pGBKT7 bait constructs (C1C2, C1P<sub>1</sub>P<sub>2</sub>P<sub>3</sub>C<sub>2</sub>, C1A<sub>1</sub>P<sub>2</sub>A<sub>3</sub>C<sub>2</sub>, C1A<sub>1</sub>A<sub>2</sub>A<sub>3</sub>C<sub>2</sub>, C0C1, C1 and C2) were mated individually with each putative positive prey in Y187. The C0C1 bait fragment was used as a negative control for the C1C2 interaction assay, as it is approximately the same size and charge as the C1C2 region. The experimental procedures were as follows:

Each of the yeast strains used was plated onto the appropriate nutritional selection plates (AH109-pGBKT7 baits on SD<sup>-W</sup> plates; Y187 putative positive preys on SD<sup>-L</sup> plates). These plates were incubated for 2-5 days in a Sanyo MIR262 stationary ventilated incubator. A single colony from these agar plates were used for each test mating experiments, which was performed in 1ml YPDA media in a 2ml microcentrifuge tube. The matings were incubated overnight at 30°C, shaking at 200rpm, in a YIH DER model LM-530 shaking incubator. Following the overnight incubation, 100 $\mu$ l of the mating cultures were plated onto SD<sup>-L-W</sup> agar

plates and incubated for 4-5 days at 30°C in a Sanyo MIR262 stationary ventilated incubator. After the incubation period, the colonies on each plate were transferred to TDO agar plates for four days, incubated at 30°C. Following this incubation, the mating mix was transferred to QDO agar plates and incubated for seven days at 30°C. On days 4 and 7, respectively, growth of yeast on these plates was assessed.

Additionally, to assess the hypothesised autoregulatory role of the C0C1 region, bait constructs encoding domains C0C2 in which the MyBPC motif represents the different phosphorylation states (C0C2, C0P<sub>1</sub>P<sub>2</sub>P<sub>3</sub>C2, C0A<sub>1</sub>P<sub>2</sub>A<sub>3</sub>C2, C0A<sub>1</sub>A<sub>2</sub>A<sub>3</sub>C2) were also mated individually with the putative positive preys, in the manner described for C1C2 baits.

## **2.16 CO-IMMUNOPRECIPITATION (Co-IP)**

Once putative positive interactors for the C1C2 region, under different phosphorylation conditions, had been identified by means of the Y2H experiments (Section 2.15), the interactions were confirmed using *in vitro* co-immunoprecipitation (Co-IP) analysis.

### **2.16.1 Creating an RNase-free experimental environment**

To reduce the possibility of RNase contamination during transcription/translation (Section 2.16.2) and Co-IP experiments (Section 2.16.3), all surfaces and instrumentation used in these experiments were wiped thoroughly using RNase Zap wipes (Ambion Inc, Austin, Texas, USA). Only pipette tips and microcentrifuge tubes certified RNase free by the manufacturer (Porex, Fairburn, Georgia, USA) were used.

### **2.16.2 Transcription and translation of baits and preys**

Following the identification of the putative interactors (Section 2.15), these prey plasmids were isolated from yeast Y187 (Section 2.1.3), shuttled into *Ecoli* DH5α (Section 2.13.1) for plasmid midi-scale preparation (Section 2.1.1) and subsequently PCR amplified using the ADHA-F and AD-R primers under conditions described in section 2.2.5. The PCR fragment generated comprised the prey insert linked to the HA-antibody epitope and a T7 promoter sequence, which is crucial for *in vitro* transcription. The eight pGBKT7 baits (C1C2, C1P<sub>1</sub>P<sub>2</sub>P<sub>3</sub>C2, C1A<sub>1</sub>P<sub>2</sub>A<sub>3</sub>C2, C1A<sub>1</sub>A<sub>2</sub>A<sub>3</sub>C2, C0C2, C0P<sub>1</sub>P<sub>2</sub>P<sub>3</sub>C2, C0A<sub>1</sub>P<sub>2</sub>A<sub>3</sub>C2, and C0A<sub>1</sub>A<sub>2</sub>A<sub>3</sub>C2) were also amplified using the BK-Myc and BK-R primers under conditions described in section 2.2.5, thereby generating a PCR fragment comprising either the C1C2 region or the C0C2 region representing the different phosphorylation states of the cMyBPC motif respectively, linked to the Myc-antibody and a T7 promoter sequence. The PCR fragments were then transcribed and translated using the TNT® Quick Coupled Transcription/Translation system (Promega Corp.), as per manufacturer's instructions. Following translation, 2μl of the reaction mixture was added to 15μl SDS loading dye (Appendix I) and electrophoresed in a 15% SDS polyacrylamide gel (Section 2.3.2; Appendix I). *In vitro* translated proteins were visualised using autoradiography (Section 2.4).

### **2.16.3 Co-IP of translated PCR products**

Once the PCR products had been translated into the respective bait- and prey-fusion peptides (Section 2.16.2), the products were co-immunoprecipitated (Figure 2.3) to assess the interaction identified by Y2H. In brief, 5µl bait and 5µl prey were mixed in a sterile, RNase-free 1.5ml microcentrifuge tube and incubated at room temperature for 1 hour, with mixing by gently tapping the tube every 15 minutes. Following the incubation, 1µl Myc-antibody (5µg/ml) (Roche Biosciences, Palo Alto, CA, USA) was added to the mixture. The sample was then incubated at room temperature for 1 hour. Subsequently, 10µl pre-washed protein G agarose (Appendix I) (Kirkegaard and Perry Laboratories, Gaithersburg, MD, USA) and 135µl Co-IP buffer (Appendix I) were added to each mixture. The sample was rotated on a Labnet rotor (Labnet Inc, NJ, USA) at 10rpm at 4<sup>0</sup>C for 1 hour and was subsequently washed five times with TBST (Appendix I).

Immunoprecipitation experiments with the baits using the Myc-antibody (Roche Biosciences), as well as each of the putative preys, using the HA-antibody (Roche Biosciences), were performed in conjunction with the Co-IP experiments to serve as controls. In brief, 5µl of each bait was individually mixed with 1µl Myc-antibody in separate sterile, RNase-free 1.5ml microcentrifuge tubes and incubated at room temperature for 1 hour. In separate 1.5ml microcentrifuge tubes, 5µl of each putative prey interactor was incubated with 5µl HA-antibody (Roche Biosciences). In addition, a protein G agarose control was included to assess whether the protein G itself was interacting non-specifically with the prey protein. For this reaction, 5µl of the prey protein was incubated in the absence of an antibody. Each of these tubes was also incubated at room temperature for 1 hour. Following the incubation, 10µl pre-washed protein G agarose (Appendix I) and 135µl Co-IP was added to each tube. The samples were rotated on a Labnet rotor (Labnet Inc, NJ, USA) at 10rpm at 4<sup>0</sup>C for 1 hour and were subsequently washed five times with TBST. To minimise background interactions the number of wash steps using TBST were increased to ten. Fifteen microlitres SDS loading dye was added to each sample which was subsequently incubated at 95<sup>0</sup>C for 5 minutes. The samples were then loaded onto a 15-20% SDS polyacrylamide gel (Section 2.3.2) and visualised using autoradiography (Section 2.4).

### Single

#### immunoprecipitations

#### Co-immunoprecipitations

#### Protein G Control

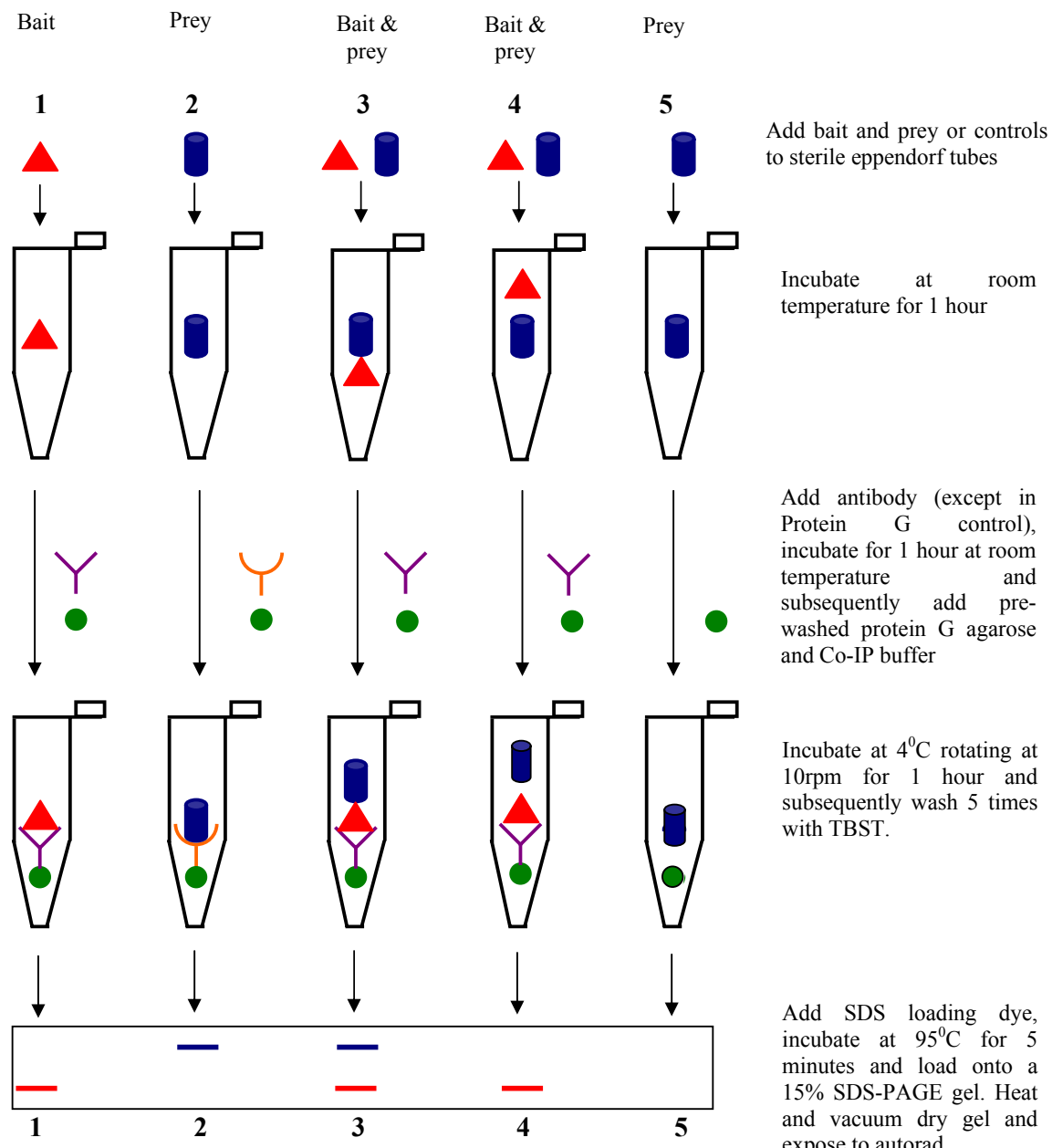


**Figure 2.3.** Schematic representation of the Co-IP protocol. Bait ; Prey ; Anti-Myc Antibody ; Anti-HA Antibody ; Protein G agarose Experiments 1 and 2 represent the immunoprecipitation of bait and prey using the appropriate antibodies. On a 15% SDS-PAGE gel, the immunoprecipitation is represented by a single band as seen in lanes 1 and 2. Experiment 3 represents a Co-IP reaction showing an interaction between bait and prey. This interaction is seen as two bands (lanes 3) on the gel; one band for each protein. Experiment 4 shows a Co-IP reaction where bait and prey do not interact with each other. After the 5 TBST washes, unbound proteins are washed away, leaving only proteins bound to the Myc-antibody and hence only one band is seen in lane 4. Experiment 5 shows the Protein G agarose control. As this is a negative control, prey should not interact with the Protein G agarose in the absence of an antibody, hence there should be no band in lane 5.

## 2.17 IN VIVO CO-LOCALISATION

The *in vivo* co-localisation assay was used to assess proposed protein-protein interactions in a true cellular environment. The proteins of interest were expressed, in mammalian cells, as fusion proteins with different fluorescent protein tags and were viewed using a fluorescence microscope housed at the Department of Physiology (University of Stellenbosch). The images acquired were subsequently processed for co-localisation. In the present study the GFP (green fluorescent protein), YFP (yellow fluorescent protein) and RFP (red fluorescent protein; produced by the DsRed vector) tags were utilised.

### 2.17.1 Co-localisation assay

Following co-transfection with the appropriate combination of vectors (Section 2.13.3), the H9C2 cells were allowed to differentiate for 7-10 days (Section 2.13.4). Just before image acquisition the culture media was removed and replaced with culture media containing a 1:200 dilution of the nucleic acid stain, Hoechst H-33342 (Sigma). This dye stains the nuclear material blue and is required for orientation purposes during the acquisition of images for the Z-stack. The cells were then photographed immediately using an Olympus IX 81 motorised inverted microscope (Olympus). Image analysis was performed using the CellR software (Olympus). The excitation and emission spectra, and filter requirements are indicated in Table 2.12.

**Table 2.12.** Excitation and emission spectra, and filter requirements of fluorescent proteins used in *in vivo* co-localisation

Fluorescent protein	Excitation	Emission	Filter set
GFP <sup>2</sup>	395nm	510nm	GFP
EYFP	514nm	527nm	YFP
DsRed-Monomer	557nm	585nm	TxRed
Hoechst H-33342*	351nm	460nm	DAPI

\* Nuclear stain, not a fluorescent protein tag.

In order to co-localise the tagged proteins in three dimensions, Z-stacks were performed. Double-labelled images, using the co-transfected samples, were acquired at different focal planes which were processed by the CellR software to determine co-localisation. The order of image acquisitions in multi-colour were as follows: for example, first a GFP image was taken at the lowest stack level and then a RFP image was taken at the same level. The camera then moved to the second lowest image and once again a GFP image was taken followed by a RFP image. This sequence was repeated for each layer until the last image was taken. The highest and lowest stack position was determined by first focusing on the nucleus of the cell to be imaged then taking the image out of focus by moving the objective up (top of the cell) then down (bottom of the cell). The co-ordinates of the top and bottom of the cell were recorded by the software. Image stacks were collected at 0.26µm intervals in the plane of the optical axis using a 60X oil immersion objective. Each co-localised image was produced from the average of 25 frames.

The image acquisition and analysis for the co-localisation of the GFP:YFP and GFP:DsRed protein pairs were performed differently. Since the spectra of GFP and YFP overlap, the excitation and imaging of the

YFP-labelled structures occurs with the GFP filter set and vice versa. Spectral imaging and linear unmixing made it possible to separate and resolve the contribution of the GFP and YFP to the total signal in each colour channel. To ‘unmix’ the spectral information, it was necessary to determine the spectral properties of the individual fluorochromes (single transfections; Table 2.12) under the same imaging conditions used for the multi-labelled samples (co-transfections; Table 2.12): i.e. the system had to be calibrated for each fluorochrome. This was performed by first taking reference GFP and YFP images of single-labelled samples with the same filter set (excitation and emission filter) as used for the images of double-labelled specimen. Spectral unmixing was then performed using the CellR software (Olympus) and involved initial calibration (using the reference images) and subsequent unmixing. The processed double-labelled GFP:YFP images were then co-localised. For the GFP:RFP co-localisations, images were acquired using the co-transfected samples and were processed for co-localisation in the same way as the GFP:YFP processed double-labelled images, except that unmixing was not required. Single images of the Hoechst staining of the nuclei and phase view of the cells were captured. These images were not required by the software for determining co-localisation, but provided context for the expression of the fluorescent proteins.

## 2.18 BIOLUMINESCENCE RESONANCE ENERGY TRANSFER (BRET)

Bioluminescence resonance energy transfer is based on the non-radiative energy transfer (RET) between a bioluminescent donor moiety and a fluorescent acceptor moiety. The energy transfer efficiency is highly dependent on the distance between the donor and the acceptor moieties and their relative orientation with respect to each other. In most RET-based assays, the typical effective distance between the donor and the acceptor is 10 to 100 angstroms ( $\text{\AA}$ ); a range that correlates well with most biological interactions, thus making RET an excellent tool for monitoring macromolecular interactions (Pfleger and Eidne, 2003; Prinz *et al.*, 2006).

BRET uses a luciferase (Rluc, 35kDa) isolated from the sea pansy *Renilla reniformis* as the donor and the proprietary coelenterazine substrate DeepBlueC (DBC) (Perkin Elmer). In the presence of oxygen, Rluc catalyses the transformation of DBC into coelenteramide, with concomitant light emission peaking at 395nm (blue light). When a suitable acceptor (GFP<sup>2</sup>, a GFP variant, 27kDa) is in close proximity, the blue light energy emitted by the Rluc/DBC reaction is captured by the GFP acceptor through RET and results in an emission of green light at 510nm. A change in the fluorescence/luminescence ratio allows protein-protein interactions to be quantitatively analysed (Pfleger and Eidne, 2003; Prinz *et al.*, 2006).

The interactions between thick (cMyBPC) and thin filaments (ACTC1 and cTNI) could not be assessed by *in vivo* co-localisation (Section 2.17), as it is already known that thick and thin filaments overlap in the sarcomere and thus appear to share the same subcellular space at the resolution of conventional and even confocal microscopy. Thus, BRET assays were employed to evaluate the interaction of cMyBPC with ACTC1 and cTNI, respectively, in differentiated cardiac cells. As the energy transfer between Rluc and GFP is distance dependent, it was necessary to engineer two cMyBPC-Rluc constructs covering the C1C2 region.

The first construct C1C10 would generate a fusion protein with the Rluc-tag on the N-terminus of domain C1, while construct C2C10 would generate a fusion protein with the Rluc-tag on the N-terminus of domain C2. By this approach, the interacting cMyBPC domain (C1, the MyBPC-motif or C2) may also be defined. In addition, the constructs needed to span to the end of domain C10, to allow the fusion construct when expressed to take its place in the sarcomere and assume its quaternary arrangement. ACTC1 and cTNI were generated as C-terminus fusion proteins to the GFP-tag, respectively. In concurrent experiments, each putative prey construct was co-transfected with either Rluc-C1C10 or Rluc-C2C10. A number of control transfections were performed to verify the data generated (Table 2.9).

In addition, the proposed interaction of domains C2, C3 and C7 with C10, respectively, were also evaluated using this assay. These N-terminus:C-terminus cMyBPC interactions were assessed by cloning PCR products representing domains C2C10, C3C10 and C7C10 individually into the GFP<sup>2</sup>-MCS-Rluc vector (Section 2.9.2). This vector generated, for example with C2C10 construct, a fusion protein comprising the GFP-tag on the N-terminus of domain C2 and the Rluc-tag on the C-terminus of domain C10. Thus, if there was an interaction between domains C2 and C10 (in differentiated cardiac cells) there would be an energy transfer between the GFP and Rluc tags, which would be measured. The construct of C-terminus domains, C7C10, was included to serve as a control for this novel approach.

### 2.18.1 BRET assay

Once the H9C2 cells had been transfected with the appropriate combination of vectors (Section 2.13.3) and were allowed to differentiate into myotubes (Section 2.13.4), the cells were visualised using an Olympus IX 81 motorised inverted microscope (Olympus) to confirm successful transfection by monitoring the GFP expression before proceeding with the BRET assay. pRluc expression cannot be visualised directly, as the substrate DeepBlueC is required for its excitation, and is toxic to cells over an extended period of time. Once the GFP expression was confirmed, the number of cells in each well was determined. Briefly, cells were trypsinised (200µl trypsin in each well) as described in section 2.12.2; after 5 minutes, 400µl growth media was added; the cells were gently resuspended and transferred to a 12ml Greiner tube.

To perform a cell count, 20µl of the cell suspension was applied to a haemocytometric cell count chamber (Appendix II). The approximate cell count for each sample was recorded. The cells were then pelleted by centrifugation at 1000rpm for 3 minute using a Sorval® GLC-4 General Laboratory centrifuge, followed by removal the supernatant. The pellet was resuspended at 1x10<sup>6</sup>cells/ml in PBS/gelatine solution (Appendix I). These cells were split for the control and isoproterenol assays.

For the control assay, 45µl of each cell suspension was added to a separate well in a 96-well white polystyrene plate. A working solution of the DeepBlueC (250µM; Appendix I) was prepared just prior to use, as it does not store well. The Synergy HT luminometer (BioTek Instruments Inc., Vermont, USA) was prewarmed to 37°C and then programmed to dispense 10µl PBS, one well at a time, followed by 5µl

DeepBlueC (final concentration 5 $\mu$ M). The cells were incubated for 45 seconds followed by 3 consecutive readings, with a 10 second integration time, with 400/30 and 516/20 filters.

To assess the effect of phosphorylation of the MyBPC-motif, mediated by CamK-II and PKA, cells were exposed to isoproterenol before performing the BRET assay. For the isoproterenol assay, 5 $\mu$ l of 65mM CaCl<sub>2</sub> (Appendix I) was added to 45 $\mu$ l of the cell suspension and following an incubation of 10 minutes, 5 $\mu$ l of 10X isoproterenol (Appendix I) was then added, as this has been demonstrated previously to result in maximal trisphosphorylation of cMyBPC in skinned cardiac trabeculae (McClellan *et al.*, 2001). The cells were incubated for a further 10 minutes and subsequently transferred to the luminometer to be read in the same manner as the control assay.

The BRET ratio was determined by subtracting the ratio of the GFP emission over the Rluc emission for a cell sample containing only the Rluc construct from the same ratio for a sample containing the putatively interacting GFP and Rluc fusion proteins (Pfleger *et al.*, 2006) (Appendix II).

### **2.18.2 Statistical Analysis**

Statistical comparison of BRET ratios between samples and controls was performed using the Statistica software package (Statsoft Inc. Oklahoma, USA). Statistical comparisons were carried out using a one-way analysis of variance (ANOVA) followed by Bonferroni's multiple comparison post-test, comparing all pairs.

## CHAPTER THREE: RESULTS

INDEX	PAGE
<b>3.1 Y2H ANALYSIS OF DOMAIN C1C2 OF cMyBPC UNDER DIFFERENT PHOSPHORYLATION CONDITIONS OF THE MyBPC-MOTIF</b>	<b>105</b>
<b>3.1.1 Y2H bait constructs</b>	<b>105</b>
<b>3.1.1.1 Sequence analysis of the pGBK-bait constructs</b>	<b>105</b>
<b>3.1.1.2 Phenotype test</b>	<b>105</b>
<b>3.1.1.3 Toxicity test</b>	<b>105</b>
<b>3.1.1.4 Mating efficiency of AH109 transformed with bait construct</b>	<b>106</b>
<b>3.1.2 Y2H screening of pretransformed cardiac cDNA library</b>	<b>106</b>
<b>3.1.2.1 pGBK-C1C2 library screen</b>	<b>107</b>
<b>3.1.2.2 pGBK-C1P<sub>1</sub>P<sub>2</sub>P<sub>3</sub>C2 library screen</b>	<b>112</b>
<b>3.1.2.3 pGBK-C1A<sub>1</sub>P<sub>2</sub>A<sub>3</sub>C2 library screen</b>	<b>116</b>
<b>3.1.2.4 pGBK-C1A<sub>1</sub>A<sub>2</sub>A<sub>3</sub>C2 library screen</b>	<b>121</b>
<b>3.1.3 Y2H in summary</b>	<b>126</b>
<b>3.1.4 Yeast-Two Hybrid Protein-Protein Interaction Assays</b>	<b>126</b>
<b>3.1.4.1 Comparison of prey coiled-coil domain structure to myosin subfragment 2</b>	<b>131</b>
<b>3.2 CO-IMMUNOPRECIPITATION</b>	<b>132</b>
<b>3.3 THREE-DIMENSIONAL <i>IN VIVO</i> CO-LOCALISATION USING FLUORESCENCE MICROSCOPY</b>	<b>141</b>
<b>3.4 BIOLUMINESCENCE RESONANCE ENERGY TRANSFER ASSAY (BRET)</b>	<b>143</b>
<b>3.4.1 C1C10 cMyBPC versus cTNI</b>	<b>144</b>
<b>3.4.2 C1C10 cMyBPC versus ACTC1</b>	<b>145</b>
<b>3.4.2 C2C10 cMyBPC versus cTNI</b>	<b>145</b>
<b>3.4.3 C2C10 cMyBPC versus ACTC1</b>	<b>146</b>
<b>3.4.3 cMyBPC-cMyBPC interaction</b>	<b>147</b>
<b>3.5 CORRELATION OF DATA BETWEEN Y2H AND VERIFICATION ASSAYS</b>	<b>148</b>

### **3.1 Y2H ANALYSIS OF DOMAIN C1C2 OF cMyBPC UNDER DIFFERENT PHOSPHORYLATION CONDITIONS OF THE MyBPC-MOTIF**

#### **3.1.1 Y2H bait constructs**

Bait constructs pGBK-C1C2, pGBK-C1A<sub>1</sub>A<sub>2</sub>A<sub>3</sub>C2, pGBK-C1A<sub>1</sub>P<sub>2</sub>A<sub>3</sub>C2 and pGBK-C1P<sub>1</sub>P<sub>2</sub>P<sub>3</sub>C2 were used to screen cardiac cDNA libraries, in separate experiments. The pGBK-C0C2, pGBK-C0A<sub>1</sub>A<sub>2</sub>A<sub>3</sub>C2, pGBK-C0A<sub>1</sub>P<sub>2</sub>A<sub>3</sub>C2 and pGBK-C0P<sub>1</sub>P<sub>2</sub>P<sub>3</sub>C2 bait constructs were generated to assess the role of domain C0 on the interaction between the C1C2 baits and the putative interactor clones identified by Y2H.

##### **3.1.1.1 Sequence analysis of the pGBK-bait constructs**

DNA sequence analysis of the pGBK-bait constructs (pGBK-C1C2, pGBK-C1A<sub>1</sub>A<sub>2</sub>A<sub>3</sub>C2, pGBK-C1A<sub>1</sub>P<sub>2</sub>A<sub>3</sub>C2, pGBK-C1P<sub>1</sub>P<sub>2</sub>P<sub>3</sub>C2, pGBK-C0C2, pGBK-C0A<sub>1</sub>A<sub>2</sub>A<sub>3</sub>C2, pGBK-C0A<sub>1</sub>P<sub>2</sub>A<sub>3</sub>C2 and pGBK-C0P<sub>1</sub>P<sub>2</sub>P<sub>3</sub>C2) were performed to verify that the integrity of the sequence and the reading frame had been maintained. Results of the sequence analysis showed that pGBK-baits were in the correct reading frame and that the integrity of the nucleotide sequence of the insert had been preserved through the multiple rounds of PCR amplifications used to generate the site-directed mutagenesis fragments. The substitution of the correct base pairs to mimic the presence or absence of phosphorylation was also verified from sequence analysis.

##### **3.1.1.2 Phenotype test**

The yeast strain AH109 transformed with the individual bait constructs was able to grow on the appropriate selection media (SD<sup>-W</sup> and SD<sup>-U</sup>), but was unable to grow on selection media lacking other essential amino acids (SD<sup>-A</sup>, SD<sup>-L</sup>, SD<sup>-H</sup>) (Section 2.14.1). This confirmed that the phenotype of the AH109 strain was retained after each transformation.

##### **3.1.1.3 Toxicity test**

In order to establish whether the various C0C2 and C1C2 pGBK-bait constructs were toxic to yeast strain AH109, growth curves were generated (Section 2.14.2). In concurrent experiments, the growth of the respective pGBK-baits transformed into AH109 was compared to the growth of yeast AH109 transformed with non-recombinant pGBK. The slope of the linearised test curves were similar to the slope of AH109 transformed with non-recombinant pGBK, indicating that the bait constructs had no toxic effect on the growth of the yeast (Figure 3.1).

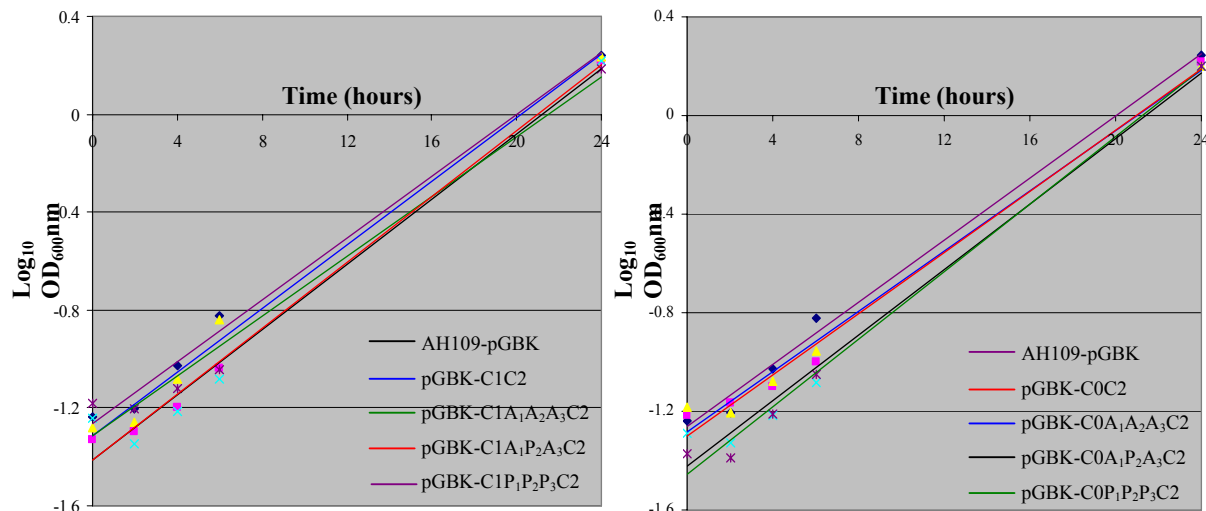


**Figure 3.1.** Linear growth curves of yeast strain AH109 transformed with non-recombinant pGBK and pGBK-cMyBPC bait constructs. In order to determine whether the bait constructs had toxic effects on the AH109 strain, the growth rate of the pGBK-bait transformants were compared to the non-recombinant pGBK. The growth rate was determined by calculating the slope of each of the curves. The slopes were comparable indicating that the bait constructs had no toxic effect on the growth of the host yeast strain.

### 3.1.1.4 Mating efficiency of AH109 transformed with bait construct

In order to determine whether the transformation of the pGBK-bait had significantly affected the mating ability of the AH109 host strain, small-scale yeast mating was performed (Section 2.14.3). The mating efficiency of each bait transformant and pTD1.1 was compared to the mating efficiency of pTD1.1 and pGBK53. The mating efficiency results show that pGBK-baits did not impede the mating efficiency of AH109, as the mating efficiency of the tests were higher than the minimum 2% recommended by the manufacturer of the MATCHMAKER Y2H system (Table 3.1).

**Table 3.1.** Effect of bait constructs in pGBK, Y2H bait vector, on AH109 mating efficiency

Mating tests	Mating efficiency
pGBK53 (AH109) x PTD1.1 (Y187)	10.8
C1C2 (AH109) x PTD1.1 (Y187)	7
C1A <sub>1</sub> A <sub>2</sub> A <sub>3</sub> C2 (AH109) x PTD1.1 (Y187)	19
C1A <sub>1</sub> P <sub>2</sub> A <sub>3</sub> C2 (AH109) x PTD1.1 (Y187)	8.6
C1P <sub>1</sub> P <sub>2</sub> P <sub>3</sub> C2 (AH109) x PTD1.1 (Y187)	25.2
C0C2 (AH109) x PTD1.1 (Y187)	8
C0A <sub>1</sub> A <sub>2</sub> A <sub>3</sub> C2 (AH109) x PTD1.1 (Y187)	10
C0A <sub>1</sub> P <sub>2</sub> A <sub>3</sub> C2 (AH109) x PTD1.1 (Y187)	18
C0 P <sub>1</sub> P <sub>2</sub> P <sub>3</sub> C2 (AH109) x PTD1.1 (Y187)	11

### 3.1.2 Y2H screening of pretransformed cardiac cDNA library

Presented in this chapter are the results of four independent library screens. The pGBK-C1C2 and pGBK-C1P<sub>1</sub>P<sub>2</sub>P<sub>3</sub>C2 library screens were performed in our laboratory just prior to the present study, but the data from these screens were included to complete the profile of cMyBPC putative interactors for the cMyBPC

motif, under various phosphorylation states, investigated in the present study. As a result, the presentation of data for the earlier library screens and the library screens performed during the course of the present study (pGBK-C1A<sub>1</sub>A<sub>2</sub>A<sub>3</sub>C2 and pGBK-C1A<sub>1</sub>P<sub>2</sub>A<sub>3</sub>C2 library screens) differ slightly. Verification studies on interactions identified in all four screens were undertaken in this study, and these are thus presented in the same format.

### 3.1.2.1 pGBK-C1C2 library screen

Approximately 1.3x10<sup>6</sup> cardiac cDNA clones were screened by the pGBK-C1C2 bait. Four hundred and sixty yeast clones were able to activate the *HIS3* reporter gene, as judged by growth on TDO plates (Table 3.2 column A) of which only 162 clones were able to activate the *ADE2* reporter gene, as judged by growth on QDO plates (Table 3.2 column B). A further 59 clones were eliminated by the X- $\alpha$ -galactosidase assay, as these clones were unable to activate the colourimetric reporter gene *MEL1* (Table 3.2 column C). The remaining 103 clones were nucleotide sequenced and the identity of each clone was determined by mining online nucleotide and protein sequence databases. Of the clones nucleotide sequenced, 83 were eliminated as putative interactors of the pGBK-C1C2 bait because their subcellular localisation (as determined using Proteome Analyst [<http://pa.cs.ualberta.ca:8080/pa/pa/index.html>] and ESLpred [<http://www.imtech.res.in/raghava/eslpred>]) would place them in a cellular compartment incompatible with MyBPC's localisation. Table 3.3 represents only those 20 clones whose open reading frame (ORF) had significant protein matches and which were considered putative positive interactors of pGBK-C1C2. Clones with currently no known subcellular localisation or function were not excluded from further investigation, as this information, although it may become available with the complete annotation of the human genome, could not currently add insight into the function of the N-terminus of cMyBPC. The same procedure to determine subcellular localisation and function was followed for the pGBK-C1P<sub>1</sub>P<sub>2</sub>P<sub>3</sub>C2 (Section 3.1.2.2), pGBK-C1A<sub>1</sub>P<sub>2</sub>A<sub>3</sub>C2 (Section 3.1.2.3) and pGBK-C1A<sub>1</sub>A<sub>2</sub>A<sub>3</sub>C2 (Section 3.1.2.4) library screens.

Subsequently, heterologous bait mating was performed on the 20 putative preys, to assess the specificity of interaction of these preys with the pGBK-C1C2 bait (Table 3.4). Where a prey was represented by multiple clones in the pGBK-C1C2 and pGBK-C1P<sub>1</sub>P<sub>2</sub>P<sub>3</sub>C2 library screens, only a single clone was subject to heterologous mating

**Table 3.2.** Activation of nutritional and colourimetric reporter genes by prey-C1C2 interaction. Tabulated are representative scoring of the 460 clones that activated the *HIS3* reporter gene, 162 clones that activated the *ADE2* reporter gene and 103 clones that were able to activate the *MEL1* reporter gene.

Clone #	A		B	C
	Growth on TDO ( <i>HIS3</i> activation)	Growth on QDO ( <i>ADE2</i> activation)	X- $\alpha$ -galactosidase assay (colour) ( <i>MEL1</i> activation)	
C1	++++	++++	++ (medium blue)	
C13	++++	++++	++ (medium blue)	
C29	++++	++++	+++ (dark blue)	
C42	++++	+	+ (no blue)	
C54	++++	+++	++ (medium blue)	
C70	++++	++++	+++ (dark blue)	
C75	++++	++++	++ (medium blue)	
C81	++++	++	++ (medium blue)	
C92	++++	+++	++ (medium blue)	
C93	++++	+	+++ (dark blue)	
C127	++++	+	+ (no blue)	
C129	++++	+++	+ (light blue)	
C132	++++	+	++ (medium blue)	
C134	++++	++	+++ (dark blue)	
C141	+++	++	+ (light blue)	
C143	++++	++	+++ (dark blue)	
C182	++++	++++	+++ (dark blue)	
C193	+++	+++	+++ (no blue)	
C212	++++	+++	++ (medium blue)	
C213	++++	++++	+++ (dark blue)	
C282	++++	++++	+ (light blue)	
C300	+++	+	+ (no blue)	
C312	++++	++++	++ (medium blue)	
C319	++++	++++	+++ (dark blue)	
C325	++++	++	+ (light blue)	
C353	+++	+	+ (no blue)	
C363	++++	++	++ (medium blue)	
C374	++++	+++	++ (medium blue)	
C412	++++	+++	+ (light blue)	
C415	++++	+++	+ (light blue)	
C449	++++	++++	++ (no blue)	
C475	+++	+	+ (no blue)	

Colonies in blue font activated *HIS3*, *ADE2* and *MEL1* reporter genes. TDO= solid media lacking Leu, Trp and His; QDO= solid media lacking Leu, Trp, His and Ade. Growth of colonies on solid media: ++++= very good, +++)= good, ++)= weak, +)= very weak, -)= no growth.

**Table 3.3.** Identification of C1C2 putative interactor clones from the Y2H cardiac cDNA library screen. Putative interactors represented by multiple clones are shown first, arranged from highest to lowest activators of nutritional and colourimetric reporter genes. Putative interactors represented by a single clone are arranged in the same manner.

Clone #	Genomic hit BLASTN			In-frame protein hit BLASTP		
	Identity	Accession #	Accession #	Size of peptide encoded by insert (aa)	Cellular localisation	Domains
		E-value	E-value			
C70	<i>Homo sapiens</i> chromosome 1 open reading frame 108 (C1orf108) hypothetical protein LOC79647	NM_024595 (0.0)	NP_078871.1 (2e-37)	99	Cytoplasm; nucleus	None
C93	<i>Homo sapiens</i> chromosome 1 open reading frame 108 (C1orf108) hypothetical protein LOC79647	NM_024595 (0.0)	NP_078871.1 (2e-37)	92	Cytoplasm; nucleus	None
C134	<i>Homo sapiens</i> chromosome 1 open reading frame 108 (C1orf108) hypothetical protein LOC79647	NM_024595 (0.0)	NP_078871.1 (2e-37)	92	Cytoplasm; nucleus	None
C143	<i>Homo sapiens</i> chromosome 1 open reading frame 108 (C1orf108) hypothetical protein LOC79647	NM_024595 (0.0)	NP_078871.1 (2e-37)	92	Cytoplasm; nucleus	None
<sup>‡</sup> C81	<i>Homo sapiens</i> troponin I type 3 (cardiac) (TNNI3)	NM_000363 (0.0)	NP_000354.4 (1e-27)	244	Thin filament	Troponin
<sup>‡</sup> C312	<i>Homo sapiens</i> troponin I type 3 (cardiac) (TNNI3)	NM_000363 (0.0)	NP_000354.4 (1e-27)	244	Thin filament	Troponin
<sup>‡</sup> C363	<i>Homo sapiens</i> troponin I type 3 (cardiac) (TNNI3)	NM_000363 (0.0)	NP_000354.4 (1e-27)	244	Thin filament	Troponin

Clone	Genomic hit			In-frame protein hit		
	BLASTN			BLASTP		
	Identity #	Accession #	Accession #	Size of peptide encoded by insert (aa)	Cellular localisation	Domains
<sup>‡</sup> C212	<i>Homo sapiens</i> heat shock 27 kDa protein family, member 7, (cardiovascular) (HSPB7)	NM_014424 (0.0)	NP_055239.1 (6e-70)	189	Cytoplasm	HSP20/alpha crystalline
<sup>‡</sup> C374	<i>Homo sapiens</i> heat shock 27 kDa protein family, member 7, (cardiovascular) (HSPB7)	NM_014424.3 (0.0)	NP_055239.1 (6e-70)	189	Cytoplasm	HSP20/alpha crystalline
<sup>‡</sup> C141	<i>Homo sapiens</i> heat shock 27 kDa protein family, member 7, (cardiovascular) (HSPB7)	NM_014424.3 (0.0)	NP_055239.1 (6e-70)	135	Cytoplasm	HSP20/alpha crystalline
C132	<i>Homo sapiens</i> heat shock 27 kDa protein 3 (HSPB3)	NM_006308 (0.0)	NP_006299.1 (3e-74)	150	Cytoplasm	HSP20/alpha crystalline
C13	<i>Homo sapiens</i> phosphoglucomutase 5 (PGM5)	NM_021965 (0.0)	NP_068800.2 (6e-68)	567	Cytoplasm; junction; adherens junction	PGM_PMM I, II, III & IV, Phosphoglucomutase/ phosphomannomutase, alpha/beta/alpha domain
C92	<i>Homo sapiens</i> phosphoglucomutase 5 (PGM5)	NM_021965 (0.0)	NP_068800.2 (6e-68)	188	Cytoplasm; junction; adherens junction	PGM_PMM Phosphoglucomutase/ phosphomannomutase, alpha/beta/alpha domain
<sup>‡</sup> C29	<i>Homo sapiens</i> actinin, alpha 2 (ACTN2)	NM_001103 (0.0)	NP_001094.1 (3e-141)	550	Z-disc	Spectrin
C182	<i>Homo sapiens</i> phosphodiesterase 4D interacting protein (myomegalin) (PDE4DIP), transcript variant 4	NM_001002810 (0.0)	NP_055459.3 (1e-70)	173	Sarcomere	Microtubule associated

Clone	Genomic hit			In-frame protein hit		
	BLASTN			BLASTP		
	Identity #	Accession #	Accession #	Size of peptide encoded by insert (aa)	Cellular localisation	Domains
C213	<i>Homo sapiens</i> ankyrin repeat and SOCS box-containing 2 (ASB2)	NM_016150.3 (0.0)	NP_057234.2 (1e-93)	568	Cytoplasm	Ankyrin repeats; suppressors of cytokine signalling
<sup>‡</sup> C319	<i>Homo sapiens</i> GRINL1A combined protein (Gcom1)	NM_001018100.1 (0.0)	NP_001018100.1 (2e-65)	433	Cytoplasm; nucleus	Myosin tail
C54	<i>Homo sapiens</i> parvin, alpha (PARVA)	NM_018222.2 (0.0)	NP_060692.1 (7e-70)	211	Cytoskeleton; cytoplasm	Calponin
<sup>‡</sup> C412	<i>Homo sapiens</i> myosin binding protein C, cardiac (MYBPC3)	NM_000256 (0.0)	NP_000247.2 (2e-26)	513	Thick filament; Sarcomere	C5-C10 FnIII and Ig
C415	<i>Homo sapiens</i> leiomodin 3 (foetal) (LMOD3)	NM_198271.2 (1e-113)	NP_938012.2 (5e-64)	526	Cytoskeleton; cytoplasm	Leucine-rich repeats, ribonuclease inhibitor-like subfamily; Tropomodulin

Only those clones with in-frame ORF's with significant protein matches are represented. <sup>‡</sup>Clones investigated further in the present study.

**Table 3.4.** Interaction of C1C2 preys with heterologous baits in specificity tests. Tabulated are the scores of the clones considered as putative interactors.

Colony #	pGBK-C1C2	pGBK-PKDd10	pGBK53	pGBKT7
C13	+++	-	-	+
C29	++	-	-	-
C54	++	+	+++	+
C70	+	-	-	-
C81	++	-	+	++
C132	+	+	++++	+
C141	+	-	++	-
C182	+	-	-	-
C212	+++	-	+	+
C213	++	-	+++	-
C312	+	-	+	-
C319	+	-	+	-
C363	+	-	-	-
C374	+++	-	++	+
C412	++	++	++	+
C415	-	-	+	-

Colonies scored after 7 days on QDO. QDO= solid media lacking Leu, Trp, His and Ade. Growth of colonies on solid media: ++++= very good, +++= good, ++= weak, + = very weak, - = no growth.

### 3.1.2.2 pGBK-C1P<sub>1</sub>P<sub>2</sub>P<sub>3</sub>C2 library screen

Library titer calculations estimated that 1.3x10<sup>6</sup> cardiac cDNA clones were screened with pGBK-C1P<sub>1</sub>P<sub>2</sub>P<sub>3</sub>C2 bait (trisphosphorylated bait mimic). Five hundred yeast clones were able to activate the *HIS3* reporter gene, as judged by growth on TDO plates (Table 3.5 column A) of which only 353 clones were able to activate the *ADE2* reporter gene, as judged by growth on QDO plates (Table 3.5 column B). A further 121 clones were eliminated by the X- $\alpha$ -galactosidase assay (Table 3.5 column C). Two hundred and thirty two clones were then nucleotide sequenced and the identity of each clone was determined by mining online nucleotide and protein sequence databases. Of the clones nucleotide sequenced, 214 were eliminated as putative interactors of the pGBK-C1P<sub>1</sub>P<sub>2</sub>P<sub>3</sub>C2 bait because of their subcellular localisation and function, as described in section 3.1.2.1. Table 3.6 represents only those 18 clones whose open reading frame (ORF) had significant protein matches and which were considered putative positive interactors of pGBK-C1P<sub>1</sub>P<sub>2</sub>P<sub>3</sub>C2. Subsequent heterologous bait mating assays assessed the 18 putative positive clone's specificity for interaction with the pGBK-C1P<sub>1</sub>P<sub>2</sub>P<sub>3</sub>C2 bait (Table 3.7). MYBPC3 (P213, P319 and P62), PDE4DIP (P403, P272 and P205) and GRINL1A (P2 and P81) clones were also identified as putative interactors by the pGBK-C1C2 screen (Section 3.1.2.1).

**Table 3.5.** Activation of nutritional and colourimetric reporter genes by prey-C1P<sub>1</sub>P<sub>2</sub>P<sub>3</sub>C2 interaction. Tabulated are representative scoring of the 500 clones that activated the *HIS3* reporter gene, 353 clones that activated the *ADE2* reporter gene and 232 clones that were able to activate the *MEL1* reporter gene.

Colony #	<b>A</b>		<b>B</b> <i>X</i> - $\alpha$ -galactosidase assay (colour)	<b>C</b> <i>X</i> - $\alpha$ -galactosidase assay (colour)
	Growth on TDO ( <i>HIS3</i> activation)	Growth on QDO ( <i>ADE2</i> activation)		
P2	++	+		+ (medium blue)
P5	+++	+++		+++ (light blue)
P6	+++	+++		+++ (light blue)
P11	++	+		+ (no blue)
P16	++++	+++		++ (medium blue)
P18	+++	+++		++ (no blue)
P30	++++	+++		++ (light blue)
P45	++	+		+ (light blue)
P62	+++	++		++ (light blue)
P67	+++	++		++ (light blue)
P77	++	+		+ (no blue)
P80	+++	++		++ (light blue)
P81	++	+		+ (medium blue)
P118	++	+		+ (dark blue)
P149	++	+		++ (light blue)
P164	++	+		+ (dark blue)
P175	++	+		+ (medium blue)
P180	++++	+++		+++ (light blue)
P182	++	+		+ (medium blue)
P192	++	+		+ (no blue)
P205	+++	++		+ (medium blue)
P213	++++	+++		+++ (light blue)
P223	++++	++		++ (medium blue)
P224	++	+		+ (dark blue)
P228	++	++		++ (no blue)
P237	+++	++		++ (medium blue)
P238	+++	++		++ (medium blue)
P259	++++	+++		+ (light blue)
P267	+++	++		+ (dark blue)
P272	+++	++		+ (light blue)
P286	+++	++		++ (light blue)
P319	++++	+++		+++ (light blue)
P353	++	+		+ (no blue)
P398	+++	++		+ (light blue)
P399	+++	++		+ (light blue)
P403	+++	+++		+++ (light blue)
P420	+++	++		+ (light blue)
P461	+++	+++		+++ (no blue)
P465	++	+		+ (medium blue)

Colonies in blue font activated *HIS3*, *ADE2* and *MEL1* reporter genes. TDO= solid media lacking Leu, Trp and His; QDO= solid media lacking Leu, Trp, His and Ade. Growth of colonies on solid media: ++++= very good, +++)= good, ++)= weak, +)= very weak, -)= no growth.

**Table 3.6.** Identification of C1P<sub>1</sub>P<sub>2</sub>P<sub>3</sub>C2 putative interactor clones from the Y2H cardiac cDNA library screen. Putative interactors represented by multiple clones are shown first, arranged from highest to lowest activators of nutritional and colourimetric reporter genes. Putative interactors represented by a single clone are arranged in the same manner.

Clone#	Identity	Genomic hit		In-frame protein hit			
		BLASTN		BLASTP			
		Accession #	E-value	Accession #	E-value	Size of peptide encoded by insert (aa)	Cellular Localisation Domains
<sup>‡</sup> P286	<i>Homo sapiens</i> actin, alpha, cardiac muscle 1 (ACTC1)	NM_005159 (0.0)		NP_005150 (1e-89)		129	Thin filament sarcomere Actin
<sup>‡</sup> P267	<i>Homo sapiens</i> actin, alpha, cardiac muscle 1 (ACTC1)	NM_005159 (0.0)		NP_005150 (1e-89)		245	Thin filament sarcomere Actin
<sup>‡</sup> P182	<i>Homo sapiens</i> actin, alpha, cardiac muscle 1 (ACTC1)	NM_005159 (0.0)		NP_005150 (1e-89)		164	Thin filament sarcomere Actin
P259	<i>Homo sapiens</i> actin, beta (ACTB)	NM_001101 (0.0)		AAH23548.1 (8e-34)		76	Cytoplasm; cytoskeleton Actin
<sup>‡</sup> P213	<i>Homo sapiens</i> myosin binding protein C, cardiac (MYBPC3)	NM_000256 (0.0)		NP_000247.2 (2e-26)		349	Thick filament sarcomere C7-C10 FnIII and Ig
P319	<i>Homo sapiens</i> myosin binding protein C, cardiac (MYBPC3)	NM_000256 (0.0)		NP_000247.2 (2e-26)		54	Thick filament sarcomere C10 Ig
<sup>‡</sup> P62	<i>Homo sapiens</i> myosin binding protein C, cardiac (MYBPC3)	NM_000256 (0.0)		NP_000247.2 (2e-26)		237	Thick filament sarcomere C8-10 FnIII and Ig
P403	<i>Homo sapiens</i> phosphodiesterase 4D interacting protein (myomegalin) (PDE4DIP), transcript variant 4	NM_001002810 (0.0)		NP_055459.3 (1e-70)		173	Sarcomere Microtubule associated
<sup>‡</sup> P205	<i>Homo sapiens</i> phosphodiesterase 4D interacting protein (myomegalin) (PDE4DIP), transcript variant 4	NM_001002810 (0.0)		NP_055459.3 (1e-70)		173	Sarcomere Microtubule associated

Clone#	Genomic hit			In-frame protein hit			
	BLASTN			BLASTP			
	Identity	Accession #	Accession #	Size of peptide encoded by insert (aa)	Cellular Localisation	Domains	
<sup>‡</sup> P272	<i>Homo sapiens</i> phosphodiesterase 4D interacting protein (myomegalin) (PDE4DIP), transcript variant 4	NM_001002810 (0.0)	NP_055459.3 (1e-70)	135	Sarcomere		Microtubule associated
P2	<i>Homo sapiens</i> GRINL1A combined protein (Gcom1), transcript variant 12	NM_001018100 (0.0)	NP_001018100.1 (2e-65)	197	Cytoplasm; nucleus		Myosin tail
<sup>‡</sup> P81	<i>Homo sapiens</i> GRINL1A combined protein (Gcom1), transcript variant 12	NM_001018100 (0.0)	NP_001018100.1 (2e-65)	132	Cytoplasm; nucleus		Myosin tail
P175	<i>Homo sapiens</i> calponin 1, basic, smooth muscle (CNN1)	NM_001299.4 (0.0)	NP_001290.2 (1e-104)	240	Cytoplasm; cytoskeleton		Calponin
P465	<i>Homo sapiens</i> calponin 1, basic, smooth muscle (CNN1)	NM_001299 (0.0)	NP_001290.2 (1e-88)	177	Cytoplasm; cytoskeleton		Calponin
P223	<i>Homo sapiens</i> chaperonin containing TCP1, subunit 7 (eta) (CCT7)	NM_001009570.1 (0.0)	NP_001009570.1 (1e-83)	172	Cytoplasm		TCP-1 chaperonin family, eta subunit
P238	<i>Homo sapiens</i> supervillin (SVIL)	NM_021738.1 (0.0)	NP_003165.1 (1e-15)	41	Actin cytoskeleton; plasma membrane; nucleus		Villin headpiece domain
P80	<i>Homo sapiens</i> filamin C, gamma (actin binding protein 280) (FLNC)	NM_001458.2 (0.0)	NP_001449.3 (2e-91)	182	Z-discs; actin cytoskeleton		Filamin-type Ig domains
P398	FLJ21347	NM_022827.2 (0.0)	NP_073738.2 (4e-101)	602	Unknown		Thioredoxin domain

Only those clones with in-frame ORF's with significant protein matches are represented. <sup>‡</sup>Clones investigated further in the present study.

**Table 3.7.** Interaction of C1P<sub>1</sub>P<sub>2</sub>P<sub>3</sub>C2 preys with heterologous baits in specificity tests. Tabulated are the scores of the clones considered as putative interactors.

Colony #	pGBK-C1P <sub>1</sub> P <sub>2</sub> P <sub>3</sub> C2	pGBK-p35	pGBK53	pGBKT7
P2	+++	-	+	-
P62	++++	-	++++	++++
P80	+++	-	+++	++
P81	++	-	+	-
P175	+++	-	++	-
P182	+++	-	+++	-
P205	++	-	+++	-
P213	+	-	+	-
P223	+	-	+++	-
P238	++	-	++	++
P259	+++	-	+++	-
P267	+++	-	+++	-
P272	++	-	+++	-
P286	+++	-	+++	-
P319	++	-	++++	++++
P398	-	-	-	-
P403	++	-	+++	-
P465	+++	-	+++	-

Colonies scored after 7 days on QDO. QDO= solid media lacking Leu, Trp, His and Ade. Growth of colonies on solid media: ++++= very good, +++= good, ++= weak, + = very weak, - = no growth.

### 3.1.2.3 pGBK-C1A<sub>1</sub>P<sub>2</sub>A<sub>3</sub>C2 library screen

The pGBK-C1A<sub>1</sub>P<sub>2</sub>A<sub>3</sub>C2 bait (monophosphorylated mimic) was used to screen approximately 1.3x10<sup>6</sup> cardiac cDNA clones. One thousand six hundred and eighty yeast clones were able to activate the *HIS3* reporter gene, as judged by growth on TDO plates (Table 3.8 column A) of which only 1035 clones were able to activate the *ADE2* reporter gene, as judged by growth on QDO plates (Table 3.8 column B). The X- $\alpha$ -galactosidase assay eliminated 897 clones (Table 3.8 column C). Subsequent heterologous bait mating assays eliminated 124 clones (Table 3.9) as they activated the transcription of reporter genes in the presence of heterologous baits, and were thus considered as false positives. As hundreds of clones were selected for during each round of assessment, the clones shown the Tables 3.8 and 3.9 are representatives of the clones screened by the pGBK-C1A<sub>1</sub>P<sub>2</sub>A<sub>3</sub>C2 bait. As a result of these increasingly stringent elimination steps, only fourteen of the original clones were, thus, classified as putative interactor clones and were nucleotide sequenced. The identities of the clones as determined by mining online sequence databases are shown in Table 3.10. Three clones were eliminated from further study because their cellular localisation would place them in a cellular compartment incompatible with MyBPC's sarcomeric localisation while one clone was out of frame. ACTN2 (APA9) was also identified by the pGBK-C1C2 screen (Section 3.1.2.1).

**Table 3.8.** Activation of nutritional and colourimetric reporter genes by prey-C1A<sub>1</sub>P<sub>2</sub>A<sub>3</sub>C<sub>2</sub> interaction. Tabulated are representative scoring of the 1680 clones that activated the *HIS3* reporter gene, 1035 clones that activated the *ADE2* reporter gene and 138 clones that were able to activate the *MEL1* reporter gene.

Clone #	<b>A</b>		X- $\alpha$ -galactosidase assay (colour)	
	Growth on TDO			
	( <i>HIS3</i> activation)	( <i>ADE2</i> activation)		
APA8	++++	+++	++ (medium blue)	
APA9	+++	+++	+++ (light blue)	
APA17	++++	+++	++ (no blue)	
APA26	++++	++++	++ (medium blue)	
APA38	+++	++++	++++ (dark blue)	
APA84	++++	++++	++++ (dark blue)	
APA122	++++	++++	+++ (no blue)	
APA162	++++	+++	+++ (light blue)	
APA163	++++	++++	++ (light blue)	
APA164	+++	+++	++ (dark blue)	
APA169	++++	++++	+++ (light blue)	
APA209	++++	+++	++ (no blue)	
APA231	++++	+++	+++ (dark blue)	
APA232	++++	+++	+++ (dark blue)	
APA257	++++	++++	++++ (dark blue)	
APA342	+++	++	++ (no blue)	
APA397	++++	+++	+++ (medium blue)	
APA409	++++	++++	++++ (dark blue)	
APA491	+++	++++	+++ (light blue)	
APA524	++++	++++	++ (light blue)	
APA528	++++	+++	+++ (medium blue)	
APA534	+++	++++	++ (medium blue)	
APA535	++++	+++	+++ (light blue)	
APA543	++++	+++	+++ (dark blue)	
APA682	++++	+++	+++ (no blue)	
APA794	++++	++++	+++ (medium blue)	
APA826	+++	++++	+++ (dark blue)	
APA834	+++	++++	+++ (light blue)	
APA923	++++	+++	+++ (medium blue)	
APA1004	++++	++++	+++ (no blue)	
APA1011	++++	+++	+++ (dark blue)	
APA1045	++++	++++	++ (light blue)	
APA1096	++++	+++	+++ (dark blue)	
APA1135	+++	++++	++++ (light blue)	
APA1138	+++	+++	+++ (no blue)	
APA1149	++++	+++	+++ (medium blue)	
APA1588	+++	++++	+++ (no blue)	
APA1641	++++	+++	+++ (dark blue)	

Colonies in blue font activated *HIS3*, *ADE2* and *MEL1* reporter genes. TDO= solid media lacking Leu, Trp and His; QDO= solid media lacking Leu, Trp, His and Ade. Growth of colonies on solid media: ++++= very good, +++)= good, ++= weak, += very weak, -= no growth

**Table 3.9.** Interaction of C1A<sub>1</sub>P<sub>2</sub>A<sub>3</sub>C2 preys with heterologous baits in specificity tests. Tabulated are representative scores of the 138 clones that were screened.

Clone #	pGBK-C1A <sub>1</sub> P <sub>2</sub> A <sub>3</sub> C2	pGBK-Reeler	pGBK53	pGBKT7
APA8	++++	++++	++++	++++
<b>APA9</b>	<b>+++</b>	-	-	-
APA26	+++	-	+++	+++
APA38	++	-	++	++++
APA84	++++	++++	-	++++
<b>APA162</b>	<b>++++</b>	-	-	-
<b>APA163</b>	<b>++++</b>	<b>++</b>	-	-
APA164	+++	-	-	+++
<b>APA169</b>	<b>+++</b>	-	-	-
<b>APA231</b>	<b>++++</b>	<b>++</b>	-	-
<b>APA232</b>	<b>++++</b>	<b>++</b>	-	-
APA257	+++	-	-	+++
APA397	+++	+++	-	++++
APA409	+++	<b>++</b>	-	<b>++</b>
<b>APA491</b>	<b>++++</b>	-	-	-
<b>APA524</b>	<b>+++</b>	-	-	-
APA528	++++	++++	++++	++++
APA534	+++	+++	+++	+++
<b>APA535</b>	<b>++++</b>	-	-	-
<b>APA543</b>	<b>++</b>	-	-	-
APA794	+++	+++	+++	+++
APA826	+++	+++	-	<b>++</b>
<b>APA834</b>	<b>++++</b>	-	-	-
APA923	++++	++++	-	+++
APA1011	++++	++++	++++	++++
<b>APA1045</b>	<b>++</b>	-	-	-
APA1096	+++	+++	-	<b>++</b>
<b>APA1135</b>	<b>+++</b>	<b>++++</b>	-	-
APA1146	++++	+++	<b>++</b>	<b>++</b>
APA1149	++++	++++	+++	-
<b>APA1641</b>	<b>++++</b>	-	-	-

Colonies scored after 7 days on QDO. QDO= solid media lacking Leu, Trp, His and Ade. Growth of colonies on solid media: ++++= very good, +++)= good, ++= weak, += very weak, -= no growth. Clones in bold blue font were selected for further study.

**Table 3.10.** Identification of the fourteen C1A<sub>1</sub>P<sub>2</sub>A<sub>3</sub>C<sub>2</sub> putative interactor clones from the Y2H cardiac cDNA library screen. Putative interactors represented by multiple clones are shown first, arranged from highest to lowest activators of nutritional and colourimetric reporter genes. Putative interactors represented by a single clone are arranged in the same manner.

Clone #	Identity	Genomic hit BLASTN		In-frame protein hit BLASTP		
		Accession #	Accession #	Size of peptide encoded by insert (aa)	Cellular localisation	Domains
		E-value	E-value			
‡APA491	<i>Homo sapiens</i> COMM domain containing 4 (COMM4)	NM_017828.3 (0.0)	NP_060298.2 (6e-92)	199	Cytoplasm	COMM
‡APA524	<i>Homo sapiens</i> COMM domain containing 4 (COMM4)	NM_017828.3 (0.0)	NP_060298.2 (1e-95)	199	Cytoplasm	COMM
‡APA535	<i>Homo sapiens</i> enolase 3 (beta, muscle) (ENO3)	NM_053013.1 (0.0)	NP_001967.1 (4e-160)	434	Cytoplasm; Z-disc and M-line of sarcomere	Enolase
‡APA163	<i>Homo sapiens</i> enolase 3 (beta, muscle) (ENO3)	NM_053013.1 (0.0)	NP_001967.1 (1e139)	364	Cytoplasm; Z-disc and M-line of sarcomere	Enolase
‡APA232	<i>Homo sapiens</i> uveal autoantigen with coiled-coil domains and ankyrin repeats (UACA)	NM_018003.2 (0.0)	NP_001008225.1 (1e-71)	155	Cytoplasm; golgi; plasma membrane	Myosin tail
‡APA162	<i>Homo sapiens</i> uveal autoantigen with coiled-coil domains and ankyrin repeats (UACA)	NM_018003.2 (0.0)	NP_001008225.1 (3e-77)	155	Cytoplasm; golgi; plasma membrane	Myosin tail
‡APA231	<i>Homo sapiens</i> spectrin repeat containing, nuclear envelope 1 (SYNE1)	NM_033071.1 (0.0)	NP_892006.1 (5e-106)	255	Sarcomere; nuclear membrane	Spectrin
‡APA9	<i>Homo sapiens</i> actinin, alpha 2 (ACTN2)	NM_001103.1 (0.0)	NP_001094.1 (3e-141)	550	Z-disc	Spectrin

Clone #	Genomic hit				In-frame protein hit		
	BLASTN				BLASTP		
	Identity	Accession #	Accession #	Size of peptide encoded by insert (aa)	Cellular localisation	Domains	
		E-value	E-value				
APA543	<i>Homo sapiens</i> adaptor-related protein complex 2, beta 1 subunit (AP2B1)	NM_001030006.1 (0.0)	NP_001273.1 (2e-122)	302	Cytoplasm	Alpha-adaptin C2 Beta-adaptin-app-C	
APA1641	<i>Homo sapiens</i> eukaryotic translation initiation factor 4A, isoform 2 (EIF4A2)	NM_001967.3 (0.0)	NP_001407.1 (2e-123)	284	Nucleus	Helicase C	
‡APA1135	<i>Homo sapiens</i> guanine nucleotide binding protein (G protein), beta polypeptide 2-like 1 (GNB2L1)	NM_006098.4 (8e-170)	NP_006089.1 (1e-75)	224	Cytoplasm	WD40	
APA834	<i>Homo sapiens</i> hypothetical protein BC002926 (LOC90379)	NM_138353.2 (0.0)	NP_612362.2 (4e-118)	219	Nucleus	None	
APA169	<i>Homo sapiens</i> phosphoprotein enriched in astrocytes 15	BC010469.1 (0.0)	No similarity	N/A	N/A	N/A	
APA1045	<i>Homo sapiens</i> ubiquitin-conjugating enzyme E2 variant 1 (UBE2V1)	NM_022442.3 (0.0)	NP_954673.1 (4e-38)	90	Nucleus	Ubiquitin conjugating enzyme E2 catalytic domain	

Thirteen of the fourteen C1A<sub>1</sub>P<sub>2</sub>A<sub>3</sub>C2 putative interactor clones had in-frame ORF's with significant protein matches. <sup>‡</sup>Clones investigated by the present study.

### **3.1.2.4 pGBK-C1A<sub>1</sub>A<sub>2</sub>A<sub>3</sub>C2 library screen**

Library titer calculations estimated that  $1.3 \times 10^6$  cardiac cDNA clones were screened with pGBK-C1A<sub>1</sub>A<sub>2</sub>A<sub>3</sub>C2 bait (dephosphorylated bait mimic). Four hundred and thirty seven yeast clones were able to activate the *HIS3* reporter gene, as judged by growth on TDO plates (Table 3.11 column A) of which only 225 clones were able to activate the *ADE2* reporter gene, as judged by growth on QDO plates (Table 3.11 column B). A further 86 clones were eliminated by the X- $\alpha$ -galactosidase assay (Table 3.11 column C) and subsequent heterologous bait mating assays eliminated 123 clones (Table 3.12). As hundreds of clones were selected for during each round of assessment, the clones shown the Tables 3.11 and 3.12 are representatives of the clones screened by the pGBK-C1A<sub>1</sub>A<sub>2</sub>A<sub>3</sub>C2 bait. Sixteen clones were thus classified as putative interactor clones and were nucleotide sequenced. The identity of each clone was determined by mining online nucleotide and protein sequence databases, shown in Table 3.13. All clones had in-frame ORF's with significant protein matches. Twelve of the 16 clones sequenced were eliminated from further study due to their incompatible subcellular localisation described in section 3.1.2.1. Of the three clones prioritised, SYNE1 (AAA179) was also identified by the pGBK-C1A<sub>1</sub>P<sub>2</sub>A<sub>3</sub>C2 screen (APA231) and GRINL1A (AAA143) was identified by the pGBK-C1C2 (C319; Section 3.1.2.1) and pGBK-C1P<sub>1</sub>P<sub>2</sub>P<sub>3</sub>C2 (P2 and P81; Section 3.1.2.2) screens.

**Table 3.11.** Activation of nutritional and colourimetric reporter genes by prey-C1A<sub>1</sub>A<sub>2</sub>A<sub>3</sub>C2 interaction. Tabulated are representative scoring of the 437 clones that activated the *HIS3* reporter gene, 225 clones that activated the *ADE2* reporter gene and 139 clones that were able to activate the *MEL1* reporter gene.

Colony #	<b>A</b>		X- $\alpha$ -galactosidase assay (colour)	
	Growth on TDO			
	( <i>HIS3</i> activation)	( <i>ADE2</i> activation)		
AAA3	++++	++++	+++ (dark blue)	
AAA9	++++	++	++ (light blue)	
AAA15	++++	++++	++++ (medium blue)	
AAA18	++++	++++	++++ (medium blue)	
AAA19	++++	++++	++++ (dark blue)	
AAA21	++++	++	++ (medium blue)	
AAA23	+++	+++	++ (no blue)	
AAA28	++++	+++	++ (light blue)	
AAA47	++++	+++	+++ (dark blue)	
AAA52	++++	+++	- (no blue)	
AAA61	++++	++	++ (medium blue)	
AAA67	++++	++++	++++ (dark blue)	
AAA79	++++	+++	++ (light blue)	
AAA84	++++	+++	+++ medium blue)	
AAA92	++++	++	++ (light blue)	
AAA98	++++	+++	+++ (medium blue)	
AAA100	++++	++	++ (medium blue)	
AAA116	++++	++	- (no blue)	
AAA119	++++	++++	+++ (dark blue)	
AAA127	++++	++	- (no blue)	
AAA130	++++	+++	+++ (dark blue)	
AAA133	++++	+++	++ (light blue)	
AAA143	++++	++++	++++ (medium blue)	
AAA144	++++	++++	+++ (dark blue)	
AAA165	+++	+++	+++ (no blue)	
AAA179	++++	++++	++++ (medium blue)	
AAA188	++++	++++	++++ (dark blue)	
AAA195	++++	+++	+++ (medium blue)	
AAA197	++++	+++	+++ (dark blue)	
AAA209	++++	+++	+ (medium blue)	
AAA210	++++	+++	++ (no blue)	
AAA225	++++	+++	+ (medium blue)	
AAA233	++++	+++	- (no blue)	
AAA255	+++	+++	+++ (no blue)	
AAA326	++++	+++	++ (light blue)	
AAA422	++++	+++	++ (medium blue)	
AAA425	++++	++++	+++ (dark blue)	
AAA437	++++	++++	++ (medium blue)	

Colonies in blue font activated *HIS3*, *ADE2* and *MEL1* reporter genes. TDO= solid media lacking Leu, Trp and His; QDO= solid media lacking Leu, Trp, His and Ade. Growth of colonies on solid media: ++++= very good, +++)= good, ++= weak, + = very weak, - = no growth.

**Table 3.12.** Interaction of C1A<sub>1</sub>A<sub>2</sub>A<sub>3</sub>C2 preys with heterologous baits in specificity tests. Tabulated are representative scores of the 139 clones that were screened.

Colony #	pGBK-C1A <sub>1</sub> A <sub>2</sub> A <sub>3</sub> C2	pGBK-Reeler	pGBK53	pGBKT7
<b>AAA3</b>	++	++	-	-
<b>AAA9</b>	+++	-	-	+
AAA15	++++	++++	++++	++++
<b>AAA18</b>	++++	++++	-	-
<b>AAA19</b>	++++	++++	-	-
AAA21	++++	++++	++++	++++
<b>AAA28</b>	++++	+	-	+
AAA47	++++	++++	-	++++
AAA61	++++	++++	+	++++
<b>AAA67</b>	++++	++	-	-
<b>AAA79</b>	+++	-	-	-
AAA84	++++	++++	++++	++++
<b>AAA92</b>	++	-	-	+
<b>AAA98</b>	+++	-	-	-
AAA100	++++	++++	++++	++++
<b>AAA119</b>	++++	++++	-	-
AAA130	+	++++	++++	++++
<b>AAA133</b>	+	++	-	+
<b>AAA143</b>	++	-	-	-
<b>AAA144</b>	+	++++	-	-
<b>AAA179</b>	++++	++++	+	+
AAA188	+	++++	+++	+++
<b>AAA195</b>	++	++++	-	-
<b>AAA197</b>	+++	++	-	-
AAA209	++++	++++	++++	++++
AAA225	++	++++	++++	++++
AAA326	++++	+	-	++++
AAA422	+	++++	+++	++
AAA425	++	++++	++++	++++
AAA437	++++	++++	-	++++

Colonies scored after 7 days on QDO. QDO= solid media lacking Leu, Trp, His and Ade. Growth of colonies on solid media: ++++= very good, +++= good, ++= weak, + = very weak, - = no growth. Clones in bold blue font were selected for further study.

**Table 3.13.** Identification of the sixteen C1A<sub>1</sub>A<sub>2</sub>A<sub>3</sub>C2 putative interactor clones from the Y2H cardiac cDNA library screen. Putative interactors represented by multiple clones are shown first, arranged from highest to lowest activators of nutritional and colourimetric reporter genes. Putative interactors represented by a single clone are arranged in the same manner.

Clone #	Genomic hit			In-frame protein hit		
	BLASTN		BLASTP			
	Identity	Accession #	Accession #	Size of peptide encoded by insert (aa)	Cellular localisation	Domains
AAA67	<i>Homo sapiens</i> SWI/SNF related, matrix associated, actin dependent regulator of chromatin, subfamily b, member 1 (SMARCB1)	NM_003073.3 (0.0)	NP_001007469.1 (7e-97)	250	Nucleus	SNF5/ SMARCB1
AAA197	<i>Homo sapiens</i> SWI/SNF related, matrix associated, actin dependent regulator of chromatin, subfamily b, member 1 (SMARCB1)	NM_003073.3 (0.0)	NP_001007469.1 (1e-141)	283	Nucleus	SNF5/ SMARCB1
AAA19	<i>Homo sapiens</i> serpin peptidase inhibitor, clade H (heat shock protein 47), member 1, (collagen binding protein 1) (SERPINH1)	NM_001235.2 (1e-168)	NP_001226.2 (9e-49)	345	Endoplasmic reticulum; golgi	HSP47
‡AAA3	<i>Homo sapiens</i> troponin T type 2 (cardiac) (TNNT2)	NM_000364.2 (3e-147)	NP_001001430 (7e-70)	258	Troponin complex	Troponin
AAA119	<i>Homo sapiens</i> solute carrier family 25 (mitochondrial carrier; phosphate carrier), member 3 (SLC25A3)	NM_005888 (0.0)	NP_957009.1 (6e-177)	339	Mitochondrion	None
AAA144	<i>Homo sapiens</i> collagen, type I, alpha 2 (COL1A2)	NM_000089.3 (0.0)	NP_000080.2 (1e-85)	162	Extracellular matrix	COLF1

Clone #	Genomic hit		In-frame protein hit				
	BLASTN		BLASTP				
	Identity	Accession #	Accession #	Size of peptide encoded by insert (aa)	Cellular localisation	Domains	
		E-value	E-value				
AAA18	<i>Homo sapiens</i> suppressor of var1, 3-like (SUPV3L1)	NM_003171.2 (0.0)	NP_003162.2 (0.0)	455	Mitochondrion	Helicase C	
<sup>‡</sup> AAA179	<i>Homo sapiens</i> spectrin repeat containing, nuclear envelope 1 (SYNE1)	NM_182961.1 (0.0)	NP_892006.2 (8e-126)	261	Sarcomere; nuclear membrane	Spectrin	
<sup>‡</sup> AAA143	<i>Homo sapiens</i> GRINL1A combined protein (Geom1)	NM_001018100.1 (0.0)	NP_001018100.1 (2e-65)	179	Cytoplasm; nucleus	Myosin tail	
AAA98	<i>Homo sapiens</i> chromosome 2 open reading frame 29 (C2orf29)	NM_017546.3 (0.0)	NP_060016.2 (1e-70)	304	Cytoplasm	None	
AAA195	<i>Homo sapiens</i> electron-transfer-flavoprotein, alpha polypeptide (ETFA)	NM_000126.2 (0.0)	NP_000117.1 (3e-111)	302	Mitochondrion	ETF_alpha	
AAA28	<i>Homo sapiens</i> eukaryotic translation initiation factor 4A, isoforms 2(EIF4A2)	NM_001967.3 (0.0)	NP_001407.1 (1e-84)	197	Nucleus	Helicase C	
AAA9	<i>Homo sapiens</i> zinc finger protein 668 (ZNF668)	NM_024706 (0.0)	NP_078982 (8e-143)	309	Nucleus	Zinc finger	
AAA79	<i>Homo sapiens</i> zinc finger protein 219 (ZNF219)	NM_016423 (0.0)	NP_057507 (1e-71)	334	Nucleus	C2H2 zinc finger	
AAA92	<i>Homo sapiens</i> prosaposin (variant Gaucher disease and variant metachromatic leukodystrophy) (PSAP)	NM_001042466.1 (0.0)	NP_001035931.1 (9e-129)	247	Lysosome	Saposin/surfactant protein-B A-type	
AAA133	<i>Homo sapiens</i> ATP synthase, H <sup>+</sup> transporting, mitochondrial F0 complex, subunit d (ATP5H)	NM_006356.2 (0.0)	NP_006347.1 (3e-84)	161	Mitochondrion	Mt_ATP_synthase_D	

All sixteen C1A<sub>1</sub>A<sub>2</sub>A<sub>3</sub>C2 putative interactor clones had in-frame ORF's with significant protein matches. <sup>‡</sup>Clones investigated by the present study.

### 3.1.3 Y2H in summary

In total, 3077 clones that activated 3 reporter genes (Table 3.14) were screened as putative interactors of domains C1C2 of cMyBPC, under the native and different phosphorylation mimic states of the cMyBPC motif. Based on subcellular localisation and function, 27 in-frame clones were prioritised as putative positive interactors of domains C1C2 cMyBPC (Table 3.14). As we were particularly interested in cMyBPC's role in the regulation of cardiac contractility, select thick and thin filament proteins, in addition to proteins that are known to associate with these sarcomeric filaments, were selected for investigation in the present study. Further, putative positive preys from the C1A<sub>1</sub>P<sub>2</sub>A<sub>3</sub>C2 and C1A<sub>1</sub>A<sub>2</sub>A<sub>3</sub>C2 library screen were also included. A detailed description of these 13 putative positive preys (ACTC1, MYBPC3, cTNI, COMMD4, ACTN2, PDE4DIP, ENO3, HSPB7, cTNT, GRINL1A, SYNE1, UACA and GNB2L1) are presented in the following chapter (Discussion). Some of these putative positive preys are represented by multiple clones which were all included in further investigations in this study. The follow-up of the remaining 14 clones falls outside the scope of this thesis, but will be screened in future studies in our laboratory.

**Table 3.14.** Summary of clones screened by Y2H

Library screen	Growth on TDO (activation of HIS3)	Growth on QDO (activation of ADE2)	X-α-galactosidase assay (activation of MEL1)	Eliminated by heterologous mating	Clones sequenced	Clones prioritised*
C1C2	460	162	103	N/A	103	12
C1P <sub>1</sub> P <sub>2</sub> P <sub>3</sub> C2	500	353	232	N/A	232	7
C1A <sub>1</sub> P <sub>2</sub> A <sub>3</sub> C2	1680	1035	138	124	14	6
C1A <sub>1</sub> A <sub>2</sub> A <sub>3</sub> C2	437	225	139	123	16	2

\*Multiple clones considered once, in order of the screen identified in.

### 3.1.4 Yeast-Two Hybrid Protein-Protein Interaction Assays

Direct Y2H protein-protein interaction assays were performed to determine whether the prioritised putative interactor preys, identified by the four library screens, interacted specifically with the cMyBPC motif (and had a preference for a particular phosphorylation mimic) or whether the interactions were driven by domains C1 or C2, flanking the cMyBPC motif (Assay 1). Additionally, the role of the cardiac-specific region N-terminus to C1 was assessed to determine whether the role of this region was analogous to the role of the regulatory tail of titin kinase (Mayans *et al.*, 1998; Section 1.9.3.2.2), and autoregulated the interactions of the C1C2 region (Assay 2). Graphical representation of data from Assay 1 in Appendix VI.

For assay 1, the pGBK-C0C1 bait was used as a negative control as this region is similar in size and charge to domains C1C2 (Kunst *et al.*, 2000) (Table 3.15).

### *Putative MyBPC-motif interactors*

ACTN2 and COMMD4 interacted strongly with pGBK-C1C2, pGBK-C1A<sub>1</sub>A<sub>2</sub>A<sub>3</sub>C2 and pGBK-C1A<sub>1</sub>P<sub>2</sub>A<sub>3</sub>C2, weakly (ACTN2) or not at all (COMMD4) with pGBK-C1P<sub>1</sub>P<sub>2</sub>P<sub>3</sub>C2, and not at all with pGBK-C1 or pGBK-C2, indicating that the region of interaction of these two proteins was with the cMyBPC motif (Table 3.15). This pattern of interactions also suggest that the interactions were phosphorylation dependent, and are analogous to the interaction of myosin S2 with the cMyBPC motif: When the cMyBPC motif is unphosphorylated it interacts with myosin S2, but upon PKA-dependent phosphorylation of the cMyBPC motif the interaction with myosin S2 is abolished (Gautel *et al.*, 1995; Section 1.9.3.5.9.1).

### *Interactions with MyBPC-motif flanking domains*

The interaction of ACTC1 with the cMyBPC N-terminus was not phosphorylation dependent, as ACTC1 interacted strongly and indiscriminately with all pGBK-C1C2 phosphorylation-mimics, pGBK-C0C1 and pGBK-C2. Further, ACTC1 interacted weakly (P182) or not at all (P267 and P286) with pGBK-C1 suggesting that actin-binding sites exist N-terminus of C1 and within domain C2, possibly including the cMyBPC motif.

The interaction of cTNT does not appear to be phosphorylation dependent as it interacted strongly with pGBK-C1C2, pGBK-C1A<sub>1</sub>A<sub>2</sub>A<sub>3</sub>C2, pGBK-C1A<sub>1</sub>P<sub>2</sub>A<sub>3</sub>C2 and pGBK-C1P<sub>1</sub>P<sub>2</sub>P<sub>3</sub>C2. cTNT did not interact with pGBK-C1 and only interacted weakly with pGBK-C2, indicating that the region of interaction may also involve the cMyBPC motif, however, it is not dependent on the phosphorylation state of the bait.

cTNI interacted fairly strongly with pGBK-C1C2, pGBK-C1A<sub>1</sub>A<sub>2</sub>A<sub>3</sub>C2, pGBK-C1P<sub>1</sub>P<sub>2</sub>P<sub>3</sub>C2 and pGBK-C2 respectively, and not at all with pGBK-C1. The interaction of pGBK-C1A<sub>1</sub>P<sub>2</sub>A<sub>3</sub>C2 with the individual cTNI clones was ambiguous as there was no interaction between C363 and pGBK-C1A<sub>1</sub>P<sub>2</sub>A<sub>3</sub>C2, while a strong interaction existed between C81 and pGBK-C1A<sub>1</sub>P<sub>2</sub>A<sub>3</sub>C2. Thus, not considering the ambiguous interactions of pGBK-C1A<sub>1</sub>P<sub>2</sub>A<sub>3</sub>C2 with the cTNI clones, the region of interaction appears to be with domain C2, and possibly the cMyBPC motif, irrespective of its phosphorylation status on a qualitative level. Clone C312 of cTNI interacted much weaker than the C363 and C81 clones, which represent the same region of the protein as C312, and may reflect alterations to the yeast fitness by repeated freeze-thawing cycles and culturing or plasmid load.

The alteration in yeast fitness may also explain the variable interactions of HSPB7 with the pGBK-C1C2 baits. The three clones (C141, C374 and C212) interacted very weakly or not at all with the cMyBPC baits, and specifically did not interact with pGBK-C1C2 in the protein-protein interaction assays, although HSPB7 was originally identified as a putative interactor in the library screen using this bait. However, C212 and C374 interacted with domain C2 consistently.

**Table 3.15.** Y2H direct protein-protein interaction assay investigating bait:prey interactions between the C1C2 phosphorylation-mimics (Assay1) and the effect of domain C0, using C0C2 phosphorylation-mimics (Assay 2).

Prey ID & Clone No	Size of peptide encoded by insert	Domains	ASSAY 1						ASSAY 2			
			C0C1	C1	C2	C1C2	C1A <sub>1</sub> A <sub>2</sub> A <sub>3</sub> C2	C1A <sub>1</sub> P <sub>2</sub> A <sub>3</sub> C2	C1P <sub>1</sub> P <sub>2</sub> P <sub>3</sub> C2	A <sub>1</sub> A <sub>2</sub> A <sub>3</sub>	C0	
										C2	C0	C0
<b>Actinin, alpha 2 (ACTN2)</b>												
APA9	550aa	Spectrin	+	-	-	+++	+++	+++	+++	+	-	-
C29	550aa	Spectrin	-	-	-	++++	++	+++	+++	+	+	+
<b>COMM Domain 4 (COMMD4)</b>												
APA524	199aa	COMM	-	-	-	+	++	+++	-	-	-	-
APA491	199aa	COMM	-	-	-	+++	+++	+++	-	-	-	-
<b>Actin (ACTC1)</b>												
P267	245aa	Actin	+++	-	+++	++++	++++	++++	+++	-	-	-
P182	164aa	Actin	+++	+	+++	+++	+++	+++	++	-	-	-
P286	129aa	Actin	++	-	+++	+++	++++	+++	+++	-	-	-
<b>Troponin I (cTNI)</b>												
C363	244aa	Troponin	-	-	++	++	++	-	++	-	-	-
C312	244aa	Troponin	-	-	+	-	+	+	-	-	-	-
C81	244aa	Troponin	-	-	+++	+++	+++	+++	+++	-	-	-
<b>Troponin T (cTNT)</b>												
AAA3	258aa	Troponin	+	-	+	++++	+++	+++	++++	+	+	-

Colonies scored after 7 days on QDO media (solid media lacking Leu, Trp, Ade, His). Growth of colonies on solid media: ++++= very good, +++)= good, ++)= weak, +)= very weak, -)= no growth. aa=amino acids

Prey ID & Clone No	Size of peptide encoded by insert	Domains	ASSAY 1						ASSAY 2			
			C0C1	C1	C2	C1C2	C1A <sub>1</sub> A <sub>2</sub> A <sub>3</sub> C2	C1A <sub>1</sub> P <sub>2</sub> A <sub>3</sub> C2	C1P <sub>1</sub> P <sub>2</sub> P <sub>3</sub> C2	A <sub>1</sub> A <sub>2</sub> A <sub>3</sub>	C0	
									C2	C2	C2	
<b>Cardiac myosin binding protein C (cMyBPC)</b>												
C412	513aa	C5-c10	+++	++++	+++	++++	++++	++++	++++	++++	++++	++++
P62	237aa	C8-c10	++++	++++	++++	++++	++++	++++	++++	++++	++++	++++
P213	349aa	C7-c10	-	-	++	+++	+	+++	++	+	+	+
<b>Heat shock 27 kDa protein, member 7 (HSPB7)</b>												
C212	189aa	HSP20/alpha crystalline	-	-	+	+	-	-	-	-	-	-
C374	189aa	HSP20/alpha crystalline	-	-	+	-	-	-	-	-	-	-
C141	135aa	HSP20/alpha crystalline	-	-	-	-	+	-	-	-	-	++
<b>Phosphodiesterase 4D interacting protein (PDE4IP)</b>												
P272	135aa	Microtubule associated	+++	+++	+++	+++	+++	+++	+++	++	++	++
P205	173aa	Microtubule associated	+++	+++	+++	+++	+++	+++	+++	++	++	++
<b>Enolase beta (ENO3)</b>												
APA163	364aa	Enolase	-	++	++	++	++	+++	++	-	-	-
APA535	434aa	Enolase	+	+	+	++++	++++	++++	++++	-	-	-

Prey ID & Clone No	Size of peptide encoded by insert	Domains	ASSAY 1						ASSAY 2			
			C0C1	C1	C2	C1C2	C1A <sub>1</sub> A <sub>2</sub> A <sub>3</sub> C2	C1A <sub>1</sub> P <sub>2</sub> A <sub>3</sub> C2	C1P <sub>1</sub> P <sub>2</sub> P <sub>3</sub> C2	A <sub>1</sub> A <sub>2</sub> A <sub>3</sub>	C0	
										C2	C2	C2
<b>GRINL1A combined protein</b>												
C319	433aa	Myosin tail	-	-	-	-	++	+++	++	-	-	-
P81	132aa	Myosin tail	-	-	-	+++	+++	++	++	-	-	-
AAA 143	179aa	Myosin tail	-	-	-	++++	+++	++++	++++	+	+	+
<b>Spectrin repeat containing, nuclear envelope 1 (SYNE1)</b>												
APA 231	255aa	Spectrin	++	+++	++	++++	++++	+++	++++	++++	++++	++++
AAA 179	261aa	Spectrin	++	++++	++	++++	++++	++++	++++	++++	++++	++++
<b>Uveal autoantigen with coiled-coil domains and ankyrin repeats (UACA)</b>												
APA 232	155aa	Myosin tail	++	++	++	++++	++++	++++	++++	-	-	-
APA 162	155aa	Myosin tail	+	+	+	++++	++++	++++	++++	-	-	-
<b>Guanine nucleotide binding protein (G protein), beta polypeptide 2-like 1 (GNB2L1)</b>												
APA 1135	224aa	WD40	++	++	++	++	++	++	++	-	-	-

Colonies scored after 7 days on QDO media (solid media lacking Leu, Trp, Ade, His). Growth of colonies on solid media: ++++= very good, +++= good, ++= weak, += very weak, - = no growth. aa= amino acids

SYNE1 (APA231 and AAA179), UACA (APA232 and APA162), GNB2L1 (APA1135), ENO3 (APA535) and PDE4DIP (P272 and P205) interacted with pGBK-C1, pGBK-C2 and the pGBK-C1C2 phosphorylation-mimics, irrespective of phosphorylation status. These interactions possibly reflect the prey proteins' ability to non-specifically interact with Ig-like domains.

All GRINL1A clones interacted with pGBK-C1A<sub>1</sub>A<sub>2</sub>A<sub>3</sub>C2 and pGBK-C1A<sub>1</sub>P<sub>2</sub>A<sub>3</sub>C2. pGBK-C1C2 interacted with only two GRINL1A clones (P81 and AAA143) while pGBK-C1P<sub>1</sub>P<sub>2</sub>P<sub>3</sub>C2 interacted with clones C319, P81 and AAA143. None of the GRINL1A clones interacted with pGBK-C0C1, pGBK-C1 and pGBK-C2. Overall, the region of interaction for GRINL1A appeared to be with the cMyBPC motif, irrespective of phosphorylation status, although the extent of interaction varied.

C412 and P62, encoding C-terminus regions of cMyBPC, interacted strongly with all the N-terminus cMyBPC baits. As cMyBPC has the ability to interact with itself, to form the proposed trimeric collar around the thick filament (Moolman-Smook *et al.*, 2002), the interaction of clones C412 and P62 with the cMyBPC baits possibly reflect this ability. Clone P213 did not interact as strongly with the cMyBPC baits and the significance of this variability is unclear. This discrepancy may explained by alterations to the yeast fitness by repeated freeze-thawing cycles and culturing or plasmid load.

#### *Effect of C0-Pro-Ala-region on interactions*

The interactions of COMMD4, ACTC1, cTNI, ACTN2, cTNT, GRINL1A, UACA, GNB2L1 and ENO3 with the C1C2 region were abolished when the interactions were assessed with the C0C2 baits (pGBK-C0C2, pGBK-C0A<sub>1</sub>A<sub>2</sub>A<sub>3</sub>C2, pGBK-C0A<sub>1</sub>P<sub>2</sub>A<sub>3</sub>C2 and pGBK-C0P<sub>1</sub>P<sub>2</sub>P<sub>3</sub>C2). Domain C0 did not interfere with the interactions of PDE4DIP, SYNE1 and cMyBPC with the C1C2 region (Table 3.15).

#### **3.1.4.1 Comparison of putative prey coiled-coil structure to myosin subfragment 2**

A number of preys that were not immediately physiologically plausible interactors of cMyBPC were identified in the four library screens (ACTN2, ENO3, GRINL1A, SYNE1, UACA and GNB2L1). In order to investigate whether these proteins may be similar to the  $\alpha$ -helical coiled-coils of myosin S2, which may help explain these apparent non-specific interaction, the secondary structures of these proteins were investigated for coiled-coil secondary structures. All of these preys except ENO3 and GNB2L1 have coiled-coil regions. These preys were then compared to myosin S2, to establish whether such a similarity could explain the C1C2 region's affinity for them.

Since the three-dimensional structures of these putative preys had not yet been solved, a sequence analysis approach was used to compare the preys to myosin S2 (Section 2.6.2). GRINL1A (z-score 4.35; confidence 95%), UACA (z-score 5.02; confidence 95%) and ACTN2 (z-score 8.41; confidence 99%) were homologous to myosin S2, while this was not the case for the other putative preys. Additionally, SYNE1 has homology to the rod domain of ACTN2 (z-score 7.13; confidence 99%). Although, of these myosin S2-similar preys, only

ACTN2 interacted with C1C2 in a manner analogous to myosin S2, the homology to myosin S2 may explain the interaction of these preys with the C1C2 cMyBPC region. Thus, based on these findings the interactions of UACA, GRINL1A, ACTN2 and SYNE1 with cMyBPC were not investigated any further.

### 3.2 CO-IMMUNOPRECIPITATION

Since it is possible for the GAL4 domains to autonomously activate transcription of reporter genes, it was necessary to verify bait-prey interactions in the absence of these domains. Thus, the prioritised ligands for the various C1C2 baits were *in vitro* co-immunoprecipitated with the cMyBPC baits (C0C2, C0A<sub>1</sub>A<sub>2</sub>A<sub>3</sub>C2, C0A<sub>1</sub>P<sub>2</sub>A<sub>3</sub>C3, C0P<sub>1</sub>P<sub>2</sub>P<sub>3</sub>C2, C1C2, C1A<sub>1</sub>A<sub>2</sub>A<sub>3</sub>C2, C1A<sub>1</sub>P<sub>2</sub>A<sub>3</sub>C3, C1P<sub>1</sub>P<sub>2</sub>P<sub>3</sub>C2), using peptides fused only to cMyc- (bait) or HA-tags (preys), but lacking GAL4 domains (Figures 3.3-15). The *in silico* predicted sizes of the baits and preys, in addition to the actual size of the fusion proteins, as observed on a 15% SDS-PAGE gel (Figure 3.2), are shown in Table 3.16.

Of the eight proteins assessed for interactions with the various cMyBPC baits, three demonstrated clear interactions. HSPB7 (Figure 3.3), PDE4DIP (Figure 3.4), ACTC1 (Figure 3.5) showed interaction both with C0C2 phosphorylation-mimics (pGBK-C0C2, pGBK-C0A<sub>1</sub>A<sub>2</sub>A<sub>3</sub>C2, pGBK-C0A<sub>1</sub>P<sub>2</sub>A<sub>3</sub>C2 and pGBK-C0P<sub>1</sub>P<sub>2</sub>P<sub>3</sub>C2) and C1C2 phosphorylation-mimics (pGBK-C1C2, pGBK-C1A<sub>1</sub>A<sub>2</sub>A<sub>3</sub>C2, pGBK-C1A<sub>1</sub>P<sub>2</sub>A<sub>3</sub>C2 and pGBK-C1P<sub>1</sub>P<sub>2</sub>P<sub>3</sub>C2).

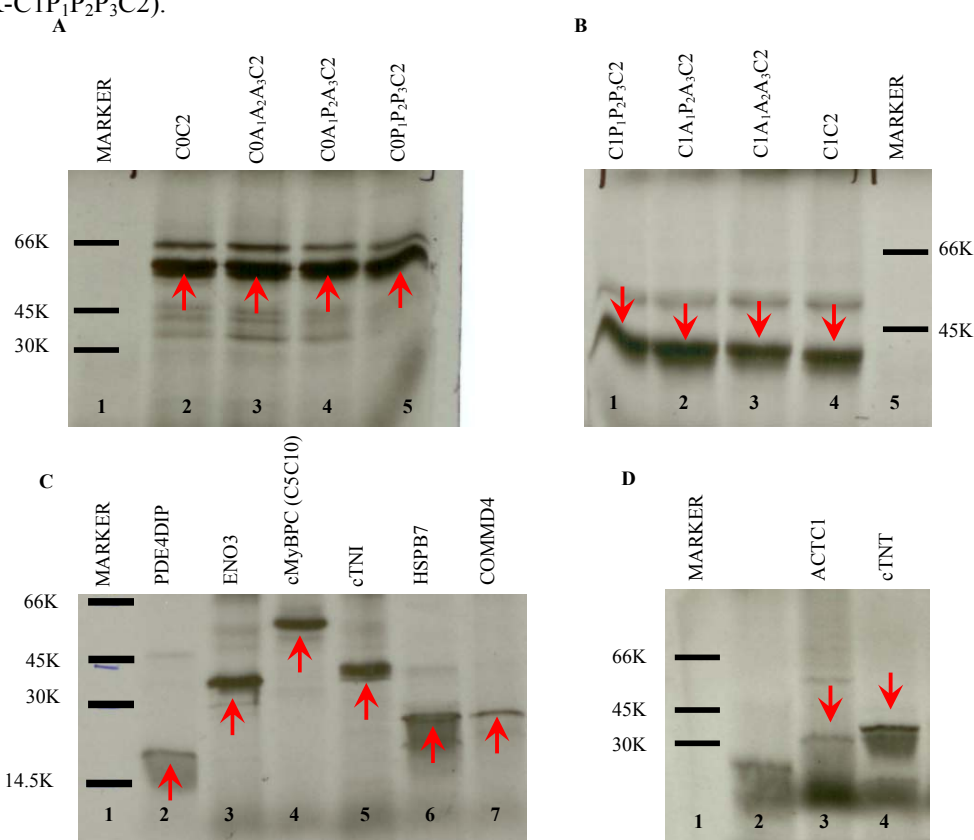


**Figure 3.2.** Autoradiograph of radioactive-labelled proteins from coupled *in vitro* transcription-translation reactions (15% SDS-PAGE gel). A and B show translated bait-mimics of C0C2 and C1C2 representing various phosphorylation states of the cMyBPC motif. C and D show translated prey proteins. Lanes A1, B6, C1 and D1 show the positions of the non-radioactive High-Range Rainbow™ molecular weight marker bands, as transferred from the dried polyacrylamide gel. The red arrow indicates the band of interest. Lane D2 shows the translation of protein not used in the present study.

**Table 3.16.** Predicted molecular weights and approximate molecular weights of fusion proteins used in the co-immunoprecipitation analysis.

Cloned insert	No of predicted amino acids	Predicted size (kDa)	Antibody tag and linker (kDa)	Size by electrophoresis* (kDa)
Myc-C0C2	460	49.6	1.4	~50
Myc-C0A <sub>1</sub> A <sub>2</sub> A <sub>3</sub> C2	460	49.6	1.4	~50
Myc-C0A <sub>1</sub> P <sub>2</sub> A <sub>3</sub> C2	460	49.6	1.4	~50
Myc-C0P <sub>1</sub> P <sub>2</sub> P <sub>3</sub> C2	460	49.6	1.4	~50
Myc-C1C2	308	34.3	1.4	~40
Myc-C1A <sub>1</sub> A <sub>2</sub> A <sub>3</sub> C2	308	34.3	1.4	~40
Myc-C1A <sub>1</sub> P <sub>2</sub> A <sub>3</sub> C2	308	34.3	1.4	~40
Myc-C1P <sub>1</sub> P <sub>2</sub> P <sub>3</sub> C2	308	34.3	1.4	~40
HA-HSPB7 (C212)	189	20.8	2.3	~25
HA-PDE4DIP (P205)	173	20.6	2.3	~20
HA-ACTC1 (P267)	245	27.2	2.3	~30
HA-COMMD4 (APA491)	199	21.7	2.3	~25
HA-cTNT (AAA3)	258	29.7	2.3	~35
HA-ENO3(APA163)	364	39.3	2.3	~42
HA-cTNI(C312)	244	27.2	2.3	~40
HA-cMyBPC (C412; C5C10)	513	57.4	2.3	~60

\* Size by electrophoresis was determined on a 15% SDS-PAGE mini gel. The prey clone used for Co-IP is indicated within brackets.

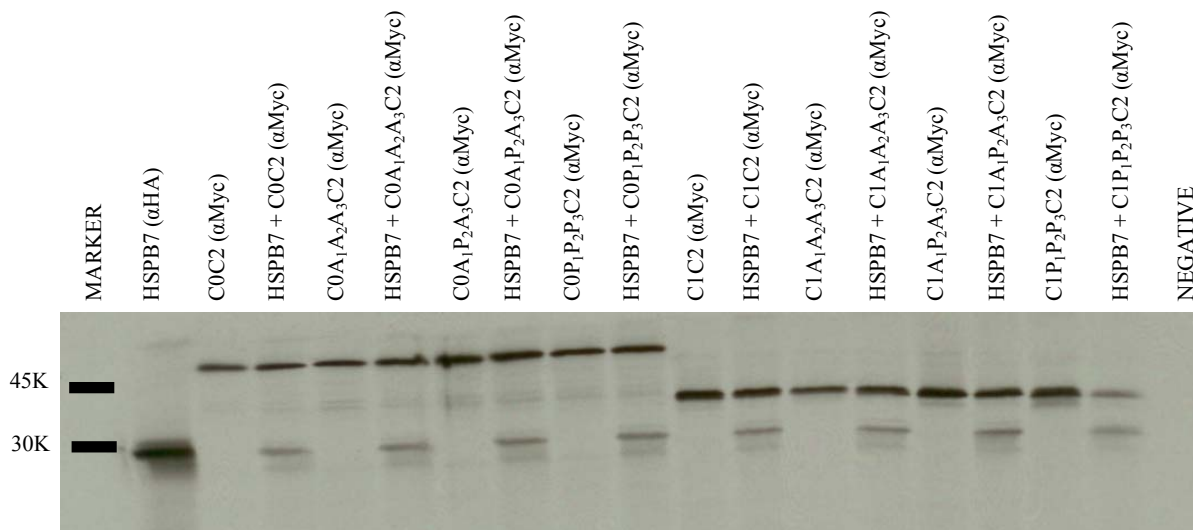


**Figure 3.3.** Autoradiograph of 20% SDS-PAGE gel showing the Co-IP of C0C2 and C1C2 cMyBPC phosphorylation-mimics with HSPB7 protein. The antibody used for immunoprecipitation is indicated within brackets. Two bands in each Co-IP lane in conjunction with a clear negative control lane suggests that HSPB7 interacted with the bait phosphorylation mimic.

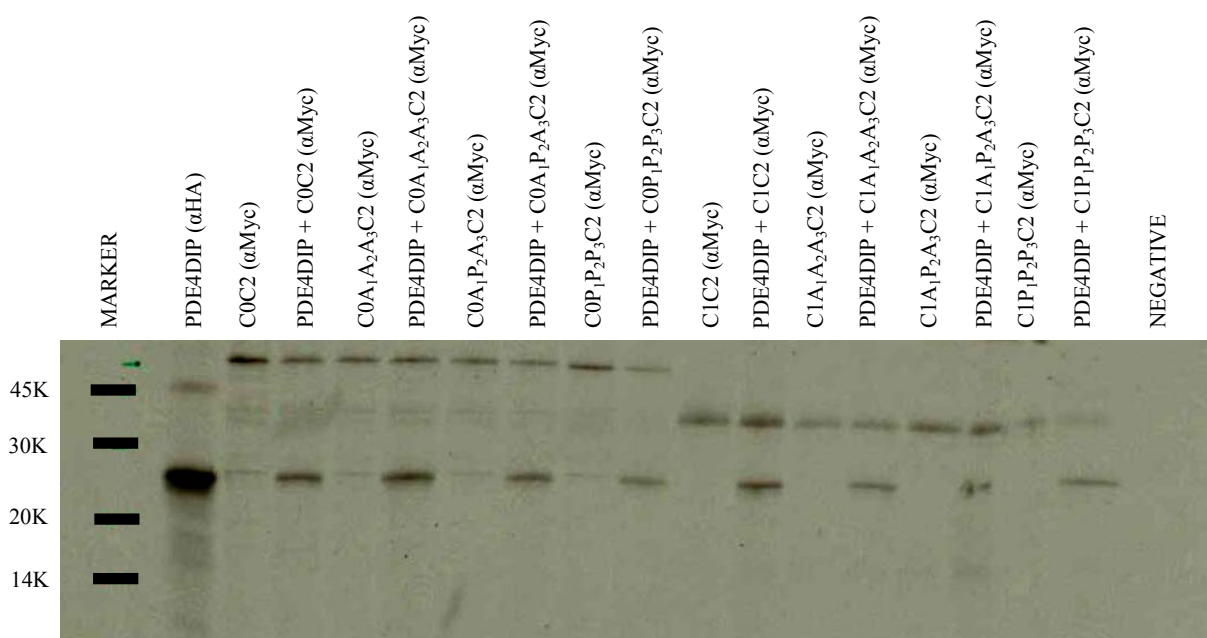


**Figure 3.4.** Autoradiograph of 20% SDS-PAGE gel showing the Co-IP of C0C2 and C1C2 cMyBPC phosphorylation-mimics with PDE4DIP protein. The antibody used for immunoprecipitation is indicated within brackets. Two bands in each Co-IP lane in conjunction with a clear negative control lane suggests that PDE4DIP interacted with the bait phosphorylation mimic.

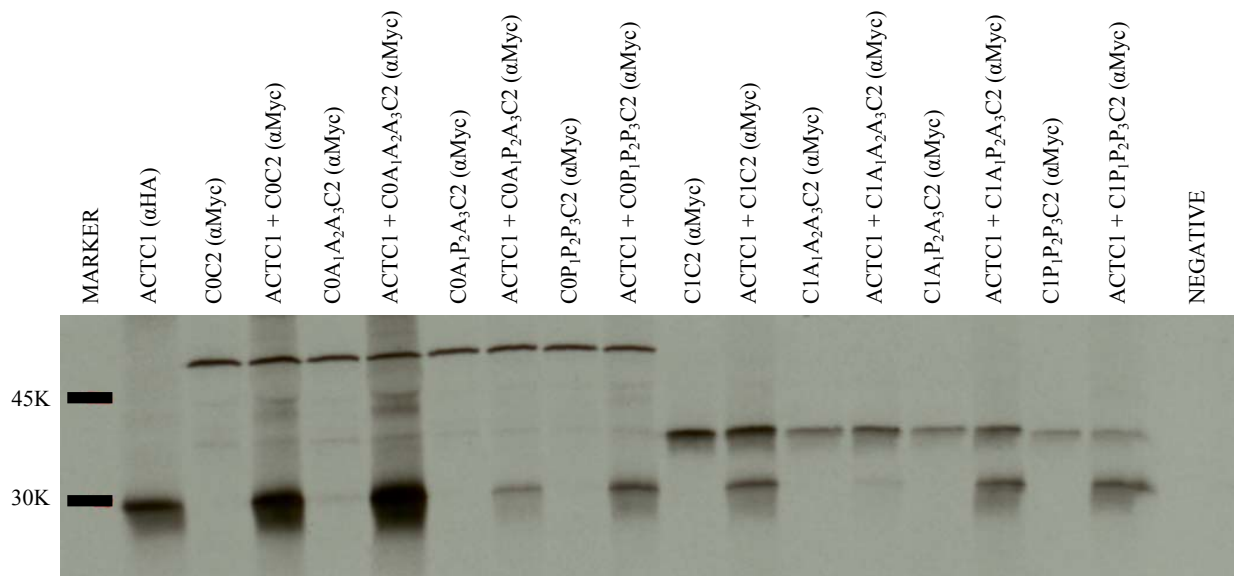


**Figure 3.5.** Autoradiograph of 17.5% SDS-PAGE gel showing the Co-IP of C0C2 and C1C2 cMyBPC phosphorylation-mimics with ACTC1 protein. The antibody used for immunoprecipitation is indicated within brackets. Two bands in each Co-IP lane in conjunction with a clear negative control lane suggests that ACTC1 interacted with the bait phosphorylation mimic.

The negative control reaction for five Co-IP analyses were somewhat confounded by the prey proteins' non-specific interaction with the protein G agarose. Densitometer analysis of these negative control lanes on the relevant autoradiographs was used to quantify the contaminating prey protein, and this value was subtracted from each prey band in the Co-IP lanes as a background contribution to band intensity (Figure 3.6, 3.8, 3.10, 3.12, and 3.14).

Since the amount of prey protein pulled down in the Co-IP interaction lanes was less than that in the negative control lane for COMMD4 (Figure 3.6-7) and cTNT (Figure 3.8-9), these interactions could be considered as negative, as assessed by Co-IP. For the ENO3 (Figure 3.10-11) and cTNI (Figure 3.12-13) interactions, only the C0C2 Co-IP's could be assessed, since the densitometer software could not resolve the C1C2 Co-IP bait-prey bands which were not well separated on the gel, despite using up to 20% (0.5mm thickness) vertical PAGE gels. For these two proteins (ENO3 and cTNI), little prey protein was calculated to be pulled down by the C0C2 baits (after subtraction of the background) and it could be considered that these proteins interact very weakly with C0C2, in a Co-IP setting. When the background was subtracted from the cMyBPC (C5C10):cMyBPC (C1C2 and C0C2) interactions (Figure 3.14-15), evidence for interaction was seen for all baits.



**Figure 3.6.** Autoradiograph of 17.5% SDS-PAGE gel showing the Co-IP of C0C2 and C1C2 phosphorylation-mimics with COMMD4 protein. The antibody used for immunoprecipitation is indicated within brackets.

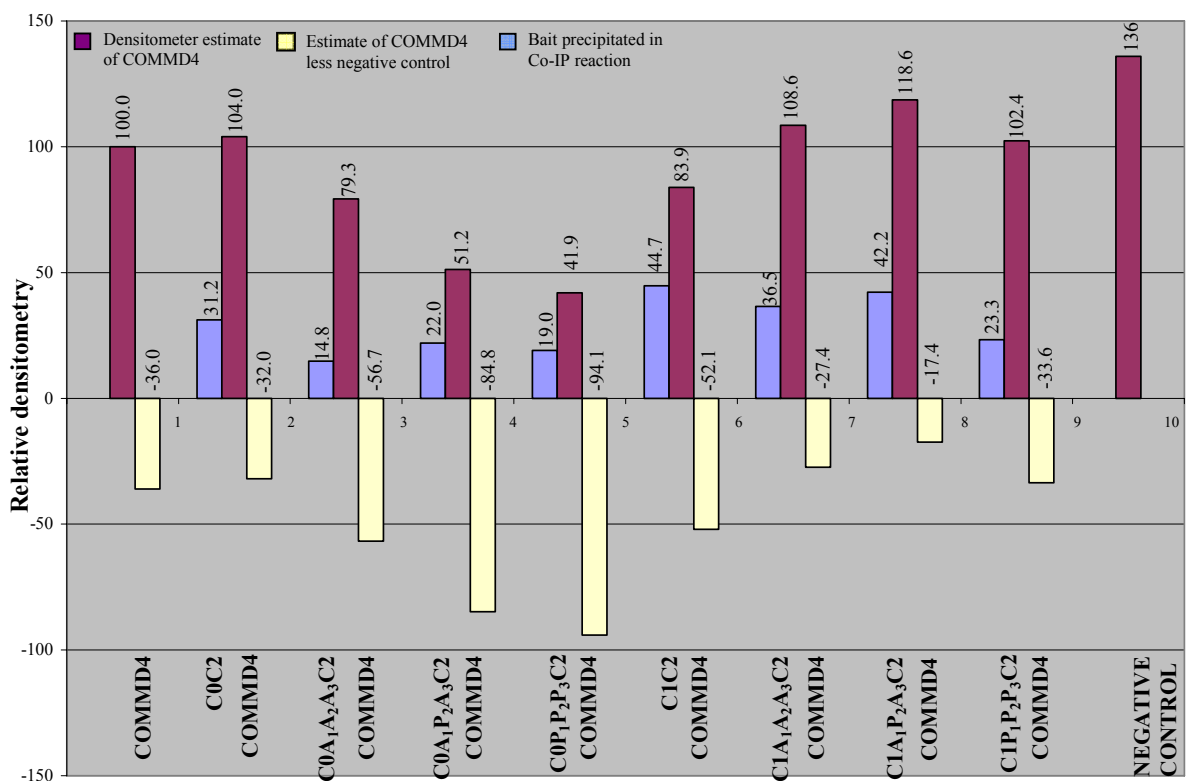


**Figure 3.7.** Densitometer estimate of COMMD4 precipitated in the Co-IP lanes only. The yellow bar in lanes 2-9 shows that the amount of COMMD4 precipitated after the negative control (lane 10) has been subtracted is less than the negative control and therefore COMMD4 does not precipitate with the C0C2 and C1C2 baits, respectively. The estimate amount of each protein is indicated above the bars.

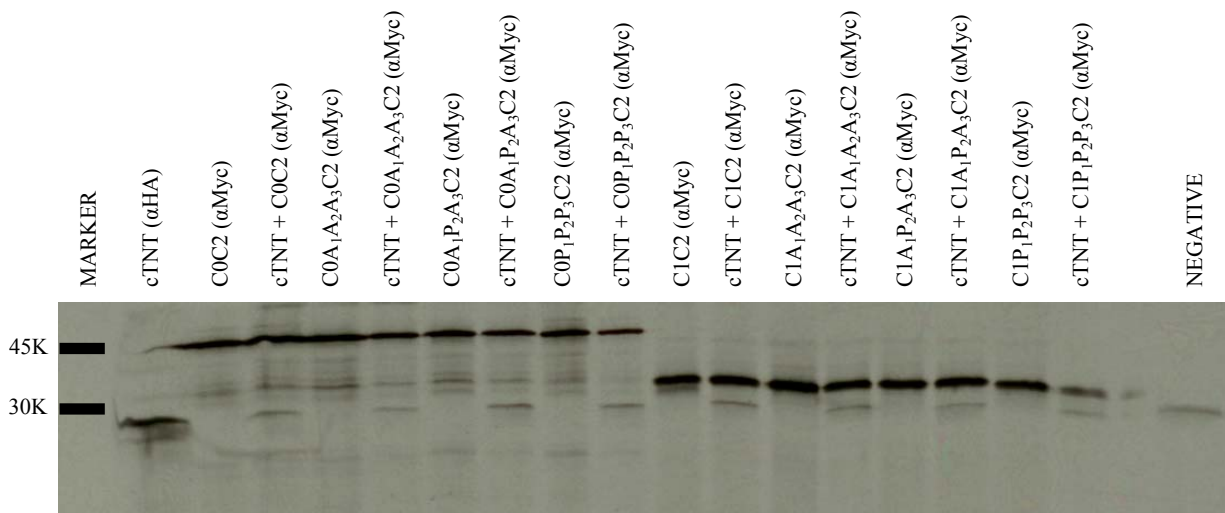


**Figure 3.8.** Autoradiograph of 20% SDS-PAGE gel showing the Co-IP of C0C2 and C1C2 phosphorylation-mimics with cTNT protein. The antibody used for immunoprecipitation is indicated within brackets.

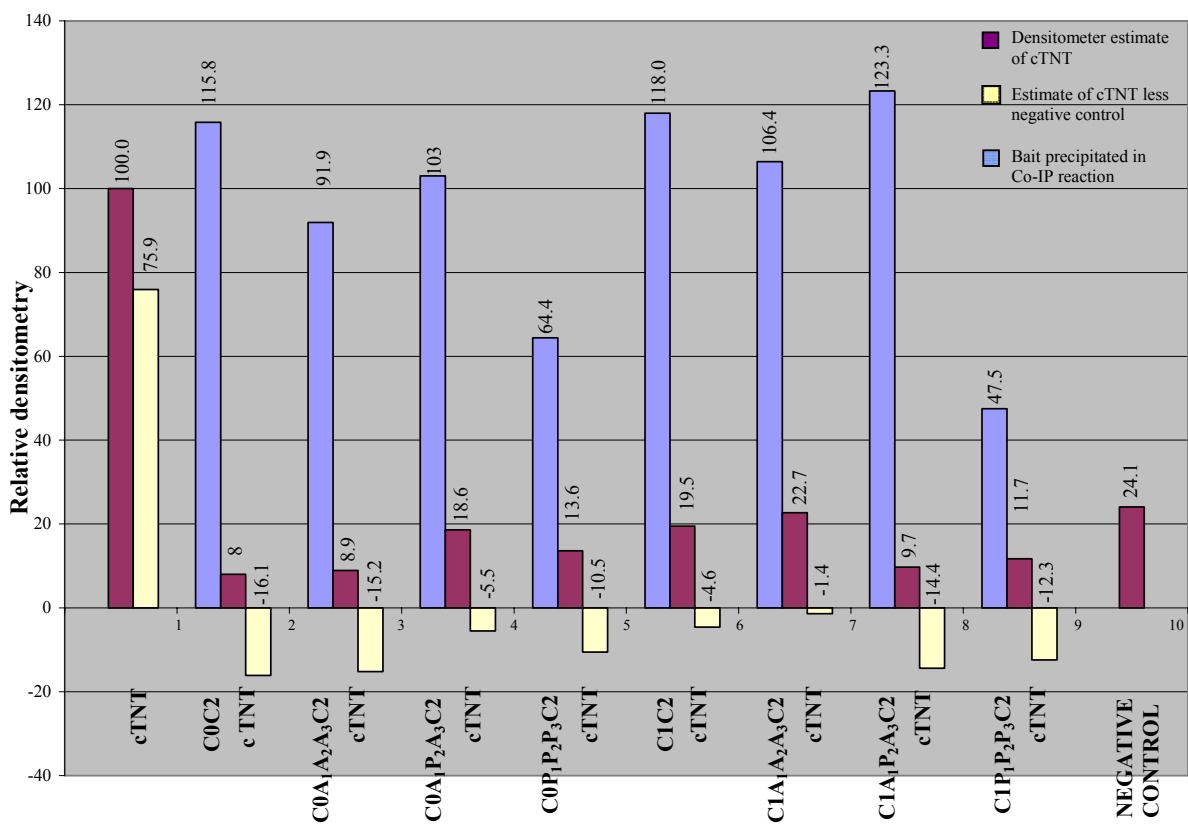


**Figure 3.9.** Densitometer estimate of cTNT precipitated in the Co-IP lanes only. The yellow bar in lanes 2-9 shows that the amount of cTNT precipitated after the negative control (lane 10) has been subtracted is less than the negative control and therefore cTNT does not precipitate with the C0C2 and C1C2 baits, respectively. The estimate amount of each protein is indicated above the bars.

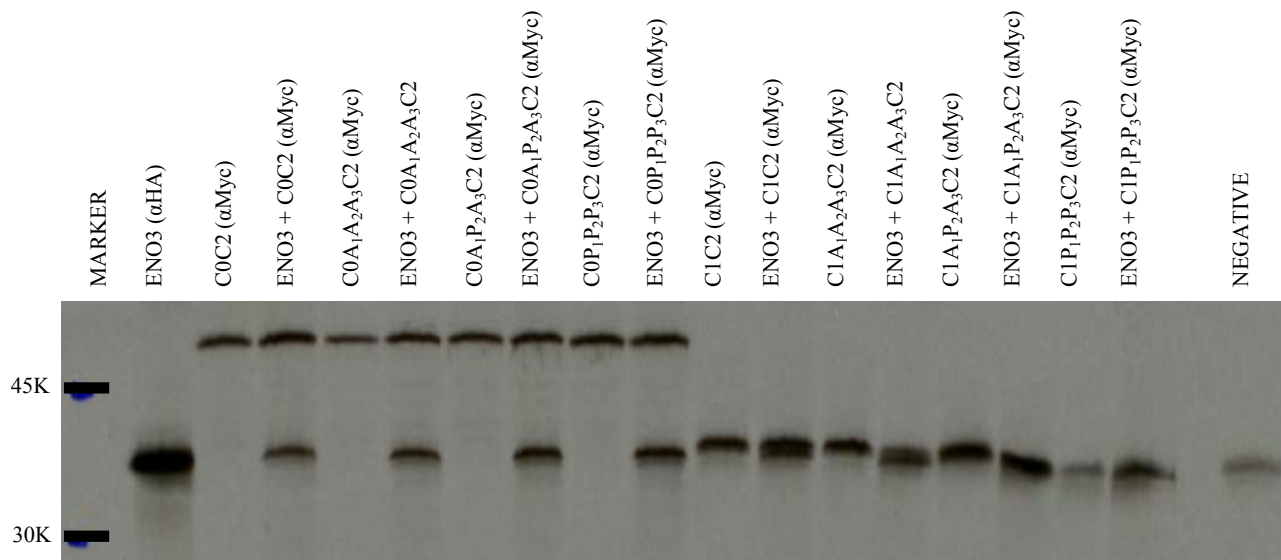


**Figure 3.10.** Autoradiograph of 20% SDS-PAGE gel showing the Co-IP of C0C2 and C1C2 phosphorylation-mimics with ENO3 protein. The antibody used for immunoprecipitation is indicated within brackets.

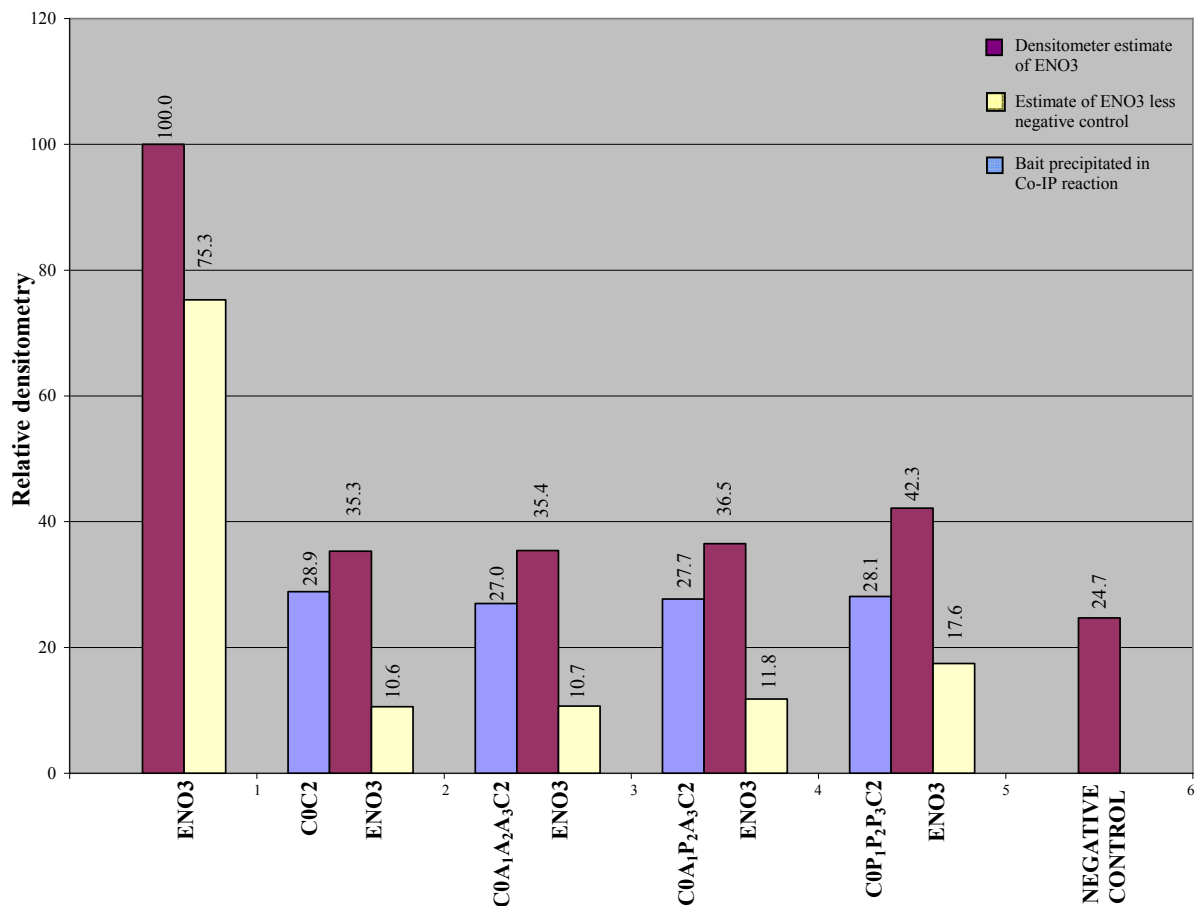


**Figure 3.11.** Densitometer estimate of ENO3 precipitated in the Co-IP lanes only. The yellow bar in lanes 2-9 shows that the amount of ENO3 precipitated after the negative control (lane 10) has been subtracted is more than the negative control and therefore ENO3 precipitates with the C0C2 baits. Estimate values for the ENO3+C1C2 baits could not be determined as the bands separated too close together. The estimate amount of each protein is indicated above the bars.

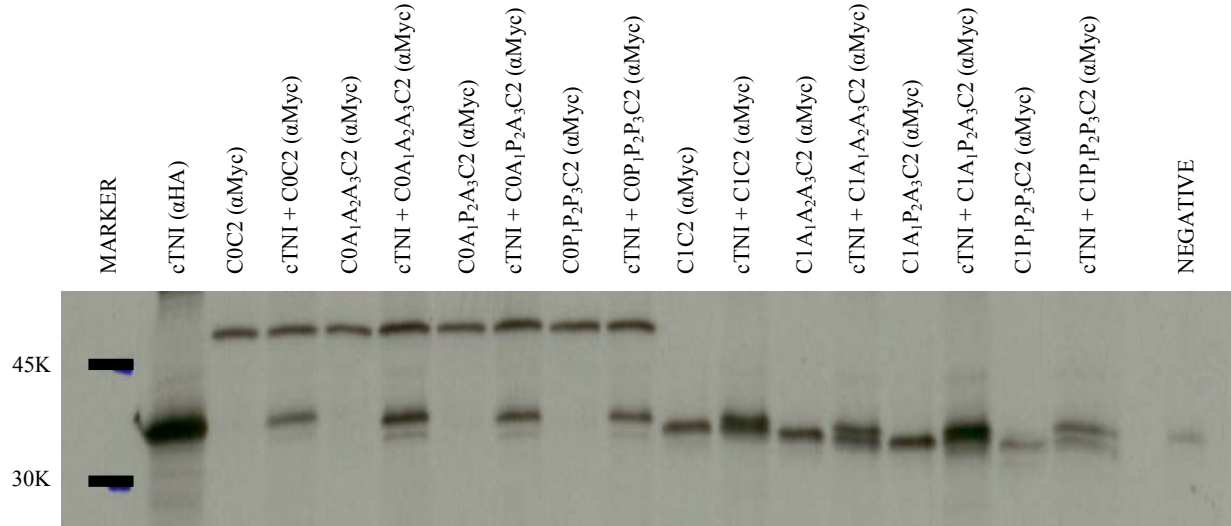


**Figure 3.12.** Autoradiograph of 20% SDS-PAGE gel showing the Co-IP of C0C2 and C1C2 phosphorylation-mimics with cTNI protein. The antibody used for immunoprecipitation is indicated within brackets.

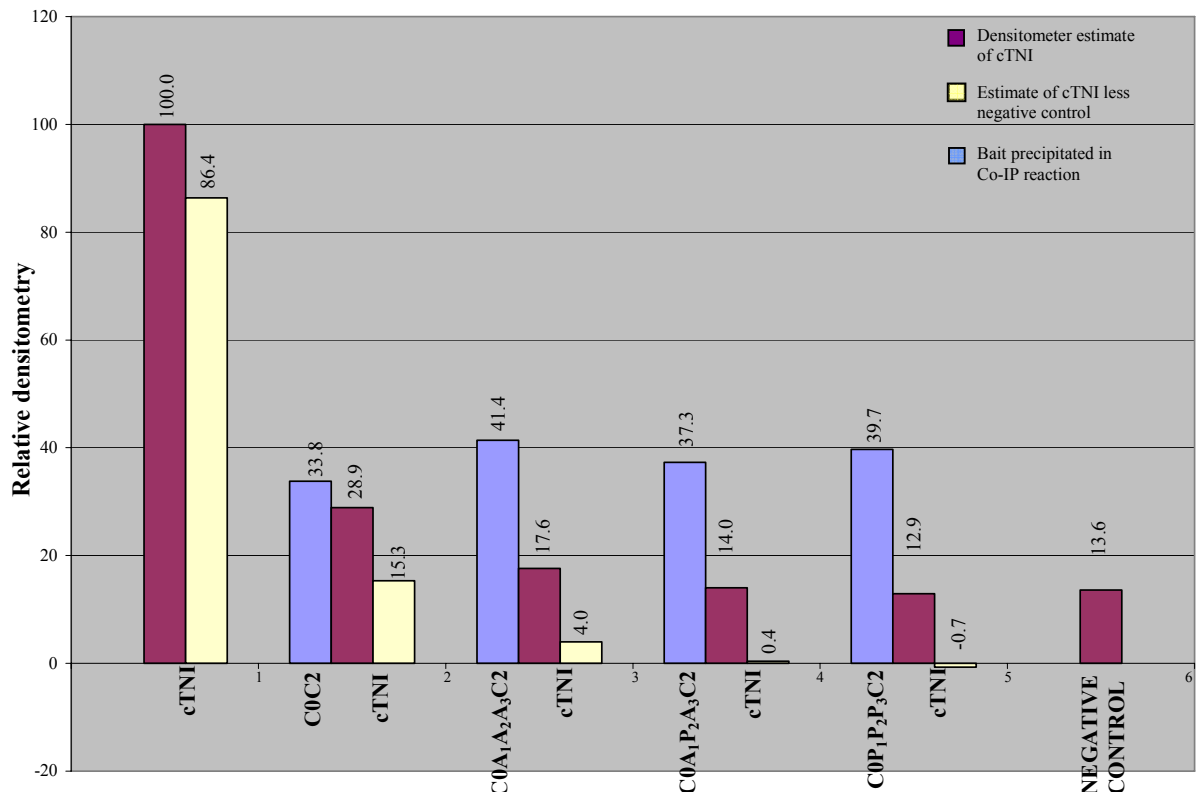


**Figure 3.13.** Densitometer estimate of cTNI precipitated in the Co-IP lanes only. The yellow bar in lanes 2-9 shows that the amount of cTNI precipitated after the negative control (lane 10) has been subtracted is more than the negative control and therefore cTNI precipitates with the C0C2 baits (except the C0P<sub>1</sub>P<sub>2</sub>P<sub>3</sub>C2+cTNI interaction). Estimate values for the cTNI+C1C2 baits could not be determined as the bands separated too close together. The estimate amount of each protein is indicated above the bars.



**Figure 3.14.** Autoradiograph of 20% SDS-PAGE gel showing the Co-IP of C0C2 and C1C2 phosphorylation-mimics with cMyBPC (C5C10) protein. The antibody used for immunoprecipitation is indicated within brackets.

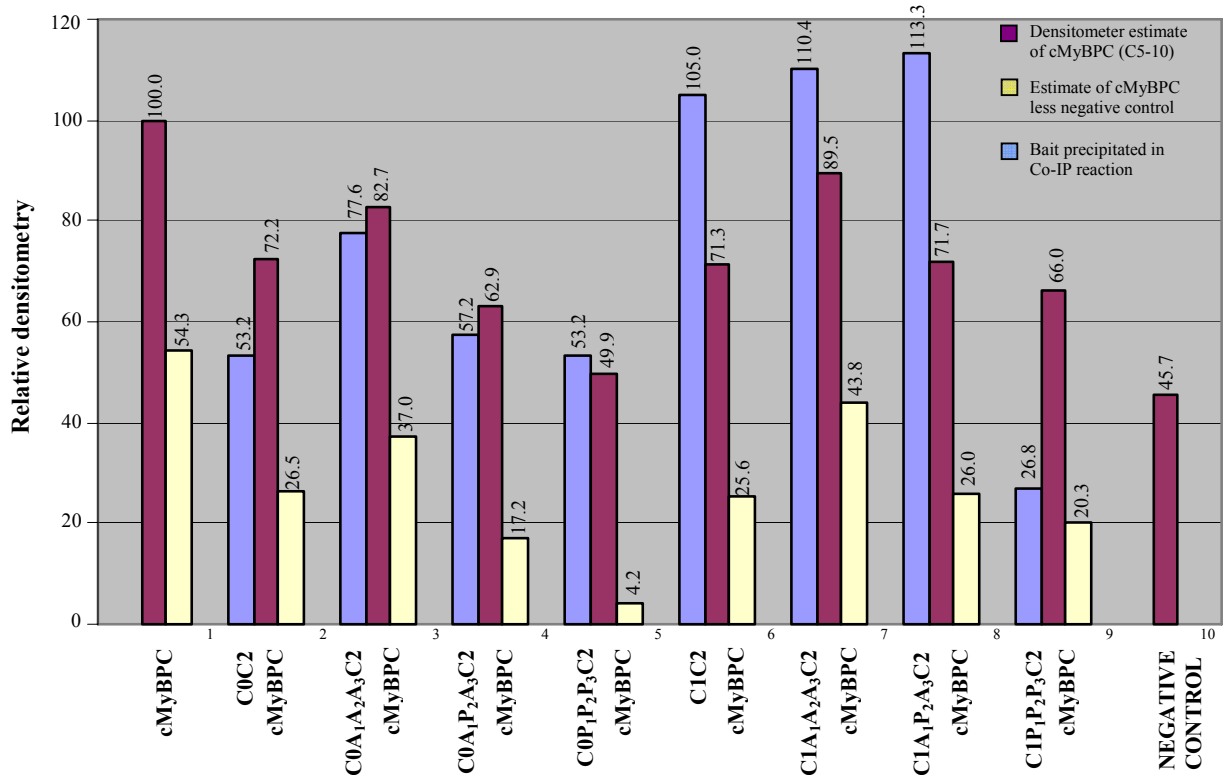


**Figure 3.15.** Densitometer estimate of cMyBPC (C5-10) precipitated in the Co-IP lanes only. The yellow bar in lanes 2-9 shows that the amount of cMyBPC (C5-10) precipitated after the negative control (lane 10) has been subtracted is more than the negative control and therefore cMyBPC (C5-10) precipitates with the C0C2 and C1C2 baits, respectively. The estimate amount of each protein is indicated above the bars.

### 3.3 THREE-DIMENSIONAL IN VIVO CO-LOCALISATION USING FLUORESCENCE MICROSCOPY

*In vivo* co-localisation using fluorescence microscopy was employed to assess the interaction of cMyBPC with PDE4DIP, COMMD4, HSPB7 and ENO3, respectively. By this technique, cMyBPC was shown to exist in the same 3D subcellular space as COMMD4 (Figure 3.16), PDE4DIP (Figure 3.17), HSPB7 (Figure 3.18), and ENO3 (Figure 3.19), respectively. The panels of images presented represent a single frame of the 25 images that were captured for the Z-stack. In all these figures, images A-C shows a single colour channel, while image D shows an overlay of the four colour channels used. To improve contrast for the overlayed images of cMyBPC:COMMD4 and cMyBPC:PDE4DIP, the YFP expression was artificially coloured red instead of yellow.

In all samples cMyBPC-GFP showed cytoplasmic expression, which was stronger and more diffuse compared to that of either of the RFP-tagged proteins (ENO3 and HSPB7), which had a more punctate expression pattern. The expression of the YFP-tagged proteins (COMMD4 and PDE4DIP) was diffuse, although PDE4DIP also demonstrated distinct areas of punctate cytoplasmic expression. The area of co-localisation (3.16-19 Image C) as determined from the Z-stack analysis was also punctate; the exception to this was PDE4DIP:cMyBPC co-localisation, which was somewhat more wide spread. None of the proteins investigated in this study showed any nuclear expression.

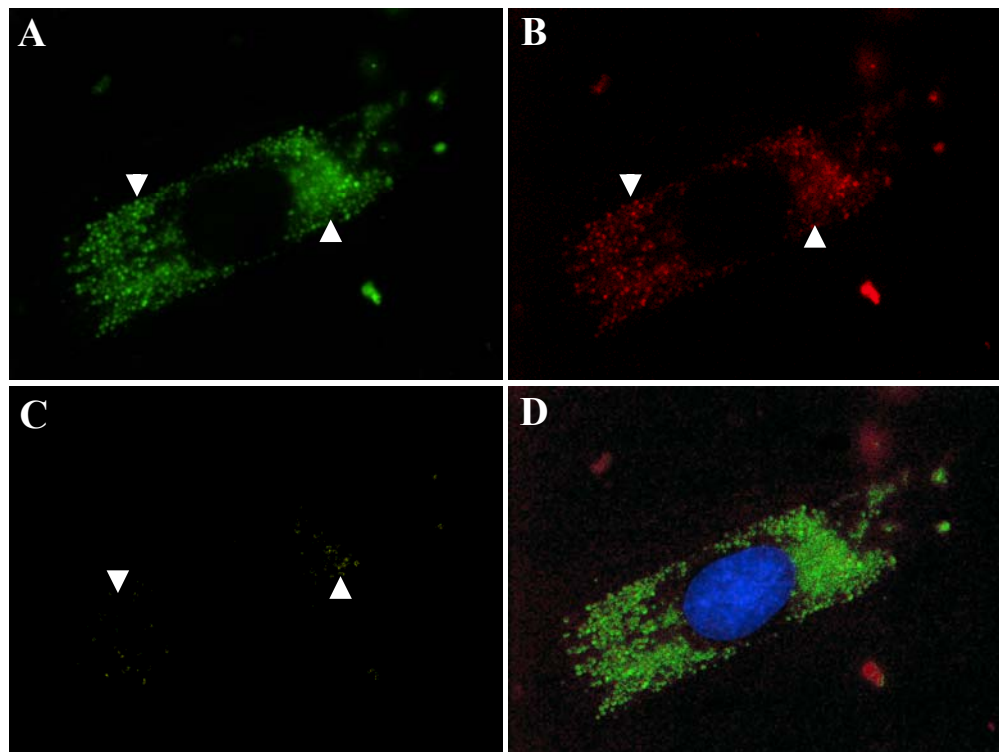


**Figure 3.16.** Live cell fluorescence imaging of COMMD4 and cMyBPC co-localisation in differentiated H9C2 cardiac myocytes. (A) GFP-tagged C1C10 cMyBPC (green). (B) YFP-tagged COMMD4 (red). (C) Co-localisation of COMMD4 and C1C10 cMyBPC generated from Z-stack (yellow). (D) Overlay of images A-C with Hoechst H-33342 labelling of the nuclei (blue). Magnification: 60X oil immersion before 70% reduction.

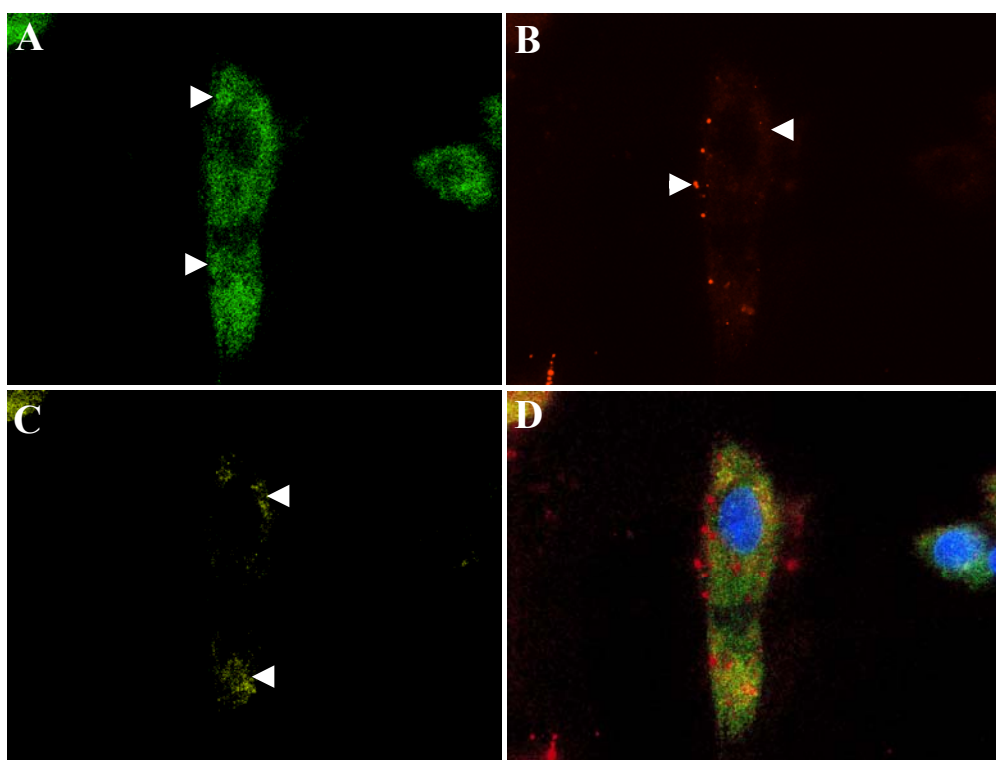


**Figure 3.17.** Live cell fluorescence imaging of PDE4DIP and cMyBPC co-localisation in differentiated H9C2 cardiac myocytes. (A) GFP-tagged C1C10 cMyBPC (green). (B) YFP-tagged PDE4DIP (red). (C) Co-localisation of PDE4DIP and C1C10 cMyBPC generated from Z-stack (yellow). (D) Overlay of images A-C with Hoechst H-33342 labelling of the nuclei (blue). Magnification: 60X oil immersion before 70% reduction.

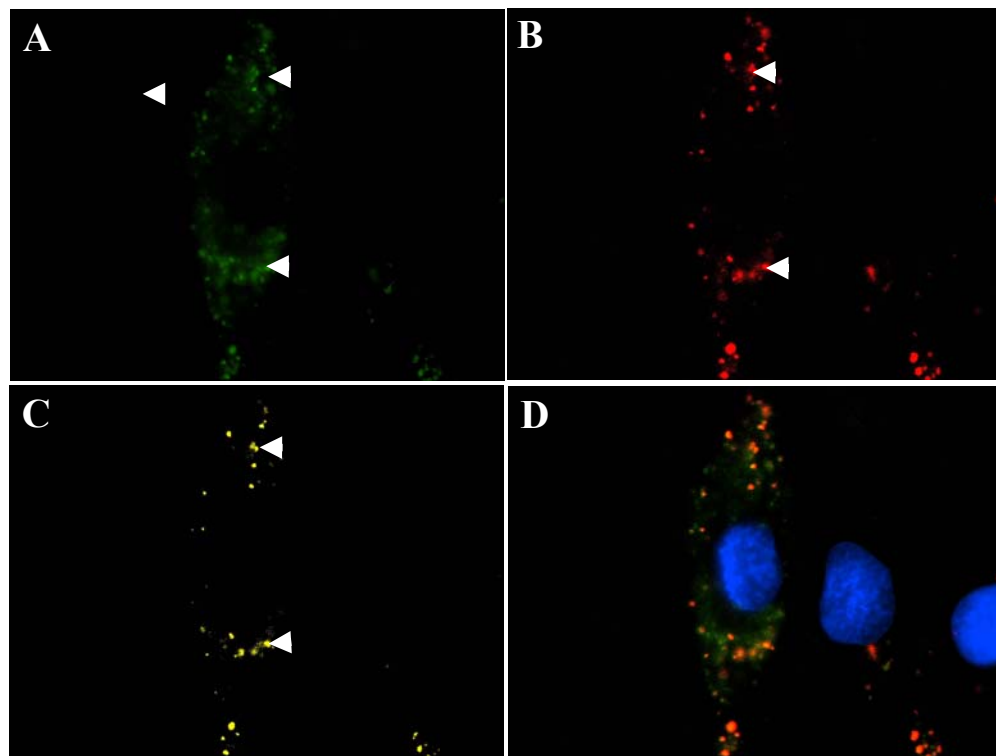


**Figure 3.18.** Live cell fluorescence imaging of HSPB7 and cMyBPC co-localisation in differentiated H9C2 cardiac myocytes. (A) GFP-tagged C1C10 cMyBPC (green). (B) RFP-tagged HSPB7 (red). (C) Co-localisation of HSPB7 and C1C10 cMyBPC generated from Z-stack (yellow). (D) Overlay of images A-C with Hoechst H-33342 labelling of the nuclei (blue). Magnification: 60X oil immersion before 70% reduction.

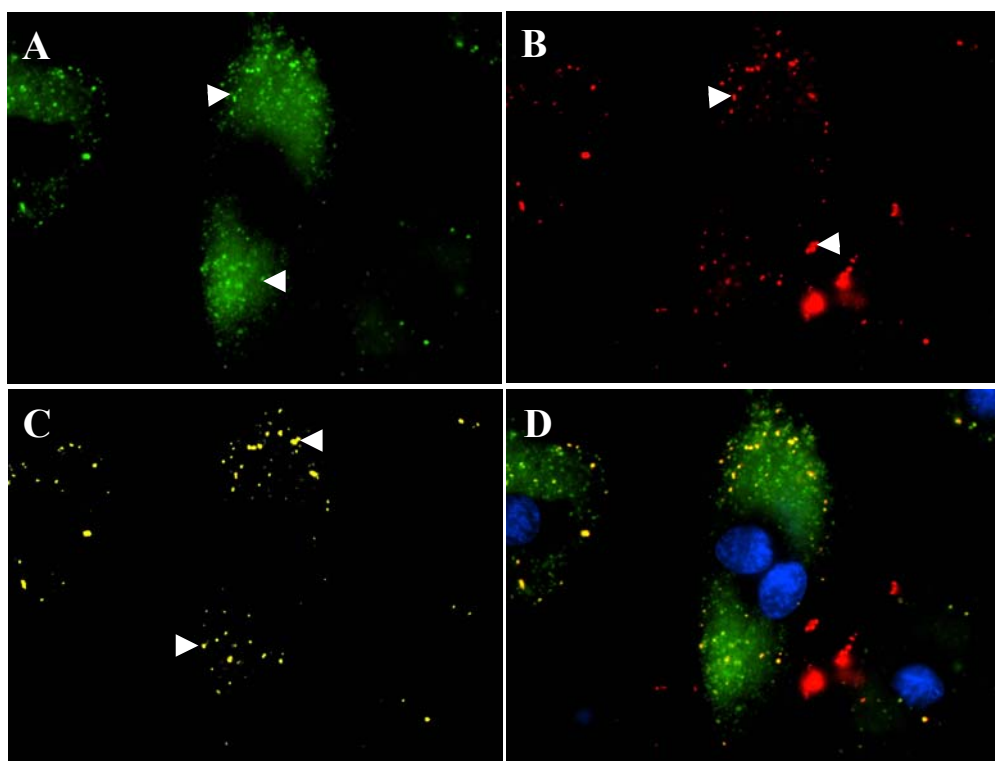


**Figure 3.19.** Live cell fluorescence imaging of ENO3 and cMyBPC co-localisation in differentiated H9C2 cardiac myocytes. (A) GFP-tagged C1C10 cMyBPC (green). (B) RFP-tagged ENO3 (red). (C) Co-localisation of ENO3 and C1C10 cMyBPC generated from Z-stack (yellow). (D) Overlay of images A-C with Hoechst H-33342 labelling of the nuclei (blue). Magnification: 60X oil immersion before 70% reduction.

### 3.4 BIOLUMINESCENCE RESONANCE ENERGY TRANSFER ASSAY (BRET)

BRET assays were employed to assess the interactions of cMyBPC with cTNI and ACTC1 in live cells. These interactions could not be assessed by *in vivo* co-localisation as thick and thin filaments are known to overlap in the sarcomere and data from co-localisation would not provide any additional information. In addition, the proposed interaction of domains C2, C3 with C10 (Section 1.9.3.5.6.1) were also examined using this assay, and interaction of domain C7 and C10 was chosen as a control in the latter assay. Due to time constraints, and as the Co-IP results of cTNT and cMyBPC (C5C10) were not positive, the verification of these putative interactions were not investigated in the present study, but will be included in future studies.

For each bait:prey interaction to be assessed, BRET assays were performed under two different conditions, viz. the first to test bait:prey interaction with cMyBPC in its native state and the second assay to test the interaction of the prey with cMyBPC when it is trisphosphorylated, mediated by CamK-II and PKA after cells had been stimulated with calcium and isoproterenol (McClellan *et al.*, 2001). Following the calculation of the BRET ratio for each bait:prey interaction in differentiated H9C2 cells, it was compared to its own controls (bait control [particular bait co-transfected with the empty GFP<sup>2</sup>-C3 vector] and prey controls [particular prey co-transfected with the empty pRLuc-C1 vector]) and to the transfection control. A positive

BRET interaction was inferred if the BRET ratio was significantly higher than the controls, as determined by ANOVA and post-hoc Bonferroni multiple comparison tests.

### 3.4.1 C1C10 cMyBPC versus cTNI

An interaction between C1C10 cMyBPC and cTNI in unstimulated H9C2 cells (cMyBPC in native conformation) was suggested by an increase in the BRET ratio of the cMyBPC/cTNI co-transfected cells over all controls (Figure 3.20 A). However, the mean standard deviation for the combined experiments was large and thus the difference between the BRET ratio for the C1C10 cMyBPC/cTNI interaction compared to the controls (C1C10 control, cTNI control and transfection control, respectively) did not reach statistical significance at the  $p<0.05$  level.

Under  $\text{Ca}^{2+}$  and isoproterenol stimulation, the BRET ratio for all samples were reduced, and the C1C10 cMyBPC/cTNI ratio was dampened to a level comparable to the controls (Figure 3.20 B), suggesting that the interaction between C1C10 cMyBPC and cTNI was abrogated. The difference in the BRET ratio for C1C10 cMyBPC/cTNI in unstimulated cells was not statistically different when compared to the BRET ratio for the C1C10 cMyBPC/cTNI interaction in stimulated cells. Bonferroni matrices are appended (Appendix VII).

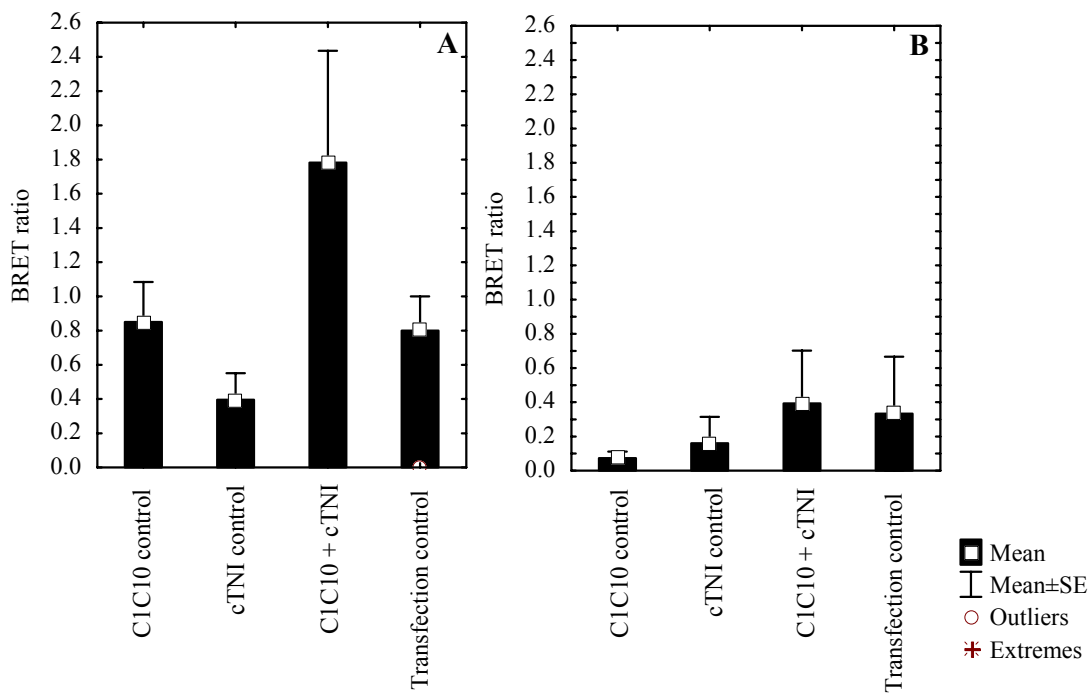


**Figure 3.20.** Bar graph of BRET values determined from differentiated H9C2 cardiac myocytes co-transfected with cTNI-GFP and C1C10 cMyBPC-Rluc, and respective controls. Values represent means  $\pm$ S.E for five independent transfections. Experiments were performed in duplicate and statistical comparisons were carried out using a one-way analysis of variance (ANOVA) followed by Bonferroni's multiple comparison post-test, comparing all pairs. Graph A shows the respective interactions in unstimulated cells while graph B shows the same interactions in cells stimulated for maximal cMyBPC phosphorylation. There were no statistically significant differences between the C1C10 cMyBPC/cTNI pair and either the C1C10 cMyBPC control or the cTNI control in either stimulated or unstimulated cells, respectively.

### 3.4.2 C1C10 cMyBPC versus ACTC1

In unstimulated H9C2 cells (cMyBPC in its native conformation) there appeared to be an interaction between C1C10 cMyBPC and ACTC1 (Figure 3.21 A). This interaction was not statistically significant when compared to the controls, due to the large mean standard deviation. In cells stimulated for maximal cMyBPC phosphorylation this interaction appeared to be abolished (Figure 3.21 B), as the BRET ratio was decreased when compared to the BRET ratio of the C1C10 cMyBPC/ACTC1 interaction in unstimulated cells (Bonferroni matrices in Appendix VII).

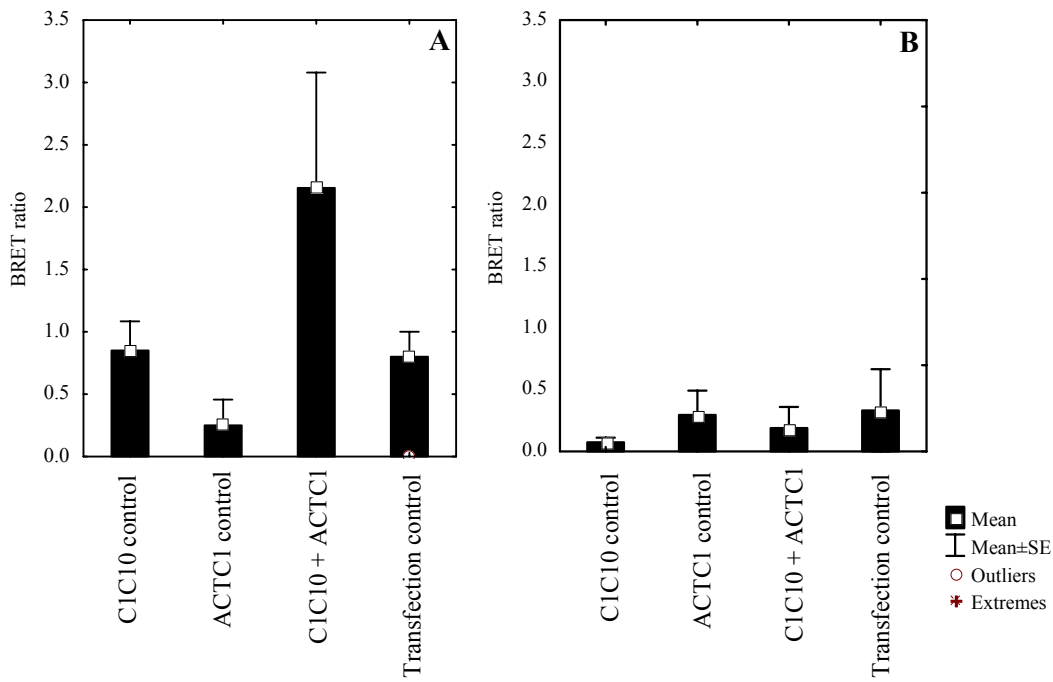


**Figure 3.21.** Bar graph of BRET values determined from differentiated H9C2 cardiac myocytes co-transfected with ACTC1-GFP and C1C10 cMyBPC-Rluc, and respective controls. Values represent means  $\pm$ S.E for five independent transfections. Experiments were performed in duplicate and statistical comparisons were carried out using a one-way analysis of variance (ANOVA) followed by Bonferroni's multiple comparison post-test, comparing all pairs. Graph A shows the respective interactions in unstimulated cells while graph B shows the same interactions in cells stimulated for maximal cMyBPC phosphorylation. There were no statistically significant differences between the C1C10 cMyBPC/ACTC1 pair and either the C1C10 cMyBPC control or the ACTC1 control in either stimulated or unstimulated cells, respectively.

### 3.4.2 C2C10 cMyBPC versus cTNI

Although the BRET ratio for the C2C10 cMyBPC/cTNI interaction and the respective controls was not significantly different (Figure 3.22 A), an interaction between C2C10 cMyBPC and cTNI was suggested. As only two independent experiments were performed the mean standard deviation for the combined experiments was large. When the cells were stimulated for maximal cMyBPC phosphorylation, there was a decrease in the BRET ratio for the C2C10 cMyBPC/cTNI interaction (Figure 3.22 B) when compared to the unstimulated cells (Bonferroni matrices in Appendix VII).

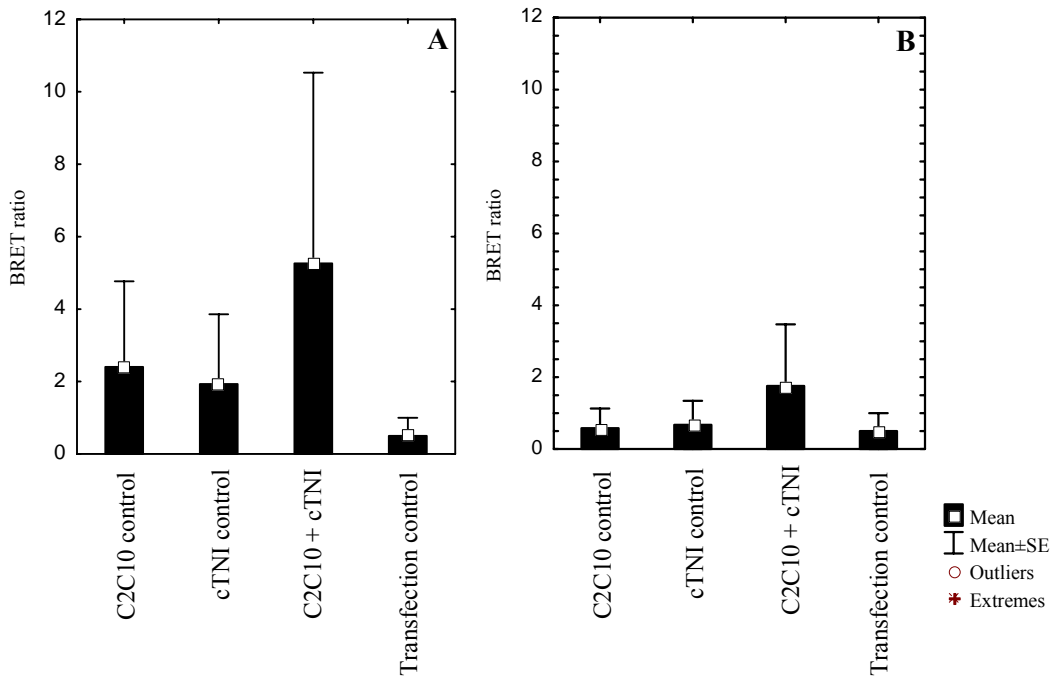


**Figure 3.22.** Bar graph of BRET values determined from differentiated H9C2 cardiac myocytes co-transfected with cTNI-GFP and C2C10 cMyBPC-Rluc, and respective controls. Values represent means  $\pm$ S.E for two independent transfections. Experiments were performed in duplicate and statistical comparisons were carried out using a one-way analysis of variance (ANOVA) followed by Bonferroni's multiple comparison post-test, comparing all pairs. Graph A shows the respective interactions in unstimulated cells while graph B shows the same interactions in cells stimulated for maximal cMyBPC phosphorylation. There were no statistically significant differences between the C2C10 cMyBPC/cTNI pair and either the C2C10 cMyBPC control or the cTNI control in either stimulated or unstimulated cells, respectively.

### 3.4.3 C2C10 cMyBPC versus ACTC1

In both independent experiments conducted to assess the interaction between C2C10 cMyBPC and ACTC1, the C2C10 control had a higher BRET ratio than the C2C10 cMyBPC/ACTC1 interaction, in unstimulated cells (Figure 3.23 A), suggesting perhaps a lack of interaction between domain C2 and ACTC1. The BRET ratios, in cells simulated for maximal cMyBPC phosphorylation, were lower (Figure 3.23 B) compared to the unstimulated cells (Bonferroni matrices in Appendix VII).

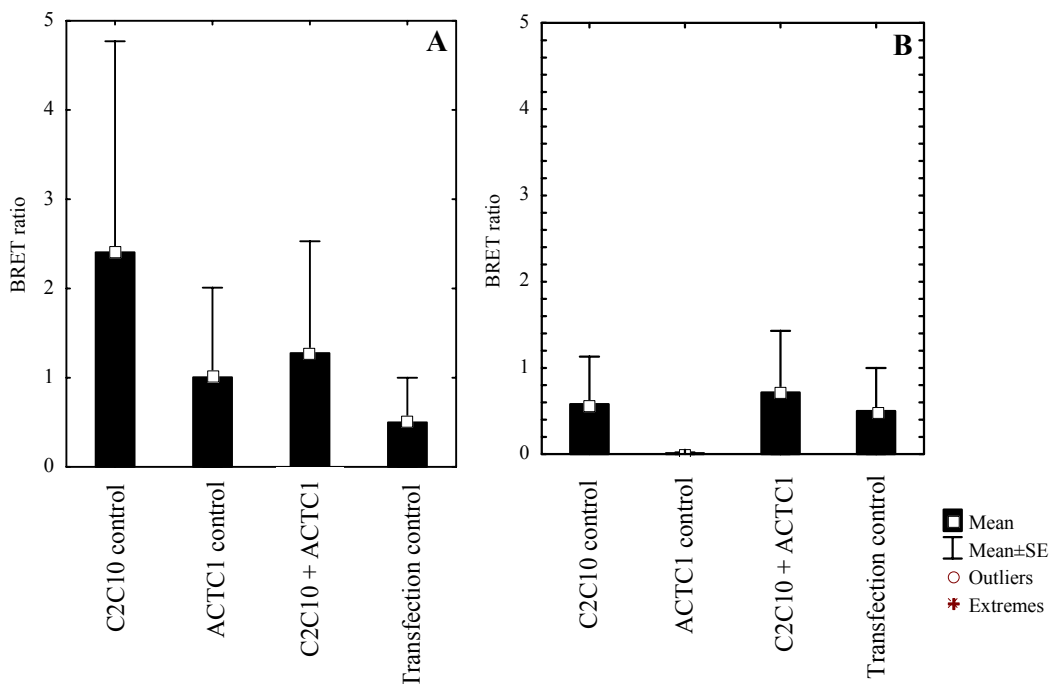


**Figure 3.23.** Bar graph of BRET values determined from differentiated H9C2 cardiac myocytes co-transfected with ACTC1-GFP and C2C10 cMyBPC-Rluc, and respective controls. Values represent means  $\pm$ S.E for two independent transfections. Experiments were performed in duplicate and statistical comparisons were carried out using a one-way analysis of variance (ANOVA) followed by Bonferroni's multiple comparison post-test, comparing all pairs. Graph A shows the respective interactions in unstimulated cells while graph B shows the same interactions in cells stimulated for maximal cMyBPC phosphorylation. There were no statistically significant differences between the C2C10 cMyBPC/ACTC1 pair and either the C2C10 cMyBPC control or the ACTC1 control in either stimulated or unstimulated cells, respectively.

### 3.4.3 cMyBPC-cMyBPC interaction

Two independent experiments were conducted to assess the interaction of domain C10 with domain C2 or C3. In addition, as a system where a single construct with an N-terminus Rluc and C-terminus GFP label was used to assess these interactions, a construct assessing interaction of domains C7 and C10, which has been shown previously by Y2H, Co-IP and surface plasmon resonance, was included to test this novel system. However, due to the large mean standard deviation of the two combined experiments and the high BRET ratio for the transfection control, no assessment of these interactions could be made (Figure 3.24) (Bonferroni matrices in Appendix VII).

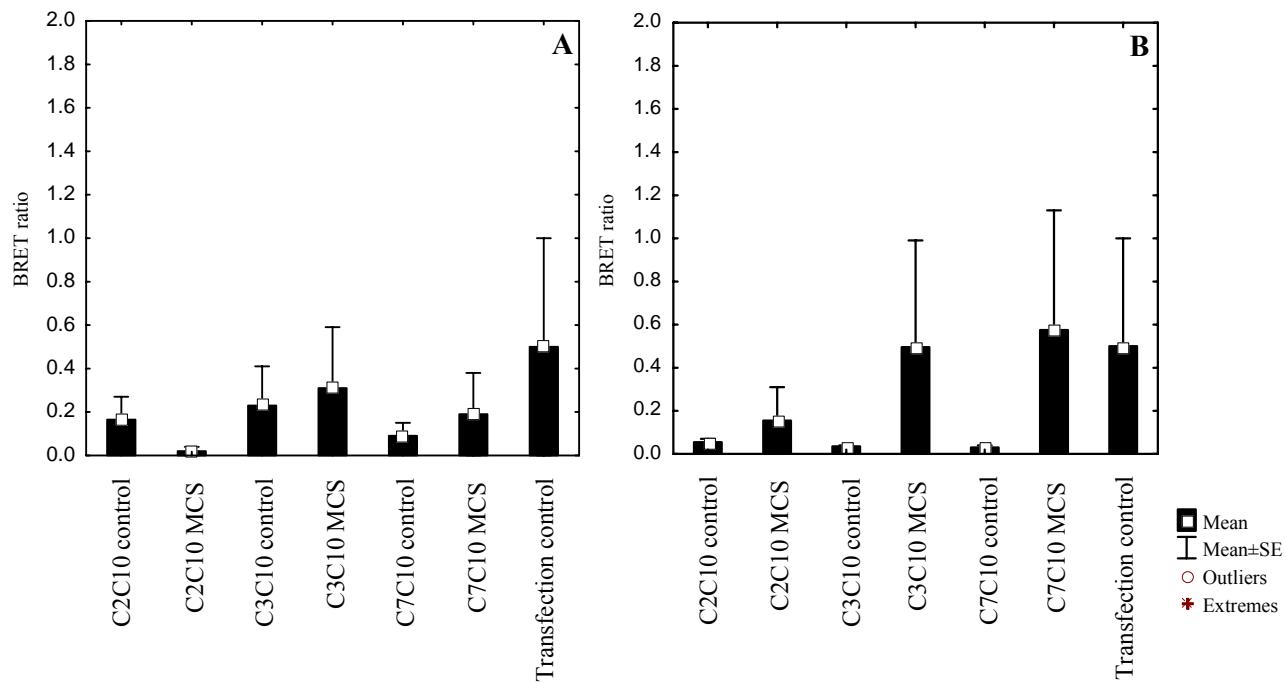


**Figure 3.24.** Bar graph of BRET values determined from differentiated H9C2 cardiac myocytes co-transfected with C2C10 MCS, C3C10 MCS, C7C10 MCS, and the respective controls. Values represent means  $\pm$ S.E for two independent transfections. Experiments were performed in duplicate and statistical comparisons were carried out using a one-way analysis of variance (ANOVA) followed by Bonferroni's multiple comparison post-test, comparing all pairs. Graph A shows the respective interactions in unstimulated cells while graph B shows the same interactions in cells stimulated for maximal cMyBPC phosphorylation. There were no statistically significant differences between each of the tests and the controls in either stimulated or unstimulated cells, respectively.

### 3.5 CORRELATION OF DATA BETWEEN Y2H AND VERIFICATION ASSAYS

#### C1C2 interactions

The interaction of N-terminus cMyBPC with HSPB7 and PDE4DIP, respectively, is supported by all three methods employed in this study (viz. Y2H, Co-IP and co-localisation data) (Table 3.17). The interaction of cMyBPC with COMMD4 and ENO3 is supported by Y2H and co-localisation data, although the Co-IP data was inconclusive. Y2H and BRET data supports the respective interactions between ACTC1 and cTNI with N-terminus cMyBPC, although the BRET data are not statistically significant. The interaction between C-terminus and N-terminus cMyBPC is only supported by Y2H and Co-IP data, while interaction between cTNT and cMyBPC is only suggested by Y2H data.

#### Effect of C0-Pro-Ala-region on interactions

For the interactions with domains C0C2, the Co-IP data was consistent for the interactions of COMMD4 (negative), PDE4DIP (positive), cMyBPC (positive) and cTNT (negative) with this region, while ambiguous results were achieved by Co-IP for the interactions of ACTC1, HSPB7, cTNI and ENO3, when compared to the Y2H data (Table 3.17).

**Table 3.17.** Correlation of data between Y2H direct protein-protein interactions and Co-IP\*.

Protein	C1C2 REGION*			C0C2 REGION*		
	Y2H	Co-IP	In vivo co-localisation	BRET	Y2H	Co-IP
COMMD4	+	-	+	Not tested	-	-
ACTC1	+	+	Not tested	+ <sup>§</sup>	-	+
cTNI	+	N/A	Not tested	+ <sup>§</sup>	-	+
cTNT	+	-	Not tested	Not tested	-	-
				N-terminus		
cMyBPC	+	+	Not tested	vs C-terminus	+	+
				Inconclusive		
HSPB7	+	+	+	Not tested	-	+
PDE4DIP	+	+	+	Not tested	+	+
ENO3	+	N/A	+	Not tested	-	+

\*Interactions considered irrespective of phosphorylation status. N/A=Bait and prey in Co-IP reaction could not be separated by SDS-PAGE; + = positive interaction; - = negative interaction; <sup>§</sup>interaction suggested but not significant

## CHAPTER FOUR: DISCUSSION

INDEX	PAGE
<b>4.1 YEAST TWO-HYBRID ANALYSIS TO IDENTIFY INTERACTORS OF DOMAINS C1C2 OF cMyBPC</b>	<b>152</b>
<b>4.1.2 Preys excluded from further study</b>	<b>153</b>
<b>4.1.3 Preys chosen for further study</b>	<b>154</b>
<b>4.1.3.1 COILED-COIL INTERACTORS</b>	<b>154</b>
<b>4.1.3.1.1 <math>\alpha</math>-Actinin 2 (ACTN2)</b>	<b>154</b>
<b>4.1.3.1.2 Glutamate Receptor, Ionotropic, NMDA-Like 1A (GRINL1A)</b>	<b>155</b>
<b>4.1.3.1.3 Uveal Autoantigen With Coiled-Coil Domains And Ankyrin Repeats (UACA)</b>	<b>156</b>
<b>4.1.3.1.4 Spectrin Repeat Containing, Nuclear Envelope 1 (SYNE1)</b>	<b>156</b>
<b>4.1.3.2 THIN FILAMENT INTERACTORS</b>	<b>157</b>
<b>4.1.3.2.1 Cardiac Troponin I (cTNI)</b>	<b>157</b>
<b>4.1.3.2.2 Cardiac Troponin T (cTNT)</b>	<b>158</b>
<b>4.1.3.2.3 Actin (ACTC1)</b>	<b>159</b>
<b>4.1.3.3 THICK FILAMENT INTERACTORS</b>	<b>161</b>
<b>4.1.3.3.1 Cardiac Myosin-Binding Protein C (cMyBPC)</b>	<b>161</b>
<b>4.1.3.4 PROTEIN TURNOVER/DEGRADATION</b>	<b>164</b>
<b>4.1.3.4.1 Copper Metabolism Gene MURR1 Domain 4 (COMMD4)</b>	<b>164</b>
<b>4.1.3.4.2 Heat Shock 27 kDa Protein Family, Member 7 (Cardiovascular)</b>	<b>167</b>
<b>4.1.3.5 KINASE ADAPTORS</b>	<b>168</b>
<b>4.1.3.5.1 Phosphodiesterase-4D-Interacting Protein (PDE4DIP)</b>	<b>169</b>
<b>4.1.3.5.2 Guanine Nucleotide-Binding Protein Subunit Beta-2-Like 1 (GNB2L1)</b>	<b>170</b>
<b>4.1.3.6 ENZYME INTERACTORS</b>	<b>170</b>
<b>4.1.3.6.1 <math>\beta</math>-Enolase (ENO3)</b>	<b>170</b>
<b>4.2 Y2H PROTEIN-PROTEIN INTERACTION STUDIES</b>	<b>172</b>
<b>4.2.1 Limitations of Y2H analysis</b>	<b>173</b>
<b>4.3 VERIFICATION STUDIES</b>	<b>174</b>
<b>4.3.1 Co-IP</b>	<b>174</b>
<b>4.3.2 Three-dimensional <i>in vivo</i> co-localisation</b>	<b>175</b>
<b>4.3.2.1 Limitations of <i>in vivo</i> co-localisation</b>	<b>175</b>
<b>4.3.3 BRET</b>	<b>176</b>
<b>4.3.3.1 Limitation of BRET</b>	<b>176</b>

<b>4.4 IMPLICATIONS FOR THE N-TERMINUS cMyBPC</b>	<b>178</b>
<b>4.5 FUTURE STUDIES</b>	<b>182</b>
<b>4.6 CONCLUSION</b>	<b>183</b>

## CHAPTER FOUR: DISCUSSION

As described in section 1.9.3.5, cMyBPC is a large multi-domain protein that is located in the C-zone of the sarcomere, anchored to LMM and titin *via* C-terminus domains. Further, the C-terminus domains have been proposed to form a collar around the thick filament in association with two other cMyBPC molecules to regulate the structure of the thick filament (Moolman-Smook *et al.*, 2002). Thus, while the function and some of interactors of the C-terminus are known, the N-terminus of this protein is not as well characterised.

Thus, far actin (Section 1.9.3.5.10) and myosin (Section 1.9.3.5.9.3) have been suggested as putative interactors of the N-terminus. While the former may involve interaction with domains C0 or the region between C0 and C1, the myosin S2 binding site is located within the C1C2 fragment. This region comprises two Ig domains connected by a linker sequence of ~100 amino acids known as the MyBPC motif. In the cardiac isoform, this motif contains three phosphorylation sites (Gautel *et al.*, 1995). Phosphorylation is mediated by PKA and/or a  $\text{Ca}^{2+}$ /calmodulin regulated kinase upon  $\beta$ -adrenergic stimulation and modulates the interaction of N-terminus cMyBPC with myosin S2. Furthermore, phosphorylation of MyBPC results in a rearrangement of the myosin S1 crossbridges and the structure of the thick filament (Weisberg and Winegrad, 1996; Levine *et al.*, 2001) which has an impact on muscle performance (McClellan *et al.*, 2001). Thus, this region seems to have vital importance as a regulator of cardiac contractility, as is further emphasised by the identification of mutations linked to hypertrophic cardiomyopathy in myosin S2 that leave the structure of the S2 coiled-coil intact but interferes with binding to cMyBPC (Gruen and Gautel, 1999b). Since the N-terminus (C0C2) has a rigid scaffolding structure and sufficient length to extend into the interfilament space (Jeffries *et al.*, 2008), it is possible that this region may interact with other sarcomeric proteins that may facilitate its proposed function as regulator of cardiac contractility.

As part of a long term investigation in our laboratory to identify the interactors of cMyBPC, we have used the Y2H approach to identify interactors of the N-terminus of this protein. The present study has focused specifically on the C1C2 region of cMyBPC. Four cardiac cDNA libraries were screened using “baits” that represented the various phosphorylation states of the cMyBPC motif, to identify the interactors of this region. Further, the hypothesised function of domain C0 as a regulator of the interaction between the putative interactors identified and the C1C2 region was investigated by direct Y2H protein-protein interaction assays.

### 4.1 YEAST TWO-HYBRID ANALYSIS TO IDENTIFY INTERACTORS OF DOMAINS C1C2 OF cMyBPC

Four independent library screens were performed and a total of 3077 clones that were able to activate three reporter genes were screened as putative interactors of C1C2 cMyBPC (Section 3.1). Following selection for the activation of nutritional and colourimetric reporter genes, heterologous mating and bioinformatics investigation, 27 in-frame cardiac cDNA clones (Table 3.3, 3.6, 3.10, 3.13) were prioritised as putative interactors of C1C2 cMyBPC.

A number of clones were pulled out multiple times by the same bait (e.g. C1orf108, TNNI3, HSPB7, PGM5, ACTC1, MYBPC3, PDE4DIP, GRINL1A, CNN1, COMMD4, ENO3, and UACA; Table 3.3, 3.6, 3.10, 3.13). In addition, a number of clones (e.g. ACTN2, PDE4DIP, GRINL1A, MYBPC3 and SYNE1) were identified as putative interactors of more than one phosphorylation-mimic state of the C1C2 bait. Since the overlap between Y2H screens using the same bait protein has been observed to be less than 15% (Zhou and Veenstra, 2007), the significance of pulling the same clone out multiple times in the same screen and between screens, is less likely to be a two-hybrid artefact and more likely to be biologically significant (Parrish *et al.*, 2006).

#### 4.1.2 Preys excluded from further study

For all four library screens, proteins were excluded for the following reasons:

##### *No significant protein matches*

While the insert sequence of clones had significant DNA matches in the NCBI database (<http://www.ncbi.nlm.nih.gov>), many of these inserts were not in-frame according to the reading frame dictated by the upstream GAL4 domain and had no significant protein matches in the database when translated. This is a result of a limitation of the commercially available cDNA libraries which are derived from oligo-dT primed cDNA, viz. that only one out of six of all cloned inserts are in-frame with the transcription factor activation domain (van Criekinge and Beyaert, 1999). Thus, as the peptides encoded by such constructs were short and physiologically irrelevant, these preys were excluded from any further analysis.

##### *Incompatible cellular compartments*

It is unlikely that protein-protein interactions are possible between proteins separated by subcellular compartmentalisation *in vivo*. Therefore, proteins localised to subcellular compartments incompatible with cMyBPC's C-zone sarcomeric (cytosolic) localisation were excluded from further study. For some proteins, the subcellular localisation has not yet been experimentally determined and thus online subcellular localisation tools (Section 2.6) were used to predict their localisation based on amino acid sequence information (Hua and Sun, 2001; Emanuelsson *et al.*, 2001; Nair and Rost, 2002). These prediction tools are somewhat restricted in their function as they have a limited accuracy for predicting subcellular localisation and they also have limited coverage of the number of subcellular regions (Lu *et al.*, 2003). The limited coverage is apparent, for instance, by their inability to predict the subcellular localisation for FLJ21347 (Table 3.6). For the present study, preys that were localised exclusively to the nucleus, mitochondria, lysosome, golgi, endoplasmic reticulum or that were secreted into the extracellular matrix were excluded as putative positive interactors of cMyBPC as their localisation do not co-incide with the cytosolic, sarcomeric C-zone localisation of cMyBPC (Table 3.3, 3.6, 3.10, 3.13). Preys that had a cytoplasmic localisation were retained as putative interactors as it is possible for these proteins to have access to cMyBPC anchored to the thick filament of the sarcomere.

#### **4.1.3 Preys chosen for further study**

Based on evidence from the literature and Y2H protein-protein interaction data (Table 3.15), the putative positive preys investigated by the present study fell into six broad groups, i.e. coiled-coil interactors (Section 4.1.3.1), thin filament interactors (Section 4.1.3.2), thick filament interactors (Section 4.1.3.3), protein turnover/degradation interactors (Section 4.1.3.4), kinase adaptor interactors (Section 4.1.3.5) and enzyme interactors (Section 4.1.3.6). Representatives of each of these categories of putative interactors were investigated further and the consequences for an interaction with cMyBPC are discussed in the following sections. The remaining putative interactors from the four library screens that were not investigated in the present study will be screened in future studies in our laboratory.

##### **4.1.3.1 COILED-COIL INTERACTORS**

The putative interactors in this category have coiled-coil secondary structure homologous to myosin S2 (except SYNE1), the often reported interactor of C1C2 cMyBPC. Although the Y2H protein-protein interaction data showed that these preys (except ACTN2) did not interact with C1C2 cMyBPC in a manner analogous to the phosphorylation-dependent interactions between C1C2 and myosin S2 (Section 1.9.3.5.9.1), these interactions may point to the ability of the C1C2 region to interact with proteins that bear some structural resemblance to myosin S2. Myosin S2 itself was not pulled out as an interactor of C1C2 cMyBPC in any of the Y2H assays, most likely because of the limitations of the cDNA library. The range of insert sizes of the commercial cDNA libraries employed in this study is 0.4-4kb, and cDNA inserts for this library were generated by reverse transcription of cardiac mRNA from oligo-dT priming at the 3'-end of transcripts. Thus, it is unlikely to find an abundance of cDNAs that represent the N-terminus of large proteins such as myosin heavy chain (5.8kb).

Although these preys with homology to myosin S2 support the interaction of myosin S2 with C1C2 cMyBPC, their subcellular localisation (ACTN2 at the Z-disc; GRINL1A associated with membranous glutamate receptors and UACA localised around the nuclear membrane) is incompatible with the C-zone cMyBPC localisation. Thus these are most likely non-physiological interactions, driven by structural homology of these proteins to myosin S2. Since the C1C2/myosin S2 interaction has been the subject of many studies and is well characterised, preys homologous to myosin S2 (ACTN2, GRINL1A and UACA) were not investigated beyond the Y2H protein-protein interaction assay.

###### **4.1.3.1.1 $\alpha$ -Actinin 2 (ACTN2)**

In cardiac muscle, ACTN2 is the predominant protein component of the sarcomeric Z-disc, where it forms a lattice structure that anchors actin and stabilises the muscle contractile apparatus (Sjöblom *et al.*, 2008). In addition to its mechanical role, ACTN2 interacts with a host of proteins involved in a variety of signalling and metabolic pathways, linking the cytoskeleton to different transmembrane proteins in a variety of junctions, regulating the activity of a number of receptors, and serving as a scaffold to connect the

cytoskeleton to diverse signalling pathways (Sjöblom *et al.*, 2008). This protein and its interactors have been described in section 1.5.

#### *ACTN2 and C1C2 cMyBPC*

ACTN2 was identified by the C1C2 (C29) and C1A<sub>1</sub>P<sub>2</sub>A<sub>3</sub>C3 (APA9) library screens as a putative interactor of C1C2 cMyBPC. The Y2H protein-protein interaction assay showed that ACTN2 had specificity for the cMyBPC motif, judged by the inability of these clones to bind to flanking domains, C1 or C2 (Table 3.15). These interactors bound to the cMyBPC motif in a manner analogous to the phosphorylation-influenced interaction of myosin S2. However, ACTN2 has structural homology to myosin S2 and has a subcellular localisation (Z-disc) that is incompatible with cMyBPC's localisation. Thus, ACTN2 was considered a spurious interactor.

#### **4.1.3.1.2 Glutamate Receptor, Ionotropic, NMDA-Like 1A (GRINL1A)**

The four GRINL1A transcripts (C319, P2, P81, AAA143) identified as putative interactors of C1C2 cMyBPC corresponded to the Gcom1 transcript which has the largest GRINL1A reading frame identified (550 amino acids) so far. The amino acid sequence of Gcom proteins resemble those of yotiao (Lin *et al.*, 1998) and the N-terminus of proteins that interact with the NR1 *N*-methyl-*D*-aspartate (NMDA) receptor subunit (NR2 and NR3) in neurons. Yotiao, a 210 kDa AKAP, is responsible for linking PKA to the transmembrane ion channel KCNQ1 in the heart (Marx *et al.*, 2002). Gcom1 co-localises with mouse NR1 NMDA receptor subunit in the plasma membrane of rat hippocampal neurons and it is therefore hypothesised that Gcom1 interacts with the NMDA receptor or other ionotropic glutamate receptors to modulate glutamate neurotransmission (Roginski *et al.*, 2004).

#### *GRINL1A and C1C2 cMyBPC*

The Y2H protein-protein interaction assay showed that all four GRINL1A clones interacted specifically with the cMyBPC motif, although the interactions were not affected by phosphorylation status of the cMyBPC motif (Table 3.15). Protein sequence analysis (Section 3.1.4.1) showed that GRINL1A has coiled-coil secondary structure homologous to myosin S2. Additionally ACTN2, which also has homology to myosin S2, interacts with transmembrane proteins such as the NR1 and NR2B subunits of the NMDA glutamate receptor (Michailidis *et al.*, 2007). It is possible that GRINL1A interacts with C1C2 cMyBPC for these reasons. Although, the possibility that it acts as an AKAP (based on similarity to the AKAP yotiao) cannot be excluded, at present there is no evidence in the literature to support such a role for GRINL1A as an AKAP in the heart. For these reasons and because of GRINL1A's proposed subcellular localisation to membranous glutamate receptors, it was considered a spurious/non-physiological interactor and was not investigated further than the Y2H assay.

#### **4.1.3.1.3 Uveal Autoantigen With Coiled-Coil Domains And Ankyrin Repeats (UACA)**

UACA (also known as nuclinc) is a novel protein which contains six ankyrin repeats and a rod-like tail sequence composed of heptapeptide repeats characteristic of  $\alpha$ -helical coiled-coils. This protein localises to the cytoplasm, especially around the nuclear membrane, in mammalian cells and is proposed to function in the apoptotic process (Sakai *et al.*, 2004). UACA is a component of the apoptosome complex which is also composed of apoptotic protease activating factor 1 (APAF1) and pro-caspase 9. UACA is suggested to regulate APAF1 expression and plays an important role in the regulation of stress-induced apoptosis. It also promotes apoptosis by regulating the redistribution of APAF1 into the nucleus after proapoptotic stress and down-regulates the expression of galactin 3 by inhibiting nuclear factor kappa-beta (NF- $\kappa$ B) signalling (Liu *et al.*, 2004).

##### *UACA and C1C2 cMyBPC*

The region of interaction between UACA and C1C2 cMyBPC could not be determined as the UACA clones (APA232 and APA162; Table 3.15) interacted with domains C1 and C2 individually as well as with the complete domain C1C2. Further, interaction with the cMyBPC motif was not phosphorylation-status dependent. The homology between UACA and myosin S2 (Section 3.1.4.1) as well as the C-zone incompatible localisation of UACA, suggests that this may be a non-specific interaction with C1C2 cMyBPC, driven by the structural similarity of UACA to myosin S2.

#### **4.1.3.1.4 Spectrin Repeat Containing, Nuclear Envelope 1 (SYNE1)**

Spectrin repeat containing nuclear envelope 1 (also known as enaptin and nesprin 1) comprises a spectrin-like rod domain and a klarsicht-related C-terminus. Antibodies directed against the C-terminus end of SYNE1 showed that the protein was present predominantly in the nuclear envelope and to a lesser degree within the nucleus, while studies with N-terminus antibodies showed that in addition to nuclear envelope localisation, a significant amount of this protein was present in the sarcomeres of both cardiac and skeletal muscle. The staining pattern was consistent with localisation at muscle Z-disc where SYNE1 may interact with actin and ACTN2, and function as a scaffolding protein (Zhang *et al.*, 2002)

##### *SYNE1 and C1C2 cMyBPC*

Y2H protein-protein interaction assays showed that SYNE1 clones (APA231 and AAA179) interacted strongly with all cMyBPC baits, including the individual domains flanking the MyBPC-motif, such that the region of interaction on C1C2 could not be mapped (Table 3.15). SYNE1 has significant homology to the rod domain of ACTN2, and not to myosin S2. Since ACTN2 has been considered a spurious interactor, combined with the Z-disc localisation of SYNE1, it was also regarded as a non-physiological interactor of C1C2 cMyBPC.

#### 4.1.3.2 THIN FILAMENT INTERACTORS

##### 4.1.3.2.1 Cardiac Troponin I (cTNI)

cTNI is a component of the troponin complex that regulates the contractile apparatus in a  $\text{Ca}^{2+}$  dependent manner and has been described in detail in section 1.9.3.4.2. Three cTNI clones were identified as cMyBPC interactors by the pGBK-C1C2 library screen (C81, C363 and C312) and the direct Y2H protein-protein interaction assays suggested that these clones interacted with domain C2, although interaction with the cMyBPC motif (irrespective of phosphorylation status) could not be excluded (Table 3.15). The cTNI interaction with the C1C2 phosphorylation-mimics could not be confirmed by Co-IP due to technical constraints: While there was adequate separation (judged visually; Figure 3.12) between cTNI and the C1C2 phosphorylation-mimics on the autoradiograph, the densitometer could not distinguish between the bands. Thus, the protein in the negative control lane could not be subtracted to determine the relative amount of cTNI that was precipitated in the Co-IP reaction.

The molecular weight of cTNI as determined by SDS-PAGE (Figure 3.2) was different to that expected from *in silico* calculations (Table 3.16) and the literature. The larger than expected protein may be accounted for by an in-frame insertion of 102 base pairs of 5'UTR of *TNNI3*, between the GAL4AD domain and the *TNNI3* start codon. This additional sequence does not BLASTp to an in-frame ORF but its effect on either the Y2H or the Co-IP interaction with the cMyBPC baits is unknown.

For the BRET assay, the additional 102 base pair sequence was not present in the construct as gene-specific primers were designed for cloning of the sequence into the relevant BRET vector. The BRET data suggested that there may be an interaction between cTNI and cMyBPC, but due to the large mean standard deviation, this finding was not statistically significant. The BRET ratios were higher for the GFP-cTNI/Rluc-C1C10 (Figure 3.20) and GFP-cTNI/Rluc-C2C10 (Figure 3.22) pairs compared to the controls when the cardiomyocytes were unstimulated than when they were stimulated for maximal phosphorylation of cMyBPC. (It should be noted that not all sarcomeric cMyBPC is thought to be replaced by the tagged exogenous proteins; hence, stimulation of the H9C2 cells for PKA activation is proposed to result in maximal phosphorylation of the endogenous cMyBPC, and adaptation of the sarcomere and the quaternary structure of endogenous and exogenous cMyBPC, accordingly). The BRET results suggested that cTNI may be an interactor of unphosphorylated cMyBPC. Further, the higher BRET ratio for the GFP-cTNI/Rluc-C2C10 interaction compared to the GFP-cTNI/Rluc-C1C10 interaction, when plotted on the same scale (data not shown), confirmed the Y2H interaction data which suggested an interaction between domain C2 and cTNI. As only two independent assays were performed for the Rluc-C2C10/GFP-cTNI interaction and standard deviations between these assays were large, more BRET assays need to be performed to achieve lower standard deviations, before final conclusions about this interaction can be drawn. As the average length of an Ig domain is measured to be 4nm long, it is possible that the region of interaction may also include cMyBPC motif, which is also proposed to be Ig-like (Jeffries *et al.*, 2008). An interaction that spans

2 Ig domains (2x 4nm) is within the range (less than 10nm) to be detected by BRET (Pfleger and Eidne, 2006).

There is currently no evidence in the literature for a direct interaction between cTNI and cMyBPC. A link between cMyBPC and cTNI may be extrapolated from the findings of Razumova *et al* (2006) which showed that a C1C2 fragment bound to actin and dramatically increased filament sliding speeds at low  $\text{Ca}^{2+}$  concentrations only in the presence of troponin and tropomyosin (Section 1.9.3.5.10). Further, cosedimentation experiments showed that in addition to actin, troponin and tropomyosin were also pelleted with the C1C2 fragment (Razumova *et al.*, 2006). However, the individual components of the troponin complex were not used in separate experiments to single out the C1C2 interactor.

In a recent study by Sadayappan *et al* (2008), PKA-mediated phosphorylation of cTNI was shown to result in a conformational change that repositioned the acidic NcTNI to facilitate an interaction with the basic residues within the inhibitory region of cTNI (Section 1.9.3.4.1.1). Since the cMyBPC motif is also high in basic residues and shares homology to the inhibitory region of cTNI (Figure 4.1), an interaction between cTNI and C1C2 (containing the cMyBPC motif) is also possible. It could be speculated that, in this setting, sufficiently high concentrations of the C1C2 fragment may have competed with the NcTnC for binding to the NcTNI, which are known to interact under low  $\text{Ca}^{2+}$  concentrations and in the absence of NcTNI phosphorylation (Section 1.9.2). This may bring about dissociation of NcTNI and NcTnC, enhancing interaction of NcTnC with the switch region of cTNI and triggering conformational changes in the thin filament that promote the formation of cross-bridges and activates filament sliding in a manner analogous to activation of the thin filament by  $\text{Ca}^{2+}$ . However, to determine whether such activation is relevant *in vivo*, further investigation is required.

C1C2 cMyBPC cTNI inhibitory region	DSYDRASKVYLFELHITDAQPAFTGSYRCEVSTKDKFDCSNFNLTVHEAM
C1C2 cMyBPC cTNI inhibitory region	GTGDL DLLSAFRRTSLAGGRRISD SHEDTGILDFSSLLKKRDSFRTPRD -----GK-----FKRP-- *: * : :
C1C2 cMyBPC cTNI inhibitory region	SKLEAPAEEDVWEILRQAPPSEYERIAFQYGVTDLRLGMLKRLKGMRDEK -----TLRRVR----- *: * : :
C1C2 cMyBPC cTNI inhibitory region	KSTA FQKKLEPAYQVSKGHKIRLTVELADHDAEVKWKLNGQEIQMSGSKY
C1C2 cMyBPC cTNI inhibitory region	IFESIGAKRTLTIQSCLADDAAYQCVVGGEKCSTELFVKEP

**Figure 4.1** CLUSTAL W multiple sequence alignment showing the homology between C1C2 cMyBPC and the inhibitory region of cTNI.

#### 4.1.3.2.2 Troponin T (cTNT)

As described in section 1.9.3.4.2, cTNT is a component of the troponin complex that regulates cardiac contractility in a  $\text{Ca}^{2+}$ -dependent manner. cTNT is important not only for fixing of the troponin components

to the actin-tropomyosin filament, but it also plays an important role in the regulation of actomyosin ATPase activity (Filatov *et al.*, 1999).

#### *cTNT and C1C2 cMyBPC*

Y2H protein-protein interaction data showed that cTNT interacted very weakly with domain C2 and not at all with domain C1, suggesting that cTNT interacted with the cMyBPC motif and that the interaction was not phosphorylation-dependent (Table 3.15). However, the Co-IP experiment did not support the interaction between cTNT and cMyBPC (Figure 3.8-9), because of this and due to time constraints; this interaction was not tested by BRET. The Co-IP data, combined with the fact that, unlike the other thin filament components (actin and cTNI), cTNT was only identified once, suggests that this may be a physiologically irrelevant interaction. However, since an interaction between a component of the thin filament and N-terminus cMyBPC is likely (Razumova *et al.*, 2006), the possibility that the interactor is cTNT cannot be excluded.

#### **4.1.3.2.3 Actin (ACTC1)**

Several studies have shown that N-terminus cMyBPC can bind to actin, although the region of interaction appears to differ among studies, depending on the experimental system used (Section 1.9.3.5.10). The Y2H protein-protein interaction data of the present study suggests that there is more than one actin-binding region on the N-terminus cMyBPC: site/s N-terminus to C1 as well as sites involving domain C2 and possibly including the cMyBPC motif (Table 3.15). The interaction with the cMyBPC motif does not appear to be phosphorylation-dependent, as actin interacted in a qualitatively similar manner with all the C1C2 phosphorylation-mimics. Since a bait construct consisting only of domain C0 was not included in the assay, the actin-binding region N-terminus of C1 was not isolated further to either C0 or the pro-ala-rich linker (or a combination). These findings do however support the studies of Squire *et al* (2003) and Kulikovskaya *et al* (2003a) who proposed actin-binding sites N-terminus to C1. The suggestion by Squire *et al* (2003) that the pro-ala-rich linker can bind actin was shown by homology modelling and was not experimentally validated, while Kulikovskaya *et al* (2003a) showed by immunoprecipitation methods that C0-containing constructs bound to actin. The affinity for actin was greater when C0C2 was used (Kulikovskaya *et al.*, 2003a), suggesting that the actin-binding region may span C0 and the pro-ala-rich linker. In their investigations, a fragment containing C1C2 did not bind to actin.

The findings of Kulikovskaya *et al* (2003a) were contrasted by the study of Razumova *et al* (2006), which showed (in an *in vitro* motility assay) that C1C2, but not C0C1, was able to bind to actin (Section 1.9.3.5.10). The differences in these studies with regard to the cMyBPC/actin interaction may relate to the presence of the troponin complex and tropomyosin (in the Razumova study). Although the inability of C0C1 in this setting to bind to the thin filament (containing actin) cannot be explained, this study is corroborated by that of Herron *et al* (2006), which showed that C0C2 and C0C1 constructs expressed in cardiomyocytes do not bind to the I-band. Furthermore, cosedimentation experiments by Razumova *et al* (2006) showed that, in addition to actin, C1C2 pelleted with troponin and tropomyosin, thus these proteins may also be able to bind

to C1C2. In the present study, Y2H interaction assays also showed that an actin-binding region resides within the cMyBPC motif and/or domain C2, rather than in C1 (Table 3.15). Unfortunately it is not possible to test for interaction with the cMyBPC motif independent of domains C1 and C2 as the cMyBPC region appears to require the flanking domains for stability (Gruen and Gautel, 1999).

The interaction between actin and C1C2 cMyBPC was further confirmed by Co-IP in the present study (Figure 3.5). Although all the C1C2 baits precipitated with actin, the intensity of the actin band varied between the baits which suggested that some baits had a lower affinity for actin than others. The C1A<sub>1</sub>A<sub>2</sub>A<sub>3</sub>C2 bait had the lowest affinity for actin; a finding not confirmed by the Y2H interaction assay data (Table 3.15), which showed that actin interacted with the C1C2 baits with similar affinity. As the Y2H interaction assay is a qualitative assessment of the interactions, quantitative β-galactosidase assays should be performed to assess the strength of these interactions. The amount of actin available for interaction with C1A<sub>1</sub>A<sub>2</sub>A<sub>3</sub>C2 bait in the Co-IP experiments may be an explanation for the small amount pulled down, although care was taken to add an equal volume of prey to each reaction. It is also possible that during the process of PCR amplification or *in vitro* transcription/translation there was some occult modification of the C1A<sub>1</sub>A<sub>2</sub>A<sub>3</sub>C2 bait that made an interaction between actin and C1A<sub>1</sub>A<sub>2</sub>A<sub>3</sub>C2 bait less favourable in this setting.

Co-IP also showed that there was an interaction between actin and the C0C2 baits (Figure 3.5). This finding was not confirmed by Y2H interaction data, which rather suggested that the C0-pro-ala-rich region interfered with the actin interactions of the C0C2 baits. An explanation for the contrasting data could be that the *in vitro* transcription/translated C0C2 protein, Myc-tagged, but lacking the GAL4-binding domain region, was in a conformation that did not allow C0C1 to block the interaction with actin as seemed to occur in the Y2H assay. The co-immunoprecipitation of actin with C0C2 baits is not an artefact of Co-IP, as the negative control lane shows that actin did not interact non-specifically with the protein G agarose. Therefore, the presence of actin in the Co-IP lane is as a result of specific interaction with the various C0C2 baits. The intensity of the actin bands Co-IPed with the C0C2 phosphorylation-mimics also varied, with C0A<sub>1</sub>A<sub>2</sub>A<sub>3</sub>C2 having the greatest affinity for actin while C0A<sub>1</sub>P<sub>2</sub>A<sub>3</sub>C2 having the weakest affinity for actin. Again, the variation in intensity of the actin bands may be due to the same reasons as mentioned above.

To confirm the interactions observed by Y2H and Co-IP in an *in vivo* setting, BRET assays were performed. Although not statistical greater due to the large standard deviations, the mean BRET ratio for the Rluc-C1C10/GFP-actin interaction was higher than that of the experimental controls (Figure 3.21A), suggesting that cMyBPC in the unphosphorylated state may interact with actin. When the differentiated cardiac myocytes were stimulated for maximal phosphorylation of the cMyBPC motif by exposure to Ca<sup>2+</sup> and isoproterenol, this interaction appeared to be abolished, as the test BRET ratio was dampened to control levels (Figure 3.21B). The mean BRET ratio for the C2C10-Rluc control was higher than that of the test reaction, suggesting that no interaction took place between domain C2 and actin (Figure 3.23A). However,

the data from this latter study was based on only two experiments, and resulted in particularly large standard deviations, so caution should be used in interpretation of these results, which also contradicted published studies as well as Y2H data from the present study.

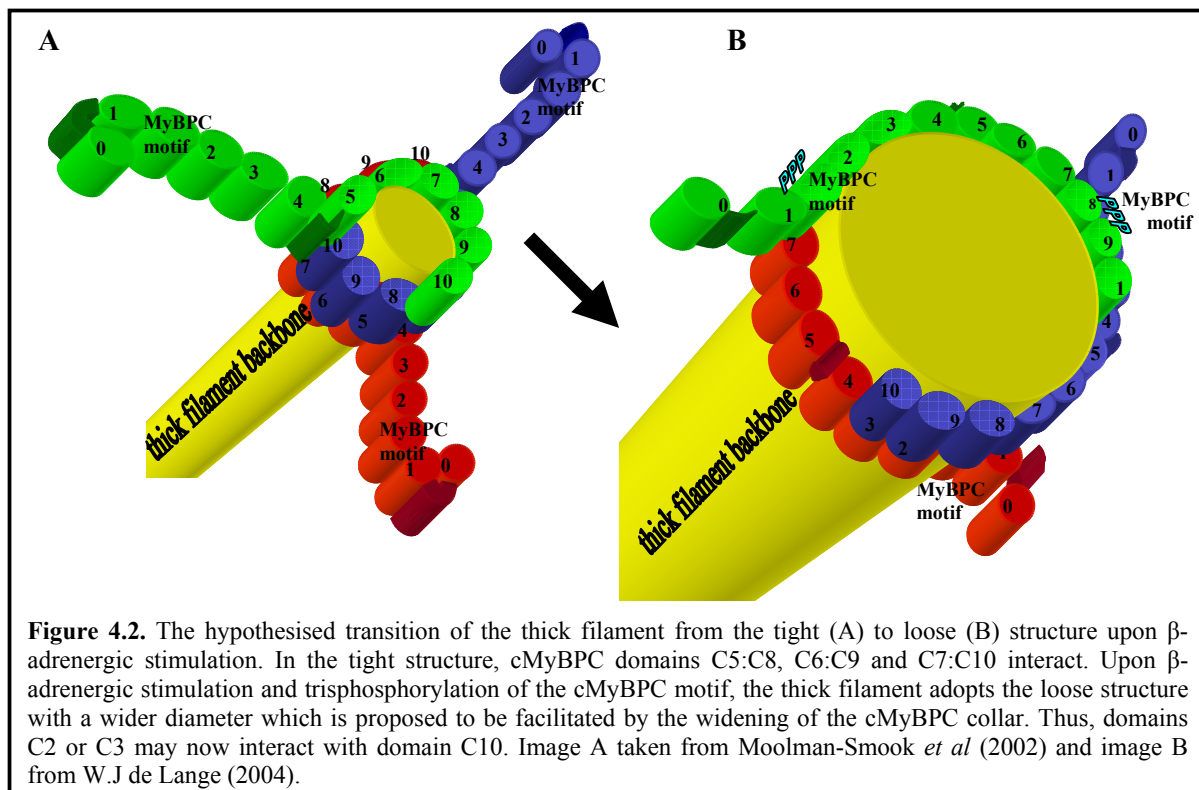
#### 4.1.3.3 THICK FILAMENT INTERACTORS

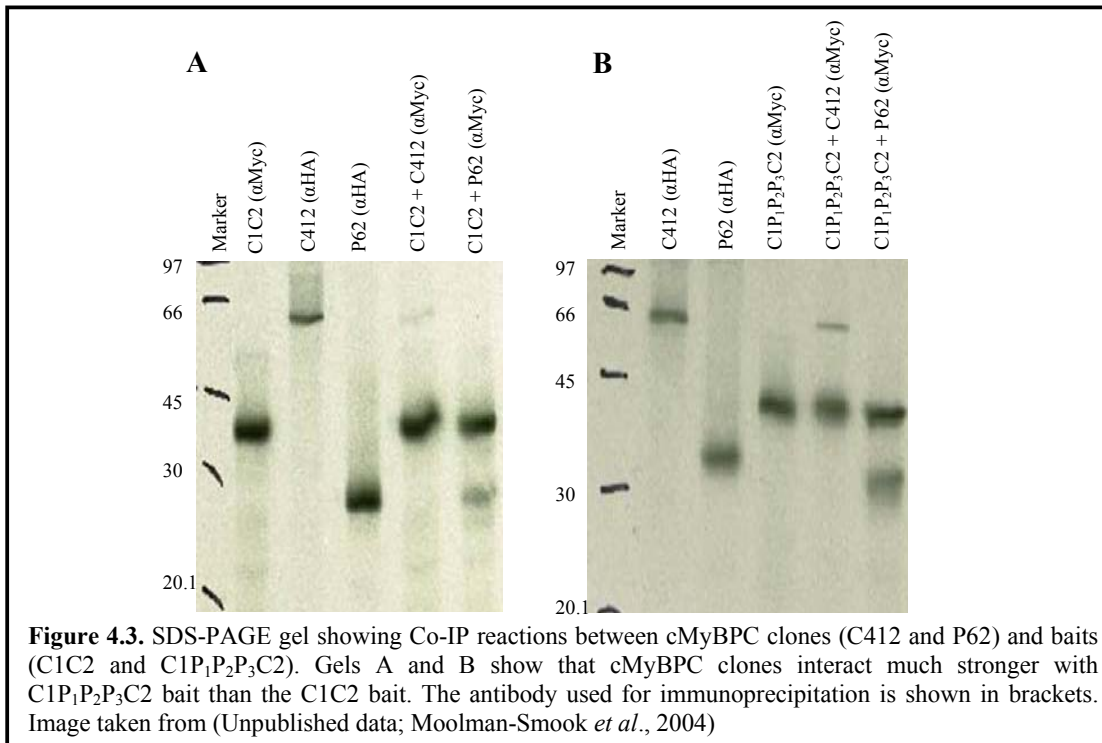
##### 4.1.3.3.1 Myosin-Binding Protein C

A previous Y2H library screen performed in our laboratory using domain C7 as “bait” identified a partial domain C10 clone as an interactor (W.J de Lange, 2004); this interaction was subsequently confirmed by surface plasmon resonance with  $K_a = \sim 1 \times 10^5$  (E Flashman, personal communication). This interaction was consistent with the proposed interaction between these domains as suggested by the trimeric collar model when the cMyBPC motif was unphosphorylated and the thick filament backbone diameter was narrow (Figure 4.2A). De Lange’s study explored the theoretical effect of cMyBPC phosphorylation on collar dimensions, as cMyBPC di- or triphosphorylation by PKA has been shown to result in the expansion of the thick filament backbone (Levine *et al.*, 2001). A trimeric cMyBPC collar would have to accommodate this change by abrogating intermolecular interactions between domains C5:C8, C6:C9 and C7:C10 and either completely breaking apart and reforming or assuming a looser conformation. The latter suggestion was favoured by De Lange, although the possibility that the collar may be completely abrogated under certain circumstances cannot be excluded. Based on thick filament backbone dimensions, De Lange speculated that upon the thick filament taking on a “loose” conformation, and with domain C10 firmly anchored to myosin and possibly titin, interaction would shift from existing between central cMyBPC domains and extreme C-terminus domains (C9 and/or C10), to between the latter domains and N-terminus domains of cMyBPC in the vicinity of the C1C2 region. (W.J de Lange, 2004). Therefore, constructs encoding domain C2 or C3 were tested for interactions with constructs encoding C9, C10 and C9C10 in Y2H interaction assays; these showed that domain C3 interacted specifically with domain C10. A fragment spanning C2C3 was not included in these assays. These findings suggested that conditions exist under which domain C10 can interact with either C7 or C3. This data, coupled with the observed changes in the thick filament back bone diameter upon cMyBPC phosphorylation, led to the proposed “loose” collar conformation depicted in Figure 4.2B. Upon cMyBPC PKA-dependent phosphorylation, the “loose” collar would allow the thick filament to expand and adopt the loose structure which has been associated with increased crossbridge cycling (described in section 1.9.3.5.11.2). This “loose” collar model was significant in aiding the interpretation of data obtained from the various Y2H library screens of C1C2 phosphorylation-mimics and subsequent verification assays in the present study.

The pGBK-C1C2 and pGBK-C1P<sub>1</sub>P<sub>2</sub>P<sub>3</sub>C2 library screens identified three cMyBPC clones (P213, C412 and P62) as putative interactors of domains C1C2. The clone encoding the largest peptide (C412) corresponded to a fragment representing from about midway through domain C5 to domain C10 (sequence accession number: NM\_000256; 513aa), the smallest clone (P62) represented midway through domain C8 to domain C10 (sequence accession number: NM\_000256; 237aa) while P213 was intermediate in size, encoded a

partial domain C7 to C10 (sequence accession number: NM\_000256; 349aa). Co-IP experiments of P62, C412, the unphosphorylated C1C2 and trisphosphorylated C1C2 baits (Figure 4.3), performed prior to the present study, showed that the trisphosphorylated bait (C1P<sub>1</sub>P<sub>2</sub>P<sub>3</sub>C2) had a greater affinity for the cMyBPC clones (C412 and P62; representing C-terminus domains) than the unphosphorylated bait (C1C2). These results could be interpreted in the following manner: when the cMyBPC motif is phosphorylated, N-terminus domains make direct contact with C-terminus domains (observed as C1P<sub>1</sub>P<sub>2</sub>P<sub>3</sub>C2 interacting strongly with C412 and P62, Figure 4.3) while when the cMyBPC motif is unphosphorylated, an interaction between C1C2 is not favoured with C-terminus domains (observed as weak interactions of C1C2 with C412 and P62, Figure 4.3). This differential affinity of C1C2 for C-terminus domains (depending on the phosphorylation status of the cMyBPC motif) lent support for a hypothesised transition from the “tight” to “loose” collar conformation upon PKA-dependent phosphorylation to accommodate changes in the thick filament. Since domain C3 was not part of the constructs used in this Co-IP assay, and considering the interaction observed between domains C3 and C10 by De Lange, it may be considered that interactions between N- and C-terminus domains are not perfectly juxtaposed; thus, the region of interaction with domain C10 may be staggered and include part of domain C2.





To further map the region of interaction of the three cMyBPC clones, identified in the present study, with the N-terminus of cMyBPC, additional Y2H interaction assays were performed. The Y2H interaction data of the present study showed that all three cMyBPC clones (P213, P62 and C412) interacted with domain C2 as well as with phosphorylation-mimics of both C1C2 and C0C2 cMyBPC (Table 3.15). These interactions may reflect the proposed interaction between domain C2/C3 and C10 when the thick filament is in the loose conformation. Furthermore, all of the cMyBPC clones interacted with C1 and C0C1 in the interaction assays, thus it is possible that domain C1 is also involved when the collar is loosened, in a manner which is not completely clear. While these qualitative Y2H interaction data did not mirror the findings of the previous Co-IP data (Figure 4.3), quantitative β-galactosidase assays may provide greater insight into the strength of these interactions. Co-IP experiments performed during the course of the present study, using clone C412 (Figure 3.14-15) confirmed the interactions with C1C2 and C0C2 phosphorylation-mimics as observed by the Y2H interaction assay.

The BRET assays to confirm the N-terminus cMyBPC interactors of domain C10 (C2 or C3) could not provide any further clarification to collar dynamics upon PKA phosphorylation, due to technical constraints (Figure 3.24): as the positive control for this assay, viz. the interaction between domains C7 and C10, did not yield the expected results. Due to time constraints, these technical issues could not be resolved. Thus, while the present study has not resolved all the issues concerning the precise nature of interactions between C-terminus and N-terminus domains of cMyBPC, it has provided further evidence for interaction between these cMyBPC regions. Further investigations are needed to refine the precise domain:domain interactions as well as the circumstances under which these interactions occur.

#### **4.1.3.4 PROTEIN TURNOVER/DEGRADATION**

##### **4.1.3.4.1 Copper Metabolism Gene *MURRI* Domain 4 (COMMD4)**

COMMD4 is member of the family of ten COMM (Copper Metabolism gene *MURRI*) domain-containing (COMMD) proteins (COMMD1-10), found in all vertebrates, which are characterised by the presence of a highly conserved and unique C-terminus COMM domain and an  $\alpha$ -helical-rich N-terminus region that is divergent across members of the family. The COMM domain not only defines this family of proteins, but functions as a critical interface for protein-protein interactions (Burstein *et al.*, 2005). Since the COMMD family has only recently been identified, the members of this family, including COMMD4, have not been extensively studied and the function(s) of COMMD4 and COMMD proteins in general is inferred based on the data available for COMMD1. COMMD1 is widely expressed in adult tissue and is distributed throughout the cell, including the nucleus as well as perinuclear organelles (Burstein *et al.*, 2005; Burstein *et al.*, 2004; Klomp *et al.*, 2003). COMM1 has been shown to participate in two apparently distinct activities, regulation of the transcription factor NF- $\kappa$ B and control of copper metabolism (Burstein *et al.*, 2005).

All members of the COMMD family are capable of inhibiting NF- $\kappa$ B transcriptional activity and the COMM domain plays a critical role in this process (Burstein *et al.*, 2005; de Bie *et al.*, 2006). NF- $\kappa$ B is a transcription factor that is associated with the development of cardiac hypertrophy, cell survival and inflammation, amongst other effects (Green, 2003; Karin and Lin, 2002). Interestingly, all signalling pathways that can stimulate NF- $\kappa$ B activation are necessary for the initiation and progression of hypertrophy to heart failure (Li *et al.*, 2004; Gupta *et al.*, 2008). COMMD1 facilitates the termination of the NF- $\kappa$ B response through its association with a Cullin 2-containing ubiquitin ligase. Given that COMMD1 can also interact with other Cullin proteins, it is predicted that COMMD proteins are likely to associate with other ubiquitin ligases to play a role in protein turnover (Burstein *et al.*, 2005).

Further, mutations in the *COMMD1* gene have been associated with copper toxicosis in a purebred dog population, but no mutations in this gene have been identified in human cases of copper toxicosis (van de Sluis *et al.*, 2002). COMMD1 interacts with the copper transporter (ATP7B), which is responsible for biliary copper excretion. The interaction between these molecules was mapped to the N-terminus of ATP7B, the region containing the metal-binding domains of this molecule. It has been inferred from this finding that COMMD1 somehow facilitates ATP7B-mediated copper excretion, although the mechanism for this effect is unknown (Burstein *et al.*, 2005). Interestingly, the association of copper deficiency with cardiomyopathy and other forms of cardiac disease has been well recognised (Klevay, 2000). Copper depletion-induced cardiomyopathy is characterised by concentric cardiac hypertrophy such as occurs in the pressure overloaded heart (Elshерif *et al.*, 2004). The deterioration in cardiac function and morphology is reversible upon copper repletion. In particular, copper repletion improved copper depletion-induced myocardial structural lesions, normalised depressed cardiac systolic and diastolic functions, and restored the response of cardiac muscle to  $\beta$ -adrenergic stimulation (Elshерif *et al.*, 2004).

### *COMMD4 and C1C2 cMyBPC*

The Y2H protein-protein interaction assay showed that COMMD4 had specificity for the cMyBPC motif, judged by the inability of COMMD4 to bind to flanking domains, C1 or C2 (Table 3.15). COMMD4 bound to the cMyBPC motif in a manner analogous to myosin S2 i.e. when the cMyBPC motif mimicked the unphosphorylated or minimally phosphorylated state, COMMD4 was able to interact with the C1C2 region, but upon mimicking of trisphosphorylation of the cMyBPC motif, the interaction was abolished. Protein-protein sequence analysis (Section 3.1.4.1) showed that COMMD4 has no structural or sequence homology to myosin S2 and the interaction is therefore not considered to occur based on structural similarity. The Y2H interaction between COMMD4 and cMyBPC was supported by 3D *in vivo* co-localisation in differentiated cardiac cells (Figure 3.16), although no support for interaction of these proteins was obtained in an *in vitro* setting (Co-IP; Figure 3.6-7). The reasons for Co-IP not supporting an interaction for COMMD4 and N-terminus cMyBPC are not clear. Both bait and prey controls showed that the fusion-proteins were precipitable by the respective antibodies, in addition the reagents and assay protocol was the same as for previous Co-IP experiments. One possibility is that COMMD4 may require the formation of S-S bonds to take on its tertiary structure; these bonds may form in yeast, but are not likely to occur in the *in vitro* translation system.

The observed interaction between COMMD4 and cMyBPC may explain results obtained in the study by Sarikas *et al* (2005). Sarikas *et al* (2005) showed that the expression of a mutant cMyBPC protein M7t (expressing only domains C0 and partial C1; 80% cMyBPC deletion and lacking the cMyBPC motif) was associated with peri- and intranuclear ubiquitinated aggregates that were not observed with mutant protein M6t (expressing C0 to partial deletion of domain C10; 3% cMyBPC deletion) or wild-type cMyBPC in cardiac myocytes. These aggregates were composed of mutant M7t that were marked for degradation, but could not be processed further. These findings suggested that the proteasome function was inhibited by the mutant aggregates, but the mechanism by which this occurred was not clear, leading the authors to speculate that the mutant cMyBPCs provided an unusually strong signal for degradation and effectively competed with other degradation-prone proteins for the proteasome (Sarikas *et al.*, 2005).

As COMMD proteins have been proposed to associate with ubiquitin ligases and be involved with protein turnover (Burstein *et al.*, 2005), the formation of ubiquitinated aggregates and the impairment of the UPS by the mutant cMyBPC (M7t) lacking the cMyBPC motif may be related to its inability to bind to COMMD4. It could be proposed that although these short truncated proteins went through the first step of being marked for processing, they could not be polyubiquitinated because of the inability to bind to COMMD4. The M6 mutant that retained the cMyBPC motif and thus the ability to interact with COMMD4 did not form ubiquitinated aggregates. The impairment of the UPS and excessive COMMD4 availability, in this model, may have detrimental effects on the cardiomyocyte. UPS-mediated proteolysis degrades abnormal proteins (oxidized, misfolded or mutant proteins) thereby serving as a essential quality control mechanism in the cell. The UPS also ensures timely removal of normal proteins (such as signalling proteins and transcription

regulators) when their jobs are done. If the UPS is inhibited, persistence of these proteins can lead to downstream activation of transcription, switching on processes such as the foetal gene program that result in cardiac hypertrophy (Powell, 2006).

Additionally, the lack of a substrate for COMMD4 (such as may occur in certain MyBPC HCM mutations according to the model outline above) would lead to an accumulation of COMMD4, which may result in increased clearing of copper, in turn leading to copper depletion. Cell culture models, animal models and human models have shown that copper depletion leads to cardiomyocyte hypertrophy (Elsherif *et al.*, 2004) which may have relevance to HCM. On the other hand, excessive COMMD4 could also be protective against the development of hypertrophy as COMMD proteins are proposed to inhibit NF- $\kappa$ B. However, NF- $\kappa$ B can also be activated through a number of other signalling pathways, [including phosphoinositol 3-kinase, NFAT, Ca<sup>2+</sup>-calmodulin kinase IV, Ras, gp130, and Janus kinase/signal transducers and activators of transcription-mediated signalling pathways] (Hall *et al.*, 2006), therefore COMMD inhibition of NF- $\kappa$ B may not be sufficient to inhibit this pathway. Thus, findings from this study suggest a plausible link between N-terminus truncation *MYBPC3* mutations, impairment of the UPS system and the development of cardiac hypertrophy in cMyBPC-associated HCM.

Further, the study by Kulikovskaya *et al* (2007), described in section 1.9.3.5.11.1, reported that cMyBPC existed in two different forms that produced either stable or unstable thick filaments (Kulikovskaya *et al.*, 2007). The stable form had well-ordered myosin heads and required cMyBPC phosphorylation while the unstable form was associated with disordered myosin heads and unphosphorylated cMyBPC. In tissue with intact cardiac cells, the unphosphorylated cMyBPC was more easily proteolysed, causing cMyBPC and myosin to be released. Antibody staining of the cMyBPC proteolytic fragments showed that the C5C10 region underwent proteolysis as anti-C5 or anti-C8C9 could not stain these fragments (Kulikovskaya *et al.*, 2007). It is possible that upon the release of unphosphorylated cMyBPC, COMMD4 in association with ubiquitin ligases are responsible for ubiquitinating the N-terminus cMyBPC proteolytic fragments and marking it for degradation by the UPS. Since phosphorylated cMyBPC is stable and still intact with the thick filament, COMMD4 proteins do not associate with it. This scenario may explain the Y2H data (Table 3.15), which showed that COMMD4 could not interact with phosphorylated C1C2 (C1P<sub>1</sub>P<sub>2</sub>P<sub>3</sub>C2) while less phosphorylated C1C2 mimics can interact with COMMD4.

Preliminary results of a further Y2H library screen of a cardiac cDNA library (performed in our laboratory) using COMMD4 as “bait” has identified further components of the UPS as interactors of COMMD4. These proteins, including the Down syndrome critical region 3 protein (DSCR3), sorting nexin 3 (SNX3), F-box and leucine-rich repeat protein 10 (FBXL10) and legumain (LGMLN) are involved in protein trafficking and degradation, substantiating the hypothesis that COMMD proteins, and COMMD4 in particular, are involved in protein turnover/degradation in the cardiac cell (C Swanepoel, personal communication).

#### **4.1.3.4.2 Heat Shock 27 kDa Protein Family, Member 7 (Cardiovascular)**

HSPB7 (cvHSP) is a cardiac-specific member of the small heat shock protein (sHSP) family. Members of this diverse protein family are characterised by a relatively low monomeric molecular mass (15-43 kDa) and the conserved  $\alpha$ -crystallin domain (~100 amino acid residues) located towards the C-terminus (Liberek *et al.*, 2008). The  $\alpha$ -crystallin domain is involved in the formation of both homo- and hetero-dimers, which have been observed for several sHSPs. At least 10 mammalian sHSPs have been identified, viz. HSPB1 (HSP27/28), HSPB2 (MKBP), HSPB3 (HSPL27), HSPB4 ( $\alpha$ A-crystallin), HSPB5 ( $\alpha$ B-crystallin), HSPB6 (HSP20/p20), HSPB8 (HSP22/H11), HSPB9 and HSPB10 (ODF1) (Ferns *et al.*, 2006).

Rapid synthesis of sHSPs is triggered by diverse cellular stresses, including elevated temperatures, exposure to toxins, inflammation, ischaemia and hypoxia (Pipkin *et al.*, 2003). Most HSPs function as chaperones and their essential role is to maintain normal cellular function by interacting with mal-folded proteins to either repair them or signal their degradation, thereby preventing their aggregation into large deleterious complexes (Doran *et al.*, 2007). In contrast to high-molecular-mass HSPs, sHSPs represent ATP-independent chaperones (de Jong *et al.*, 1993). In response to cellular stress, poly-disperse assemblies of sHSPs appear to disintegrate into smaller subunits, which is followed by binding to unfolding substrate and then reforming into larger complexes (Stamler *et al.*, 2005).

The induction of cytosolic HSPs is also linked to the function of the UPS. Inhibition of the UPS in cardiomyocytes leads to an increase in the expression of HSPs such as HSP27, which renders early cardioprotection against sublethal heat stress (Stangl *et al.*, 2002). Further, there is a dramatic increase in HSPB7 and  $\alpha$ B-crystallin expression in aged rat muscle (Doran *et al.*, 2007), which agrees with a study by Yamaguchi *et al* (2007) on aged human fibers. Since a variety of cellular and molecular changes occur during aging (including fiber type shifting-induced remodelling of the contractile apparatus and reduced capacity of the UPS), the upregulation of HSPs may represent an auto-protective mechanism to prevent the deleterious accumulation of non-functional protein aggregates and counteract severe muscle damage (Doran *et al.*, 2007). Further,  $\alpha$ B-crystallin has been shown to interact with components of the SCF E3 ubiquitin ligase complex (Section 1.7.3; Pickart and Eddins, 2004).

Specifically, HSPB7 is preferentially expressed in cardiovascular tissues, where it is known to interact with  $\alpha$ -filamin (or actin-binding protein 280), providing stability to the dimerised filamin (Krief *et al.*, 1999). In muscle cells, HSPB7 exists in complex with HSP22, HSP27, HSPB2, HSP20 and  $\alpha$ B-crystallin (Fontaine *et al.*, 2005). These hetero-dimers and hetero-oligomer complexes of sHSPs are poorly defined and essentially nothing is known about their functional significance. Since there is little literature on the role of HSPB7 in the myocardium, studies on other sHSP that complex with HSPB7 and share the conserved  $\alpha$ -crystallin domain in the myocardium may provide some insight on the function of HSPB7 by taking the “guilt by association” approach.

$\alpha$ B-Crystallin comprises 3-5% of the total soluble protein content of cardiac muscle, and it moves from the general distribution of the cytosol to cardiac myofibrils following ischaemia to protect the myofibrils from extensive structural damage (Golenhofen *et al.*, 1999). Also,  $\alpha$ B-crystallin interacts with the N2B region of titin (Section 1.6) where atomic force microscopy show that it stabilises titin's Ig domains and decreases the probability of Ig domain unfolding under conditions of stress such as  $\beta$ -adrenergic stimulation (Bullard *et al.*, 2004).

In addition to  $\alpha$ B-crystallin (Morrison *et al.*, 2004), HSP20 (Fan *et al.*, 2005) and HSP27 have been shown to offer cardioprotection under conditions of stimulated ischaemia/reperfusion injury (Martin *et al.*, 1997). HSP27 protects cTNI and cTNT from ischaemia/reperfusion induced degradation by preventing their proteolytic cleavage (Lu *et al.*, 2008). Such protection may result in restored post-ischaemic myofilament response to  $\text{Ca}^{2+}$  and improvement post-ischaemic contractile function (Lu *et al.*, 2008). Since sHSPs share the  $\alpha$ -crystallin domain, researchers suggested that other members of the sHSP family might also have protective effects. Thus, HSPB7 may also perform such functions although this has not been shown experimentally. Interestingly, HSP27 also localises to a quantitative trait locus for cardiac hypertrophy in a rat model (Hammert *et al.*, 1996), while activation of HSP20 increases myocyte shortening by increasing  $\text{Ca}^{2+}$  uptake (Pipkin *et al.*, 2003); hence sHSPs influence both myocyte structure and function.

#### *HSPB7 and C1C2 cMyBPC*

The present study has shown by Y2H analyses (Table 3.15), Co-IP (Figure 3.3) and 3D *in vivo* co-localisation (Figure 3.18), that HSPB7 is an interactor of cMyBPC. Both small HSPs and phosphorylated cMyBPC (Sadayappan *et al.*, 2006) have been shown to be cardioprotective against ischaemic/reperfusion injury. It is possible that HSPB7 and cMyBPC may work together to protect the myocardium from this kind of injury. Alternately, HSPB7 may interact with cMyBPC, protecting it during ischaemic injury and preventing cMyBPC cleavage, analogous to HSP27 interacting with cTNI and cTNT (Lu *et al.*, 2008). Further, it is also possible that HSPB7 interacts with the N-terminus cMyBPC upon  $\beta$ -adrenergic stimulated phosphorylation to stabilise the region, similar to the interaction of  $\alpha$ B-crystallin and titin N2B region (Bullard *et al.*, 2004). The N-terminus may also require additional support during contraction/relaxation if it bound to the thin filament (data from present study) to ensure that these Ig domains do not unfold during the stress of enhanced cardiac contractility. These hypotheses are speculative and require experimental verification.

#### **4.1.3.5 KINASE ADAPTORS**

The generation of ubiquitous second messengers (cAMP, cGMP and  $\text{Ca}^{2+}$ ) in response to many different extracellular stimuli requires tight regulation to ensure appropriate and specific cellular responses. This is achieved by subcellular compartmentalisation, which places signalling enzymes from the same or from different pathways in close proximity to their target, within signalling complexes. Binding of signalling enzymes to such complexes is mediated by proteins that are collectively termed adaptor proteins

(Schechtman and Mochly-Rosen, 2001). A number of adaptor proteins have been described: specifically, A-kinase anchoring protein (AKAP) anchors PKA, while receptors for activated C-kinase (RACK) anchor PKC. Substrate specificity is not exclusive, as AKAPs interact with other signalling proteins such as phosphodiesterases (PDEs; Section 1.5.11) and phosphatases, while RACKs (Section 4.1.3.4.2) are also known to have multiple interactors.

#### 4.1.3.5.1 Phosphodiesterase-4D-Interacting Protein (PDE4DIP)

Myomegalin or PDE4DIP (phosphodiesterase-4D-interacting protein) is a novel protein with structural/scaffold properties, which localises to the sarcomere in cardiac and skeletal muscle. Y2H analyses using myomegalin as “bait” to screen a skeletal muscle library has identified a phosphodiesterase, PDE4D, as an interacting partner (Verde *et al.*, 2001). As described in section 1.5.11, the PDE superfamily is responsible for the local degradation of second messengers and the type 4 PDEs are specifically involved in the degradation of cAMP second messengers, which activate PKA. Due to its association with this PDE component, myomegalin/PDE4DIP is proposed to function in cAMP signal compartmentalisation as an AKAP, bringing PDE4D to a site in muscle cells where several steps in the cAMP signalling cascade take place. This cascade is particularly relevant to cMyBPC, which is a PKA target, during  $\beta$ -adrenergic stimulation.

Further, the importance of appropriate compartmentalisation of second messengers is highlighted in the study by Fink *et al* (2001), where the disruption of the AKAP-mediated PKA anchoring in cardiac myocytes altered contractile function during  $\beta$ -adrenergic stimulation. Test myocytes were more responsive to the increased intracellular  $\text{Ca}^{2+}$  concentration resulting from activation of  $\beta$ -adrenergic signalling. Also, PKA-dependent phosphorylation of cTNI and cMyBPC (upon  $\beta$ -adrenergic stimulation) were significantly reduced in cells which showed decreased compartmentalisation of PKA due to the disruption of the AKAP-mediated PKA anchoring compared to control cells. These findings demonstrate that, in response to  $\beta$ -adrenergic stimulation, cardiomyocyte function and substrate phosphorylation by PKA is regulated by targeting of PKA by AKAPs (Fink *et al.*, 2001).

#### PDE4DIP and C1C2 cMyBPC

The Y2H direct protein-protein interaction assay showed that both PDE4DIP clones (P272 and P205) interacted with the cMyBPC baits in a manner such that the region of interaction of PDE4DIP on the N-terminus cMyBPC could not be mapped (Table 3.15). As PDE4DIP showed no structural or sequence homology to myosin S2 (which may have accounted for its interaction with N-terminus cMyBPC) and given the probability that PDE4DIP functions as an AKAP, being able to interact with a phosphodiesterase and possibly cMyBPC (a PKA target), PDE4DIP was considered a putative true interactor of cMyBPC and was followed up by verification studies. Co-IP reactions (Figure 3.4) confirmed the interaction between PDE4DIP and the C1C2 region, while 3D *in vivo* co-localisation (Figure 3.17) showed that PDE4DIP and cMyBPC share the same subcellular space within the cardiac cell.

As part of a larger study in our laboratory to build the cMyBPC interactome, PDE4DIP (isoform 4) was used as “bait” to screen a cardiac cDNA library and multiple PKA targets, including cTNI, were identified (G Uys, personal communication). Additionally, in this study, Y2H interaction assays showed that PDE4DIP interacted directly with two PKA regulatory isoforms, PRKAR1A and PRKAR2A. Interaction with at least one PKA regulatory subunit is a condition for a protein to be classified as an AKAP. These findings lend support for the hypothesis that PDE4DIP acts as an AKAP in cardiac muscle. Thus, PKA may dock to the N-terminus of cMyBPC by means of PDE4DIP in order to effect phosphorylation of the MyBPC motif and cTNI.

#### **4.1.3.5.2 Guanine Nucleotide-Binding Protein Subunit Beta-2-Like 1 (GNB2L1)**

Guanine nucleotide-binding protein subunit beta-2-like 1 (GNB2L1) or RACK1 (Receptors for Activated C-Kinase 1) is a WD40-repeat containing protein that forms part of a family of adaptors proteins called RACK’s (Schechtman and Mochly-Rosen, 2001). RACKS were originally shown to serve as binding proteins for PKC; however, a wide variety of proteins such as Src, integrin  $\beta$ -subunits,  $\gamma$ -aminobutyric acid (GABA) receptors and PDE4D5 have been shown to be interactors. The functional consequences of the interaction between PDE4D5 and GNB2L1 have not been elucidated, but the most probable role is that recruited PDE4D5 controls cAMP levels in the vicinity of the complex and thus regulates the PKA-driven phosphorylation of GNB2L1-associated proteins (Houslay and Adams, 2003). Further, RACK1 has been shown to function as a “raft” or shuttling protein which moves the signalling complex from one cellular site to another, likely resulting in different molecular events at each site depending on the available substrate (Schechtman and Mochly-Rosen, 2001).

#### *GNB2L1 and C1C2 cMyBPC*

GNB2L1 interacted with the C1C2 region in a similar manner to PDE4DIP, and the region of interaction on C1C2 could not be mapped to any particular domain within this region (Table 3.15). Further, GNB2L1 does not share any structural or sequence homology to myosin S2, and so is not likely to be a false interaction driven by similarity to another C1C2 interactor. Adaptors are capable of binding to a number of different enzymes concomitantly, therefore, the fact that the cMyBPC motif is not a substrate for PKC *in vivo* may not be relevant to discount GNB2L1 as a putative interactor of C1C2 cMyBPC, as other PKC sites may exist on cMyBPC. Its interaction with PDE4D5 suggests that GNB2L1 may also be involved in cAMP signalling and may be relevant to cMyBPC phosphorylation. So, while GNB2L1 was not investigated further than the Y2H protein-protein interaction assay in the present study, it should form part of other studies investigating AKAPs in the heart in our laboratory.

#### **4.1.3.6 ENZYME INTERACTORS**

##### **4.1.3.6.1 $\beta$ -Enolase (ENO3)**

Cytosolic enzymes that supply energy for movement and transport are not distributed uniformly throughout the cytoplasm, but are located in particular areas of the cell. This distribution is especially important for

muscle cells, which intermittent high-energy requirements. Under these conditions, ATP is derived primarily from glycolysis (Suarez, 2003). One of the terminus steps of glycolysis, the conversion of 2-phospho-D-glycerate (2-PGA) to 2-phosphoenolpyruvate (PEP), is catalysed by the enzyme enolase (2-phospho-D-glycerate hydrolase). In striated muscles, enolase is a dimeric protein formed from three subunits ( $\alpha$ ,  $\beta$ , and  $\gamma$ ) which are encoded by different genes, *ENO1*, *ENO3* and *ENO2*, respectively (Feo *et al.*, 1990). The  $\alpha\alpha$  homodimer accounts for the entire enolase activity during early embryogenesis, and is also the isoform expressed in most adult tissues. However, in the brain and in striated muscles (two tissues with high energy requirements), an isoform transition occurs:  $\alpha\gamma$  and  $\gamma\gamma$  isoforms are expressed in the brain, while  $\alpha\beta$  and  $\beta\beta$  isoforms occur in striated muscles (Comi *et al.*, 2001). The isoform transition in skeletal muscle cells results from a differential regulation of the  $\alpha$ - and  $\beta$ -enolase mRNA levels. Postnatally, there is a large increase in total enolase activity due to the specific accumulation of  $\beta\beta$ -enolase, whereas the  $\alpha\alpha$ -enolase decreases to negligible levels. Additionally, the thyroid hormone partially controls the expression of enolase in developing striated muscles (Merkulova *et al.*, 2000).

In the sarcomere,  $\beta$ -enolase has been localised to both the Z-disc and M-line (Keller *et al.*, 2000). At the M-line,  $\beta$ -enolase interacts with creatine kinase (Foucault *et al.*, 2000), which also interacts with other metabolic enzymes (such as phosphofructokinase and adenylate kinase) and is linked to M-line titin *via* interaction with adaptor protein FHL2 (described in section 1.5.5) (Lange *et al.*, 2006). FHL2 is also targeted to the I-band, where it interacts with the N2B region of titin, linking the metabolic enzyme complex to this region. Recruitment of metabolic enzymes to the sarcomere has previously been suggested to provide a structural role (Clark *et al.*, 2002), thus these complexes may provide additional stability to the I-band and M-lines. Taken together, these findings show that metabolic enzyme complexes are common in the sarcomere at sites of high energy demand (Lange *et al.*, 2006). The finding in the present study of an interaction between  $\beta$ -enolase and C1C2 cMyBPC suggests that a full ATP-producing segment containing glycolytic enzymes may also be operating in the C-zone.

#### *$\beta$ -Enolase and C1C2 cMyBPC*

The Y2H interaction data showed that  $\beta$ -enolase interacted with both domains C1 and C2, thus specificity to a region within the C1C2 region could not be established (Table 3.15). While Co-IP reactions could not be assessed as the C1C2 phosphorylation-mimics and  $\beta$ -enolase migrated together by SDS-PAGE (Figure 3.10), 3D *in vivo* co-localisation showed that  $\beta$ -enolase and cMyBPC exist in the same subcellular space within the mature cardiac cell (Figure 3.19). Thus, this study provides the first evidence of the association of cMyBPC with a glycolytic enzyme, viz.  $\beta$ -enolase. cMyBPC is phosphorylated during  $\beta$ -adrenergic stimulation (Section 1.9.3) which, in association with other proteins, works to increase the power output of the myocardium during the “fight-fright-flight” response. The energy requirement during this brief bout of work is supplied by glycolysis; therefore it is plausible that it would be advantageous for an energy producing complex to associate with cMyBPC.

Further, another enzyme AMP-activated kinase (AMPK) which is involved in cardiac energy homeostasis has been identified as an interactor of domain C8 of cMyBPC (Harding, personal communication). When AMPK is activated it functions to protect the cell from critical ATP depletion by activating glycolysis and fatty acid uptake during hypoxic stress or extreme metabolic demand (Blair *et al.*, 2001). Mutations in the gene which encodes the  $\gamma$ 2 subunit of AMPK underlie some cases of HCM. Considering  $\beta$ -enolase's role in local energy production and the proposed interaction with cMyBPC, it is an ideal candidate to screen for HCM-associated mutations or investigate as a modifier of the hypertrophic phenotype in HCM.

#### 4.2 Y2H PROTEIN-PROTEIN INTERACTION STUDIES

Y2H direct protein-protein interaction studies were used to determine whether the phosphorylation status of the cMyBPC motif influenced the interaction between the putative positive interactors and the C1C2 region of cMyBPC (Table 3.15). cMyBPC is a sarcomeric-anchored protein and the constraints of a lattice may be critical for the manner and nature of its interactions with other proteins; therefore data from Y2H interaction assays between fragments of protein should be interpreted with this in mind.

##### *C1C2 interactions*

The negative control, C0C1, used for the assay may not have been ideal for all investigations, as it contained a domain (C1) that is a part of the bait constructs subject to investigation by the same assays; on the other hand, it allowed investigation of interactions of the C0-pro-ala-rich region in a more natural conformation. Some preys interacting with domain C1 also interacted with the pGBK-C0C1 construct [cMyBPC (C412 and P62), PDE4DIP (P272 and P205); Table 3.15], and it is not clear whether these preys are also interactors of domain C0 and/or the pro-ala-rich linker. Inclusion of a bait construct encoding only domain C0, in these assays, may have helped in discriminating the region involved in the interaction.

##### *C0C2 interactions*

The C0-pro-ala-rich region does indeed appear to interfere with the interactions of the C1C2 region with some, but not all, putative positive preys, in this setting. No interactions were seen between any of the C0C2 baits and COMMD4, actin, cTNI, ENO3, GRINL1A, UACA and GNB2L1. These preys interacted strongly with the C1C2 region, therefore the lack of interaction with the C0C2 baits indicates interference by the C0-pro-ala-rich region. This interference appears to be constitutive as the C0-pro-ala-rich linker region is able to block the interaction with domain C1C2 under all phosphorylation conditions. This may not be the case inside a cardiac cell where the interactors of domain C0/pro-ala-rich linker are present (actin or myosin has been suggested; section 1.9.3.5.9-10) and the steric constraint of a sarcomeric lattice may affect the observed regulatory activity of C0-pro-ala-rich region on the interactions of the C1C2 region. These sarcomeric factors are not present in the yeast cell and this may be the reason why C0C1 interferes with these interactions under all phosphorylation conditions. This however does not explain why the C0-pro-ala-rich region does not interfere with the C1C2 interactions of cMyBPC clones, PDE4DIP and SYNE1. However, it may be that the C0-pro-ala-rich region constrains interactions with particular binding surfaces within the C1C2 region (each

Ig domain is considered to have at least four possible binding surfaces), and that these interactors make use of alternate binding surfaces of the C1C2 region. The functional role of the C0-pro-ala-rich region with regard to the interactions of C1C2 is not entirely clear and may best be investigated within the context of muscle cells.

#### 4.2.1 Limitations of Y2H analysis

Y2H is an extremely powerful assay with which to identify novel protein-protein interactions by screening libraries of tissue-specific cDNAs. The use of the yeast host can be considered an advantage for the investigation of mammalian protein interactions, in that it is an *in vivo* technique which bears a greater resemblance to higher eukaryotic systems than a system based on a bacterial host (Sobhanifar, 2003).

This technique does have some limitations which do not necessarily reduce the usefulness of the technology. Standard Y2H library assay approaches generally underestimate the number of interactions because forced subcellular localisation of bait and prey in the yeast nucleus may preclude certain interactions from taking place, such as those involving integral membrane proteins. In addition, interactions that require specific post-translational modifications (such as disulphide bridge formation, glycosylation, or phosphorylation) may not be detectable by Y2H unless the enzymes responsible for the modification happen to be present in the yeast (Cusick *et al.*, 2005). Also, certain proteins, when expressed in the yeast or targeted to the nucleus, may become toxic to the host, while other proteins may degrade essential yeast proteins or proteins whose presence is required for the assay (Sobhanifar, 2003).

The greatest disadvantage of using the Y2H system for identifying protein-protein interactions is its false-positive detection rate. This system detects a significant number of interactions that have no obvious or testable biological significance. Technical false-positives can be eliminated from screens by rigorous testing of reporter gene activation and heterologous mating. However, when technical false-positives are fully accounted for, there may still remain interactions that are reproducibly real and do not involve binding to the GAL4 domains or direct interaction with DNA, but are not plausible based on existing functional annotation of the proteins involved. These interactions may well be biological false-positives that arise from the forced, out-of-context expression of baits and preys. However, this is not necessarily the case as there is a growing list of “moonlighting” proteins performing multiple, apparently unrelated functions. Many moonlighting proteins are metabolic enzymes with additional functional activity, although numerous signalling, structural and nucleic acid binding proteins are also multifunctional (Jeffery, 2003; Sriram *et al.*, 2005).

As a consequence of these specificity issues, independent verification of a putative protein-protein interaction is essential. There are two distinct aspects to validating Y2H interactions. One is to determine if the two-hybrid reporter activity is indicative of a true specific binary protein interaction. This can be addressed by demonstrating the interaction with a different assay, such as the co-immunoprecipitation approach used in the present study. The second, much more important question is whether the interaction

takes place *in vivo* where it plays some functional role in the organism (Parrish *et al.*, 2006); to address this question, co-localisation in live, physiologically relevant cells were used in the present study.

#### 4.3 VERIFICATION STUDIES

##### 4.3.1 Co-IP

The Y2H vectors (pGBKT7 and pACT2) are designed with antibody tags and a T7 promoter sequence, to allow *in vitro* transcription/translation of the clones, facilitating Co-IP experiments as a verification approach. Therefore, this technique allows for rapid assessment of protein-protein interactions following Y2H identification. Additionally, the organisation of the vector allows generation of putative interactor-epitope tagged fusion proteins, excluding the GAL4 domains, thus allowing bait-prey interactions to be tested in the absence of these transcription factor domains and excluding any role for these domains in the proposed interaction. Co-IP was used to verify the bait-prey interactions identified in the various library screens, as well as to assess the effect of the various phosphorylation-mimic states on the proposed interactions.

For the C1C2 region, Co-IP confirmed the interactions of actin, cMyBPC (C5C10), HSPB7 and PDE4DIP with this region. No interactions of C1C2 cMyBPC with either COMMD4 or TNNT2 was observed, while the C1C2 cMyBPC interactions with cTNI and β-enolase could not be assessed because the bait and prey peptides separated too closely to each other. The negative control reactions for five of the Co-IP experiments were contaminated by the prey protein's non-specific interaction with the protein G agarose in the absence of an antibody. This was problematic, as the prey protein precipitated in the Co-IP reaction could not completely be attributed to the interaction with the bait. Using pre-washed protein G agarose is an accepted way of reducing this non-specific interaction, and was employed in this study; however neither this precaution, nor increasing the number of wash steps or increasing the stringency of the wash buffer could minimise the non-specific interaction. Therefore, in order to facilitate analyses of these interactions, the autoradiographs of samples with non-specific protein G interaction were scanned using a densitometer and the density of bands in the protein G control lanes subsequently subtracted as background from the densities in the Co-IP reaction lanes. However, in some cases proteins that were not well separated on the gel not be distinguished as separate bands by the densitometer. Furthermore, varying the acrylamide concentration of the gels (15-20%) did not improve separation of proteins with similar masses in this study. Western blots performed in our laboratory using the radio-labelled proteins from the *in vitro* transcription/translation reactions and either the HA- or cMyc-antibodies revealed multiple bands on the autoradiograph, presumably originating from the rabbit reticulocyte system used, that complicated the interpretation of the data. A solution to this problem may be to perform western blots on proteins derived from *in vivo* Co-IP, preferably using monoclonal antibodies against the endogenous proteins of interest.

For the COMMD4 and cTNT interaction with the C1C2 baits, the Co-IP experiment showed that there were no interactions with C1C2, in contrast to the Y2H data. Further, Co-IP suggested interactions between the

C0C2 phosphorylation-mimics and each of HSPB7, actin,  $\beta$ -enolase, and cTNI, in contrast to the Y2H data. As Co-IP is an *in vitro* assay, and made use of a rabbit reticulocyte system in this study, the physiological activity, and the proper folding of the translated proteins cannot be determined, while any post-translational modification, which may still have taken place to some extent within the yeast, is likely to be absent. Furthermore, it is also possible that during PCR amplification of the insert or during transcription nucleotide modifications were introduced, leading to altered proteins that alter the nature of the interactions compared to that observed in yeast.

#### **4.3.2 Three-dimensional *in vivo* co-localisation**

Conventional co-localisation determines if proteins share the same subcellular space by overlaying 2-dimensional images captured in the different colour channels. In this study, the tagged proteins were determined to be co-localised by performing a z-stack analysis which considers co-localisation throughout the depth of the cell, i.e. in a third dimension. By this technique cMyBPC (C1C10) was shown to occupy the same subcellular space as HSPB7,  $\beta$ -enolase, PDE4DIP and COMMD4, respectively. Cells mock transfected with water were used as negative controls. These control cells were also differentiated and photographed using the same conditions as the test cells, and no GFP, YFP or RFP expression was observed. The morphology of the mock transfected and negative control cells were also indistinguishable. It has been previously shown that over-expression of cMyBPC-GFP was completely benign: the cardiomyocytes were able to effectively regulate the overall stoichiometry of the cMyBPC pool (Yang *et al.*, 1998).

As the spectra of GFP and YFP overlapped, the co-localisation of cMyBPC with COMMD4 and PDE4DIP were performed differently compared to the GFP-RFP co-localisations. Separate images of GFP- and YFP-only transfections were acquired for the process of spectral unmixing. This is one of the important considerations when choosing fluorescent protein tags to be used in co-localisation studies, as the emission and excitation spectra of the fluorescent protein need to be sufficiently far apart to avoid bleed through. However, this problem can be overcome by the use of spectral unmixing, although it requires additional, time-consuming software manipulation and may result in a decrease in the co-localisation signal.

##### **4.3.2.1 Limitations of *in vivo* co-localisation**

The other considerations when choosing fluorescent protein tags is that the pair should have a high quantum yield, have low sensitivity to the cellular environment (ionic interactions, pH) and should be photo stable (Berggard *et al.*, 2007).

Although in most cases completely inert, the GFP-tag is quite large (24x42 $\text{\AA}$  in diameter; Ormö *et al.*, 1996) and may interfere with normal behaviour of the target protein (Falk and Lauf, 2001). Furthermore, over-expression and/or tagging may sometimes cause a protein to become incorrectly localised. Therefore, as an alternative to transient expression of tagged proteins, the localisation of endogenous proteins can be studied. This, however, requires the availability of highly specific primary antibodies raised against the proteins of

interest. A potential problem with detection of endogenous protein is that the components of the protein complex may not be expressed sufficiently in the cell lines studied to facilitate detection by antibodies (Berggard *et al.*, 2007).

The resolution of the conventional light microscope is limited by the diffraction of light to approximately 200nm, with objects that are closer together than this appearing as a single object (Lalonde *et al.*, 2008). For the present study, z-stack images were taken 260nm (0.26μm) apart, suggesting that considerable distances may actually separate proteins that appear co-localised by fluorescence microscopy. So while it is possible to determine if two proteins share the same subcellular space using this technique, it is not possible to tell if they actually associate. Thus, co-localisation should be considered as one of several pieces of evidence for a protein-protein interaction, but, like Co-IP, on its own it is insufficient to conclude that two proteins are in a complex (Lalonde *et al.*, 2008). This optical resolution limit can be overcome by using the technique of BRET.

#### 4.3.3 BRET

As described in section 2.18, the typical effective distance between the BRET donor and the acceptor is 10 to 100 angstroms (Å); a range that correlates well with most biological interactions (Pfleger and Eidne, 2003; Prinz *et al.*, 2006), thus making this an excellent tool to investigate the interactions between cMyBPC and the thin filaments, which share the same compartment within the sarcomere. The efficiency of resonance energy transfer (RET) depends on the relative orientation of the energy donor and acceptor, and decreases with the sixth power of their distance. Therefore if RET occurs, it indicates that the two partners interact physically rather than merely being co-localised in the same vicinity (Subramanian *et al.*, 2006).

True positive and negative control interactors expressed in the same subcellular compartment and at the same level as the test fusion proteins were not available for the present study. Therefore, the bait-Rluc and prey-GFP controls in addition to the mock-transfection control were used as the negative controls, while BRET ratio values of the test interaction that was statistically higher than the negative controls were considered as indicative of a positive interaction.

##### 4.3.3.1 Limitation of BRET

The power of BRET lies in the possibility of studying protein interactions in real time *in vivo*; however this technique is technically and experimentally demanding. BRET assays are generally carried out in a 96-well plate format with 50μl of cell suspension per well, containing approximately 50000 cells. Despite the apparently higher sensitivity of BRET, it has a very low signal output; as a result, more cells are needed to achieve sufficiently high luminescence levels, which also require long integration times (Pfleger and Eidne, 2006).

The large mean standard deviation observed in the BRET assays in the present study was likely due to the small number of replicates in each assay. Since for each test (C1/C2C10 cMyBPC versus actin/cTNI) two assay were performed (with and without  $\text{Ca}^{2+}$ /isoproterenol treatment), only four replicates per sample were possible. To try to reduce the large deviation, qualitative similar data from independent assays were pooled together, but did not reduce the standard deviation to desired levels. More experiments with additional replicates are required to be performed to reduce the deviation, but due to time constraints and the fact that BRET is technically and experimentally demanding, more assays could not be performed.

Interpretation of data from the BRET assays were further complicated by the high background contribution of the transfection (Figure 3.20A-21A) and bait/prey controls (Figure 3.23A). Also, compared to the actin and cTNI BRET assays (Figure 3.20-23), the mean BRET ratio for MCS assay (Figure 3.24) was very low (<1.6). The reduced BRET ratio could be due to a smaller amount of fusion protein available for the interaction being tested. This could possibly point to a lower transfection efficiency of cardiac myocytes, which are notorious for being difficult to transfect. A solution to this problem could possibly be the generation of a stable cell line expressing the various fusion constructs. In the present study, the cardiac myocytes were transiently transfected, which resulted in a mixed population of cells with a range of expression levels that may account for the large mean standard deviation. With a stable cell line, it may be possible to get a stronger more stable BRET signal from uniform expressing cells (Pfleger and Eidne, 2006). Additionally, knockdown of the endogenous cMyBPC may be advisable: As at least three cMyBPC proteins are localised in seven to nine of the 43nm-apart transverse stripes (Flashman *et al.*, 2004), as many cMyBPC-Rluc-tagged proteins need to be incorporated into the sarcomere in close proximity to the GFP-tagged interactors for BRET to occur. The likelihood that this happens with high efficiency in all sarcomeres in every cell is low, therefore variable readings within and between experiments are likely to occur, and may explain the large standard deviations observed in the present study. Further, since the endogenous proteins (actin, troponin I and cMyBPC) were also present they may have competed with the tagged proteins and reduced the number of donor-acceptor interactions (Pfleger and Eidne, 2006).

BRET requires proper orientation of the donor and acceptor dipoles without the interference of the interacting proteins. Before performing the test BRET assays, several optimisation experiments were performed to determine the most efficient BRET pair from the several C-terminus and N-terminus Rluc and GFP<sup>2</sup> fusion protein combinations that were generated. The combination with the strongest BRET signal above the background was chosen. Further, it was important to optimise the assay conditions with respect to the transfection conditions to avoid non-specific RET due to molecular crowding (Prinz *et al.*, 2006).

Steric hindrance by the rather large reporter proteins fused to the proteins of interest could hamper protein interaction. This problem could possibly be overcome by using smaller reporter proteins (e.g. *Gaussia princeps* luciferase, 20 kDa). Alternate labelling approaches that could be investigated include tetracysteine-

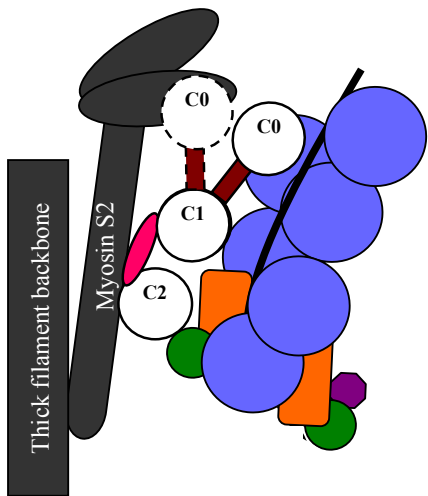
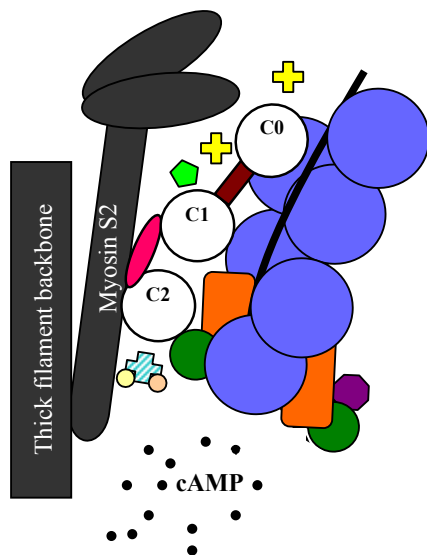
biarsenical system (Hoffman *et al.*, 2005); fluorescent nanoparticles (Lian *et al.*, 2004) or quantum dots (Clapp *et al.*, 2006).

#### 4.4 IMPLICATIONS FOR THE N-TERMINUS cMyBPC

The Y2H approach was used to identify interactors of C1C2 cMyBPC, with a view to identifying interactors that may point to additional functions or pathways in which the N-terminus region may be involved. By this approach, the putative interactors identified and verified by the present study indicate that N-terminus cMyBPC interacts with at least four different classes of proteins i.e. thin filament proteins (actin and cTNI), adaptor proteins (PDE4DIP), protein degradation/turnover proteins (COMMD4 and HSPB7) and energy producing enzymes ( $\beta$ -enolase). In addition, the N-terminus is able to interact with C-terminus domains of cMyBPC. Among these proteins, only actin has previously been proposed as an interactor, while the remaining interactions, to our knowledge, are novel. It is intriguing that deregulation of those pathways that these proteins are involved in result in cardiac dysfunction. Considering that only 60% of HCM-causing mutations have been identified, the putative positive interactors, and other components of the pathways that they are involved in, are ideal candidates to be interrogated for HCM-causing mutations or modifiers of the HCM phenotype.

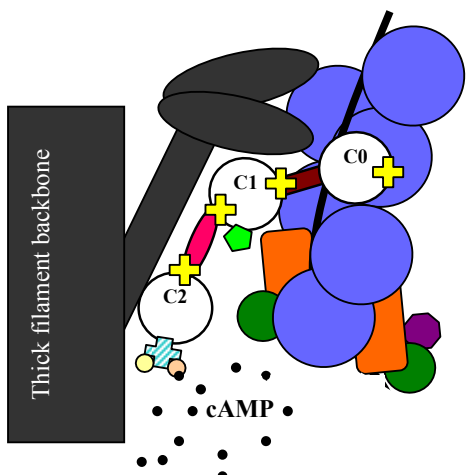
The interaction between myosin S2 and C1C2 has been well described, thus the question arises whether these newly proposed interactors compete with myosin S2 for C1C2 binding or whether a number of proteins can interact simultaneously, or consecutively. As described in earlier sections (Section 1.9.3.5.9.3 and 1.8.3.5.10), the N-terminus's binding partners are influenced by the phosphorylation status of the cMyBPC motif. The following scenario is put forward to account for the various interactions that are possible for the N-terminus cMyBPC and the potential implications of such interactions for the regulation of cardiac contractility. According to the BRET and Y2H interaction data of the present study, when the cMyBPC motif is unphosphorylated (thus, in contact with myosin S2, restraining the myosin heads from making contact with actin), domain C2 and/or the cMyBPC motif interacts with cTNI while C1 may interact with actin (Figure 4.4A). Additionally, the myosin heads appear disordered and the thick filament backbone has a narrow diameter, with the cMyBPC collar arranged around the backbone (Figure 4.2A).

As cMyBPC is anchored to the thick filament and titin *via* C-terminus regions, N-terminus interactions with the thin filament would cross-link the thin and thick filaments and provide mechanical and structural stability to the C-zone in the A-band. Such a hypothesis is supported in mouse models where cMyBPC-deficient myocardium is overly compliant and dilates as it is not be able to provide the requisite transmural wall stress at normal LV chamber dimensions to accommodate normal LV pressure (Palmer *et al.*, 2004a). This transmural wall stress is suggested to be provided as a result of cMyBPC's interaction with LMM and titin, but the cross-linking of the thick and thin filaments may also contribute to this end. Alternatively, an interaction with cTNI and/or actin may point to a mechanism whereby cMyBPC is able to activate the thin filament analogous to  $\text{Ca}^{2+}$  activation. The conditions and reasons for such activation is not apparent and may

**A****B**

When cMyBPC is unphosphorylated: cMyBPC motif interacts with myosin S2; domain C2 interacts with cTNI; C1 makes contact with actin; the pro-ala-rich linker supports domain C0 to interact with the myosin head. Alternatively both the pro-ala-rich linker and C0 interact with actin. The thick filament backbone has a narrow diameter. (see text for further details)

Upon a rise in second messenger cAMP that activates PKA, the following components are recruited to cMyBPC in anticipation of cMyBPC phosphorylation: PDE4DIP in association with PKA and PDE4D; β-enolase and HSPB7. (see text for further details)

**C**

cAMP activates PKA, which docks to the N-terminus via PDE4DIP. The N-terminus contacts β-enolase to support generation of energy for enhanced contractility. Upon cMyBPC phosphorylation by PKA: myosin S2 is released, freeing the myosin heads; the thick filament diameter increases, taking the myosin heads closer to actin, promoting interaction myosin/actin interaction; domain C2 may no longer interact with cTNI; C1-pro-ala-rich linker-C0 may interact with actin or other interactors. Cardiovascular heat shock protein (HSPB7) makes multiple contacts with the N-terminus providing additional stability during this period of stress. (see text for details)

Orange square	Troponin T
Blue circle	Actin
Green circle	Troponin I
White circle	cMyBPC Ig domain
Purple circle	Troponin C
Pink oval	cMyBPC motif
Black arrowhead	Myosin heads
Black bar	Myosin subfragment 2 (S2)
Cyan plus sign	PDE4DIP
Yellow circle	PDE4D
Orange circle	PKA
Green diamond	β-enolase
Yellow plus sign	Cardiovascular heat shock protein (HSPB7)
Curly bracket	Tropomyosin

**Figure 4.4.** Proposed interactions for the N-terminus cMyBPC. See text for details

be extended from the study of Razumova *et al* (2006) where C1C2 was able to activate thin filament mobility only in regulated thin filaments under conditions of low  $\text{Ca}^{2+}$  concentrations. It may also be possible that the C1C2 interactions facilitate the positioning of the pro-ala-rich linker and/or domain C0 for favourable interactions with actin, myosin or as yet unidentified interactor/s (Figure 4.4A). An interaction between the pro-ala-rich linker and a myosin component has been suggested by Herron *et al* (2006), who observed that exogenous addition of fragments containing the pro-ala-rich linker to the cardiac myocytes resulted in the activation of force production in the absence of  $\text{Ca}^{2+}$  (Section 1.9.3.5.9.3). Finally, the N-terminus interactions with cTNI and actin may contribute to the internal load (described in section 1.9.3.5.11.6) that is hypothesised to be the mechanism by which cMyBPC slows down crossbridge cycling.

Recent work by Nagayama *et al* (2007) reported that some of MyBPC's roles (such as slowing early contraction, increasing stiffness and sustaining systole, as well as enhancing relaxation at faster heart rates) are PKA-independent, and suggested that these constraints on contraction/relaxation was due to interactions between cMyBPC and other sarcomeric proteins. This perhaps is achieved through direct contact with the thin filament components, such as actin and the troponins as suggested in the present study. These N-terminus interactions are plausible, as recent studies have shown that the length of the cMyBPC motif and the flanking domains, C1 and C2 is sufficient to span the interfilament space and interact with the thin filament and/or other interactors (Jeffries *et al.*, 2008).

Upon  $\beta$ -adrenergic stimulation, the elevation in the levels of diffusible second messenger cAMP which activates PKA to phosphorylate a number of  $\text{Ca}^{2+}$  handling and sarcomeric proteins is proposed to trigger the following sequence of events. Only the PKA-mediated phosphorylation of cMyBPC will be included as the phosphorylation of other sarcomeric proteins and the consequences on cardiac dynamics have been described in previous sections (1.8.3.2-4). Membrane depolarisation which causes the release of a small quantity of  $\text{Ca}^{2+}$  via voltage-gated L-type channels possibly activates CamK-II, associated with cMyBPC, and adds the first phosphate to site B in the cMyBPC motif. It is plausible that this step occurs now since *in vivo* studies have shown that the addition of the first phosphate occurs at a  $\text{Ca}^{2+}$  concentration below that necessary for muscle contraction (McClellan *et al.*, 2001). This reaction induces a change in the thick filament from the disordered structure to a tight structure (myosin heads lying along the backbone). The transient increase in the cytosolic  $\text{Ca}^{2+}$  concentration is not sufficient to directly activate the myofilaments, but instead serves as a trigger to release  $\text{Ca}^{2+}$  from the sarcoplasmic reticulum via ryanodine receptors (Bers, 2005). The release of greater quantities of  $\text{Ca}^{2+}$  through  $\text{Ca}^{2+}$ -induced  $\text{Ca}^{2+}$  release results in an increase in  $\text{Ca}^{2+}$  affinity for TNC and subsequent conformational changes in TNC and cTNI (described in section 1.9.2) that culminate in the release of the inhibitory region from actin supporting actin-myosin contact and force generation.

Concurrently, to enhance cardiac contractility, cMyBPC is phosphorylated in the proposed following sequence of events. In anticipation of additional work and the requirement to provide additional energy to power the enhanced contractility, cMyBPC makes contact with  $\beta$ -enolase (a component of the energy

producing glycolytic complex) to facilitate production of ATP (Figure 4.4B/C). At the same time, the signalling complex “raft” comprising PDE4DIP, PKA, PDE4D and perhaps other signalling molecules, make contact with the N-terminus cMyBPC in close vicinity to the cMyBPC motif and cTNI. The interaction of  $\beta$ -enolase and PDE4DIP with the N-terminus cMyBPC may only be transient, lasting for the duration of  $\beta$ -adrenergic stimulation. Activation of PKA by cAMP results in the addition of the second and third phosphates to sites A and C of the MyBPC-motif (di- and trisphosphorylated MyBPC), producing greater order in myosin heads and looser packing of the myosin backbone (Levine *et al.*, 2001). The phosphorylation-induced release of the cMyBPC motif from myosin S2 releases the constraint from the myosin head; the contacts between C5:C8, C6:C9 and C7:C10 are abrogated; the collar loosens, now forming contacts between domains C2/C3 and C10, which allows the thick filament backbone diameter to expand (Figure 4.2B), taking a subset myosin heads close to the thin filament allowing a higher force development.

During this time it is uncertain whether domain C0 (and even pro-ala-rich-linker) is still attached to actin, myosin or have new interacting partners. If this region interacts with actin, as suggested by Kulikovskaya *et al* (2003a), when cMyBPC is phosphorylated, this interaction could also act as a load on contraction. Thus, the N-terminus may provide a consistent load against contraction. A possible function for the uninterrupted interaction of C0 and/or the pro-ala-rich linker with actin is so that some of the energy of systole could be stored by cMyBPC, which could assist in the filling of the heart during diastole. For cMyBPC to store energy effectively during systole, it must not detach and attach to actin during the contraction because attachment and detachment would dissipate the energy stored (Kulikovskaya *et al.*, 2003a) (Section 1.9.3.5.11.6). It is also uncertain what the interactors of domains C1C2 during this time may be. As suggested by the Razumova *et al* (2006) study, where a C1C2 fragment interacted with actin to slow down thin filament motility either in regulated or unregulated filaments (under high  $\text{Ca}^{2+}$  conditions), C1C2 may also aid in slowing down crossbridge kinetics by interacting with actin (Razumova *et al.*, 2006). Further work is required to establish the physiological significance and plausibility of these proposed interactions for the working heart.

As contractility is enhanced, upon  $\beta$ -adrenergic stimulation, and the pro-ala-rich linker and domain C0 are extended into the interfilament space to interact with its ligands, the N-terminus may require support to prevent the Ig domains from unravelling during this period of additional stress. This support may come from the association of the cardiac-specific heat shock protein, HSPB7, which has been shown to interact with cMyBPC in the present study (Figure 4.4C). This interaction with the N-terminus cMyBPC may also be a transient interaction for the duration of the additional stress.

Not all the interactors of the N-terminus cMyBPC that have been identified by this study may interact with cMyBPC when it is associated with the thick filament. As discussed in section 4.1.3.4.1, COMMD4 may interact with the dephosphorylated cMyBPC that has been released from the thick filament. COMMD4 may

function with other ubiquitin ligases to polyubiquitinate cMyBPC and mark it for degradation by the UPS. Thus, the N-terminus may regulate the turnover/degradation cycle of cMyBPC further highlighting the importance of this region.

The ability of the pro-ala-rich linker and domain C0 to regulate interactions of C1C2 and its interactors has been observed by the Y2H interaction assay (Table 3.15). This may represent a self-regulatory mechanism of the N-terminus, the function of which is unclear. Whether this is possible within the muscle cell, and the conditions under which this may occur, are not yet apparent and warrant further investigation.

Another question that needs to be asked is whether it is possible for one region of cMyBPC to have so many interactors. As cMyBPC may exist in 3 to 4 different forms within the cell based on the number of phosphates added to the cMyBPC motif, these forms may be associated with different interactors. The Y2H library screens of the present study corroborates this suggestion as, even though there was overlap in the identities of preys identified between screens, there were interactors that were unique to each phosphorylation-mimic bait. Further, the N-terminus C1C2 cMyBPC region comprises two Ig domains, each with four potential interaction surfaces and is thus able to accommodate many more interactors.

Since experimental data on human protein-protein interactions is still scarce, bioinformatics methods have been used to predict human protein-protein interactors from experimentally derived interactions in other organisms such as yeast, worm and fruitfly (Ramirez *et al.*, 2007). Calculations of the number of interactions per protein based on, for example, the yeast interactome suggests that there are ~3-10 interactors per protein. This estimate does not even take into account complicating factors such as alternative mRNA splicing or post-transcriptional modification, both of which produce many more protein species and hence more interactions (Bork *et al.*, 2004). Further, the number of genes in the human genome is ~25000 compared to the ~6000 of *S.cerevisiae*, suggesting more human proteins and thus more interactions. Thus, it is entirely possible that N-terminus cMyBPC may have as many interactors as suggested by the present study.

Thus, the present study has identified and verified numerous novel interactors of the N-terminus of cMyBPC. These interactors may shed light on the dynamics of PKA-mediated phosphorylation (PDE4DIP), the turnover of cMyBPC in the sarcomere (COMMD4), the preservation of cMyBPC integrity (HSPB7) and the means to generate energy ( $\beta$ -enolase). In addition, this study has identified means by which cMyBPC may be able to regulate cardiac dynamics by direct contact with cTNI and actin, independent of PKA-mediated phosphorylation.

#### 4.5 FUTURE STUDIES

The novel interactors of C1C2 cMyBPC identified and verified by the present study warrants further investigation to fully understand the nature of the interaction and the relevance to cMyBPC. The identification of these preys suggests other pathways in which cMyBPC may be involved and these need to

be interrogated in the context of HCM, cardiac hypertrophy *per se* and heart failure. Therefore, the putative interactors confirmed as interactors of the C1C2 region should be considered as candidates to screen in association studies and mutation screens. As part of the on going study to identify cMyBPC interactors, the interactors verified should be used as “baits” in future cDNA library screens to build the cMyBPC interactome. This approach has already begun with COMMD4 (C Swanepoel, personal communication) and PDE4DIP (G Uys, personal communication) library screens having being completed. Interactors being verified in these screens overlap with those identified by the present study. This lends support for the interactors of the present study and bodes very well for our interactome mapping.

Furthermore, the putative interactors that fell outside the scope of this study need to be investigated. For the interactors verified, stably transfected cell lines need to be generated in order to improve the BRET assays. Finer mapping of the amino acids involved in cMyBPC interactions should be performed together with studies which may determine how HCM-causing cMyBPC mutations in the C1C2 region affect ligand binding. Finally, it needs to be determined when and how these interactions with C1C2 take place within the living cell, whether these interactors compete with myosin S2 for interaction or whether the regions of interaction are distinct from the myosin S2 binding site. Quantitative  $\beta$ -galactosidase assays may also assist in this regard to assess strength of interactions of various prey/phosphorylation-mimic combinations to enhance understanding of the interaction dynamics.

#### 4.6 CONCLUSION

This study has identified 27 putative interactors of domains C1C2 of cMyBPC by Y2H analyses. Thirteen of these interactors were subjected to further verification by direct Y2H protein-protein interaction assays, *in vitro* co-immunoprecipitation and 3D *in vivo* co-localisation or BRET assays. While challenges were experienced for the BRET verification of cMyBPC C-terminus domains, cTNI, actin and cTNT, these preys are still considered as putative interactors of N-terminus cMyBPC. Verification studies have shown that PDE4DIP, HSPB7,  $\beta$ -enolase and COMMD4 share the same subcellular space as cMyBPC and that preys that share homology with myosin S2 (ACTN2, SYNE1, UACA and GRINL1A) are likely to be biologically irrelevant interactors. Except for actin, the putative positive interactors identified are novel and may provide new insight into the mechanism of cMyBPC phosphorylation, degradation and to the mechanism by which cMyBPC regulates cardiac contractility. By mapping the cMyBPC interactome we may identify new targets and pathways to interrogate to determine the mechanism by which mutations in *MYBPC3* induce cardiac dysfunction. This study has identified exciting and novel interactors that will extend our knowledge of cMyBPC and will serve as a platform for many future studies.

## **APPENDIX I**

### **1. BACTERIAL PLASMID PURIFICATION SOLUTIONS**

#### **Cell Suspension Solution**

50mM Tris-HCl, pH 7.5	2.5ml 1M Tris
10mM EDTA	1ml 0.5M EDTA
Sterile water to a final volume of 50ml	

#### **Cell Lysis Solution**

0.2M NaOH	2.5ml 4M NaOH
1% SDS	5ml
Sterile water to a final volume of 50ml	

#### **Neutralisation Solution**

1.32M KOAc, pH 4.8	13.2ml 5M KOAc
Sterile water to a final volume of 50ml	

### **2. YEAST TRANSFORMATION REAGENTS**

#### **1M LiAc**

LiAC	5.1g
Make up to 50ml with sterile water.	

#### **100mM LiAc**

1M LiAC	5ml
Make up to 50ml with sterile water	

#### **50% PEG 4000**

PEG 4000	25g
Make up to 50ml with sterile water	

### **3. YEAST PLASMID PURIFICATION SOLUTIONS**

#### **Yeast Lysis Buffer**

SDS	1%
Triton X-100	2%
NaCl	100mM
Tris, pH 8	10mM
EDTA, pH8	1mM

#### **4. ELECTROPHORESIS STOCK SOLUTIONS**

##### **10% Ammonium Persulphate**

Ammonium persulphate (Merck)	10g
Sterile water	10ml
Mix well and stock at 4°C	

##### **20X SB Stock Solution**

di-Sodium tetraborate decahydrate	38.14g
Sterile water to a final volume of 1 litre	

##### **1X SB Solution**

20X SB solution	50ml
Sterile water to a final volume of 1 litre.	

##### **SDS-PAGE Resolving Gel Buffer (4X)**

Tris base	109.2g
ddH <sub>2</sub> O	330ml
10% SDS	24ml
pH to 8.8 using 1M HCl. Make up to 600ml using ddH <sub>2</sub> O	

##### **SDS-PAGE Stacking Gel Buffer (4X)**

Tris base	36.3g
ddH <sub>2</sub> O	330ml
10% SDS	24ml
pH to 6.8 using 1M HCl. Make up to 600ml using ddH <sub>2</sub> O	

##### **10X SDS-PAGE Running Buffer**

Tris base	30g
Glycine	144g
10% SDS	100ml
Add ddH <sub>2</sub> O to a final volume of 1L	

##### **1X SDS-PAGE Running Buffer**

10X SDS-PAGE running buffer	100ml
Sterile water to a final volume of 1 litre	

## 5. GELS

### 1% Agarose Gel

Agarose	1g
SB buffer (1X)	100ml

Microwave for 1 minute on maximum power and add 5µl ethidium bromide (10mg/ml) when temperature of  $\approx 55^{\circ}\text{C}$  is reached.

### 2% Agarose Gel

Agarose	2g
SB buffer (1X)	100ml

Microwave for 1 minute on maximum power and add 5µl ethidium bromide (10mg/ml) when temperature of  $\approx 55^{\circ}\text{C}$  is reached.

### 15% SDS-PAGE Stacking Gel

Sterile water	2.56ml
10% SDS	40µl
SDS-PAGE stacking gel buffer (4X)	1ml
Acrylamide (40%)	390µl
APS (10%)	30µl
TEMED	6µl

Makes two gels for the Bio-Rad Mini gel apparatus system (Bio-Rad Laboratories, Hercules, CA, USA).

### 15% SDS-PAGE Resolving Gel

Sterile water	4.82ml
10% SDS	100µl
SDS-PAGE resolving gel buffer (4X)	1.25ml
Acrylamide (40%)	3.75ml
APS (10%)	80µl
TEMED	6µl

Makes two gels for the Bio-Rad Mini gel apparatus system (Bio-Rad Laboratories, Hercules, CA, USA).

### 20% SDS-PAGE Stacking Gel

Sterile water	8.8ml
SDS-PAGE stacking gel buffer (4X)	3.2ml
Acrylamide (40%)	950µl
APS (10%)	134µl

TEMED 13.4 $\mu$ l  
 Makes two gels for the Modular Vertical Electrophoresis system (VS20CBS, Cleaver Scientific, Warwickshire, United Kingdom).

### **20% SDS-PAGE Resolving Gel**

Sterile water	8.8ml
SDS-PAGE resolving gel buffer (4X)	8.8ml
Acrylamide (40%)	17.6ml
APS (10%)	350 $\mu$ l
TEMED	35 $\mu$ l

Makes two gels for the Modular Vertical Electrophoresis system (VS20CBS, Cleaver Scientific, Warwickshire, United Kingdom).

## **6. LOADING DYES**

### **Ethidium Bromide Stock (10mg/ml)**

Ethidium bromide (Sigma)	500mg
Sterile water	50ml

Stir well on magnetic stirrer for 4 hours and store in a dark container at 4°C

### **Bromophenol Blue Loading Dye**

Bromophenol blue	0.1% (w/v)
Sterile water to a final volume of 100ml.	Store at 4°C

### **SDS Loading Dye**

1M Tris-HCl (pH6.8)	50mM
DTT	100mM
SDS	2%
Bromophenol blue	0.1%
Glycerol	10%

## **7. MOLECULAR SIZE MARKERS**

### **$\lambda$ Pst Molecular Size Marker**

Bacteriophage Lambda genomic DNA	200 $\mu$ l
<i>Pst</i> I Restriction enzyme	3 $\mu$ l (30U)
Promega buffer H	30 $\mu$ l
Sterile water to a final volume of 300 $\mu$ l	

Incubate at 37°C for 3 hours, heat inactivate enzyme at 65°C for 10 minutes. Use 1 $\mu$ l of digestion product on polyacrylamide gels, or 3 $\mu$ l on ethidium bromide stained agarose gels.

Fragment sizes:

11497bp, 5077bp, 4507bp, 2838bp, 2560bp, 2459bp, 2443bp, 2140bp, 1986bp, 1700bp, 1159bp, 1093bp, 805bp, 514bp, 468bp, 448bp, 339bp, 264bp, 247bp, 211bp, 200bp, 164bp, 150bp, 94bp, 87bp, 72bp

## 8. PCR BUFFER

### 10x NH<sub>4</sub> PCR Buffer (BIOLINE UK)

Ammonium sulphate	160mM
Tris-HCl (pH 8.8)	670mM
Tween-20	0.1%

## 9. Co-IP REAGENTS

### Co-IP Buffer

1M Tris (pH-7.5)	400µl
5M NaCl	60µl
1M DTT	20µl
2ng/ml Aprotinin	50µl
50mM PMSF	200µl
Tween 20	20µl

Make up to 20 ml using sterile water.

### Pre-washed Protein G Agarose

A volume of Co-IP buffer (double the volume of the Protein G agarose) was used to wash the Protein G agarose (10µl/reaction) by centrifugation for 30 seconds. Following centrifugation, the supernatant was discarded and the pellet resuspended (double volume of Co-IP buffer) before another round of centrifugation. This procedure was repeated five times. After the final centrifugation step, the pellet was resuspended in a volume of Co-IP buffer representing the initial volume of Protein G aliquoted.

### TBST (pH 7.6)

NaCl	8g
1M Tris-HCl (pH 7.6)	20ml
Tween 20	1ml

Make up to 1L using sterile water.

## **10. SOLUTIONS USED FOR THE ESTABLISHMENT OF BACTERIAL COMPETENT CELLS**

### **CAP-Buffer**

CaCl <sub>2</sub>	2.21g
Glycerol	37.5ml
PIPES	0.76g

Sterile water to a final volume of 250ml. Adjust pH to 7.0 and store at 4°C.

## **11. BACTERIAL MEDIA**

### **LB-Media**

Bacto tryptone	5g
Yeast extract	2.5g
NaCl	5g

Sterile water to a final volume of 500ml. Autoclave and add the appropriate antibiotic (Ampicillin 25mg/l, Kanamycin 5mg/l or Zeocin™ 10mg/l) to media when temperature of ≈55°C is reached.

### **LB-Agar Plates**

Bacto tryptone	5g
Yeast extract	2.5g
NaCl	5g
Bacto agar	8g

Sterile water to a final volume of 500ml. Autoclave and add the appropriate antibiotic (Ampicillin 25mg/l, Kanamycin 5mg/l or Zeocin™ 10mg/l) to media when temperature of ~55°C is reached, prior to pouring ~20, 90mm plates. These plates were then allowed to set for 2-5 hours and stored at room temperature for up to three weeks.

## **12. YEAST MEDIA**

### **YPDA Media**

Difco peptone	10g
Yeast extract	10g
Glucose	10g
L-adenine hemisulphate (0.2% stock solution)	7.5ml

Add sterile water to a final volume of 500ml. Autoclave at 121°C for 15 minutes.

### **YPDA Agar Plates**

YPDA media	
Difco peptone	10g
Yeast extract	10g
Bacto agar	10g

Glucose	10g
L-adenine hemisulphate (0.2% stock solution)	7.5ml
Add sterile water to a final volume of 500ml and autoclave at 121°C for 15 minutes. Allow to cool to a temperature of ~55°C, before pouring ~20, 90mm plates. These plates were then allowed to set for 2-5 hours and stored at room temperature for up to three weeks.	

#### **SD<sup>-W</sup> Media**

Glucose	12g
Yeast nitrogen base without amino acids	4g
SD <sup>-W</sup> amino acid supplement	0.4g
Add sterile water to a final volume of 600ml. Adjust pH to 5.8 and autoclave at 121°C for 15 minutes.	

#### **SD<sup>-W</sup> Agar Plates**

Glucose	12g
Bacto agar	12g
Yeast nitrogen base without amino acids	4g
SD <sup>-W</sup> amino acid supplement	0.4g
Add sterile water to a final volume of 600ml. Adjust pH to 5.8 and autoclave at 121°C for 15 minutes. Allow to cool to a temperature of ~55°C, before pouring ~20, 90mm plates. These plates were then allowed to set for 2-5 hours and stored at room temperature for up to three weeks.	

#### **SD<sup>-L</sup> Media**

Glucose	12g
Yeast nitrogen base without amino acids	4g
SD <sup>-L</sup> amino acid supplement	0.4g
Add sterile water to a final volume of 600ml. Adjust pH to 5.8 and autoclave at 121°C for 15 minutes.	

#### **SD<sup>-L</sup> Agar Plates**

Glucose	12g
Bacto agar	12g
Yeast nitrogen base without amino acids	4g
SD <sup>-L</sup> amino acid supplement	0.4g
Add sterile water to a final volume of 600ml. Adjust pH to 5.8 and autoclave at 121°C for 15 minutes. Allow to cool to a temperature of ~55°C, before pouring ~20, 90mm plates. These plates were then allowed to set for 2-5 hours and stored at room temperature for up to three weeks.	

**SD<sup>L-W</sup> Media**

Glucose	12g
Yeast nitrogen base without amino acids	4g
SD <sup>L-W</sup> amino acid supplement	0.4g
Add sterile water to a final volume of 600ml. Adjust pH to 5.8 and autoclave at 121 <sup>0</sup> C for 15 minutes.	

**SD<sup>L-W</sup> Agar Plates**

Glucose	12g
Bacto agar	12g
Yeast nitrogen base without amino acids	4g
SD <sup>L-W</sup> amino acid supplement	0.4g
Add sterile water to a final volume of 600ml. Adjust pH to 5.8 and autoclave at 121 <sup>0</sup> C for 15 minutes. Allow to cool to a temperature of ~55 <sup>0</sup> C, before pouring ~20, 90mm plates. These plates were then allowed to set for 2-5 hours and stored at room temperature for up to three weeks.	

**TDO Media**

Glucose	12g
Yeast nitrogen base without amino acids	4g
SD <sup>L-W-H</sup> amino acid supplement	0.4g
Add sterile water to a final volume of 600ml. Adjust pH to 5.8 and autoclave at 121 <sup>0</sup> C for 15 minutes.	

**TDO Agar Plates**

Glucose	12g
Bacto agar	12g
Yeast nitrogen base without amino acids	4g
SD <sup>L-W-H</sup> amino acid supplement	0.4g
Add sterile water to a final volume of 600ml. Adjust pH to 5.8 and autoclave at 121 <sup>0</sup> C for 15 minutes. Allow to cool to a temperature of ~55 <sup>0</sup> C, before pouring ~20, 90mm plates. These plates were then allowed to set for 2-5 hours and stored at room temperature for up to three weeks.	

**QDO Media**

Glucose	12g
Yeast nitrogen base without amino acids	4g
SD <sup>L-W-H-Ade</sup> amino acid supplement	0.4g
Add sterile water to a final volume of 600ml. Adjust pH to 5.8 and autoclave at 121 <sup>0</sup> C for 15 minutes.	

### **QDO Agar Plates**

Glucose	12g
Bacto agar	12g
Yeast nitrogen base without amino acids	4g
SD-L-W-H-Ade amino acid supplement	0.4g

Add sterile water to a final volume of 600ml. Adjust pH to 5.8 and autoclave at 121<sup>0</sup>C for 15 minutes. Allow to cool to a temperature of ~55<sup>0</sup>C, before pouring ~20, 90mm plates. These plates were then allowed to set for 2-5 hours and stored at room temperature for up to three weeks.

### **X- $\alpha$ -Galactosidase Solution (5mg/ml)**

X- $\alpha$ -Galactosidase	25mg
Dimethylformamide	1ml

Make a 25mg/ml stock. Dilute with dimethylformamide to 5mg/ml working solution.

## **13. EUKARYOTIC CELL CULTURE MEDIA**

### **Complete Growth Media**

DMEM (4.5g/L glucose, with L-glutamine)	178ml
Foetal calf serum	20ml
Penstrep	2ml

Pre-warm to 37<sup>0</sup>C before use.

### **Serum-Free Media**

DMEM (4.5g/L glucose, with L-glutamine)	100ml
Pre-warm to 37 <sup>0</sup> C before use.	

### **Differentiating Growth Media**

DMEM (4.5g/L glucose, with L-glutamine)	196ml
Horse serum	2ml
Penstrep	2ml

Pre-warm to 37<sup>0</sup>C before use.

## **14. BIOLUMINESCENCE RESONANCE ENERGY TRANSFER ASSAY (BRET) REAGENTS**

### **D-PBS/0.5%w/v Gelatine Solution**

PBS (with MgCl <sub>2</sub> and Ca <sup>2+</sup> )	10ml
Gelatine	50µl

**10X Isoproterenol**

Isoproterenol	2.48mg
---------------	--------

Add 100ml sterile water for 1000X stock. Dilute further 1:100 with sterile water for 10x working solution. Make up as required as it cannot be stored in solution.

**65mM CaCl<sub>2</sub>**

Calcium chloride	478mg
------------------	-------

Add 50ml sterile water for a 10X working solution.

**DEEPBLUE C Stock**

Dissolve one 200ug pellet in 500ul absolute ethanol for a 1mM stock. Dilute further 1:4 in DMSO for working solution (250μM). Make up as required as it does not store well.

## APPENDIX II

### CALCULATING YEAST MATING EFFICIENCIES (Calculations based on Clontech Manual)

Count number of colonies on all plates with 30-300 colonies after 4 days

$$\# \text{colony forming units (cfu)/ml} = \frac{\text{cfu} \times 1000 \mu\text{l/ml}}{\text{volume plated (\mu l)} \times \text{dilution factor}}$$

1. Number of cfu/ml on SD<sup>L</sup> plates = viability of prey partner
  2. Number of cfu/ml on SD<sup>W</sup> plates = viability of bait partner
  3. Number of cfu/ml on SD<sup>L-W</sup> plates = viability of diploids
  4. Lowest Number of cfu/ml of SD<sup>L</sup> or SD<sup>W</sup> plates indicate limiting partner
5. Mating efficiency=  $\frac{\# \text{cfu/ml of diploids} \times 100}{\# \text{cfu/ml of limiting partner}}$

#### Library titre

Count number of colonies on all plates with 30-300 colonies after 4 days

$$\# \text{cfu/ml} = \frac{\# \text{colonies}}{\text{plating volume(ml)} \times \text{dilution factor}}$$

$$\# \text{colonies clones screened} = \# \text{cfu/ml} \times \text{final resuspension volume}$$

#### Haemocytometric cell count

A cell count using, a Neubauer haemocytometer (Superior, Berlin, Germany), was required to determine the titre of bait cultures used in the library mating experiments, as well as to determined the concentration of the H9C2 cells used in the BRET assay. Prior to counting, both the surface of the chamber and the glass cover slip was cleaned with alcohol. The glass cover slip was then placed over the counting surface; a dilution (1:100) of the sample prepared and an aliquot applied into one of the V-shaped wells. Once the area under the coverslip filled with the sample through capillary action, the counting chamber was subsequently placed on a microscope (Nikon TMS, Nikon Instruments., New York, USA) stage and the counting area was brought into focus under low magnification. The number of cells in the large central quadrant of the haemocytometer was counted and this value was used to calculate the number of cells per millilitre using the following formula:

Number of cells/ml = number of cells x dilution factor x  $10^4$  (a constant used because the depth of the haemocytometer is 0.1mm)

### BRET CALCULATIONS

The following formula (Pfleger *et al.*, 2006) was used to calculate the BRET ratio (Section 3.4) for the verification of protein-protein interactions as identified by Y2H analyses.

$$\frac{\text{Bait-prey GFP expression}}{\text{Bait-prey Rluc expression}} - \frac{\text{Bait GFP expression}}{\text{Bait Rluc expression}}$$

## APPENDIX III

### LIST OF SUPPLIERS

[ <sup>35</sup> S] methionine	PerkinElmer
Acrylamide	Merck
Agarose	Whitehead Scientific
Ammonium acetate	B&M Scientific
Ammonium persulphate	Merck
Ampicillin	Roche
Anti-cMyc	Roche
Anti-HA monoclonal antibody	Roche
Aprotinin	Roche
Autoradiography film	Kodak
β-mercapto-ethanol	Sigma
Bacteriophage Lambda genomic DNA	Promega
Bacto Agar	Merck
Bacto tryptone	Fluka
<i>BamHI</i>	Promega
Bromophenol blue	Merck
Calcium chloride	Merck
Calf intestinal alkaline phosphatase	Promega
dATP	Boehringer Mannheim
dCTP	Boehringer Mannheim
DeepBlueC	PerkinElmer
dGTP	Boehringer Mannheim
Dimethylformamide	Merck
di-Sodium tetraborate decahydrate	Merck
DMEM	Highveld biological
dNTP mix	TaKaRa
DsRed-Monomer-C1	BD Bioscience
DTT	Roche
dTTP	Boehringer Mannheim
<i>EcoRI</i>	Promega
EDTA	Boehringer Mannheim
Ethanol	Boehringer Mannheim
Ethidium bromide	Roche
Ex Taq™ polymerase	TaKaRa
Ex Taq™ polymerase Mg <sup>2+</sup> -containing reaction buffer	TaKaRa

Foetal calf serum	Delta Bioproducts
Gelatine	Sigma
GeneJuice®	Novagen
GFX® DNA purification kit	Amersham Pharmacia
Glass beads (450-600µm)	Sigma
Glucose	Kimix
Glycerol	Promega
Glycine	Kimix
H9C2	American Type Culture Collection
HCl	Merck
Herring sperm DNA	Promega
<i>Hind</i> III	Promega
Horse serum	Sigma
Hybond N+ nylon membranes	Amersham Pharmacia
In-Fusion™ 2.0 Dry-Down PCR cloning kit	BD Bioscience
Isopropanol	Merck
Isoproterenol	Sigma
K-acetate	Sigma
Kanamycin	Roche
L-adenine hemisulphate	Sigma
LiAc	Sigma
Matchmaker™ Two-hybrid system 3	BD Biosciences
MgCl <sub>2</sub>	Bioline
MgSO <sub>4</sub> .7H <sub>2</sub> O	Merck
<i>Mlu</i> I	Promega
Molecular size marker (200bp)	Promega
Na <sub>2</sub> CO <sub>3</sub>	Merck
NaCl	BDH Chemicals
Na <sub>2</sub> HPO <sub>4</sub> .7H <sub>2</sub> O	Merck
Na <sub>2</sub> H <sub>2</sub> PO <sub>4</sub> .H <sub>2</sub> O	Merck
NaOH	Sigma
<i>Nde</i> I	Promega
Oligonucleotide primers	Department of Molecular and Cell Biology, University of Cape Town (UCT), Cape Town, South Africa
<i>ortho</i> -Nitrophenyl-β-galactoside	Roche
pACT2	BD Biosciences
PBS	Sigma

pdEYFP-C1amp	RZPD
PEG4000	Merck
Penicillin/streptomycin	Highveld Biological
Peptone	Difco
pGBTKT7	BD Biosciences
pGFP <sup>2</sup> -C3	PerkinElmer
pGFP <sup>2</sup> -MCS-Rluc	PerkinElmer
Phenol/chloroform/isoamyl	Sigma
PIPES	Merck
PMSF	Roche
Protein G agarose	Kirkegaard and Perry Laboratories
<i>Pst</i> I	Promega
pSV-β-Galactosidase	Promega
QDO	BD Biosciences
Rluc-C1	PerkinElmer
RNAse wipes	Ambion
<i>Sac</i> II	Promega
SD <sup>-Ade</sup>	BD Biosciences
SD <sup>-L</sup>	BD Biosciences
SD <sup>-L-W</sup>	BD Biosciences
SD <sup>-Met</sup>	BD Biosciences
SDS	Sigma
SD <sup>-Ura</sup>	BD Biosciences
SD <sup>-W</sup>	BD Biosciences
T4 DNA Ligase	Promega
Taq polymerase	Bioline
TDO	BD Biosciences
TEMED	Sigma
TNT® Quick Coupled transcription/translation system	BD Biosciences
Tris	Merck
Tris-HCl	Merck
Triton X-100	Sigma
Trypsin	Highveld Biological
Tween 20	Merck
Whatman 3M paper	Whatman international
Wizard® Purefection plasmid purification kit	BD Biosciences
<i>Xba</i> I	Promega
X-α-galactosidase	Southern Cross

Yeast extract

Difco

Yeast nitrogen base (without amino acids)

BD Biosciences

Zeocin<sup>TM</sup>

Invitrogen

## APPENDIX IV

### BACTERIAL STRAIN PHENOTYPE

#### E.coli strain DH5 $\alpha$

$\Phi$  80d *lacZ* $\Delta$ *M15* *recA1*, *endA1*, *Gry A96 thi-1*, *hsdR17 supE44*, *relA1*, *deoR*  $\Delta$ (*lacZYA argF*)*u169*

### YEAST STRAIN PHENOTYPES

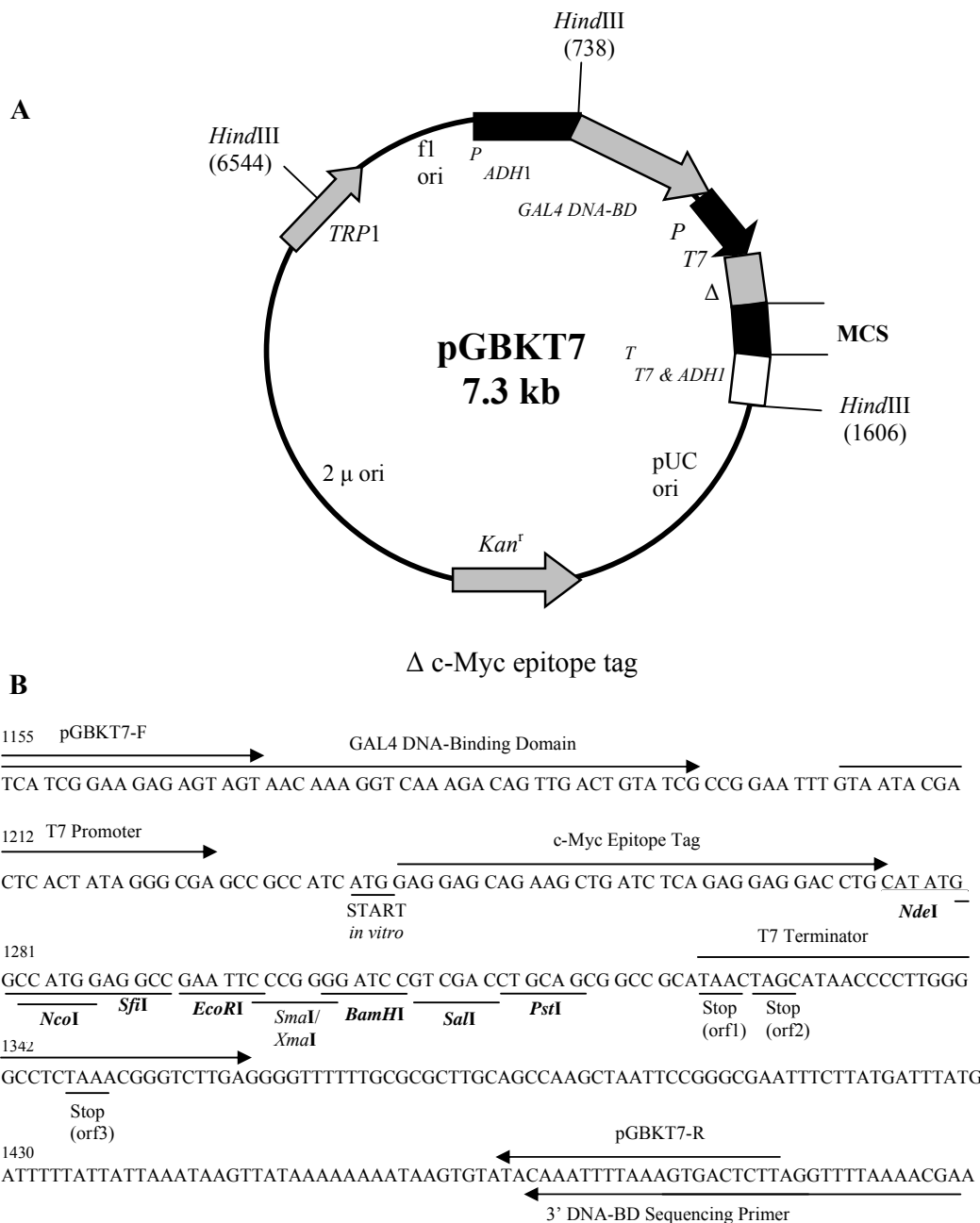
#### Yeast strain AH109

*MATa*, *trp1-901*, *leu2-3*, *ura3-5*, *his3-200*, *gal4 $\Delta$* , *gal80 $\Delta$* , *LYS2::GAL1<sub>UAS</sub>-GAL1<sub>TATA</sub>.HIS3*, *GAL2<sub>UAS</sub>-GAL2<sub>TATA</sub>-ADE2*, *URA3::MEL1<sub>UAS</sub>-MEL1<sub>TATA</sub>-lacZ* (James *et al.*, 1996)

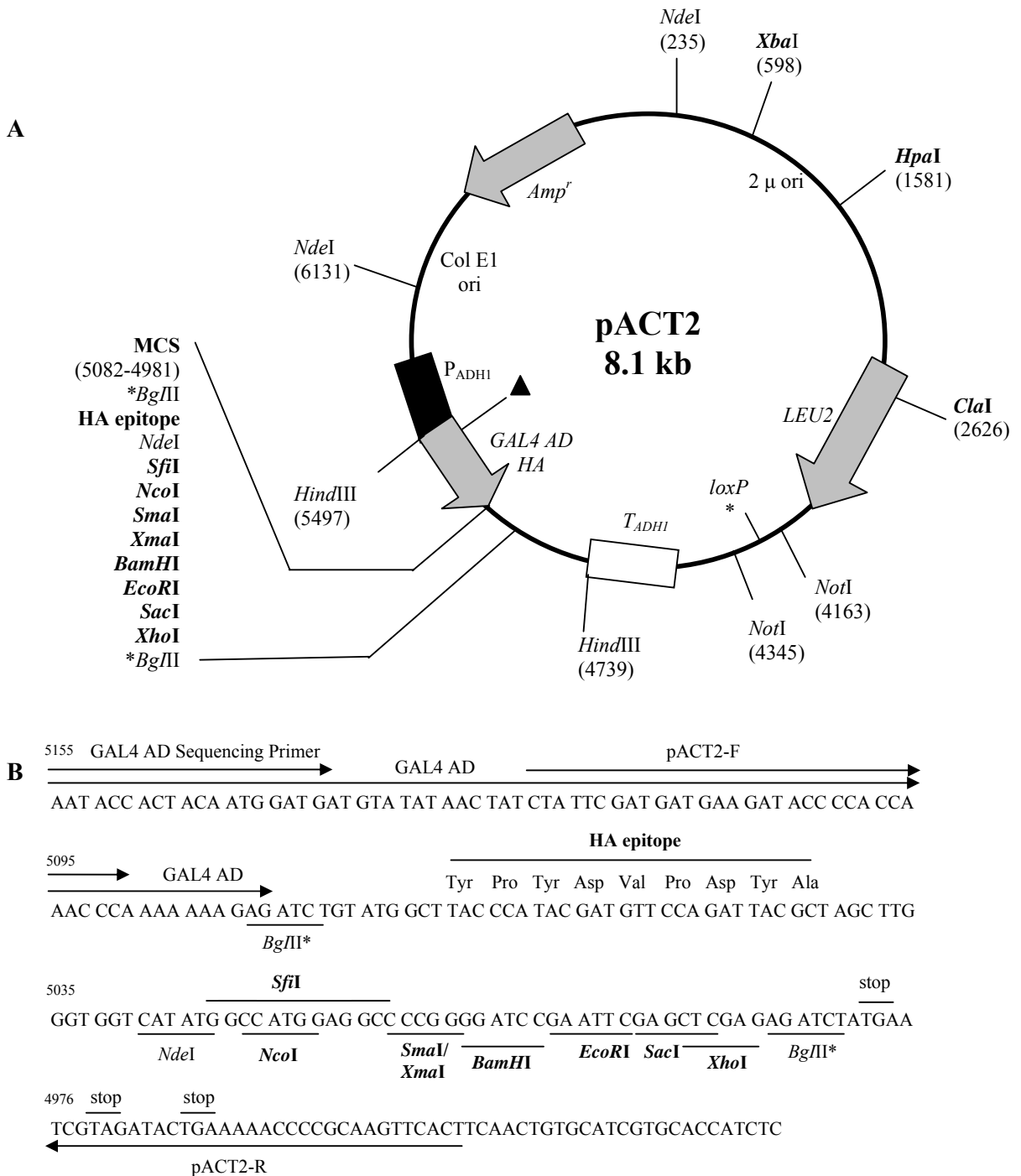
#### Yeast strain Y187

*MATa*, *ura3-52*, *his3-200*, *ade2-101*, *trp1-901*, *leu2-3*, *112*, *gal4 $\Delta$* , *met*, *gal80 $\Delta$* , *URA3::GAL1<sub>UAS</sub>-GAL1<sub>TATA</sub>-lacZ* (Harper *et al.*, 1993)

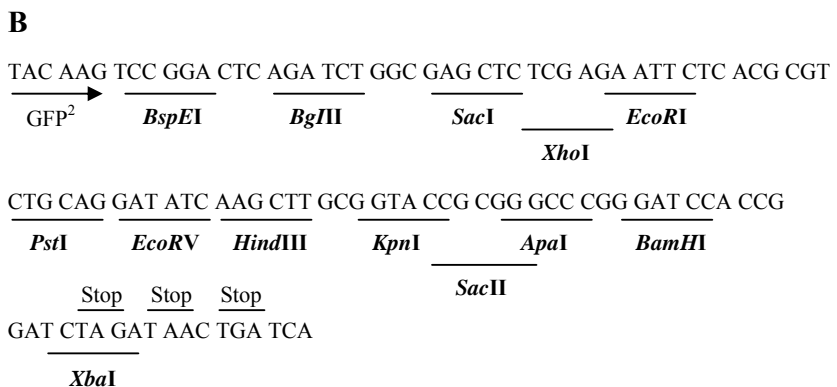
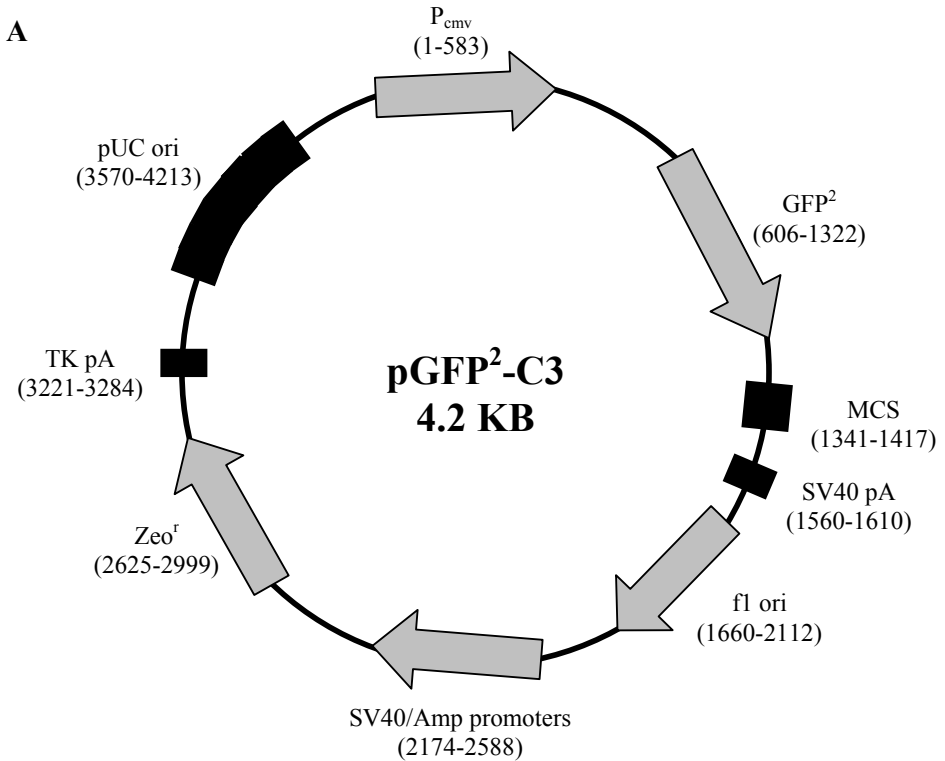
## APPENDIX V



**Restriction map and multiple cloning site of pGBK7 Y2H vector.** A) The positions of the kanamycin resistance gene ( $Kan^r$ ), the  $TRP1$  nutritional marker for selection in yeast,  $GAL4$ - $BD$  coding sequences,  $f1$  bacteriophage and  $pUC$  plasmid origins of replication, the truncated *S.cerevisiae*  $ADH1$  promoter sequence ( $P_{ADH1}$ ), the T7 RNA polymerase promoter, c-Myc epitope tag, transcription termination sequences (T7 and  $ADH1$ ) and the MCS are indicated on the map. B) Nucleotide sequence of the pGBK7 MCS. The position of all unique restriction enzyme recognition sequences, stop codons in the T7 termination sequence,  $GAL4$ - $BD$  coding sequence, T7 promoter sequence, c-Myc epitope tag, positions of the screening and sequencing primers are indicated on the sequence (redrawn from Clontech MATCHMAKER vector handbook)

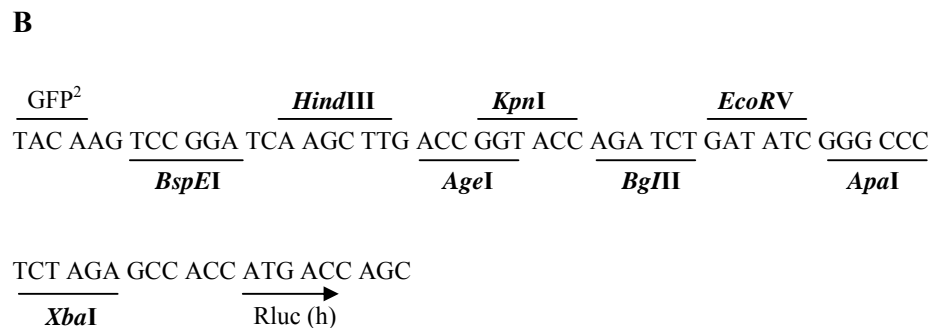
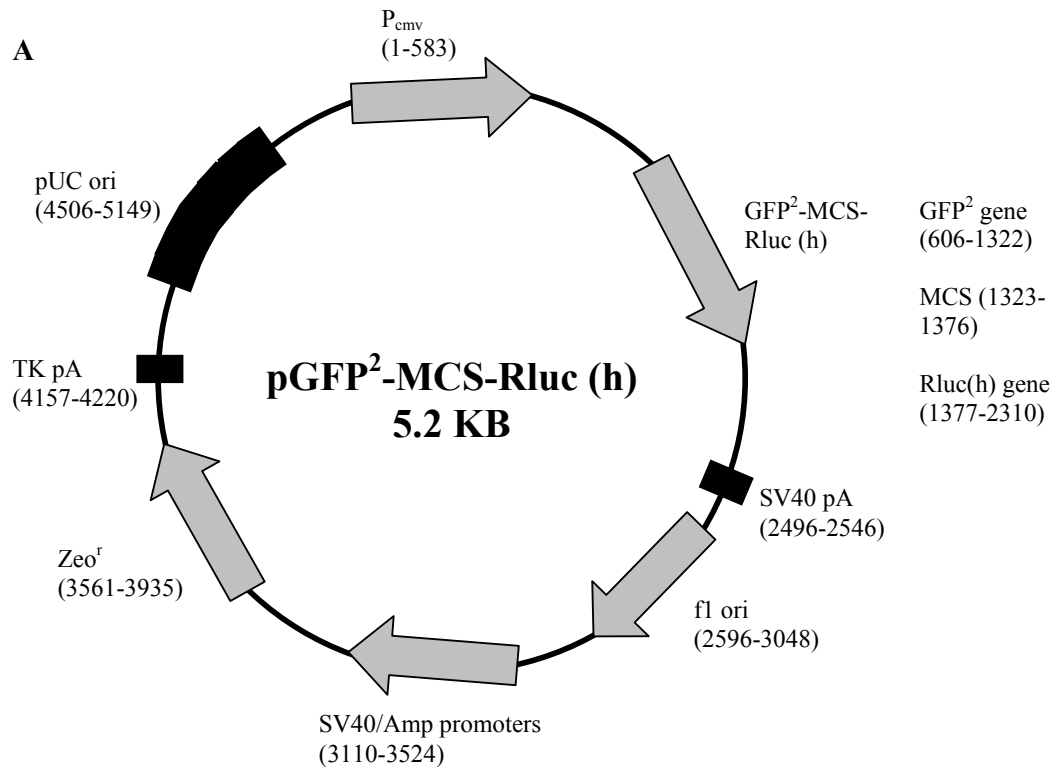


**Restriction map and multiple cloning site of pACT2 Y2H prey vector.** A) The positions of unique restriction enzyme sites are indicated in bold font. The position of the ampicillin resistance gene (*Amp*<sup>r</sup>), *LEU2*, *GAL4-AD* coding sequence, 2μ and pBR322 plasmid origin of replication, the *S.cerevisiae ADH1* promoter, *S.cerevisiae ADH1* termination sequence, Lox sites (Lox 1 and Lox 2), the haemagglutinin (HA) epitope tag and the MCS are indicated on the map. B) Nucleotide sequence of the pACT2 MCS. The position of restriction enzyme sites, stop codons, the *GAL4-AD* coding sequence, HA epitope tag, and the positions of the pACT2-F and pACT2-R primers are all indicated (redrawn from Clontech MATCHMAKER vector handbook).

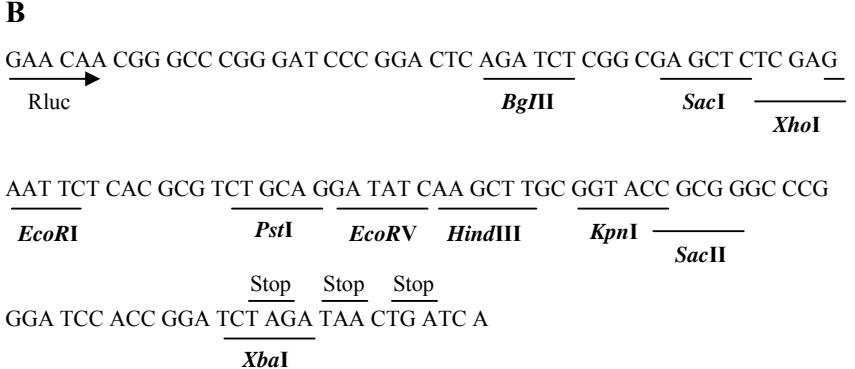
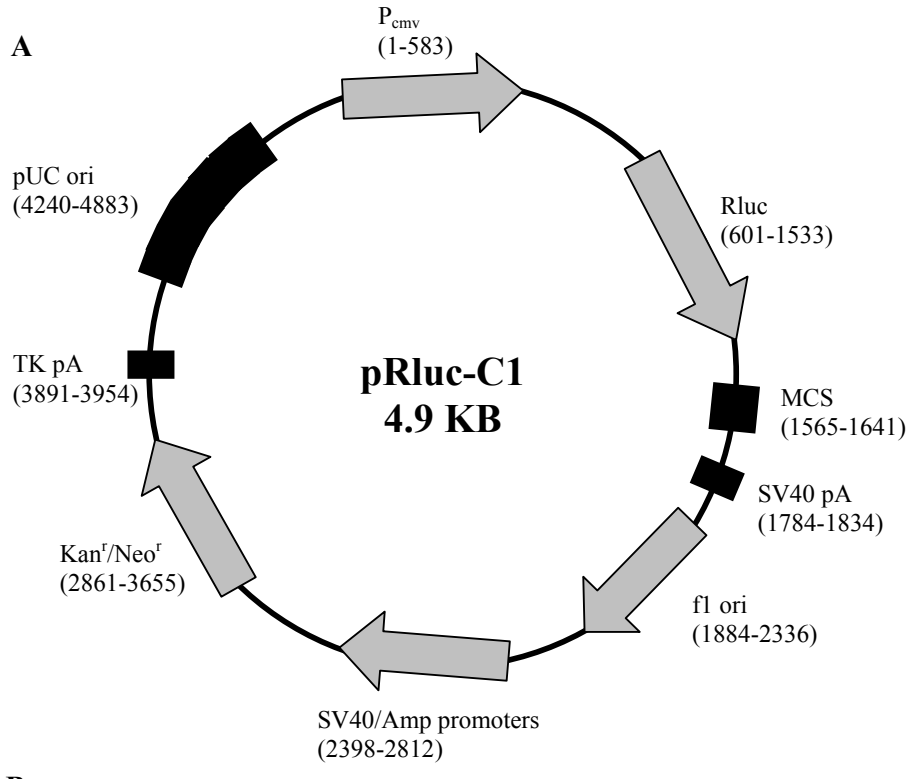


\* Frame changes characterising pGFP<sup>2</sup>-C3 occur after this site

**Restriction map and multiple cloning site of pGFP<sup>2</sup>-C3 vector.** A) The position of the P<sub>CMV</sub>, SV40 early poly (A) signal, GFP<sup>2</sup> gene, TK poly (A) signal, P<sub>SV40</sub>/P<sub>amp</sub> promoters, Zeo<sup>r</sup>, f1 origin, pUC sequences and the MCS are indicated on the map. B) Nucleotide sequence of the pGFP<sup>2</sup>-C3 MCS. The position of restriction enzyme sites and stop codons are all indicated (redrawn from BRET<sup>2</sup>™ technical data sheet).

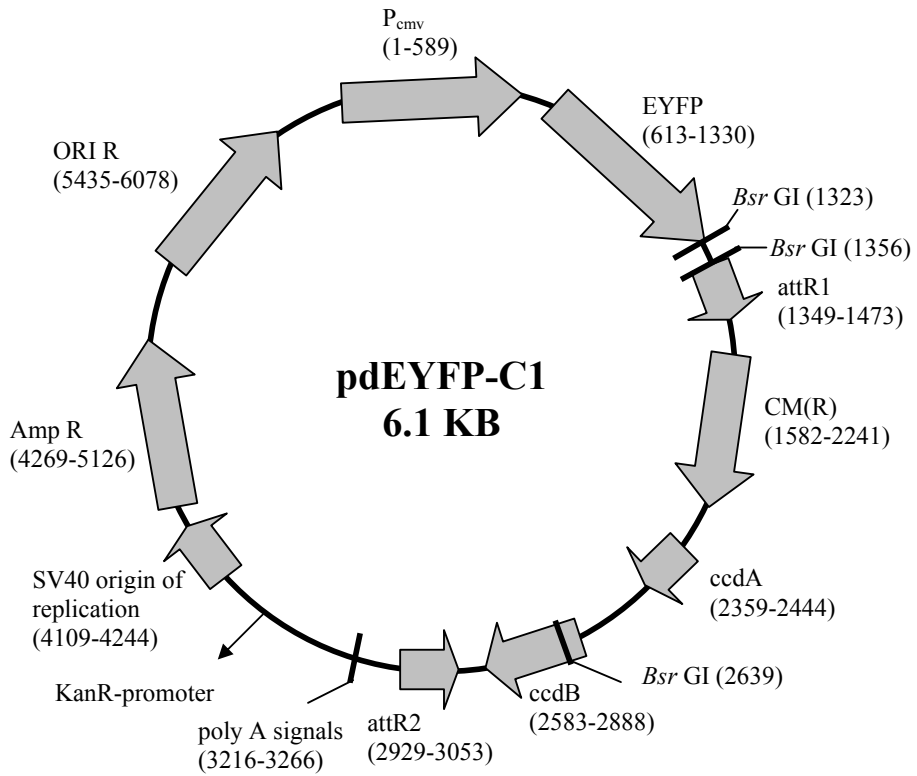


**Restriction map and multiple cloning site of pGFP<sup>2</sup>-MCS-Rluc (h) vector.** A) The position of the P<sub>CMV</sub>, SV40 early poly (A) signal, Rluc gene, GFP<sup>2</sup> gene, TK poly (A) signal, P<sub>SV40</sub>/P<sub>amp</sub>, Zeo<sup>r</sup>, f1 origin, pUC sequence and the MCS are indicated on the map. B) Nucleotide sequence of the MCS. The position of restriction enzyme sites are indicated (redrawn from BRET<sup>2</sup>™ technical data sheet).

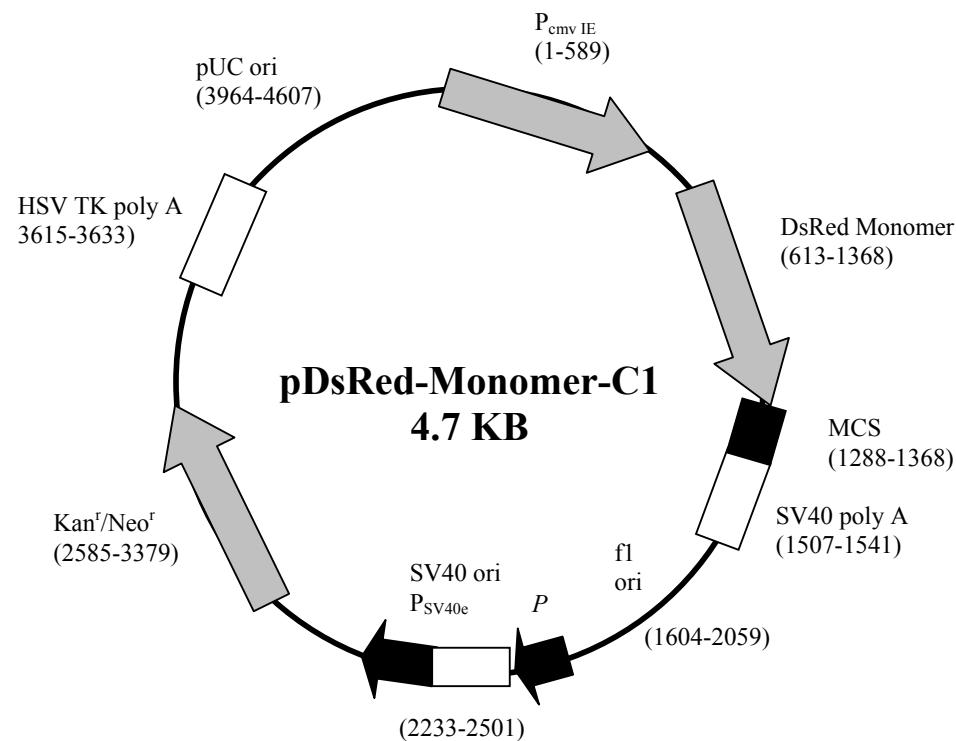


\*Frame changes characterising pRLuc-C1 occur after this site

**Restriction map and multiple cloning site of pRLuc-C1 vector.** A) The position of the P<sub>CMV</sub>, SV40 early poly (A) signal, Rluc gene, TK poly (A) signal, P<sub>SV40/Pamp</sub>, Kan/Neo<sup>r</sup>, f1 origin, pUC sequence and the MCS are indicated on the map. B) Nucleotide sequence of pRLuc-C1 MCS. The position of restriction enzyme sites and stop codons are indicated (redrawn from BRET<sup>2</sup>™ technical data sheet).



**Restriction map of pdEYFP-C1 vector.** The position of the EYFP tag, *chloramphenicol resistance* gene, *ccdB* gene, *ccdA* gene, SV40 early poly A signal, P<sub>CMV</sub> early promoter, *Kan resistance* gene, SV40 origin of replication, pUC plasmid replication origin, attR1 and attr2 recombination sites are indicated on the map (Map redrawn from RZPD vector info: <http://www.rzpd.de/info/vectors/pdEYFP-C1amp.shtml>).

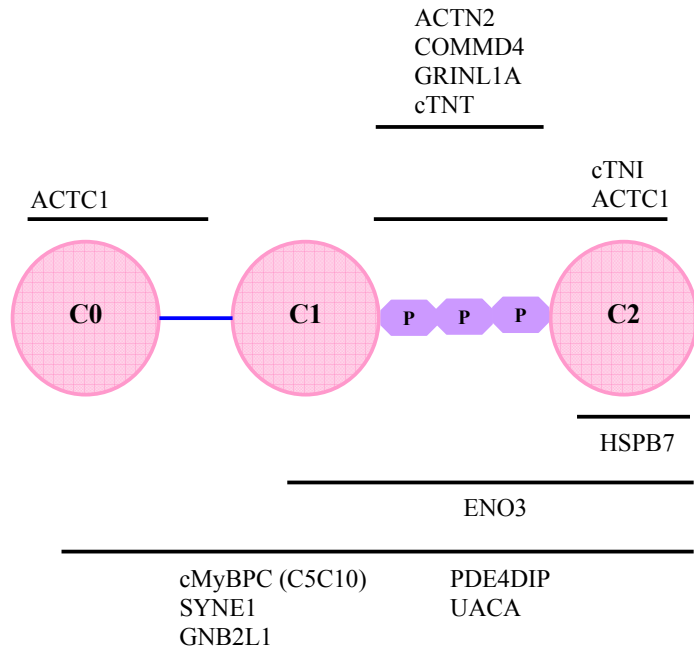


<b>DsRed-Monomer</b> TCC CAG TCC GGA CTC AGA TCT CGA GCT CAA GCT TCG AAT TCT GCA GTC GAC GGT ACC <u>XbaI</u> GCG GGC CCG GGA TCC ACC GGA TCT AGA TAA CTG ATC	<u>SacI</u> <u>XbaI</u> <u>BamHI</u> <u>HindIII</u> <u>EcoRI</u> <u>SalI</u> <u>KpnI</u>
<u>Apal</u> <u>SacII</u> <u>XmaI</u> <u>SmaI</u>	<u>STOP</u> <u>STOP</u> <u>STOP</u>

**Restriction map of pDsRed-Monomer-C1 vector.** pDsRed-Monomer-C1 is a mammalian expression vector that encodes DsRed-Monomer, a monomeric mutant derived from the tetrameric *Discosoma* sp. red fluorescent protein DsRed. The multiple cloning site (MCS) is positioned between the DsRed-Monomer coding sequence and the SV40 polyadenylation signal (SV40 poly A). The position of the fl ori, P<sub>CMV</sub> early promoter, *Kan/Neo* resistance genes, SV40 origin of replication, pUC plasmid replication origin and the Herpes simplex virus (HSV) thymidine kinase (TK) are indicated on the map (Map redrawn from Clontech vector information booklet).

## APPENDIX VI

Graphical representation of the Y2H protein-protein interaction assay data used to map the prey protein region of interaction on C0C2 of cMyBPC. Data in Table 3.15 Section 3.1.4.



## APPENDIX VII

### Bonferoni matrices for Bioluminescence resonance energy transfer assays

#### Bonferroni test; variable BRET ratio (C1C10 + TNI; NO CALCIUM)

Probabilities for Post Hoc Tests Error: Between MS = .68259, df = 16.000

Sample	{1} - .85000	{2} - .39600	{3} - 1.7820	{4} - .80000
1 C1C10 control		1.000000	0.560755	1.000000
2 TNI control	1.000000		0.104284	1.000000
3 C1C10 + TNI	0.560755	0.104284		0.471237
4 Transfection control	1.000000	1.000000	0.471237	

#### Bonferroni test; variable BRET ratio (C1C10 +TNI; CALCIUM ADDED)

Probabilities for Post Hoc Tests Error: Between MS = .17393, df = 8.0000

Sample	{1} - .07333	{2} - .16000	{3} - .39333	{4} - .33333
1 C1C10 control		1.000000	1.000000	1.000000
2 TNI control	1.000000		1.000000	1.000000
3 C1C10 + TNI	1.000000	1.000000		1.000000
4 Transfection control	1.000000	1.000000	1.000000	

#### Bonferroni test; variable BRET ratio (C1C10 + ACTC; NO CALCIUM)

Probabilities for Post Hoc Tests Error: Between MS = 1.2439, df = 16.000

Sample	{1} - .85000	{2} - .25000	{3} - 2.1540	{4} - .80000
1 C1C10 control		1.000000	0.498426	1.000000
2 ACTC control	1.000000		0.094770	1.000000
3 C1C10 + ACTC	0.498426	0.094770		0.437563
4 Transfection control	1.000000	1.000000	0.437563	

#### Bonferroni test; variable BRET ratio (C1C10 + ACTC; CALCIUM ADDED)

Probabilities for Post Hoc Tests Error: Between MS = .13545, df = 8.0000

Sample	{1} - .07333	{2} - .29667	{3} - .19000	{4} - .33333
1 C1C10 control		1.000000	1.000000	1.000000
2 ACTC control	1.000000		1.000000	1.000000
3 C1C10 + ACTC	1.000000	1.000000		1.000000
4 Transfection control	1.000000	1.000000	1.000000	

**Bonferroni test; variable BRET ratio (C2C10 + TNI; NO CALCIUM)****Probabilities for Post Hoc Tests Error: Between MS = 18.644, df = 4.0000**

Sample	{1} - 2.4050	{2} - 1.9300	{3} - 5.2650	{4} - .50000
1 C2C10 control		1.000000	1.000000	1.000000
2 TNI control	1.000000		1.000000	1.000000
3 C2C10 + TNI	1.000000	1.000000		1.000000
4 Transfection control	1.000000	1.000000	1.000000	

**Bonferroni test; variable BRET ratio (C2C10 + TNI; CALCIUM ADDED)****Probabilities for Post Hoc Tests Error: Between MS = 1.9713, df = 4.0000**

Sample	{1} - .58000	{2} - .67000	{3} - 1.7550	{4} - .50000
1 C2C10 control		1.000000	1.000000	1.000000
2 TNI control	1.000000		1.000000	1.000000
3 C2C10 + TNI	1.000000	1.000000		1.000000
4 Transfection control	1.000000	1.000000	1.000000	

**Bonferroni test; variable BRET ratio (C2C10 + ACTC; NO CALCIUM)****Probabilities for Post Hoc Tests Error: Between MS = 4.2141, df = 4.0000**

Sample	{1} - 2.4050	{2} - 1.0050	{3} - 1.2750	{4} - .50000
1 C2C10 control		1.000000	1.000000	1.000000
2 ACTC control	1.000000		1.000000	1.000000
3 C2C10 + ACTC	1.000000	1.000000		1.000000
4 Transfection control	1.000000	1.000000	1.000000	

**Bonferroni test; variable BRET ratio (C2C10 + ACTC; CALCIUM ADDED)****Probabilities for Post Hoc Tests Error: Between MS = .53191, df = 4.0000**

Sample	{1} - .58000	{2} - .01000	{3} - .71500	{4} - .50000
1 C2C10 control		1.000000	1.000000	1.000000
2 ACTC control	1.000000		1.000000	1.000000
3 C2C10 + ACTC	1.000000	1.000000		1.000000
4 Transfection control	1.000000	1.000000	1.000000	

<b>Bonferroni test; variable BRET ratio (MCS; NO CALCIUM)</b>							
<b>Probabilities for Post Hoc Tests Error: Between MS = .11769, df = 7.0000</b>							
Sample	{1} - .16500	{2} - .02000	{3} - .23000	{4} - .31000	{5} - .09000	{6} - .19000	{7} - .50000
1 C2C10 control		1.000000	1.000000	1.000000	1.000000	1.000000	1.000000
2 C2C10 MCS	1.000000		1.000000	1.000000	1.000000	1.000000	1.000000
3 C3C10 control	1.000000	1.000000		1.000000	1.000000	1.000000	1.000000
4 C3C10 MCS	1.000000	1.000000	1.000000		1.000000	1.000000	1.000000
5 C7C10 control	1.000000	1.000000	1.000000	1.000000		1.000000	1.000000
6 C7C10 MCS	1.000000	1.000000	1.000000	1.000000	1.000000		1.000000
7 Transfection control	1.000000	1.000000	1.000000	1.000000	1.000000	1.000000	

<b>Bonferroni test; variable BRET ratio (MCS; CALCIUM ADDED)</b>							
<b>Probabilities for Post Hoc Tests Error: Between MS = .23641, df = 7.0000</b>							
Sample	{1} - .05500	{2} - .15500	{3} - .03500	{4} - .49500	{5} - .03000	{6} - .57500	{7} - .50000
1 C2C10 control		1.000000	1.000000	1.000000	1.000000	1.000000	1.000000
2 C2C10 MCS	1.000000		1.000000	1.000000	1.000000	1.000000	1.000000
3 C3C10 control	1.000000	1.000000		1.000000	1.000000	1.000000	1.000000
4 C3C10 MCS	1.000000	1.000000	1.000000		1.000000	1.000000	1.000000
5 C7C10 control	1.000000	1.000000	1.000000	1.000000		1.000000	1.000000
6 C7C10 MCS	1.000000	1.000000	1.000000	1.000000	1.000000		1.000000
7 Transfection control	1.000000	1.000000	1.000000	1.000000	1.000000	1.000000	

## THESIS REFERENCES

<http://pa.cs.ualberta.ca:8080/pa/pa/index.html>

<http://www.clontech.com>

<http://www.imtech.res.in/raghava/eslpred>

<http://www.ncbi.nlm.nih.gov/BLAST/>

<http://www.ncbi.nlm.nih.gov/Entrez>

<http://www.perkinelmer.com>

Ababou A, Zhou L, Gautel M *et al.* Sequence specific assignment of domain C1 of the N-terminal myosin-binding site of human cardiac myosin binding protein C (MyBP-C). *J Biomol NMR*. 2004;29:431-432.

Ababou A, Gautel M, Pfuhl M. Dissecting the N-terminal myosin binding site of human cardiac myosin binding C: structure and myosin binding of domain C2. *J Biol Chem*. 2006;282:9204-9215.

Abbott MB, Dong W-J, Dvoretsky A *et al.* Modulation of cardiac troponin C-cardiac troponin I regulatory interactions by the amino-terminus of cardiac troponin I. *Biochemistry*. 2001;40:5992-6001.

Adamcova M, Pelouch V. Isoforms of troponin in normal and diseased myocardium. *Physiol Res*. 1999;48:235-247.

Agarkova I, Ehler E, Lange S *et al.* M-band: a safeguard for sarcomere stability? *J Muscle Res Cell Motil*. 2003;24:191-203.

Agarkova I, Perriard JC. The M-band: an elastic web that crosslinks thick filaments in the center of the sarcomere. *Trends Cell Biol*. 2005;15:477-485.

Alyonycheva TN, Mikawa T, Reinach FC *et al.* Isoform-specific interaction of the myosin-binding proteins (MyBPs) with skeletal and cardiac myosin is a property of the C-terminal immunoglobulin domain. *J Biol Chem*. 1997;272:20866-20872.

Arber S, Hunter JJ, Ross J *et al.* MLP-deficient mice exhibit a disruption of cardiac cytoarchitectural organization, dilated cardiomyopathy, and heart failure. *Cell*. 1997;88:393-403.

Au Y. The muscle ultrastructure: a structural perspective of the sarcomere. *Cell Mol Life Sci*. 2004;61:3016-3033.

Bang ML, Centner T, Fornoff F *et al.* The complete gene sequence of titin, expression of an unusual approximately 700-kDa titin isoform, and its interaction with obscurin identify a novel Z-line to I-band linking system. *Circ Res*. 2001;89:1065-1072.

Barbato JC, Huang Q-Q, Moazzem M *et al.* Proteolytic N-terminal truncation of cardiac troponin I enhances ventricular diastolic function. *J Biol Chem.* 2005;280:6602-6609.

Barral JM, Hutagalung AH, Brinker A *et al.* Role of the myosin assembly protein UNC-45 as a molecular chaperone for myosin. *Science.* 2002;295:669-671.

Bashyam MD, Savithri GR, Kumar MS *et al.* Molecular genetics of familial hypertrophic cardiomyopathy (FHC). *J Hum Genet.* 2003;48:55-64.

Berggard T, Linse S, James P. Methods for the detection and analysis of protein-protein interactions. *Proteomics.* 2007;7:2833-2842.

Bers DM, Guo T. Calcium signalling in cardiac ventricular myocytes. *Ann N Y Acad Sci.* 2005;1047:86-98.

Bertola LD, Ott EB, Griebsma S *et al.* Developmental expression of the alpha-skeletal actin gene. *BMC Evol Biol.* 2008;8:166.

Bhupathy P, Babu GJ, Periasamy M. Sarcolipin and phospholamban as regulators of cardiac sarcoplasmic reticulum Ca<sup>2+</sup> ATPase. *J Mol Cell Cardiol.* 2007;42:903-911.

Blair E, Redwood C, Ashrafian H *et al.* Mutations in the  $\gamma_2$  subunit of AMP-activated protein kinase cause familial hypertrophic cardiomyopathy: evidence for the central role of energy compromise in disease pathogenesis. *Hum Mol Genet.* 2001;10:1215-1220.

Boateng SY, Goldspink PH. Assembly and maintenance of the sarcomere. *Cardiovasc Res.* 2008;77:667-675.

Bodine SC, Latres E, Baumhueter S *et al.* Identification of ubiquitin ligases required for skeletal muscle atrophy. *Science.* 2001;294:1704-1708.

Borisov AB, Martynova MG, Russell MW. Early incorporation of obscurin into nascent sarcomeres: implication for myofibril assembly during cardiac myogenesis. *Histochem Cell Biol.* 2008;129:463-478.

Bosch-Comas A, Lindsten K, Gonzalez-Duarte R *et al.* The ubiquitin-specific protease USP25 interacts with three sarcomeric proteins. *Cell Mol Life Sci.* 2006;63:723-734.

Brenner B. Effect of Ca<sup>2+</sup> on cross-bridge turnover kinetics in skinned rabbit psoas fibers: implication for regulation of muscle contraction. *Proc Natl Acad Sci USA.* 1988;85:3265-3269.

Buckberg GD, Mahajan A, Jung B *et al.* MRI myocardial motion and fiber tracking: a confirmation of knowledge from different imaging modalities. *Eur J Cardiothorac Surg.* 2006;29:S165-S177.

Bullard B, Ferguson C, Minajeva A *et al.* Association of the chaperone alphaB-crystallin with titin in heart muscle. *J Biol Chem.* 2004;279:7917-7924.

Burkart EM, Sumandea MP, Kobayashi T *et al.* Phosphorylation or glutamic acid substitution at protein kinase C sites on cardiac troponin I differentially depress myofilament tension and shortening velocity. *J Biol Chem.* 2003;278:11265-11272.

Burstein E, Ganesh L, Dick RD *et al.* A novel role for XIAP in copper homeostasis through regulation of MURR1. *EMBO.* 2004;23:244-254.

Burstein E, Hoberg JE, Wilkinson AS *et al.* COMMD proteins, a novel family of structural and functional homologs of MURR1. *J Biol Chem.* 2005;280:22222-22232.

Buscemi N, Foster DB, Neverova I *et al.* p21-activated kinase increases the calcium sensitivity of rat triton-skinned cardiac muscle fiber bundles via a mechanism potentially involving novel phosphorylation of troponin I. *Circ Res.* 2002;91:509-516.

Calaghan SC, Trinick J, Knight PJ *et al.* A role for C-protein in the regulation of contraction and intracellular Ca<sup>2+</sup> in intact rat ventricular myocytes. *J Physiol.* 2000;528:151-156.

Carlsson L, Yu JG, Moza M *et al.* Myotilin: a prominent marker of myofibrillar remodelling. *Neuromuscul Disord.* 2007;17:61-68.

Carrier L, Knöll R, Vignier N *et al.* Asymmetric septal hypertrophy in heterozygous cMyBP-C null mice. *Cardiovasc Res.* 2004;63:293-304.

Cazorla O, Szilagyi S, Vignier N *et al.* Length and protein kinase A modulations of myocytes in cardiac myosin binding protein C-deficient mice. *Cardiovasc Res.* 2006;69:370-380.

Centner T, Yano J, Kimura E *et al.* Identification of muscle specific ring finger proteins as potential regulators of the titin kinase domain. *J Mol Biol.* 2001;306:717-726.

Chan JY, Takeda M, Briggs LE *et al.* Identification of cardiac-specific myosin light chain kinase. *Circ Res.* 2008;102:571-580.

Chang AN, Potter JD. Sarcomeric protein mutations in dilated cardiomyopathy. *Heart Fail Rev.* 2005;10:225-235.

Chen J, Kubalak SW, Minamisawa S *et al.* Selective requirement of myosin light chain 2v in embryonic heart function. *J Biol Chem.* 1998;273:1252-1256.

Chen Z, Higashiyama A, Yaku H *et al.* Altered expression of troponin T isoforms in mild left ventricular hypertrophy in the rabbit. *J Mol Cell Cardiol.* 1997;29:2345-2354.

- Chu G, Luo W, Matlib MA *et al.* Compensatory mechanisms in phospholamban knock-out mouse hearts. *Biophys J.* 1996;70.
- Chu G, Sato Y, Harrer J *et al.* Pentameric assembly of phospholamban facilitates inhibition of cardiac function in vivo. *J Biol Chem.* 1998;273:33674-33680.
- Clapp AR, Medintz IL, Mattoussi H. Förster resonance energy transfer investigations using quantum-dot fluorophores. *Chemphyschem.* 2006;7:47-57.
- Clark KA, McElhinny AS, Beckerle MC *et al.* Striated muscle cytoarchitecture: an intricate web of form and function. *Annu Rev Cell Dev Biol.* 2002;18:637-706.
- Codd MB, Sugrue DD, Gersh BJ *et al.* Epidemiology of idiopathic dilated and hypertrophic cardiomyopathy. A population-based study in Olmsted County, Minnesota, 1975-1984. *Circulation.* 1989;80:564-572.
- Colson BA, Bekyarova T, Fitzsimons DP *et al.* Radial displacement of myosin cross-bridges in mouse myocardium due to ablation of myosin binding protein-C. *J Mol Biol.* 2007;367:36-41.
- Comi GP, Fortunato F, Lucchiari S *et al.* β-enolase deficiency, a new metabolic myopathy of distal glycolysis. *Ann Neurol.* 2001;50:202-207.
- Craig R, Woodhead JL. Structure and function of myosin filaments. *Curr Opin Struct Biol.* 2006;16:204-212.
- Crawford AW, Michelsen JW, Beckerle MC. An interaction between zyxin and alpha-actinin. *J Cell Biol.* 1992;116:1381-1393.
- Cusick ME, Klitgord N, Vidal M *et al.* Interactome: gateway into systems biology. *Hum Mol Genet.* 2005;14:R171-R181.
- Davis JS, Hassanzadeh S, Winitzky S *et al.* The overall pattern of cardiac contraction depends on a spatial gradient of myosin regulatory light chain phosphorylation. *Cell.* 2001;107:631-641.
- de Bie P, van de Sluis B, Burstein E *et al.* Characterisation of COMMD protein-protein interaction in NF-κB signalling. *Biochem J.* 2006;398:63-71.
- de Jong JW, Leunissen JA, Voorter CE. Evolution of the alpha-crystallin small heat-shock protein family. *Mol Biol Evol.* 1993;10:103-126.
- de Lange WJ. An investigation of myosin binding protein C mutations in South Africa and a search for ligands binding to myosin binding protein C. *PhD Thesis.* 2004;University of Stellenbosch.
- de Tombe PP, ter Keurs HE. An internal viscous element limits unloaded velocity of sarcomere shortening in rat myocardium. *J Physiol.* 1992;454:619-642.

- de Tombe PP. Cardiac myofilaments: mechanics and regulation. *J Biomechan*. 2003;36:721-730.
- Dhoot GK, Perry SV. Expression of slow skeletal myosin binding C-protein in normal adult mammalian heart. *J Muscle Res Cell Motil*. 2005;26:143-148.
- Djinovic-Carugo K, Young P, Gautel M *et al*. Structure of the alpha-actinin rod: Molecular basis for cross-linking of actin filaments. *Cell*. 1999;98:537-546.
- Dong W-J, Robinson JM, Stagg S *et al*. Ca<sup>2+</sup>-induced conformational transition in the inhibitory and regulatory regions of cardiac troponin I. *J Biol Chem*. 2003;278:8686-8692.
- Dong W-J, An J, Xing J *et al*. Structural transition of the inhibitory region of troponin I within the regulated cardiac thin filament. *Arch Biochem Biophys*. 2006;456:135-142.
- Dong W-J, Jayasundar J, An J *et al*. Effects of PKA phosphorylation of cardiac troponin I and strong crossbridge on conformational transitions of the N-domain of cardiac troponin C in regulated thin filaments. *Biochemistry*. 2007;46:9752-9761.
- Dong W-J, Xing J, Villial M *et al*. Conformation of the regulatory domain of cardiac muscle troponin C in its complex with cardiac troponin I. *J Biol Chem*. 1999;274:31382-31390.
- Doran P, Gannon J, O'Connell K *et al*. Aging skeletal muscle shows a drastic increase in the small heat shock proteins aB-crystallin/HspB5 and cvHsp/HspB7. *Eur J Cell Biol*. 2007;86:629-640.
- dos Remedios CG, Chhabra D, Kekic M *et al*. Actin binding proteins: regulation of cytoskeletal microfilaments. *Physiol Rev*. 2003;83:433-473.
- Edes I, Kranias E. Phospholamban and troponin I are substrates for protein kinase C in vitro but not intact beating guinea pig hearts. *Circ Res*. 1990;67:394-400.
- Eijssen LM, van den Bosch BJ, Vignier N *et al*. Altered gene expression reveals possible maladaptive processes in heterozygous and homozygous cardiac myosin-binding protein C knockout mice. *Genomics*. 2008;91:52-60.
- El-Armouche A, Boknik P, Eschenhagen T *et al*. Molecular determinants of altered Ca<sup>2+</sup> handling in human chronic atrial fibrillation. *Circulation*. 2006;114:670-680.
- El-Armouche A, Pohlmann L, Schlossarek S *et al*. Decreased phosphorylation levels of cardiac myosin-binding protein-C in human and experimental heart failure. *J Mol Cell Cardiol*. 2007;43:223-229.
- Elsherif L, Jiang Y, Saari JT *et al*. Dietary copper restriction-induced changes in myocardial gene expression and the effect of copper repletion. *Exp Biol Med*. 2008;229:616-622.

Emanuelsson O, von Heijne G, Schneider G. Analysis and prediction of mitochondrial targeting peptides. *Methods Cell Biol.* 2001;65:175-187.

England PJ. The significance of phosphorylation of myosin light chains in heart. *J Mol Cell Cardiol.* 1984;16:591-595.

Epstein ND, Davis JS. Sensing stretch is fundamental. *Cell.* 2003;112:147-150.

Epstein ND, Davis JS. When is a fly in the ointment a solution and not a problem? *Circ Res.* 2006;98:1110-1112.

Falk MM, Lauf U. High resolution, fluorescence deconvolution microscopy and tagging with the autofluorescent tracers CFP, GFP, and YFP to study the structural composition of gap junctions in living cells. *Microsc Res Tech.* 2001;52:251-262.

Fan GC, Ren X, Qian J et al. Novel cardioprotective role of a small heat-shock protein, Hsp20, against ischemia/reperfusion injury. *Circulation.* 2005;111:1792-1799.

Fatkin D, Graham RM. Molecular mechanisms of inherited cardiomyopathies. *Physiol Rev.* 2002;82:945-980.

Fentzke RC, Buck SH, Patel JR et al. Impaired cardiomyocyte relaxation and diastolic function in transgenic mice expressing slow skeletal troponin I in the heart. *J Physiol.* 1999;517:143-157.

Feo S, Oliva D, Barbieri G et al. The gene for the muscle-specific enolase is on the short arm of human chromosome 17. *Genomics.* 1990;6:192-194.

Ferns G, Shams S, Shafi S. Heat shock protein 27: its potential role in vascular disease. *Int J Exp Pathol.* 2006;87:253-274.

Filatov VL, Katrukha AG, Bulgarina TV et al. Troponin: Structure, properties and mechanism of functioning. *Biochemistry.* 1999;64:969-985.

Fink MA, Zakhary DR, Mackey JA et al. AKAP-mediated targeting of protein kinase A regulates contractility in cardiac myocytes. *Circ Res.* 2001;88:291-297.

Flashman E, Redwood C, Moolman-Smook J et al. Cardiac myosin binding protein C. Its role in physiology and disease. *Circ Res.* 2004;94:1279-1289.

Flashman E, Korkie L, Watkins H et al. Support for a trimeric collar of myosin binding protein C in cardiac and fast skeletal muscle, but not in slow skeletal muscle. *FEBS Lett.* 2008;582:434-438.

Flavigny J, Souchet M, Sebillon P *et al.* COOH-terminal truncated cardiac myosin-binding protein C mutants resulting from familial hypertrophic cardiomyopathy mutations exhibit altered expression and/or incorporation in fetal rat cardiomyocytes. *J Mol Biol.* 1999;294:443-456.

Fontaine JM, Sun X, Benndorf R *et al.* Interactions of HSP22 (HSPB8) with HSP20, alphaB-crystallin, and HSPB3. *Biochem Biophys Res Commun.* 2005;337:1006-1011.

Foucault G, Vacher M, Merkulova T *et al.* Presence of enolase in the M-band of skeletal muscle and possible indirect interaction with the cytosolic muscle isoform of creatine kinase. *Biochem J.* 1999;338:115-121.

Foucault G, Vacher M, Cribier S *et al.* Interactions between β-enolase and creatine kinase in the cytosol of skeletal muscle cells. *Biochem J.* 2000;346:127-131.

Fowler VM, Sussmann MA, Miller PG *et al.* Tropomodulin is associated with the free (pointed) ends of the thin filaments in rat skeletal muscle. *J Cell Biol.* 1993;120:411-420.

Frank D, Kuhn C, Katus HA *et al.* The sarcomeric Z-disc: a nodal point in signalling and disease. *J Mol Med.* 2006;84:446-468.

Franz WM, Muller OJ, Katus HA. Cardiomyopathies: from genetics to the prospect of treatment. *Lancet.* 2001;358:1627-1637.

Freiburg A, Gautel M. A molecular map of the interactions between titin and myosin binding protein C. Implications for sarcomeric assembly in familial hypertrophic cardiomyopathy. *Eur J Biochem.* 1996;235:317-323.

Frey N, Olson EN. Calsarcin-3, a novel skeletal muscle-specific member of the calsarcin family, interacts with multiple Z-disc proteins. *J Biol Chem.* 2002;277:13998-14004.

Fritz-Six KL, Cox PR, Fischer RS *et al.* Aberrant myofibril assembly in tropomodulin-1 null mice leads to aborted heart development and embryonic lethality. *J Cell Biol.* 2003;163:1033-1044.

Fukuda N, Wu Y, Nair P *et al.* Phosphorylation of titin modulates passive stiffness of cardiac muscle in a titin isoform-dependent manner. *J Gen Physiol.* 2005;125:257-271.

Garvey JL, Kranias E, Solaro J. Phosphorylation of C-protein, troponin I and phospholamban in isolated rabbit hearts. *Biochem J.* 1988;249:709-714.

Gautel M, Zuffard O, Freiburg A *et al.* Phosphorylation switches specific for the cardiac isoform of myosin binding protein-C: a modulator of cardiac contraction? *EMBO J.* 1995;14:1952-1960.

Gautel M, Fürst DO, Cocco A *et al.* Isoform transitions of the myosin binding protein C family in developing human and mouse muscles. *Circ Res.* 1998;82:124-129.

Geier C, Gehmlich K, Ehler E *et al.* Beyond the sarcomere: CSRP3 mutations cause hypertrophic cardiomyopathy. *Hum Mol Genet*. 2008;Epub ahead of print.

Gilbert R, Kelly MG, Mikawa T *et al.* The carboxyl terminus of myosin binding protein C (MyBP-C, C-protein) specifies incorporation into the A-band of striated muscle. *J Cell Sci*. 1996;109:101-111.

Gilbert R, Cohen JA, Pardo S *et al.* Identification of the A-band localization domain of myosin binding proteins C and H (MyBP-C and MyBP-H) in skeletal muscle. *J Cell Sci*. 1999;112:69-79.

Golenhofen H, Htun P, Ness W *et al.* Binding of the stress protein alpha B-crystallin to cardiac myofibrils correlates with the degree of myocardial damage during ischemia/reperfusion in vivo. *J Mol Cell Cardiol*. 1999;31:569-580.

Gotthardt M, Hammer RE, Hubner N *et al.* Conditional expression of mutant M-line titins result in cardiomyopathy with altered sarcomere structure. *J Biol Chem*. 2003;278:6059-6065.

Granzier HL, Labeit S. Cardiac titin: an adjustable multifunctional spring. *J Physiol*. 2002;541:335-342.

Granzier HL, Labeit S. The giant protein titin. A major player in myocardial mechanics, signalling, and disease. *Circ Res*. 2004;94:284-295.

Green WC. How resting T cells deMURR HIV infection. *Nat Immunol*. 2004;5:18-19.

Gregorio CC, Trombitas K, Centner T *et al.* The NH<sub>2</sub> terminus of titin spans the Z-disc: its interaction with a novel 19-kDa ligand (T-cap) is required for sarcomeric integrity. *J Cell Biol*. 1998;143:1013-1027.

Gruen M, Prinz H, Gautel M. cAPK-phosphorylation controls the interaction of the regulatory domain of cardiac myosin binding protein C with myosin-S2 in an on-off fashion. *FEBS Lett*. 1999a;453:254-259.

Gruen M, Gautel M. Mutations in β-myosin S2 that cause familial hypertrophic cardiomyopathy (FHC) abolish the interaction with the regulatory domain of myosin-binding protein-C. *J Mol Biol*. 1999b;286:933-949.

Gulick J, Hewett TE, Klevitsky R *et al.* Transgenic remodeling of the regulatory myosin light chains in the mammalian heart. *Circ Res*. 1997;80:655-664.

Gunning P, O'Neill G, Hardeman E. Tropomyosin-based regulation of the actin cytoskeleton in time and space. *Physiol Rev*. 2008;88:1-35.

Gupta S, Young D, Maitra RK *et al.* Prevention of cardiac hypertrophy and heart failure by silencing of NF-κB. *J Mol Biol*. 2008;375:637-649.

Ha KN, Traaseth NJ, Verardi R *et al.* Controlling the inhibition of the sarcoplasmic  $\text{Ca}^{2+}$ -ATPase by tuning phospholamban structural dynamics. *J Biol Chem.* 2007;282:37205-37214.

Hagemann D, Xiao R-P. Dual site phospholamban phosphorylation and its physiological relevance in the heart. *Trends Cardiovasc Med.* 2002;12:51-56.

Hall G, Hasday JD, Rogers TB. Regulating the regulator: NF- $\kappa$ B signaling in heart. *J Mol Cell Cardiol.* 2006;41:580-591.

Harris SP, Bartley CR, Hacker TA *et al.* Hypertrophic cardiomyopathy in cardiac myosin binding protein-C knockout mice. *Circ Res.* 2002;90:594-601.

Harris SP, Rostkova E, Gautel M *et al.* Binding of myosin binding protein-C to myosin subfragment S2 affects contractility independent of a tether mechanism. *Circ Res.* 2004;95:930-936.

Hernandez OM, Jones M, Guzman G *et al.* Myosin essential light chain in health and disease. *Am J Physiol Heart Circ Physiol.* 2007;292:H1643-H1654.

Herron TJ, Korte FS, McDonald KS. Power output is increased after phosphorylation of myofibrillar proteins in rat skinned cardiac myocytes. *Circ Res.* 2001;89:1184-1190.

Herron TJ, Rostkova E, Kunst G *et al.* Activation of myocardial contraction by the N-terminal domains of myosin binding protein-C. *Circ Res.* 2006;98:1290-1298.

Herzberg O, Moult J, James MN. Calcium binding to skeletal muscle troponin C and the regulation of muscle contraction. *Ciba Found Symp.* 1986;122:120-144.

Hoffmann C, Gaietta G, Bunemann M *et al.* A FlAsH-based FRET approach to determine G protein-coupled receptor activation in living cells. *Nat Methods.* 2005;2:171-176.

Hofmann PA, Greaser M, Moss RL. C-protein limits shortening velocity of rabbit skeletal muscle fibres at low levels of  $\text{Ca}^{2+}$  activation. *J Physiol.* 1991a;439:701-715.

Hofmann PA, Hartzell HC, Moss RL. Alterations in  $\text{Ca}^{2+}$  sensitive tension due to partial extraction of C-protein from rat skinned cardiac myocytes and rabbit skeletal muscle fibers. *J Gen Physiol.* 1991b;97:1141-1163.

Hofmann PA, Lange JH. Effects of phosphorylation of troponin I and C-protein on isometric tension and velocity of unloaded shortening in skinned single cardiomyocytes from rats. *Circ Res.* 1994;74:718-726.

Holmes WB, Moncman CL. Nebulette interacts with filamin C. *Cell Motil Cytoskel.* 2008;65:130-142.

Hoshijima M. Mechanical stress-strain sensors embedded in cardiac cytoskeleton: Z disk, titin and associated structures. *Am J Physiol Heart Circ Physiol.* 2006;290:H1313-H1325.

Houdusse A, Love ML, Dominguez R *et al.* Structures of four  $\text{Ca}^{2+}$ -bound troponin C at 2.0 Å resolution: further insights into the  $\text{Ca}^{2+}$ -switch in the calmodulin superfamily. *Structure.* 1997;5:1695-1711.

Houmeida A, Holt J, Tskhovrebova L *et al.* Studies of the interaction between titin and myosin. *J Cell Biol.* 1995;131:1471-1481.

Houslay MD, Adams DR. PDE4 cAMP phosphodiesterases: modular enzymes that orchestrate signalling cross-talk, desensitization and compartmentalization. *Biochem J.* 2003;370:1-18.

Houslay MD, Baillie GS, Maurice DH. cAMP-specific phosphodiesterase-4 enzymes in the cardiovascular system. *Circ Res.* 2007;100:950-966.

Howarth JW, Meller J, Solaro J *et al.* Phosphorylation-dependent conformational transition of the cardiac specific N-extension of troponin I in cardiac troponin. *J Mol Biol.* 2007;373:706-722.

Hua S, Sun Z. Support vector machine approach for protein subcellular localization prediction. *Bioinformatics.* 2001;17:721-728.

Huxley AF. Muscle structure and theories of contraction. *Prog Biophys Biophys Chem.* 1957;7:255-318.

Huxley AF. Mechanics and models of the myosin motor. *Philos Trans R Soc Lond.* 2000;355:433-440.

Huxley HE, Brown W. The low-angle X-ray diagram of vertebrate striated muscle and its behaviour during contraction and rigor. *J Mol Biol.* 1967;30:383-434.

Huxley HE. The mechanism of muscular contraction. *Science.* 1969;164:1356-1366.

Idowu SM, Gautel M, Perkins SJ *et al.* Structure, stability and dynamics of the central domain of cardiac myosin binding protein C (MyBP-C): Implications for multidomain assembly and causes for cardiomyopathy. *J Mol Biol.* 2003;329:745-761.

James J, Osinska H, Hewett TE *et al.* Transgenic over-expression of a motor protein at high levels results in severe cardiac pathology. *Transgenic Res.* 1999;8:9-22.

James P, Inui M, Tada M *et al.* Nature and site of phospholamban regulation of the  $\text{Ca}^{2+}$  pump of sarcoplasmic reticulum. *Nature.* 1989;342:90-92.

Jansen PM, de Tombe PP. Protein kinase A does not alter unloaded velocity of sarcomere shortening in skinned rat cardiac trabeculae. *Am J Physiol.* 1997;273:H2415-H2422.

Jeffery CJ. Moonlighting proteins: old proteins learning new tricks. *Trends Genet.* 2003;19:415-417.

Jeffries CM, Whitten AE, Harris SP *et al.* Small-angle x-ray scattering reveals the N-terminal domain organization of cardiac myosin binding protein C. *J Mol Biol.* 2008;377:1186-1199.

Jideama NM, Noland TA, Raynor RL *et al.* Phosphorylation specificities of protein kinase C isozymes for bovine cardiac troponin I and troponin T and sites within these proteins and regulation of myofilament properties. *J Biol Chem.* 1996;271:23277-23283.

Jin J-P. Cloned rat cardiac titin class I and class II motifs. *J Biol Chem.* 1995;270:6908-6916.

Johannessen M, Moller S, Hansen T *et al.* The multifunctional roles of the four-and-a-half-LIM only protein FHL2. *Cell Mol Life Sci.* 2006;63:268-284.

Kadambi VJ, Ponniah S, Harrer J *et al.* Cardiac-specific overexpression of phospholamban alters calcium kinetics and resultant cardiomyocyte mechanics in transgenic mice. *J Clin Invest.* 1996;97:533-539.

Kadambi VJ, Kranias E. Phospholamban: a protein coming of age. *Biochem Biophys Res Commun.* 1997;239:1-5.

Karin M, Lin A. NF-kappaB at the crossroads of life and death. *Nat Immunol.* 2002;3:221-227.

Katz AM, Lorell BH. Regulation of cardiac contraction and relaxation. *Circulation.* 2000;102:69-74.

Keane NE, Quirk PG, Gao Y *et al.* The ordered phosphorylation of cardiac troponin I by the cAMP-dependent protein kinase-structural consequences and functional implications. *J Biol Chem.* 1997;248:329-337.

Keller A, Demeurie J, Merkulova T *et al.* Fibre-type distribution and subcellular localisation of  $\alpha$  and  $\beta$  enolase in mouse striated muscle. *Biol Cell.* 2000;92:527-535.

Kentish JC, McCloskey DT, Layland J *et al.* Phosphorylation of troponin I by protein kinase A accelerates relaxation and crossbridge cycle kinetics in mouse ventricular muscle. *Circ Res.* 2001;88:1059-1065.

Kleerekoper Q, Howarth JW, Guo X *et al.* Cardiac troponin I induced conformational changes in cardiac troponin C as monitored by NMR using site-directed spin and isotope labeling. *Biochemistry.* 1995;34:13343-13352.

Klevay LM. Cardiovascular disease from copper deficiency- a history. *J Nutr.* 2000;130:489-492.

Klomp AE, van de Sluis B, Klomp LW *et al.* The ubiquitously expressed Murr1 protein is absent in canine copper toxicosis. *J Hepatol.* 2003;39:703-709.

Kögler H. The role of cardiac myosin binding protein-C as a regulator of myofilament  $\text{Ca}^{2+}$  sensitivity. *Cardiovasc Res.* 2006;69:304-306.

Koretz JF, Irving TC, Wang K. Filamentous aggregates of native titin and binding of C-protein and AMP-deaminase. *Arch Biochem Biophys.* 1993;304:305-309.

Korte FS, McDonald KS, Harris SP *et al.* Loaded shortening, power output, and rate of force redevelopment are increased with knockout of cardiac myosin binding protein-C. *Circ Res.* 2003;93:752-758.

Koss KL, Kranias E. Phospholamban: a prominent regulator of myocardial contractility. *Circ Res.* 1996;79:1059-1063.

Krief S, Faivre J-F, Robert P *et al.* Identification and characterization of cvHsp. *J Biol Chem.* 1999;274:36592-36600.

Kulikovskaya I, McClellan G, Flavigny J *et al.* Effect of MyBP-C binding to actin on contractility in heart muscle. *J Gen Physiol.* 2003a;122:761-774.

Kulikovskaya I, McClellan G, Levine R *et al.* Effect of extraction of myosin binding protein C on contractility of rat heart. *Am J Physiol Heart Circ Physiol.* 2003b;285:H857-H865.

Kulikovskaya I, McClellan G, Levine R *et al.* Multiple forms of cardiac myosin-binding protein C exist and can regulate thick filament stability. *J Gen Physiol.* 2007;129:419-428.

Kumarapeli AR, Wang X. Genetic modification of the heart: chaperones and the cytoskeleton. *J Mol Cell Cardiol.* 2004;37:1097-1109.

Kunst G, Kress KR, Gruen M *et al.* Myosin binding protein C, a phosphorylation-dependent force regulator in muscle that controls the attachment of myosin heads by its interaction with myosin S2. *Circ Res.* 2000;86:51-58.

Labeit S, Kolmerer B. Titins: Giant proteins in charge of muscle ultrastructure and elasticity. *Science.* 1995;270:293-296.

Laing NG, Nowak KJ. When contractile proteins go bad: the sarcomere and skeletal muscle disease. *BioEssays.* 2005;27:809-822.

Lange S, Auerbach D, McLoughlin P *et al.* Subcellular targeting of metabolic enzymes to titin in heart muscle may be mediated by DRAL/FHL-2. *J Cell Sci.* 2002;63:268-284.

Lange S, Xiang F, Yakovenko A *et al.* The titin kinase domain of titin controls muscle gene expression and protein turnover. *Science.* 2005;308:1599-1603.

Lange S, Ehler E, Gautel M. From A to Z and back? Multicompartment proteins in the sarcomere. *Trends Cell Biol.* 2006;16:11-18.

Layland J, Solaro J, Shah AM. Regulation of cardiac contractile function by troponin I phosphorylation. *Cardiovasc Res.* 2005;66:12-21.

Levine R, Griffiths H, Patchell V *et al.* Study of the phosphorylatable light chains of skeletal and gizzard myosins by nuclear magnetic resonance spectroscopy. *Biochem J.* 1988;254:277-286.

Levine R, Chantler PD, Kensler RW *et al.* Effects of phosphorylation by myosin light chain kinase on the structure of Limulus thick filaments. *J Cell Biol.* 1991;113:563-572.

Levine R, Yang Z, Stull JT *et al.* Structure and functional responses of mammalian thick filaments to alterations in myosin regulatory light chains. *J Struct Biol.* 1998;122:149-161.

Levine R, Weisberg A, Kulikovskaya I *et al.* Multiple structures of thick filaments in resting cardiac muscle and their influence on cross-bridge interactions. *Biophys J.* 2001;81:1070-1082.

LeWinter MM, Wu Y, Labeit S *et al.* Cardiac titin: structure, functions and role in disease. *Clin Chim Acta.* 2007;375:1-9.

Li B, Trueb B. Analysis of the alpha-actinin/zyxin interaction. *J Biol Chem.* 2001;276:33328-22235.

Li H, Oberhauser AF, Redick SD *et al.* Multiple conformations of PEVK proteins detected by single-molecule techniques. *Proc Natl Acad Sci USA.* 2001;98:10682-10686.

Li H, Cook JD, Terry M *et al.* Calcium transients regulate patterned actin assembly during myofibrillogenesis. *Dev Dyn.* 2004;229:231-242.

Li MX, Spyracopoulos L, Sykes BD. Binding of cardiac troponin-I 147-163 induces a structural opening in human cardiac troponin-C. *Biochemistry.* 1999;38:8289-8298.

Li MX, Wang X, Sykes BD. Structural based insights into the role of troponin in cardiac muscle pathophysiology. *J Muscle Res Cell Motil.* 2004;25:559-579.

Li Y, Ha T, Gao X *et al.* NF- $\kappa$ B activation is required for the development of cardiac hypertrophy in vivo. *Am J Physiol Heart Circ Physiol.* 2004;287:H1712-H1720.

Lian W, Litherland SA, Badrane H *et al.* Ultrasensitive detection of biomolecules with fluorescent dye-doped nanoparticles. *Anal Biochem.* 2004;334:135-144.

Liberek K, Lewandowska A, Zietkiewicz S. Chaperones in control of protein aggregation. *EMBO.* 2008;27:328-335.

Lim MS, Walsh MP. Phosphorylation of skeletal and cardiac muscle C-proteins by the catalytic subunit of cAMP-dependent protein kinase. *Arch Biochem Cell Biol.* 1986;64:622-630.

Lin JW, Wyszynski M, Madhavan R *et al.* Yotiao, a novel protein of neuromuscular junction and brain that interacts with specific splice variants of NMDA receptor subunit NR1. *J Neurosci*. 1998;18:2017-2027.

Lin Z, Lu MH, Schultheiss T *et al.* Sequential appearance of muscle-specific proteins in myoblasts as a function of time after cell division: evidence for a conserved myoblast differentiation program in skeletal muscle. *Cell Motil Cytoskeleton*. 1994;29:1-19.

Lindhout DA, Boyko RF, Corson DC *et al.* The role of electrostatics in the interaction of the inhibitory region of troponin I with troponin C. *Biochemistry*. 2005;44:14750-14759.

Linke WA, Kulke M, Li H *et al.* PEVK domain of titin: an entropic spring with actin-binding properties. *J Struct Biol*. 2002;137:194-205.

Linke WA. Sense and stretchability: The role of titin and titin-associated proteins in myocardial stress-sensing and mechanical dysfunction. *Cardiovasc Res*. 2008;77:637-648.

Liu L, Sakai T, Sano N *et al.* Nucling mediates apoptosis by inhibiting expression of galectin-3 through interference with nuclear factor kB signalling. *Biochem J*. 2004;380:31-41.

Lohse MJ, Engelhardt S, Eschenhagen T. What is the role of beta-adrenergic signaling in heart failure? *Circ Res*. 2003;93:896-906.

Lu X-Y, Chen L, Cai X-L *et al.* Overexpression of heat shock protein 27 protects against ischaemic/reperfusion-induced cardiac dysfunction via stabilization of troponin I and T. *Cardiovasc Res*. 2008;Epub ahead of print.

Luo W, Grupp IL, Harrer J *et al.* Targeted ablation of the phospholamban gene is associated with markedly enhanced myocardial contractility and loss of β-agonist stimulation. *Circ Res*. 1994;75:401-409.

Lynn RW, Taylor EW. Mechanism of adenosine triphosphate hydrolysis by actomyosin. *Biochem*. 1971;10:4617-4624.

MacArthur DG, North KN. A gene for speed? The evolution and function of α-actinin-3. *BioEssays*. 2004;26:786-795.

MacDougall LK, Jones LR, Cohen P. Identification of the major protein phosphatases in mammalian cardiac muscle which dephosphorylate phospholamban. *Eur J Biochem*. 1991;196:725-734.

MacGowan GA, Du C, Koretsky AP. High calcium and dobutamine positive inotropy in the perfused mouse heart: myofilament calcium responsiveness, energetic economy, and effects of protein kinase C inhibition. *BMC Physiol*. 2001;1:12.

- Malhotra A, Huang S, Bhan A. Subunit function in cardiac myosin: effect of removal of Lc2 (18 000 molecular weight) on enzymatic properties. *Biochemistry*. 1979;18:461-466.
- Margossian SS, White H, Caulfield J *et al*. Light chain 2 profile and activity of human ventricular myosin during dilated cardiomyopathy. *Circulation*. 1992;85:1720-1733.
- Maron BJ, Gardin JM, Flack JM *et al*. Prevalence of hypertrophic cardiomyopathy in a general population of young adults. *Circulation*. 1995;92:785-789.
- Maron BJ. Hypertrophic cardiomyopathy. *Lancet*. 1997;350:127-133.
- Martin AF. Turnover of cardiac troponin subunits. *J Biol Chem*. 1981;256:964-968.
- Martin JL, Mestril R, Hilal-Dandan R *et al*. Small heat shock proteins and protection against ischemic injury in cardiac myocytes. *Circulation*. 1997;96:4343-4348.
- Marx SO, Kurokawa J, Reiken S *et al*. Requirement of a macromolecular signaling complex for beta adrenergic receptor modulation of the KCNQ1-KCNE1 potassium channel. *Science*. 2002;295:496-499.
- Mattiazzi A, Mundina-Weilenmann C, Guo Xiang C *et al*. Role of phospholamban phosphorylation on Thr<sup>17</sup> in cardiac physiological and pathological conditions. *Cardiovasc Res*. 2005;68:366-375.
- Maw MC, Rowe AJ. The reconstruction of myosin filaments in rabbit psoas muscle from solubilized myosin. *J Muscle Res Cell Motil*. 1986;7:97-109.
- Mayans OM, van der Ven PF, Wilm M *et al*. Structural basis for activation of the titin kinase domain during myofibrillogenesis. *Nature*. 1998;395:863-869.
- Maytum R, Geeves MA. Cooperativity and switching within the three-state model of muscle regulation. *Biochemistry*. 1999;38:1102-1110.
- McClellan G, Weisberg A, Winegrad S. Cyclic AMP can raise or lower cardiac actomyosin ATPase activity depending on alpha adrenergic activity. *Am J Physiol*. 1994;267:H431-H442.
- McClellan G, Kulikovskaya I, Winegrad S. Changes in cardiac contractility related to calcium-mediated changes in phosphorylation of myosin-binding protein C. *Biophys J*. 2001;81:1083-1092.
- McClellan G, Kulikovskaya I, Flavigny J *et al*. Effect of cardiac myosin-binding protein C on stability of the thick filament. *J Mol Cell Cardiol*. 2004;37:823-835.
- McConnell BK, Jones KA, Fatkin D *et al*. Dilated cardiomyopathy in homozygous myosin-binding protein-C mutant mice. *J Clin Invest*. 1999;104:1235-1244.

McElhinny AS, Kolmerer B, Fowler VM *et al.* The N-terminal end of nebulin interacts with tropomodulin at the pointed ends of the thin filaments. *J Biol Chem.* 2001;276:583-592.

McKay RT, Tripet BP, Pearlstone JR *et al.* Defining the region of troponin-I that binds to troponin-C. *Biochemistry.* 1999;38:5478-5489.

Merkulova T, Keller A, Oliviero P *et al.* Thyroid hormones differentially modulate enolase enzymes during rat skeletal and cardiac muscle development. *Am J Physiol Endocrinol Metab.* 2000;278:E330-E339.

Metzger JM, Westfall MV. Covalent and noncovalent modification of thin filament action. The essential role of troponin in cardiac muscle regulation. *Circ Res.* 2004;94:146-158.

Michailidis IE, Helton TD, Petrou VI *et al.* Phosphatidylinositol-4,5-biphosphate regulates NMDA receptor activity through a-actinin. *J Neurosci.* 2007;27:5523-5532.

Minamisawa S, Gu Y, Ross J *et al.* Post-transcriptional compensatory pathway in heterozygous ventricular myosin light chain 2-deficient mice results in lack of gene dosage effect during normal cardiac growth or hypertrophy. *J Biol Chem.* 1999;274:10066-10070.

Mizuguchi K, Deane CM, Blundell TL *et al.* HOMSTRAD: a database of protein structure alignments for homologous families. *Protein Sci.* 2008;7:2469-2471.

Montgomery DE, Chandra M, Huang Q-Q *et al.* Transgenic incorporation of skeletal TnT into cardiac myofilaments blunts PKC-mediated depression of force. *Am J Physiol Heart Circ Physiol.* 2001;280:H1011-H1018.

Moolman-Smook J, Flashman E, de Lange W *et al.* Identification of novel interactions between domains of myosin binding protein-C that are modulated by hypertrophic cardiomyopathy missense mutations. *Circ Res.* 2002;91:704-711.

Moolman JA, Reith S, Uhl K. A newly created splice donor site in exon 25 of the MyBP-C gene is responsible for inherited hypertrophic cardiomyopathy. *Circulation.* 2000;101:1396-1402.

Moos C, Mason CM, Besterman JM *et al.* The binding of skeletal muscle C-protein to F-actin and its relation to the interaction of actin with myosin subfragment-1. *J Mol Biol.* 1978;124:571-586.

Moos C, Feng IN. Effect of C-protein on actomyosin ATPase. *Biochem Biophys Acta.* 1980;632:141-149.

Morano I. Tuning the human heart molecular motors by myosin light chains. *J Mol Med.* 1999;77:544-555.

Morrison LE, Whittaker JL, Klepper RE *et al.* Roles for alphaB-crystallin and HSPB2 in protecting the myocardium from ischemia-reperfusion-induced damage in a KO mouse model. *Am J Physiol.* 2004;286:H847-H855.

Moss RL, Fitzsimons DP. Myosin light chain 2 into the mainstream of cardiac development and contractility. *Circ Res*. 2006;99:225-227.

Musa H, Meek S, Gautel M *et al*. Targeted homozygous deletion of M-band titin in cardiomyocytes prevents sarcomere formation. *J Cell Sci*. 2006;119:4322-4331.

Nagayama T, Takimoto E, Sadayappan S *et al*. Control of in vivo contraction/relaxation kinetics by myosin binding protein C. *Circulation*. 2007;116:2399-2408.

Nair R, Rost B. Inferring sub-cellular localization through automated lexical analysis. *Bioinformatics*. 2002;1:S78-S86.

Nave R, Fürst DO, Weber K. Visualization of the polarity of isolated titin molecules: a single globular head on a long thin rod as the M band anchoring domain? *J Cell Biol*. 1989;109:2177-2187.

Noland TA, Raynor RL, Kuo JF. Identification of sites phosphorylated in bovine cardiac troponin I and troponin T by protein kinase C and comparative substrate activity of synthetic peptides containing the phosphorylation sites. *J Biol Chem*. 1989;264:20778-20785.

Noland TA, Kuo JF. Protein kinase C phosphorylation of cardiac troponin T decreases  $\text{Ca}^{2+}$ -dependent actomyosin MgATPase activity and troponin T binding to tropomyosin-F-actin complex. *Journal of Biochemistry*. 1992;288:123-129.

Noland TA, Raynor RL, Jideama NM *et al*. Differential regulation of cardiac actomyosin S-1 MgATPase by protein kinase C isozyme-specific phosphorylation of specific sites in cardiac troponin I and its phosphorylation site mutants. *Biochemistry*. 1996;35:14923-14931.

Oakley CE, Hambly BD, Curmi PM *et al*. Myosin binding protein C: structural abnormalities in familial hypertrophic cardiomyopathy. *Cell Res*. 2004;14:95-110.

Oakley CE, Chamoun J, Brown LJ *et al*. Myosin binding protein-C: enigmatic regulator of cardiac contraction. *Int J Biochem Cell Biol*. 2007;39:2161-2166.

Obermann WM, Gautel M, Steiner F *et al*. The structure of the sarcomeric M band: localization of defined domains of myomesin, M protein, and the 250kD carboxy terminal region of titin by immunoelectron microscopy. *J Cell Biol*. 1996;134:1441-1453.

Obermann WM, Gautel M, Weber K *et al*. Molecular structure of the sarcomeric M-band: mapping of titin and myosin binding domains in myomesin and the identification of a potential regulatory phosphorylation site in myomesin. *EMBO*. 1997;16:211-220.

Okagaki T, Weber FE, Fischman DA *et al*. The major myosin-binding domain of skeletal muscle MyBP-C (C-protein) resides in the COOH-terminal, immunoglobulin C2 motif. *J Cell Biol*. 1993;123:619-626.

Olson EN, Williams RS. Calcineurin signaling and muscle remodeling. *Cell*. 2000;101:689-692.

Olsson MC, Patel JR, Fitzsimons DP *et al*. Basal myosin light chain phosphorylation is a determinant of Ca<sup>2+</sup>sensitivity of force and activation dependence of the kinetics of myocardial force development. *Am J Physiol*. 2004;287:H2712-H2718.

Ormö M, Cubitt AB, Kallio K *et al*. Crystal structure of the *Aequorea victoria* green fluorescent protein. *Science*. 1996;273:1392-1395.

Osadchii OE. Myocardial phosphodiesterases and regulation of cardiac contractility in health and cardiac disease. *Cardiovasc Drugs Ther*. 2007;21:171-194.

Palmer BM, McConnell BK, Li GH *et al*. Reduced cross-bridge dependent stiffness of skinned myocardium from mice lacking cardiac myosin binding protein-C. *Mol Cell Biochem*. 2004a;263:73-80.

Palmer BM, Georgakopoulos D, Janssen PM *et al*. Role of cardiac myosin binding protein C in sustaining left ventricular systolic stiffening. *Circ Res*. 2004b;94:1249-1255.

Palmer BM, Noguchi T, Wang Y *et al*. Effect of cardiac myosin binding protein-C on mechanoenergetics in mouse myocardium. *Circ Res*. 2004c;94:1615-1622.

Panaviene Z, Deng XA, Esham M *et al*. Targeting of nebulin fragments to the cardiac sarcomere. *Exp Cell Res*. 2007;313:896-909.

Papageorgopoulos C, Caldwell K, Schweingrubber H *et al*. Measuring synthesis rates of muscle creatine kinase and myosin with stable isotopes and mass spectrometry. *Anal Biochem*. 2002;309:1-10.

Parrish JR, Gulyas D, Finely RL. Yeast two-hybrid contributions to interactome mapping. *Curr Opin Biotech*. 2006;387-393.

Patel JR, Diffee GM, Huang X *et al*. Phosphorylation of myosin regulatory light chain eliminates force-dependence changes in relaxation rates in skeletal muscle. *Biophys J*. 1998;1998:360-368.

Peng J, Raddatz K, Molkentin JD *et al*. Cardiac hypertrophy and reduced contractility in hearts deficient in titin kinase region. *Circulation*. 2007;115:743-751.

Peña JR, Wolska BM. Troponin I phosphorylation plays an important role in the relaxant effect of β-adrenergic stimulation in mouse hearts. *Cardiovasc Res*. 2004;61:756-763.

Periasamy M, Bhupathy P, Babu GJ. Regulation of sarcoplasmic reticulum Ca<sup>2+</sup> ATPase pump expression and its relevance to cardiac muscle physiology and pathology. *Cardiovasc Res*. 2007;77:265-273.

Perry SV. Vertebrate tropomyosin: distribution, properties and function. *J Muscle Res Cell Motil.* 2001;22:5-49.

Persechini A, Stull JT, Cooke R. The effect of myosin phosphorylation on the contractile properties of skinned rabbit skeletal muscle fibers. *J Biol Chem.* 1985;260:7951-7954.

Pfleger KD, Eidne KA. New technologies: Bioluminescence resonance energy transfer (BRET) for the detection of real time interactions involving G-protein coupled receptors. *Pituitary.* 2003;6:141-151.

Pfleger KD, Eidne KA. Illuminating insights into protein-protein interactions using bioluminescence resonance energy transfer. *Nat Methods.* 2006;3:165-174.

Pfleger KD, Seeber RM, Eidne KA. Bioluminescence resonance energy transfer (BRET) for the real-time detection of protein-protein interactions. *Nat Protoc.* 2006;1:337-345.

Pi Y, Sreekumar R, Huang X *et al.* Positive inotropy mediated by diacylglycerol in rat ventricular myocytes. *Circ Res.* 1997;81:92-100.

Pi Y, Kemnitz KR, Zhang D *et al.* Phosphorylation of troponin I controls cardiac twitch dynamics. *Circ Res.* 2002;90:649-656.

Pi Y, Zhang D, Kara R *et al.* Protein kinase C and A sites on troponin I regulate myofilament  $\text{Ca}^{2+}$ -sensitivity and ATPase activity in the mouse myocardium. *J Physiol.* 2003;552:845-857.

Pickart CM, Eddins MJ. Ubiquitin: structures, functions, mechanisms. *Biochem Biophys Acta.* 2004;1695:55-72.

Pipkin W, Johnson JA, Creazzo TL *et al.* Localization, macromolecular associations, and function of the small heat shock-related protein HSP20 in rat heart. *Circulation.* 2003;107:469-476.

Pohlmann L, Kroger I, Vignier N *et al.* Cardiac myosin-binding protein C is required for complete relaxation in intact myocytes. *Circ Res.* 2007;101:928-938.

Powell SR. The ubiquitin-proteasome system in cardiac physiology and pathology. *Am J Physiol Heart Circ Physiol.* 2006;291:H1-H19.

Prinz A, Diskar M, Herberg FW. Application of bioluminescence resonance energy transfer (BRET) for biomolecular interaction studies. *Chembiochem.* 2006;7:1007-1012.

Radke MH, Peng J, Wu Y *et al.* Targeted deletion of titin N2B-region leads to diastolic dysfunction and cardiac atrophy. *Proc Natl Acad Sci USA.* 2007;104:3444-3449.

Rayment I, Holden HM, Wittaker M *et al.* Structure of the actin-myosin complex and its implications for muscle contraction. *Science*. 1993;261:58-65.

Rayment I, Rypniewski WR, Schmidt-Base K *et al.* Three-dimensional structure of myosin subfragment-1: a molecular motor. *Science*. 1993;261:50-58.

Razumova MV, Shaffer JF, Tu A *et al.* Effects of the N-terminal domains of myosin binding protein-C in an *in vitro* motility assay. *J Biol Chem*. 2006;281:35846-35854.

Redwood C, Moolman-Smook J, Watkins H. Properties of mutant contractile proteins that cause hypertrophic cardiomyopathy. *Cardiovasc Res*. 1999;44:20-36.

Reiffert SU, Jaquet K, Heilmeyer LM *et al.* Stepwise subunit interaction changes by mono- and bisphosphorylation of cardiac troponin I. *Biochemistry*. 1998;37:13516-13525.

Rice JJ, Winslow RL, Hunter WC. Comparison of putative co-operative mechanisms in cardiac muscle: length dependence and dynamic responses. *Am J Physiol*. 1999;276:H1734-H1754.

Ritz-Gold C, Cooke R, Blumenthal D *et al.* Light chain phosphorylation alters the conformation of skeletal muscle myosin. *Biochem Biophys Res Commun*. 1980;93:209-214.

Robia SL, Campbell KS, Kelly EM *et al.* Forster transfer recovery reveals that phospholamban exchanges slowly from pentamers but rapidly from the SERCA regulatory complex. *Circ Res*. 2007;101:1123-1129.

Roginski RS, Mohan Raj BK, Birditt B *et al.* The human GRINL1A gene defines a complex transcription unit, an unusual form of gene organization in eukaryotes. *Genomics*. 2004;84:265-276.

Rottauer W, Gautel M, Zehelein J *et al.* Novel splice donor site mutation in the cardiac myosin-binding protein-C gene in familial hypertrophic cardiomyopathy. *J Clin Invest*. 1997;100:475-482.

Rottauer W, Wessels G, Dahme T *et al.* Cardiac myosin light chain-2. A novel essential component of thick-myofilament assembly and contractility of the heart. *Circ Res*. 2006;99:323-331.

Sadayappan S, Gulick J, Osinka H *et al.* Cardiac myosin-binding protein-C phosphorylation and cardiac function. *Circ Res*. 2005;97:1156-1163.

Sadayappan S, Osinka H, Klevitsky R *et al.* Cardiac myosin binding protein C phosphorylation is cardioprotective. *Proc Natl Acad Sci USA*. 2006;103:16918-16923.

Sadayappan S, Finely N, Howarth JW *et al.* The role of the acidic N' region of cardiac troponin I in regulating myocardial function. *FASEB J*. 2008;22:1246-1257.

Sakai T, Liu L, Teng X *et al.* Nucling recruits Apaf-1/Pro-caspase-9 complex for the induction of stress-induced apoptosis. *J Biol Chem.* 2004;279:41131-41140.

Sakthivel S, Finely N, Rosevear PR *et al.* In vivo and in vitro analysis of cardiac troponin I phosphorylation. *J Biol Chem.* 2005;280:703-714.

Samarel AM. In vivo measurements of protein turnover during muscle growth and atrophy. *FASEB J.* 1991;5:2020-2028.

Sanbe A, Fewell JG, Gulick J *et al.* Abnormal cardiac structure and function in mice expressing non-phosphorylatable cardiac regulatory myosin light chain 2. *J Biol Chem.* 1999;274:21085-21094.

Sanger JW, Chowrashi P, Shaner NC *et al.* Myofibrillogenesis in skeletal muscle cells. *Clin Ortho.* 2002;403S:S153-S162.

Sanger JW, Kang S, Siebrands CC *et al.* How to build a myofibril. *J Muscle Res Cell Motil.* 2005;26:343-354.

Sarikas A, Carrier L, Schenke C *et al.* Impairment of the ubiquitin-proteasome system by truncated cardiac myosin binding protein C mutants. *Cardiovasc Res.* 2005;66:33-44.

Schaub MC, Hefti MA, Zuelling RA *et al.* Modulation of contractility in human cardiac hypertrophy by myosin essential light chain isoforms. *Cardiovasc Res.* 1998;37:381-404.

Schechtman D, Mochly-Rosen D. Adaptor proteins in protein kinase C-mediated signal transduction. *Oncogene.* 2001;20:6339-6347.

Schiaffino S, Reggiani C. Molecular diversity of myofibrillar proteins: gene regulation and functional significance. *Physiol Rev.* 1996;76:371-423.

Schlender KK, Bean LJ. Phosphorylation of chicken cardiac C-protein by calcium/calmodulin-dependent protein kinase II. *J Biol Chem.* 1990;266:2811-2817.

Schultheiss T, Lin ZX, Lu MH *et al.* Differential distribution of subsets of myofibrillar proteins in cardiac nonstriated and striated myofibrils. *J Cell Biol.* 1990;110:1159-1172.

Sébillon P, Bonne G, Flavigny J *et al.* COOH-terminal truncated human cardiac MyBP-C alters myosin filament organization. *C R Acad Sci III.* 2001;324:251-260.

Shaffer JF, Razumova MV, Tu A *et al.* Myosin S2 is not required for effects on myosin binding protein-C on motility. *FEBS Lett.* 2007;581:1501-1504.

Sjöblom B, Salmazo A, Djinovic-Carugo K. α-Actinin structure and regulation. *Cell Mol Life Sci.* 2008.

Sjostrom M, Squire JM. Fine structure of the A-band in cryosections. *J Mol Biol.* 1977;109:550-567.

Sobhanifar S. Yeast two hybrid assay: A fishing tale. *BioTeach Journal.* 2003;1:81-87.

Solaro J, Rosevear PR, Koyabashi T. The unique functions of cardiac troponin I in the control of cardiac muscle contraction and relaxation. *Biochem Biophys Res Commun.* 2008;369:82-87.

Song LS, Wang SQ, Xiao RP *et al.*  $\beta$ -Adrenergic stimulation synchronizes intracellular  $\text{Ca}^{2+}$  release during excitation-contraction coupling in cardiac myocytes. *Circ Res.* 2001;88:794-801.

Squire JM, Luther PK, Knupp C. Structural evidence for the interaction of C-protein (MyBP-C) with actin and sequence identification of a possible actin-binding domain. *J Mol Biol.* 2003;331:713-724.

Srikakulam R, Winkelmann DA. Chaperone-mediated folding and assembly of myosin in striated muscle. *J Cell Sci.* 2004;117:641-652.

Sriram G, Martinez JA, McCabe ER *et al.* Single-gene disorders: what role could moonlighting enzymes play? *Am J Hum Genet.* 2005;76:911-924.

Stamler R, Kappe G, Boelens W *et al.* Wrapping the alpha-crystallin domain fold in a chaperone assembly. *J Mol Biol.* 2005;353:68-79.

Stangl K, Gunther C, Frank T *et al.* Inhibition of the ubiquitin-proteasome pathway induces differential heat-shock protein response in cardiomyocytes and renders early cardiac protection. *Biochem Biophys Res Commun.* 2002;291:542-549.

Starr R, Offer G. Polypeptide chains of intermediate molecular weight in myosin preparations. *FEBS Lett.* 1971;15:40-44.

Steltzer JE, Patel JR, Moss RL. Acceleration of stretch activation in murine myocardium due to phosphorylation of myosin light chain. *J Gen Physiol.* 2006a;128:261-272.

Steltzer JE, Fitzsimons DP, Moss RL. Ablation of myosin-binding protein-C accelerates force development in mouse myocardium. *Biophys J.* 2006b;90:4119-4127.

Steltzer JE, Dunning SB, Moss RL. Ablation of cardiac myosin-binding protein-C accelerates stretch activation in murine skinned myocardium. *Circ Res.* 2006c;98:1212-1218.

Steltzer JE, Patel JR, Walker JW *et al.* Differential roles of cardiac myosin-binding protein C and cardiac troponin I in the myofibrillar force responses to protein kinase A phosphorylation. *Circ Res.* 2007;101:503-511.

Stepkowski D. The role of the skeletal muscle myosin light chains N-terminal fragments. *FEBS Lett.* 1995;374:6-11.

Strang KT, Moss RL.  $\beta$ -Adrenergic receptor stimulation increases unloaded shortening velocity in skinned single ventricular myocytes from rats. *Circ Res.* 1994;74:542-549.

Streeter DD, Spotnitz HM, Patel JR *et al.* Fiber orientation in the canine left ventricle during systole and diastole. *Circ Res.* 1969;24:339-347.

Suarez RK. Shaken and stirred: muscle structure and metabolism. *J Exp Biol.* 2003;206:2021-2029.

Subramanian C, Woo J, Cai X *et al.* A suite of tools and application notes for in vivo protein interaction assays using bioluminescence resonance energy transfer (BRET). *Plant J.* 2006;48:138-152.

Sweeney HL, Bowman BF, Stull JT. Myosin light chain phosphorylation in vertebrate striated muscle: regulation and function. *Am J Physiol.* 1993;264:C1085-C1095.

Sweeney HL, Yang Z, Zhi G *et al.* Charge replacement near the phosphorylatable serine of the myosin light chain mimics aspects of phosphorylation. *Proc Natl Acad Sci USA.* 1994;91:1490-1494.

Szczesna-Cordary D, Zhao J, Jones M *et al.* Phosphorylation of the regulatory light chains of myosin affects  $\text{Ca}^{2+}$  sensitivity of skeletal muscle contraction. *J Appl Physiol.* 2002;92:1661-1670.

Szczesna-Cordary D. Regulatory light chains of striated muscle myosin, structure, function and malfunction. *Curr Drug Targets Cardiovasc Haematol Disord.* 2003;3:187-197.

Szczesna-Cordary D, Guzman G, Zhao J *et al.* The E22K mutation of myosin RLC that causes familial hypertrophic cardiomyopathy increases calcium sensitivity of force and ATPase in transgenic mice. *J Cell Sci.* 2005;118:3675-3583.

Tada M. Calcium cycling proteins of the cardiac sarcoplasmic reticulum. *Circulation.* 2003;67:729-737.

Takimoto E, Soergel DG, Janssen PM *et al.* Frequency- and afterload-dependent cardiac modulation in vivo by troponin I with constitutively active protein kinase A phosphorylation sites. *Circ Res.* 2004;94:496-504.

Timson DJ, Trayer HR, Trayer IP. The N-terminus of A1-type myosin essential light chains binds actin and modulates myosin motor function. *Eur J Biochem.* 1998;255:654-662.

Tohong RH, Yamashita H, Graham ML *et al.* Impairment of muscle function caused by mutations of phosphorylation sites in myosin regulatory light chain. *Nature.* 1995;374:650-653.

Traaseth NJ, Verardi R, Torgersen KD *et al.* Spectroscopic validation of pentameric structure of phospholamban. *Proc Natl Acad Sci USA.* 2007;104:14676-14681.

Trombitas K, Freiburg A, Centner T *et al.* Molecular dissection of N2B cardiac titin's extensibility. *Biophys J.* 1999;77:3189-3196.

Van Criekinge W, Beyaert R. Yeast Two-Hybrid: State of the Art. *Biol Proced Online.* 1999;2:1-38.

van de Sluis B, Rothuizen J, Pearson PL *et al.* Identification of a new copper metabolism gene by positional cloning in a purebred dog population. *Hum Mol Genet.* 2002;11:165-173.

van Heerebeek L, Borbely A, Niessen HW *et al.* Myocardial structure and function differ in systolic and diastolic heart failure. *Circulation.* 2006;113:1966-1973.

Vatner DE, Sato N, Ishikawa Y *et al.* Beta-adrenoreceptor desensitization during the development of canine pacing-induced heart failure. *Clin Exp Pharmacol Physiol.* 1996;23:692.

Venema RC, Raynor RL, Noland TA *et al.* Role of protein kinase C in the phosphorylation of cardiac myosin light chain 2. *Biochem J.* 1993;294:401-406.

Verde I, Pahlke G, Salanova M *et al.* Myomegalin is a novel protein of the golgi/centrosome that interacts with cyclic nucleotide phosphodiesterase. *J Biol Chem.* 2001;276:11189-11198.

Vibert P, Craig R, Lehman W. Steric-model for activation of muscle thin filaments. *J Mol Biol.* 1997;266:8-14.

Vignier N, Perrot A, Schulte HD. Cardiac myosin binding protein C and familial hypertrophic cardiomyopathy with incomplete disease penetrance. *Circulation.* 2001;104.

Wannenburg T, Heijne GH, Geerdink JH *et al.* Cross-bridge kinetics in rat myocardium: effect of sarcomere length and calcium activation. *Am J Physiol Heart Circ Physiol.* 2000;279:H779-H790.

Ward DG, Cornes MP, Trayer IP. Structural consequences of cardiac troponin I phosphorylation. *J Biol Chem.* 2002;277:41795-41801.

Wattanapermpool J, Guo X, Solaro J. The unique amino-terminal peptide of cardiac troponin I regulates myofibrillar activity only when it is phosphorylated. *J Mol Cell Cardiol.* 1995;27:1383-1391.

Weigt C, Schoepper B, Wegner A. Tropomyosin-troponin complex stabilizes the pointed ends of actin filaments against polymerization and depolymerization. *FEBS Lett.* 1990;260:266-268.

Weinert S, Bergmann N, Luo X *et al.* M line-deficient titin causes cardiac lethality through impaired maturation of the sarcomere. *J Cell Biol.* 2006;173:559-570.

Weisberg A, Winegrad S. Alteration of myosin cross bridges by phosphorylation of myosin-binding protein c in cardiac muscle. *Proc Natl Acad Sci USA.* 1996;93:8999-9003.

Weisberg A, Winegrad S. Relation between crossbridge structure and actomyosin ATPase activity in rat heart. *Circ Res.* 1998;83:60-72.

Westfall MV, Turner I, Albayya FP *et al.* Troponin I chimera analysis of the cardiac myofilament tension response to protein kinase A. *Am J Physiol Cell Physiol.* 2001;280:C324-C332.

Westfall MV, Metzger JM. Troponin I isoforms and chimeras: tuning the molecular switch of cardiac contraction. *News Physiol Sci.* 2001;16:278-281.

Willis MS, Patterson C. Into the heart: the emerging role of the ubiquitin-proteasome system. *Mol Cell Cardiol.* 2006;41:567-579.

Winegrad S. Cardiac myosin binding protein C. *Circ Res.* 1999;84:1117-1126.

Witt CC, Gerull B, Davies MJ *et al.* Hypercontractile properties of cardiac muscle fibers in a knock-in mouse model of cardiac myosin-binding protein-C. *J Biol Chem.* 2001;276:5353-5359.

Wolska BM, Stojanovic MO, Luo W *et al.* Effect of ablation of phospholamban on dynamics of cardiac myocyte contraction and intracellular calcium under basal conditions and during  $\beta$ -adrenergic stimulation. *Am J Physiol.* 1996;271:391-397.

Yamaguchi T, Arai H, Katayama N *et al.* Age-related increase of insoluble, phosphorylated small heat shock proteins in human skeletal muscle. *J Gerontol A Biol Sci Med Sci.* 2007;62:481-489.

Yamamoto K, Moos C. The C-proteins of rabbit red, white and cardiac muscles. *J Biol Chem.* 1983;258:8395-8401.

Yamamoto K, Moos C. Characterisation of H-protein, a component of skeletal muscle myofibrils. *J Biol Chem.* 1984;259:7163-7168.

Yamamoto K. The binding of skeletal muscle C-protein to regulated actin. *FEBS Lett.* 1986;208:123-127.

Yamasaki R, Wu Y, McNabb M *et al.* Protein kinase-A phosphorylates titin's cardiac-specific N2B-domain and reduces passive tension in rat cardiac myocytes. *Circ Res.* 2002;90:1181-1188.

Yamasaki R, Berri M, Wu Y *et al.* Titin-actin interaction in mouse myocardium: passive tension modulation and its regulation by calcium/S100A1. *Biophys J.* 2001;81:2297-2313.

Yang Q, Sanbe A, Osinka H *et al.* A mouse model of myosin binding protein C human familial hypertrophic cardiomyopathy. *J Clin Invest.* 1998;102:1292-1300.

Yang Q, Sanbe A, Osinka H *et al.* *In vivo* modeling of myosin binding protein C familial hypertrophic cardiomyopathy. *Circ Res.* 1999;85:841-847.

Yang Q, Osinka H, Klevitsky R *et al.* Phenotypic deficits in mice expressing a myosin binding protein C lacking the titin and myosin binding domains. *J Mol Cell Cardiol*. 2001a;33:1649-1658.

Yang Q, Hewett TE, Klevitsky R *et al.* PKA-dependent phosphorylation of cardiac myosin binding protein C in transgenic mice. *Cardiovasc Res*. 2001b;51:80-88.

Young P, Ferguson S, Banuelos S *et al.* Molecular structure of the sarcomeric Z-disk: two types of titin interactions lead to an asymmetrical sorting of alpha-actinin. *EMBO J*. 1998;17:1614-1624.

Young P, Ehler E, Gautel M. Obscurin, a giant sarcomeric Rho guanine nucleotide exchange factor protein involved in sarcomere assembly. *J Cell Biol*. 2001;154:123-136.

Zhang Q, Ragnauth C, Greener MJ *et al.* The nesprins are giant actin-binding proteins, orthologous to Drosophila melanogaster muscle protein MSP-300. *Genomics*. 2002;80:473-481.

Zhou M, Veenstra TD. Proteomic analysis of protein complexes. *Proteomics*. 2007;7:2688-2697.